Optical Diamond Turning of Rapidly Solidified Aluminium Alloy Grade - 431

By

OYEKUNLE, FUNSHO ADEKUNLE

NELSON MANDELA
UNIVERSITY

Optical Diamond Turning of Rapidly Solidified Aluminium Alloy Grade - 431

By

OYEKUNLE, FUNSHO ADEKUNLE

(Student Number: *s216865093*)

Submitted in fulfilment/partial fulfilment of the requirements for

The Degree of Master of Engineering: Mechatronics in the Faculty of Engineering, the Built

Environment and Information Technology at the

Nelson Mandela University

April 2020

Promoter/Supervisor: Prof. Khaled Abou El-Hossein

Copyright Statement

The copy of this thesis has been provided on the condition that anyone who accesses it understands and recognizes that its copyright rests with the Nelson Mandela Metropolitan University and that no information derived from it may be published without the prior consent of the Author unless appropriately reference.
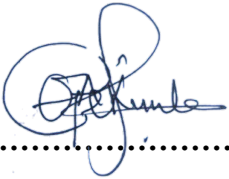
Author's Declaration

I**, Funsho Adekunle Oyekunle** hereby declare that:

- The work contained in this thesis is my own original work;

- All sources used or referred to have been documented and recognized; and

- This thesis has not been in its entirety previously submitted in full or partial fulfilment of the requirements for an equivalent or higher qualification at any educational institute for a degree.

Authors' Signature   **Date: April 2020**

………………………………

Dedication

To the saviour of the world. The author and finisher of our faith and to Iremide, the precious gift he gave me.

Acknowledgement

Abstract

The high demand for ultraprecision machining systems is increasing day by day. The technology leads to increased productivity and quality manufactured products, with an excellent surface finish. Therefore, these products are in demand in many industrial fields such as space, national defence, the medical industry and other high-tech industries.

Single point diamond turning (SPDT) is the core technology of ultraprecision machining, which makes use of single-point crystalline diamond as a cutting tool. This technique is used for machining an extensive selection of complex optical surfaces and other engineering products with a quality surface finish. SPDT can achieve dimensional tolerances in order of 0.01um and surface roughness in order of 1nm. SPDT is not restricted, but mostly applicable, to non-ferrous alloys; due to their reflective properties and microstructure that discourages tool wear.

 The focus of this study is the development of predictive optimisation models, used to analyse the influence of machining parameters (speed, feed, and depth of cut) on surface roughness. Moreover, the study aims to obtain the optimal machining parameters that would lead to minimum surface roughness during the diamond turning of Rapidly Solidified Aluminium (RSA) 431.

In this study, Precitech Nanoform 250 Ultra grind machine was used to perform two experiments on RSA 431. The first machining process, experiment 1, was carried out using pressurized kerosene mist; while experiment 2 was carried out with water as the cutting fluid. In each experiment, machine parameters were varied at intervals and the surface roughness of the workpiece was measured at each variation.

The measurements were taken through a contact method using Taylor Hobson PGI Dimension XL surface Profilometer. Acoustic emission (AE) was employed as a precision sensing technique - to optimize the machining quality process and provide indications of the expected surface roughness.

The results obtained revealed that better surface roughness can be generated when RSA 431 is diamond-turned using water as a cutting fluid, rather than kerosene mist. Predictive models for surface roughness were developed for each experiment, using response surface methodology (RSM) and artificial neural networks (ANN). Moreover, RSM was used for optimisation. Time-domain features acquired from AE signals, together with the three cutting parameters, were used

as input parameters in the ANN design. The results of the predictive models show a close relationship between the predicted values and the experimental values for surface roughness. The developed models have been compared in terms of accuracy and cost of computation - using the mean absolute percentage error (MAPE).

Abbreviations

UHPM	Ultra-high Precision Machining
RSA	Rapidly Solidified Aluminium
NDT	Non-Destructive Test
SPDT	Single-point Diamond Turning
CNC	Computer Numeric Control
AE	Acoustic Emission
AI	Artificial Intelligence
RSM	Response Surface Model
ANN	Artificial Neural Network
CAD	Computer-Aided Design
CAM	Computer-Aided Manufacturing
EDM	Electrical Discharge Machining
SEM	Scanning Electron Microscope
DoE	Design of Experiment
MRR	Material Rate Removal
RSM	Response Surface Method
SCD	Single Crystal Diamond
SPDT	Single-point Diamond Turning
BUE	Built Up Edge

FCC	Face Centre Cubic
Mpa	Mega Pascal
AE	Acoustic Emission
RMS	Root Mean Square
DSP	Digital Signal Processing
DVD	Digital Video Disc
DAC	Digital to Analog Conversion
BP	Back Propagation
RSA	Rapidly solidification of aluminium
ARMA	Auto-Regression Moving Average
MA	Moving Average
AR	Auto-Regression
DFT	Discrete Fourier Transform
PSD	Power Spectral Density
STFT	Short Time Fourier Transform
FFT	Fast Fourier Transform
DWT	Discrete Wavelet Transform
CWT	Continuous Wavelet Transform
BBD	Box-Behnken Design
MEG	Magnetoencephalogram

EEG	Electroencephalogram
ECG	Electrocardiogram
ISO	International Organization for Standardization
2FI	Two Factor Interaction

Nomenclature

f feed rate

v cutting speed

d depth of cut

R_a surface roughness

δ   the estimation error

n   the total number of measurements

i the estimated measurement for a specific run

R^2 coefficient of determination

Glossary of Terms

A

Accuracy - the condition or quality of being true, correct, or exact.

Aspherical - the property of a surface deviating slightly from a perfectly spherical shape and relatively free from aberrations.

Allowance - is a planned deviation between an exact dimension and a nominal or theoretical dimension.

Asymmetric - not symmetric; lacking symmetry or misproportioned.

Axisymmetric - being symmetrical around an axis.

B

Built up edge – is an accumulation of material against the rake face that seizes to the tool tip, separating it from the chip

C

Crystallite size - is the size of a single crystal inside a particle or grain.

D

Dynamic strain – a strain which changes with time.

G

Grain size - (or particle size) is the diameter of individual grains of sediment or the lithified particles in clastic rocks. The term may also be applied to other granular materials.

M

Miniaturization - the act of making materials on a greatly reduced scale.

Microstructure - is the very small-scale structure of a material, defined as the structure of a prepared surface of a material as revealed by a microscope above $25\times$ magnification.

N

Non-Ferrous – is a metal containing little or no iron.

P

Precision - is the mechanical exactness of a material.

Pass band filter - is an electronic circuit or device which allows only signals between specific frequencies to pass through and attenuates/rejects frequencies outside the range.

R

Roughness – the property of a lens having a coarse or uneven surface, as from projection, irregularities or breaks. A state of being not smooth.

S

Spherical - a figure having the form of a sphere; globular.

Sampling - is the process of converting a continuous signal to a discrete one.

Symmetric - having two halves which are the same, except one half is the mirror image of the other half.

T

Tolerance - the permissible range of variation in a dimension of an object.

Topography – the detailed mapping or charting of the features of a relatively small area, district, or locality.

W

Wear – a condition of a surface which infers causing deterioration or degradation of that surface.

(Adapted from [1])

List of Publications from this Work:

Adekunle Funsho Oyekunle, Hweju, Zvikomborero, Khaled Abou-El-Hossein "Genetic Algorithm Based Surface Roughness Prediction Using Acoustic Emission Signal Parameters".

Adekunle Funsho Oyekunle, Khaled Abou-El-Hossein "*Effects of Cutting Fluids on Surface Roughness in Single-Point Diamond Turning of Rapidly Solidified Aluminium Alloy (RSA 431)*".

Adekunle Funsho Oyekunle, Khaled Abou-El-Hossein "*Optimization of SPDT of RSA 431 Using water as coolant*".

Table of Contents

List of Figures

xxiii

Chapter One

1.0   Introduction

1.1   Background and significance

All manufactured engineering components depend mostly on the machining process for its quality and performance. The demand for an advanced optical and precision industry led to a significant dimensional tolerance through a simple extension of conventional machining processes and techniques.

In today's manufacturing, the emergence of newer materials and complex shapes, which are challenging to machine, has led to the introduction of ultraprecision machining (UPM). Also, the increased market call for developed, miniaturization, long reliable, better performed and quality-controlled products through accurate machining has provoked the introduction of UPM.

Since the introduction, a better quality of industrial technology has been recorded in terms of accuracy and surface quality. In recent time, the technology of ultraprecision machining has improved due to its ultra-smooth surface roughness in atomic order and nanometric range of accuracy. The finishing feature has made it suitable for the development of modern optical and precision components.

Single-point diamond turning (SPDT) is one of the ultraprecision machine tooling-processes or techniques. It was introduced in 1960 when it was used for optical turning but was only officially recognized in the mid-1970s [2, 3]. This technique makes use of diamond tool technology for the rapid production of spherical and aspheric optical lenses, mirrors, mould inserts, freeform optics and mechanical components.

Furthermore, the geometry and superior surface of these components can be manufactured in large volumes with high accuracy and precision. The position accuracy (from ±1 to ±5 nm) of UPM, in contrast to the ±1000 nm accuracy of conventional precision machines, and the sharpness together with the rigidity of the diamond tool - has made an impressive smooth mirror surface achievable.

1

SPDT is extensively used for machining non-ferrous materials like aluminium and copper due to their easy diamond-tunability, excellent reflectivity and high-corrosion resistance. Conventional aluminium can be challenging to diamond turning at a surface roughness value less than 3nm. Moreover, mirror surface components may have to undergo post-process operations such as lapping and polishing to achieve the required surface finish [4]. This process is time-consuming and capital intensive.

Optical aluminium alloys have exhibited immense advantages, including better-machined surfaces through diamond turning when compared to other non-ferrous metals like Nickel-phosphorus (NI-P) plated steel and copper alloys. The advantages are due to the unique combination of aluminium alloys properties like fine-grain microstructure free of defects, and the ability to produce a good surface finish. Finally, another advantage when compared to other alloys is minimal tool wear experienced during machining.

Meanwhile, the increasing demand for improved optical and precision components at an affordable cost has encouraged the modification of aluminium alloys through a meltspinning technique. This technique is a process of rapid solidification, which births a new generation of aluminium alloys. These new aluminium alloys are mostly applicable for the production of advanced optical precision and other engineering components, as a result of improved microstructures, and upgraded mechanical and physical properties.

1.2   Research motivation

Manufacturing engineering is a vast industry in the world today. Advanced manufacturing engineering is confident in improving the standard of living of any nation and help it to compete in the world trade markets. For this reason, huge investments are being put into manufacturing engineering for advancement to meet the increasing demand for quality and improved products, which are readily available at very low cost.

Ultraprecision machining has gained a lot of relevance in the past few years due to its application in various fields like electronics, optics, national defence, medical automobile, etc. Many organizations and some developed countries like USA, UK, China, and Japan have adopted and

invested in the technology and development of UPM as a source of economic strength and a barometer of its science and technology. Therefore, different research has been initiated.

Summarily, the technology of ultraprecision machining is not only leading in modern manufacturing technology, but it also serves as the basis for future manufacturing technologies[5]. RSA alloys are a special type of aluminium alloys typically machined by UPM for optical and precision purposes, due to their improved mechanical and physical characteristics. Ultraprecision machined components produced from RSA alloys are largely used for optical, electronic and mechanical components. Although, the realization of desired surface quality, at a limited time and minimal tool wear rate during machining, is of great significance. Therefore, attention must be directed in that regard.

For Africa to attain a competitive position alongside the developed continents in the industrial and manufacturing sector, there is a pressing need to focus on the improvement on the quality and productivity of engineering products; at low cost and within a minimum time lost. Surface roughness is one of the important parameters to determine the quality of products, and the mechanism responsible for the generation of these parameters is dynamic, complicated and process dependent. This research studies the ultraprecision cutting of RSA alloy and a model that can eliminate the laborious trial-and-error approach, reduce cost and time consumed during machining of RSA-431 is developed.

1.3   Problem statement

The driving force for advancement in machining optical aluminium for the production of precision moulds, optical devices and components, is the increase of the surface integrity at a very low cost and less production time. Ultraprecision single-point diamond turning (SPDT) has been well developed and widely used to produce a final surface without a post-polishing operation.

However, in reality, the surface of these optic materials still contains defects from variations of associated machining parameters and conditions. Consequently, affecting the performances of the optical components. To realise how these defects impress the surface quality of diamond-turned devices, the study of machinability of optical material is important.

In the last decade, SPDT has been used extensively for precision machining of non-ferrous metals, mostly aluminium. So far, little or no effort is currently placed on SPDT of rapidly solidified aluminium, RSA 431, which is a relatively new grade of RSA. This grade possesses good mechanical and physical properties like low weight, low thermal expansion and high stiffness, among others. Given the high content of silicon (40%) and magnesium in its chemical composition, it appears difficult to machine.

Therefore, the single-point machining of RSA 431 should be approached somewhat differently. These constituents in relation, to the other variation of cutting parameters like feed, speed, and depth of cut, can cause abrasion thereby influencing the surface finish when diamond-turned. Hence, there is a need for attention and interest to conduct SPDT experiments at a nanometric scale on the workpiece, to examine the possible conditions for fabricating high-quality optical surfaces.

1.4   Aim of the study

Industrial activities depend solely on machining despite recent development achieved in the near-net industrial manufacturing technique. This research aim is to study the cutting mechanisms of SPDT on RSA grade 431 and then using the knowledge, to predict the achievable level of surface roughness.

1.5   Objectives

In this research study, the listed objectives will be used to achieve the aim:

- To investigate the ultra-precision diamond turning of RSA 431 by determining the surface roughness experimentally, using kerosene mist and water respectively as cutting fluid.
- To develop predictive and optimisation models to determine the optimum machining parameters that would produce minimum surface roughness.
- To investigate and develop a model to determine the effects of machining parameters on the acoustic emissions to provide guidance for desirable surface roughness.
- To compare the performance of RSM and ANN models using the mean-absolute-percentage error (MAPE).

4

1.6   Scope of the thesis

The research investigates the single point diamond of rapidly solidified aluminium to provide a reference guide for desired surface roughness; over a range of machining parameter combinations. The scope of this research is limited to:

- Literature studies on ultraprecision machining, aluminium alloys and its machinability.
- The investigation focuses on RSA grade 431.
- Measurement of the machined surface is limited to average roughness parameters.
- The cutting parameters are limited to depth of cut, feed and cutting speed, which are varied for each experimental run.
- The effect of different cutting fluids (water and kerosene mist) on surface roughness during single point diamond turning operation.
- Acoustic emission signal recording and analysis is the main detecting technique utilised in the research.
- Development and validation of model deployable for surface roughness is the design and analysis of the experiment approach and artificial neural network (ANN).

1.7   Hypothesis

Null hypothesis:

i.   Acoustic Emission sensing technique is not suitable to monitor the ultra-high precision diamond turning of RSA-431.

ii. An artificial neural network (ANN) cannot be used to accurately predict the surface roughness of ultraprecision diamond turning of RSA-431.

iii. Response surface modelling is not suitable to analyse the effect of machining parameters in the ultraprecision diamond turning of RSA-431.

1.8   Thesis structure

The thesis presents experimental works, which generate predictive and optimisation models for surface roughness in terms of machine parameters (depth of cut, feed, and speed), during the turning of RSA-431. The organisation is introduced in the graphical design shown in Figure 1.1

Chapter1: Introduction and background

Chapter 2: Literature Review

Chapter 3: Experimental Design and Procedure

Chapter 4: Results and Discussion

Chapter 5: Conclusion and Recommendation
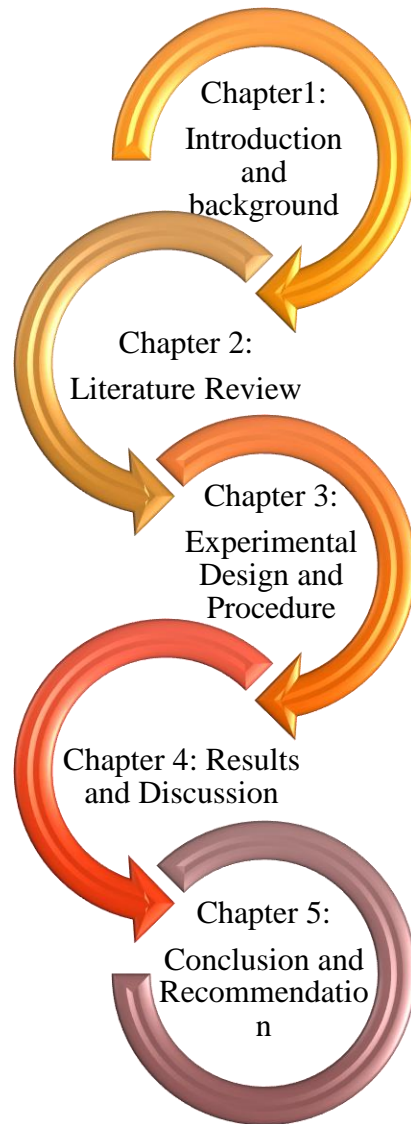
Figure 1.1: Research Approach

<div align="center">**Chapter Two**</div>

2.0 Literature Review

2.1 Brief background of manufacturing process

Since 4000 BC, human civilisation has been centred around manufacturing activities. Over the years, the industrial revolution has positively influenced engineering product, due to the introduction of high-automated machines to replace the primitive manufacturing processes like the hammering of metals for jewellery, carving of wood, hand forging and hand-filing of metal.

Industrial manufacturing is a vital source of economic strength for a nation. It is an act of making use of processes and systems to transform certain engineering materials into products of increased value. Thus, we can say manufacturing involves three building blocks, namely - processing, system and material. Processing in manufacturing involves a transformation in terms of shape, size and form of engineering material into an advanced or final product.

Processing can be in the form of machining, which is a controlled material removal process that transforms engineering materials into desired shapes or sizes with the help of cutting tools, which are stronger and harder than the material [6]. It is simply a term used to describe the material removal process of a workpiece to form chips. This, if carried out properly, adds value to the geometry and appearance of the workpiece and makes it suitable for the desired product.

However, in this present day, there is a new trend in the demand for miniaturised products at a reduced cost, better performance and on-time delivery. This can be confirmed in every manufacturing industry. To meet these huge demands, as well as overcome the challenges of more products with minimum material with less energy and manpower, micromachining was introduced.

The term micromachining can be defined as the mechanical micro-cutting techniques where the material is removed by geometrically determined cutting edges [7]. The importance of a material removal process has called for automated high-speed machine systems and tools, to improve process accuracy, increase productivity, quality of engineering components and facilitate materials that are difficult to machine. Advanced industries such as automobile, medical, aeronautics, etc now employ the use of this technology due to the high demand for materials with high physical

<div align="center">7</div>

and mechanical properties. These properties include thermal coefficient, strength-to-weight ratio, hardness, toughness, among others.

However, to have a better tool life when machining hard materials, the cutting speed needs to be reduced [8]. Thus, the machining of certain hard and other high-temperature engineering materials through the conventional method can be challenging.

2.2   Overview of precision engineering

Over the last 200 years, progress towards greater precision has led to tolerances of less than 1 micron. Although many problems in micro-engineering are yet unsolved, components can now be produced with tolerances of a few nanometres. The history of increasing machining precision has indicated that there is an ever-increasing demand for creating value-added products [9]. Today, the increase in technical complexity of engineering products, coupled with consumer's demand for the high-standard quality and reliability of these complex products at a very affordable price, have provoked the introduction of precision engineering.

In 1974, N. Taniguchi [10], a renowned Japanese researcher, illustrated the historical development of relative precision and accuracy of machining technologies and how they have changed over time, using a diagram called Taniguchi curves Figure 2.1 shows the Taniguchi curves showing the evolution of machining accuracy updated beyond the year 2000 (as shown in the red box to include a state-of-the-art manufacturing process).
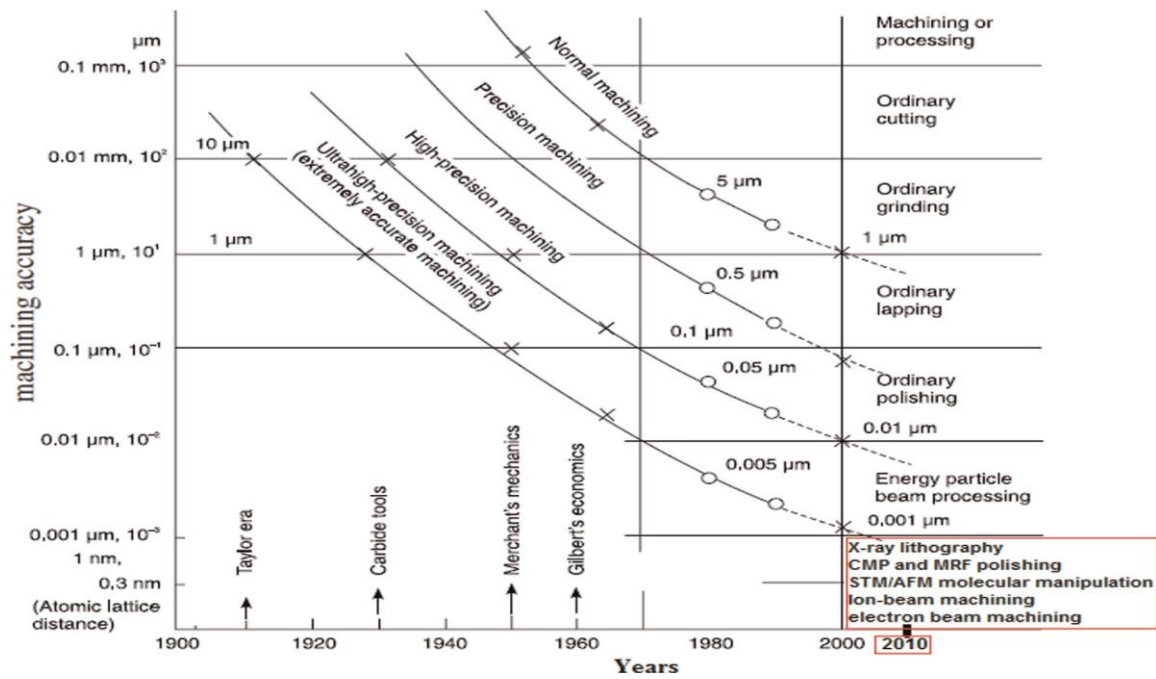
Figure 2.1: Taniguchi curves showing the evolution of machining accuracy [10].

In the curve, he depicted that it took about 20 years to improve precision by one decimal point, as shown in Table 2.1. He further predicted that machining resolution will attain 1nm in the year 2000 and according to the prediction, quite several ultraprecision machining techniques are available today. As seen in history, the change in precision machining since its invention has been significant, it can, therefore, be concluded that precision machining has come a long way and is here to stay.

Table 2.1: Summary ultraprecision evolution.

Year	1900	1920	1940	1960	1980	2000
Resolution (µm)	>10	5	0.5	0.05	0.005	0.001

Although the study of precision engineering commenced around the early 1930s, it gained significant development in the 1970s when it was used to manufacture memory discs for computer hard drives and photoreceptor components; used in many photocopier and printing machines [9, 11]. Around this time, the demands for miniaturisation and high surface quality have increased

tremendously and many engineering bodies and researchers have pursued the advancement of precision engineering.

Regardless of the pertinence of precision engineering in the manufacturing industry at that time, there was no precise definition or methodical organisation in this field. However, in the early 1990s, Nakawaza [12], a Japanese engineering educator in his book titled *Principle of Precision*, defined precision engineering as the structured combination of knowledge and principles of achieving high-precision during machining. It involves the invention of high-precision machine tools, their design, fabrication and measurement. He emphasized in his book the need to understand that priority needs to be placed on cutting tools (like single crystal tools) as much as the manufacturing processes. This agrees with the definition of precision engineering offered by the America Society of Precision Engineering (ASPE) [13] as;

> "Precision engineering is a discipline encompassing the design, development, and measurement of and for high-accuracy components. By extension, the field also includes the design of systems in which high dimensional accuracy is a central concern, as well as the design of machine tools and measuring machines to accomplish the necessary manufacture and measurement."

McKeown [14], went further in his definition from fabrication and designing. He describes precision engineering as the application of scientific skills and techniques in precision processing of materials, information processing system, control system and unmanned manufacturing system containing CAD and CAM systems. According to McKeown, the main aim of precision engineering is to achieve high accuracy, which is the ratio of tolerance to dimension.

Generally, precision engineering is often described as manufacturing to a tolerance that is smaller than 1µm, with the physical dimension of components in order of 1µm. Simply, this means the process of manufacturing and measuring engineering products in precision engineering are of precise standard. For a manufactured product to be considered precise, it must possess feature satisfactory limits, accurate dimensions, tolerance as well as allowance. Precision engineering deals with manufacturing products ranging from sizes as big as a satellite rocket launcher to

10

something as small as a microchip. It is especially applicable in the production of diamond indenters and tools, mirrors, 3d metallic mirrors, ICs memory, thin film, aspherical lenses in the optical field, etc. As a result of the individual difference in products detailed measurement, the level of precision will be determined by the purpose for which it is manufactured.

2.3   Accuracy and precision

Although, precision and accuracy are terms used in describing systems and method that measures, estimate, or predicts, the definition of precision and accuracy have been mistaken for each other and is often defined as the same. For a better understanding of precision engineering, it is important to differentiate the two terms with respect to modern machining. A graphic explanation (Figure 2.2.) is used to explain these two terms.
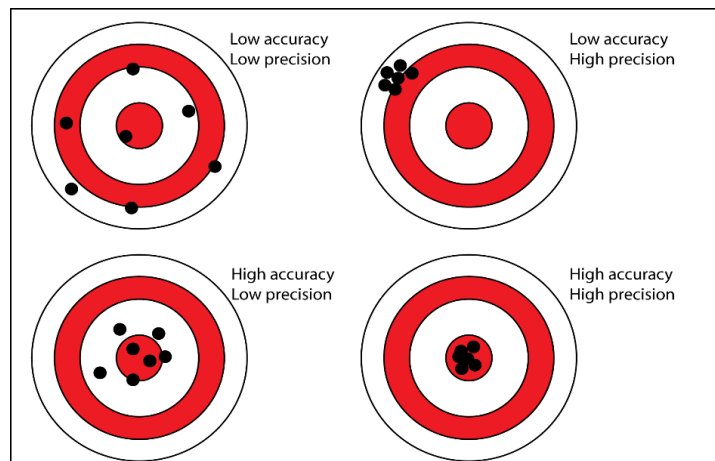
Figure 2.2: Difference between accuracy and precision

Accuracy is the degree to which a measured system produces the true or correct value of quantities of interest. In other words, it is the difference between the measured value of a system and the actual measurement. The smaller the difference, the more accurate the system.

The repeatability of the measurement system of the same standard without any error is known as precision. This implies the reliability of a system to repeat the same measurement over a few times without any error. Additionally, tolerance can simply be defined as the predictable deviation or allowance of the measurement system from the standard value. It is usually expressed as "±" [9].

2.4   Ultraprecision machining

Machining can be classified into macro, mesa, micro, and nano-scale machining as predicated on the accuracy and scale machining chart shown in Figure 2.3. It is understood that the ultraprecision machining technique applies to both micro and nano-scale cutting for ultraprecision accuracy [15].
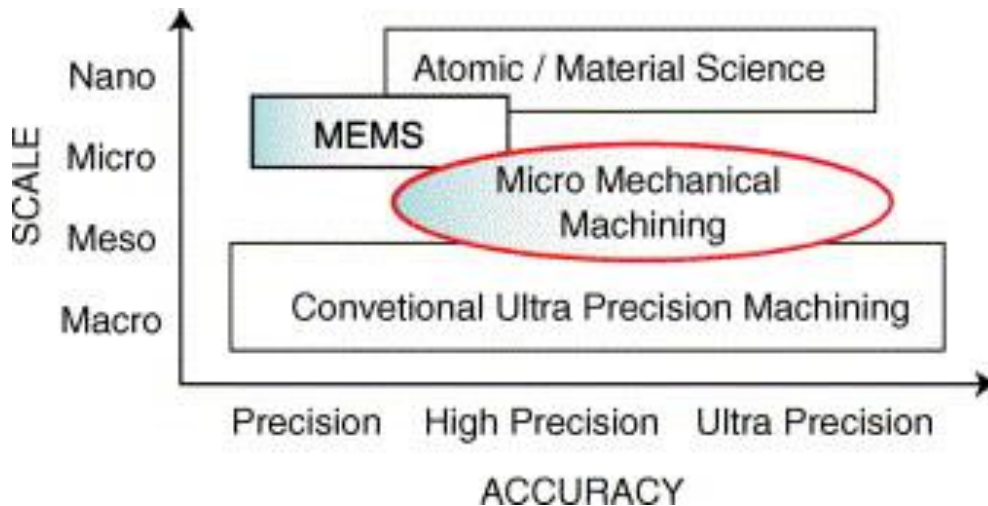
Figure 2.3: Classification of mechanical machining

Ultraprecision machining (UPM) is a representation of advanced modern manufacturing technology that deals with material removal at the lowest atomic scale. The removal action process at this small scale is called atomic bit [7] and an extreme amount of energy is needed by the machine tool in this atomic vicinity.

Taniguchi [16] used the term nanotechnology to describe UPM as the process by which the highest possible dimensional accuracy can be achieved over time. The technique of UPM is employed in the manufacturing of optical devices and other precision components with the most stringent dimension order, accuracy form in the range of 0.1 nm – 100 nm. Moreover, a surface finish at a nanometric / sub-nanometric level is attainable, which cannot be achieved through conventional machining processes and techniques.

Ultraprecision machining is not restricted to specific indexes of profile accuracy and surface roughness, it is also used in achieving intricate shapes and forms. The advanced technology of UPM today has ensured the production of complex 3-dimensional surfaces with the accuracy required for optical and precision application. The future of conventional manufacturing industries

12

like automotive and engine fabrication, aerospace, national defence, medical and other high-tech industries lie in full automated ultraprecision machining systems. These systems are required due to continuous rapid growth and demand for devices or equipment at nano level precision, which can be manufactured at a lower cost and in less time.

UPM is charged with the responsibility of promoting miniaturised products and improving their performance, stability and reliability to meet consumers' demands. However, these needs are endless, there will always be a demand for new and improved products. Therefore, the focus on ultraprecision engineering has become increasingly relevant. Ultraprecision machining is widely appreciated, not just because of the high precision and reliability it offers conventional products, but also the manufacturing of new products where high performance and miniaturisation is important.

In machining, the performance of the process is directly influenced by the machine's features. The features of UPM responsible for the accuracy and high performance can be categorised into five major sub-systems - mechanical structure, work spindle, drives, control, measurement system and control. Table 2.2 shows the prominent machine parts and their UPM features [7].

Table 2.2: Features of Single-Point Ultraprecision Machine.

Machine Parts / elements	Features
Machine base	
Provides thermal and mechanical stability, damping characteristics.	Made of cast iron, natural or epoxy granite, polymer concrete.
Work spindle	
Spindle motion errors significantly affect the surface quality and accuracy of machined features.	Both the spindle types have high rotational accuracy and rotational speeds. Aerostatic spindles are for low /medium loads, hydrostatic bearings take heavy loads.

Use aerostatic or hydrostatic, recent grooved air bearings.	
Drives	
Slides drives provide stiffness, acceleration, speed, smoothness of motion, accuracy and repeatability. Spindle drives are usually AC/DC motors. Slides are usually provided with a linear motor or friction drives.	Servo drives are used in contouring operations. Small and precise motions of tools for tool positioning and fine motion are achieved by piezoelectric actuators.
Controls	
Controls are required for linear and rotary drives, limiting, position, time switches and sensors. They also control thermal, geometrical and tool setting errors.	Multi-Axes CNC controllers are used. PC-based controls are used more recently. Feedback controls have a resolution of nm or sub-nm.
Measurement and Inspection Systems	
Provides rapid and accurate positioning of the cutting tool towards workpiece surface. It also monitors the tool-wear condition.	Online measurement and error compensation. Laser interferometer for tool position control.

The machining process of UPM is currently categorized into four fields [5]:

i. Ultraprecision cutting: This is a field of UPM where technology makes use of hard material, such as crystalline diamond, as tools. A wide nanometre range of surface roughness is achievable with these tools. Ultraprecision cutting can be in the form of

ultraprecision turning, milling, grinding, boring and ultraprecision cutting with ultrasonic vibration (compound machining).

ii. Ultraprecision grinding: This is an abrasive process of UPM that makes use of ultrafine grinding wheels, wear-resistant abrasives, low run-out spindles and machine tools with high loop stiffness. The aim is to achieve high machining precision and accuracy with superior surface roughness. Ultraprecision grinding is commonly used for machining hard and brittle materials like glass, ceramic and semiconductors – where the abrasive process is more complex and probabilistic, especially when high precision is required.

iii. Ultraprecision polishing: This combines mechanical and chemical action to achieve fine abrasiveness. This combination is carried out with the application of soft polishing tools, chemical fluids, or electric/magnetic fluid to obtain a super smooth surface with no/ minimal defect in the subsurface/surface. Although this process of UPM is complex, expensive and time-consuming, it is the main method of UPM that is responsible for the fabrication of high-precision and high-quality freeform surfaces. The quantity of material removed during the process is also small, often below several microns.

iv. Ultraprecision non-traditional machining: This involves the use of nano physical process with high energy elementary particles like photons, electrons, ions and reactive atoms; to perform direct ablation of the substrate or carry out lithography. This process is used to produce complex shapes and of this process include electronic beam figuring and ion beam figuring.

In the past few decades, the use of ultraprecision machining has revolved around the core technology of SPDT and. the effectiveness of the technology has made the two synonymous. Our focus for this research will be on ultraprecision SPDT.

2.5   Single-point diamond turning

The technique of SPDT is the pioneer of the ultraprecision turning method. The precision engineering industry has achieved great improvement in recent years, since the introduction of SPDT, which is justified by its demand for machining small and light-weight materials for high and accurate optical components.

These optical components can be used for telescopess, defense system, laser-research instruments, medical instruments, and other optical and precision applications. SPDT is a tool-based ultraprecision machining process that mainly uses single-crystal diamond as a tool that can remove material at the scale of a few atomic layers, to produce an optical quality machined surface. The form accuracy is usually within a micrometre range and the surface roughness is less than a few tens of a nanometre.

The diamond tool used in SPDT of UPM is an ultra-sharp high-purity tool with a small cutting-edge radius, capable of cutting through the minimum thickness of the workpiece, only a few micrometres or less than 1 micrometre. This cutting tool edge radius has a significant effect on the nanometric range of the SPDT surface. Micro cutting carried out on surfaces with less damaged or very thin affected layers to achieve a smooth surface using SPDT technology. Other outstanding properties like super hardness, high thermal conductivity and high wear resistance with low friction of the diamond tool, also contribute to the precision cutting ability.

Similar to other machining processes, SPDT is charged with material removal of the workpiece to desired shapes, forms and sizes. Non-ferrous materials like aluminium, copper, electroless nickel, and other soft and ductile material are the most common workpieces that can be diamond-turned to a nanometric surface finish without post-polishing processes [17, 18].

However, the technique has been improved to diamond-turn some infrared materials like silicon and germanium in the brittle-ductile region. Some difficult-to-machine materials, which are capable of transmitting light over a wide range of wavelengths required in optical and defence systems, can also be machined using the technology of SPDT to produce a surface roughness in few tens of a nanometre. Experiments have shown that a silicon machined surface using SPDT exhibited good quality surface. Nevertheless, rapid diamond tool wear experienced with these materials is still a deterministic setback [18].
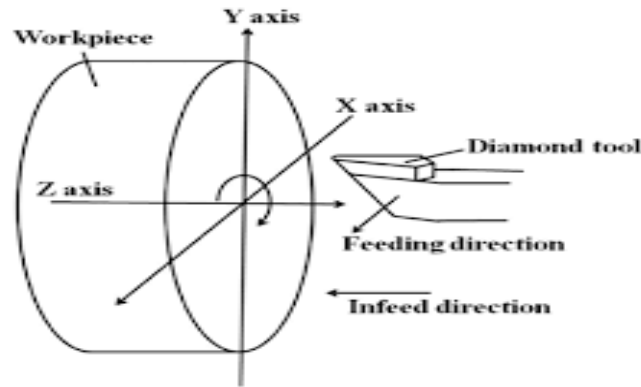
Figure 2.4: Turning operation using Single-point diamond tool (SPDT).

The introduction of diamond turning can be traced back to many centuries. The first known report of this technique was the diamond turning of hardened steel screw for dividing engines, which was carried out by Ramsden Jesse in 1779 [19]. In the early 1900s, the technology was first used for optical purpose [20]. However, the real development started during World War II when some researchers applied the technique to turn Schmidt plate masters [21, 22].

Between the 1950s and 1970s, ultraprecision SPDT gained worldwide recognition when it was used in the aerospace and national defence field in the USA. SPDT was used to machine reflective mirrors for laser fusion as well as spherical and spherical components for tactical missiles and manned spacecraft. Within this period, it was reported that Du Pont in collaboration with a nuclear weapon plant, Union Carbide Y-12, used the measuring expertise of Lawrence Livermore National Laboratory (LLNL) for modern diamond turning equipment. For instance, the SPACO machine which integrated linear motor and diamond turning technologies [21].

The introduction of ultraprecision SPDT into the weapons' laboratories has accelerated technological advances in the areas of machine design (including non-contact spindle bearings like primarily air-bearings), hydrostatic ways, non-contact drive systems, integration of displacement measuring interferometers onto the machine axes, computer numerical control (CNC), numerical compensation for repeatable errors, and precise environmental temperature and vibration control. However, SPDT was limited to ductile materials like copper and alumina for Spherical and axisymmetric aspherical lenses at the time [5].

17

From the 1980s to 1990s, SPDT began to experience recognition and investment (in terms of resources like money and manpower) from civilian industries in the USA, Europe and Asia. Soon its advanced applications became fully commercialized and widely available. A few years later, the increasing demand for aspherical lenses, Fresnel lenses and other optical and precision components led to the development of SPDT technology in the field of automobile, energy technology, medicine, information, optoelectronics, and communication. During this period, the key technology depended on by the technology of diamond turning included air spindle, laser interferometer position feedback, capacitance gauge, numerical control, three-axis or two-axis machining, brushless DC motor, pneumatic vibration isolators and temperature control [23].

At present, diamond turning has reached the nanometre level and its advancement has continuously been utilized in civilian industries and research institutes. It is also used to manufacture components like moulds for compact disc lenses, cylinders for video tape recorders, drums for plain paper copiers, computer magnetic memory disc substrates, convex mirrors for high output carbon dioxide laser resonators, spherical hearing surfaces in beryllium, copper etc., infra-red lenses made of germanium for thermal imaging systems scanners for laser printers, elliptical mirrors for YAG (Yttrium Aluminium Garnet) laser beam collectors and X-ray mirror substrates [24, 25].

The nanometric level of surface roughness and form accuracy rely on aerostatic bearing spindles and slides, high rigidity and accuracy tools, feedback control, and environmental temperature adjustment [26]. The complicated multi-axis control system of SPDT enables the machining of freeform devices in lieu of just spherical and aspherical surfaces, both of which are axisymmetric. Today, advanced machining technologies such as the fast tool servo (FTS), slow tool servo (STS), ultraprecision fly cutting (UPFC), etc. have been developed based on SPDT technology. This came about due to further demand for non-rotationally symmetric parts, complex optical profile, freeform and structural surfaces with uniform surface quality.

2.6   Surface roughness

Surface roughness otherwise known as roughness, is a description of surface texture. It can be defined as a measured combination of irregular waves or unevenness of a surface. These

irregularities are generated by the relative movement of the cutting tool profile across the geometry of a workpiece, to produce a resultant metal removal in the form of chips. Roughness is quantified by the vertical deviations of a real surface from its ideal form. High deviation indicates a rough surface, while low deviation indicates a smooth surface when measured.

Quantification is dependent on the vertical and horizontal intentness of the measuring instrument used. Surface roughness is important in engineering products due to the fundamental problems such as friction, wear, contact surface, lubrication, fatigue strength and tightness of joints. Surface roughness also influences the conduction of heat and electricity, cleanliness, surface reflectivity, the accuracy of sealing action, fatigue behaviour and load transmission of machined parts. In recent time, the accuracy of machined components in modern manufacturing through surface roughness has been convincingly demanding due to the functionality requirements of emerging new products.

2.6.1 Components of surface roughness

In machining, irregularity of surfaces is inevitable, it is caused by controllable and uncontrollable factors. Therefore, it is important to understand the geometry and the surface characteristics of a machined part. The components of a machined surface can be defined as follows (Figure 2.5):
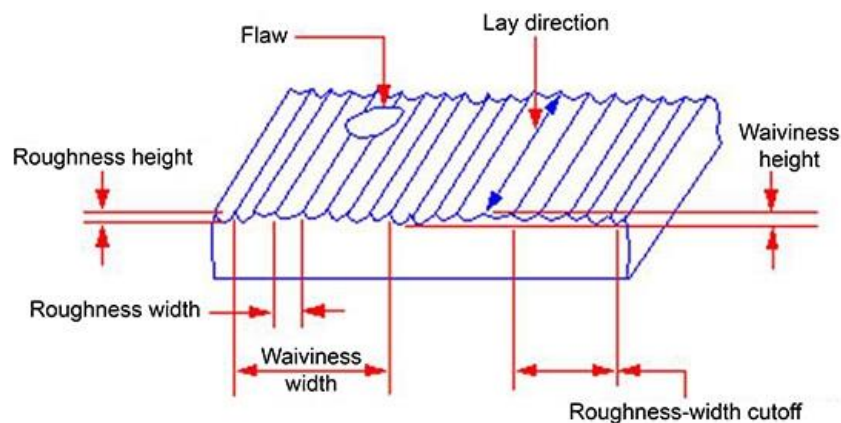
Figure 2.5: Components of a Surface [27].

19

- **Surface texture** is the nominal deviated patterns on the surface of machined material. It is also referred to as the variation in form, roughness, waviness, flaws, and lay.

- **Roughness** is the patterns produced by the action of the cutting tool on the work material. These patterns consist of finer irregularities of the surface texture.

- **Roughness height** is the average of deviations from the mean plane of the machined surface.

- **Roughness width** is the width between two successive peaks and valleys of roughness.

- **Roughness-width cut-off** is the largest spacing of irregularities of machined surface, average roughness and height are inclusive.

- **Waviness** (Figure error) is termed the irregularities produced by the action of the machining process that results in spacing greater than that of surface roughness sampling length and less than waviness sampling length. This property occurs due to machine or workpiece deflection, vibration or chatter.

- **Waviness height** is the peak-to-valley distance.

- **Waviness width** is the spacing between successive wave peaks or valleys.

- **Lay** is usually the direction the surface pattern takes, ignoring variation due to roughness and waviness.

- **Flaws** are inadvertent, unexpected and undesirable interferences impressed on the topography of a machined surface.

2.6.2   Parameters for surface roughness

Surface roughness described in terms of variation in heights of a surface when compared to a reference plane can be represented in different forms of parameters. Roughness parameters can be calculated in either two-dimensional or three-dimensional form. Two-dimensional profile analysis is widely used. Although in recent years, three-dimensional surface topography has gained much emphasis on science and engineering application [28]. Roughness parameters are classified into amplitude, spacing and hybrid parameters [29]. Table 2.3 below describes some of the roughness parameters.

Table 2.3: Surface Roughness Parameters

Parameter	Description	Mathematical expression
R_a, CLA or AA	Average roughness or centre line average or Arithmetic average	$$R_a = \frac{1}{n}\sum_{i=1}^{n}|y_i|$$
R_q, R_{RMS}	Root mean square	$$R_q = \sqrt{\frac{1}{n}\sum_{i=1}^{n}y_i^2}$$
R_p	Maximum peak height	$$R_p = max_i y_i$$
R_t	Maximum height of the profile	$$R_t = R_P - R_v$$
R_v	Maximum peak depth	$$R_v = min_i y_i$$
R_{ku}	Kurtosis	$$R_{ku} = \frac{1}{nR_q^4}\sum_{i=1}^{n}y_i^4$$
R_{sk}	Skewness	$$R_{sk} = \frac{1}{nR_q^3}\sum_{i=1}^{n}y_i^3$$
R_{zDIN}, R_{tm}	The average distance between the highest peak and lowest valley in each sampling length.	$$R_{zDIN} = \frac{1}{S}\sum_{I=1}^{S}R_{ti},$$ Where S is the number of sampling lengths, and R_{ti} is the R_t for the ith sampling length.
R_{zJIS}	Japanese industrial standard for R_z based on the five highest	$$R_{zJIS} = \frac{1}{5}\sum_{I=1}^{5}R_{pi} - R_{vi},$$

	peaks and lowest valleys over the entire sampling length.	Where $R_{pi}\, R_{vi}$ are the ith highest peak, and lowest valley respectively

Surface roughness is mostly represented by the average roughness value (R_a) and peak-to-valley, to describe general engineering and automotive components. While there is no valid explanation to this, R_q (Root mean square) is mostly used to describe optical or electronic components. This may be due to the sensitivity of R_q to plausible but false peaks and valley. Figure 2.6 shows a typical profile of surface roughness and the features used in calculating its parameters [30].
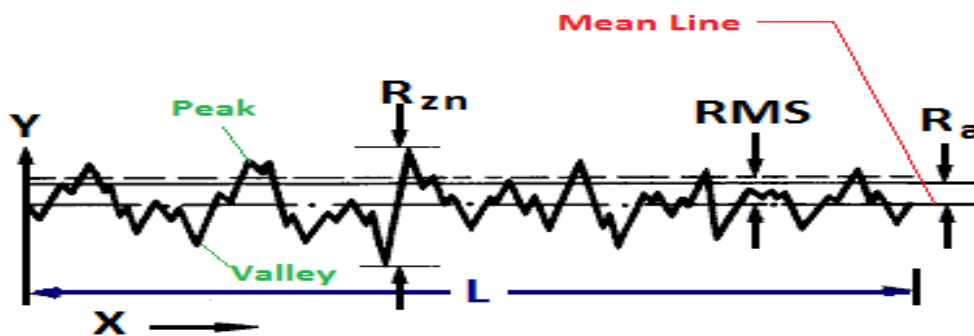
Figure 2.6: Surface roughness profile.

L = Sampling length, the length is chosen or specified to differentiate between roughness and waviness irregularities. Y = Ordinate of the profile curve, which is a function of x.

Average surface roughness (R_a) can be calculated theoretically in terms of the tool radius, r and feed marks created by the tool on the surface profile. The theoretical expression is given as;

$$R_a = 0.032 \frac{f^2}{r} \tag{2.1}$$

2.6.3 Surface roughness metrology

The measurement of surface roughness is usually carried out in two ways; contact and non-contact technique. Contact technique is an old technique that has been used for over ten decades. It is based on a stylus probe making physical contact by dragging along the test surface and numerical values at which the stylus deviates from point to points is recorded. Instruments used in contact measurement are profilometer, Tomlinson surface meter, Taylor Hobson Talysurf [31]. Non-

contact is also a common technique that makes use of an optical probe and as the name implies, it does not make any contact with the test surface. It is a common method used in non- contact measuring technique such as; interferometry, confocal microscopy, focus variation, structured light, electrical capacitance, electron microscopy, atomic force microscopy and photogrammetry [32].

The contact method of measurement provides a more reliable measurement due to its direct touch and it is characterized by a clear wave profile. However, the non-contact technique is preferred considering that it can measure soft, sensitive and smaller asperity accurately, the measurement process is fast, and it does not damage the test surface. Nevertheless, this technique is relatively new, expensive and requires enough technical know-how. The stylus method of contact technique has been the most widely used to measure surface roughness, for good resolution, easy data output, and operation. After the cutting action of the tool on the surface of work material, the stylus is dragged through a surface linearly to determine the surface roughness.

2.6.3.1   Calibration for surface roughness

The importance of surface roughness in engineering material cannot be over emphasized, especially where high precision is required. Therefore, surface roughness instrument, which contributes to the result must be monitored and standardized to ensure accurate and quality capture of data. To achieve this, a systematic calibration of surface roughness instrument must be performed. Calibration is a comparison of any measuring instrument with a known standard [1]. Equipment manufacturers have specified the calibration methods and techniques to help achieve better accuracy and uncertainty levels. Most new and sophisticated surface roughness measuring instrument has three elements - the stylus, pick up and instrument. These elements play a crucial but collective role in capturing and interpretation of data during roughness measurement. Measuring equipment consists mainly of three important elements, these are - stylus, pick up and instrument [33].

- Stylus: The stylus is connected to the lever arm and allowed runs through the machined surface using the stylus tip. The type of stylus tip is determined by the surface profile to be measured. The shape and size of the styli tips are always specified by the manufacturer. In

case of a worn-out, dirty or incorrect identified stylus, the result will be wrong. Periodic extermination of stylus' condition is extremely important.

- The pick-up: This is an electro-mechanical device that converts the surface deviations traced by the stylus and convert to digital values. A worn-out or dirty pick up will result in an incorrect movement of the stylus throughout the measuring range. The pick-up acts like a transducer and it consists of three rudiments for operation – the range for maximum vertical displacement, resolution, for minimum vertical steps and linearity, for possible identical electrical response or signal produced by a vertical movement anywhere along the total range.

- The instrument: This amplifies data converted by the pick-up. Surface deviations are always very small, therefore, for a better examination of data, the instrument must amplify or magnify the data. The amplified data are then transformed into a graph.

Calibration is a significant process in surface roughness measurement. A deviation in the condition of surface measuring instrument will lead to a significant deviation of the measured surface [34].

2.6.4 Surface roughness in diamond turning

The accuracy of any machine tool is defined by the quality of the machined surface regarding the designer's specified dimensions. Achieving high accuracy and good surface finish are ultimate machining indexes aimed by the machining technology of SPDT. High-quality surface finish at the nanometric level and form error at the sub-micrometre level are the main features characterized by ultraprecision SPDT [35, 36]. The ultraprecision has made the machining technique attractive and acceptable for machining optical and mechanical components to extremely precise requirements.

To satisfy the unending demand for high precision, accuracy, performance, reliability and longevity of optical products, the surface quality of the machined parts must meet the required manufacturing standards. For instance, the surface integrity of some materials used in the aerospace and automobile industry must be fabricated to satisfy the harsh conditions like stress and temperature it will be subjected to. Furthermore, components like injection mould and

24

compression mould inserts are machined using SPDT, to mitigate the complexity and time consumption of post-machining processes like lapping and polishing.

The surface profile of a UPM machined workpiece is often defined by irregular or random tool mark, material swelling and recovery, vibration-induced wavy, material pile-up and material crack/surface wrinkle/fracture/defect/dimple [36]. Nevertheless, many research works and machinists [25, 37-40] have successfully applied the technology of ultraprecision diamond turning for precision components and optics by virtue of the excellent surface finish within few nanometric range generated. The cutting mechanism that motivates these characteristics has also been studied.

2.6.5   Factors affecting surface roughness

Surface roughness is very important when determining the quality of optical and precision components; this is because of its vast influence on the appearance, performance, production cost as well as improvement in mechanical properties like corrosion resistant, fatigue, the load-bearing capacity of mechanical parts. The importance of surface roughness in diamond turning cannot be overemphasized. However, some types of errors; such as form, figure and finish, are still experienced by diamond-turned machined surfaces. These errors influence the integrity of workpiece surfaces and they are affected by the process, dynamic and material factors [18, 32, 36], Table 2.3 summarises these factors and details:

Table 2.4: Factors affecting surface roughness in UPM.

Factors	Details
1. Process factors	
Cutting conditions	Cutting speed, feed rate, depth of cut, etc.
Tool geometry	Edge radius, nose radius, rake angle, tool clearance, etc.
Tool wear	Crater wear, fracture wear, flank wear
Environmental conditions	Cutting Fluid
2. Dynamic factors	

Machine tool, vibration	Spindle vibration, chatter vibration, slide vibration, tool-tip vibration, tool-tip vibration, table vibration, machine-induced vibration etc.
3. Material factors	
Material property	Material property change, material swelling, and recovery, hardness, grain size, composition, internal defects, etc.

2.6.5.1 Effect of machine tool

The effect of a machine tool on surface roughness generation is crucial, as the characteristic features of the machine tool affect the surface finish. UPM has always depended on its advanced machine features like high stiffness, kinematic and dynamic characteristics for generating a superior surface finish.

Through the years, UPM has gained continuous interest and the design has evolved into an advanced machine tool, intending to improve surface finish and form accuracy. The advancement of UPM in areas like motion accuracy, stiffness, stability, and capability made it suitable to deliver the superior surface quality of optical products.

Before the invention of the air-bearing spindle in the 1960s, the ultraprecision machine tool relied on the hydrostatic bearing spindle by dint of its first-class submicron rotational accuracy [2]. With the introduction of air bearing spindle, UPM has experienced machining with low friction and low heat generation. In addition to the air bearing, high stiffness, laser position feedback with nanometric resolution and low friction hydrostatic slideways have been incorporated to improve the machining accuracy of UPM [41].

Over the years, the nanometric level of an ultraprecision machine has enjoyed enormous improvements due to some contributions by researchers in the development of ultraprecision machine tool structures. These contributions have likewise been greatly adopted for accuracy. In a bid to obviate the friction, Furukawa *et al.* [42] made use of alumina-based ceramics for the design of ultraprecision machine structure. This is due to the high stiffness, aerostatic sides and thermal stability of the material.

McKeown [43] exploited synthetic granite blocks because of its high damping properties to design some integral machine parts like the rail, base, bridge air bearing, pillar, etc. to allow the machine to withstand shock and vibration. Later, as development progressed, an ultraprecision lathe machine with air mounting, granite bed, air bearing spindle and air sliders was constructed by Kim and Kim [44].

A 5-axis ultraprecision milling machine was also designed by Keuchi *et al.* [9, 20, 45]This machine employs the ability of non-friction servo mechanisms of 1 nm translational resolution, 1×10^{-5} degree rotational resolution, and 10 nm / 200 mm slideway straightness for precision accuracy. Sriyotha *et al.* [36] accomplished 1nm motion accuracy through a non-contact mechanism by making use of aerostatic guideways and coreless linear motors.

UPM is known for its high stiffness and damping system, however, its kinematic and dynamic features are responsible for the fabrication of high-quality nanometric surface roughness and sub-micrometric form error of material. The importance of rigidity of a machine tool is incomparable, as this is used to reduce and / or eliminate oscillation and not only because of the dynamic cutting forces exerted during machining.

The ability of a machine to resist dynamic forces is called dynamic stiffness and it is one of the key factors that determine the surface accuracy of machined parts. The dynamic force is predominantly caused by the rotational movement of the machine tool's spindle and axes, which can result in relative vibration between the tool and workpiece. Spindle vibration is caused by unbalanced mass and eccentric moments in UPM [35]. This undue vibration between the tool and the workpiece often causes an error of machined form and inevitably results in a static deflection that deteriorates surface roughness. Hence, with critical consideration of dynamic properties such as spindle, machine structure and positioning of the machine tool, the surface finish can be improved.

2.6.5.2 Effect of environmental factors

Controlling the environmental conditions experienced in a work area/laboratory during precision machining within the exact limit can be depended on to achieve the good surface finish and form

accuracy. The environmental conditions include temperature, humidity, heat, acoustic vibration, electrical noise, spindle runout, slideway vibration or inhomogeneity of the workpiece material, and other dynamic force like loudspeakers, slamming of doors, etc. and seismic forces like floor-mounted machinery, footstep, outside noise from road traffic.

Some of the conditions induce vibration of machine tool, thereby causing variation between the relative movement of the cutting tool and workpiece. Another adverse influence on surface roughness is the heat that causes thermal errors experienced by the cutting tool and workpiece, which deteriorates surface roughness [46].

An experiment carried out by Moriwaki and Shamoto [47] on UPM, shows how thermal deformation experienced in the main air spindle affects machine accuracy to produce a good surface finish and further investigation shows that heat also has a significant effect on the material property to change the quality of the surface.

In precision machining, it is perceived that the total elimination of environmental influences on the machine tool every so often can somewhat be technically difficult and expensive to achieve [36, 48]. However, measures are being taken to mitigate these environmental disturbances, for instance, the introduction of acoustic enclosures or pneumatic vibration isolators for dynamic stiffness, installation of large air-conditioned and vibration-isolated room to control vibration, temperature, moisture, cleanliness [46] and the use of temperature-controlled fluid or airflow to effectively control thermal heat between the cutting tool and workpiece material in UPM available today. All these have helped to reduce the influence of environmental factors on the machine tool, which affects surface roughness.

2.6.5.3 Effect of cutting conditions

Cutting conditions are process factors influencing surface integrity in SPDT. The efficiency of the machining process can be ascertained by the result in terms of surface finish, which depends on the parameters of cutting conditions. The cutting parameters are mainly cutting speed, feed rate and depth of cut. The study of cutting parameters and the effect they have on surface quality began many centuries ago, to provide useful techniques and predictions of desired surface roughness of

components before machining. In SPDT, these parameters form a fundamental influence on machined parts.

- Cutting speed is defined as the speed at which a workpiece moves with respect to the tool. It is simply denoted by V. In turning, cutting speed is expressed mathematically as

$$V = \pi D_O N \tag{2.2}$$

  Where V = cutting speed (m/mm), D_O = outer diameter of workpiece (m), and
  N = revolution per min of the workpiece (rpm)

- Feed rate is defined as the distance the tool travels into or along the workpiece each time the point moves a certain distance over the workpiece surface. In the case of the turning process, feed is defined as the distance that the tool moves in one revolution of the workpiece. It is denoted by the symbol f and expressed mathematically as

$$f = N \times f_z \times Z \tag{2.3}$$

  Where f = feed rate (mm/rev or mm/min), f_z = feed per tooth (mm/tooth),
  N = revolution per min of the workpiece (rpm), Z = number of flute.

- Depth of cut is the distance that the tool bit moves into the workpiece. In other words, it is the perpendicular distance measured between the machined surface and the uncut surface. For turning, depth of cut is half the difference of the measured initial diameter and final diameter. It is denoted by d and expressed mathematically as

$$d = \frac{d_i - d_f}{2} \tag{2.4}$$

  Where d = depth of cut, d_i = initial diameter (m), d_f = final diameter (m)

In addition, material removal rate (MRR) in turning is the volume of chips removed in 1 min and a measurement of the productivity of metal cutting. MRR determines the speed at which metal is removed in machining and is dependent on the process parameters. MRR is calculated as

$$MRR = vfd \tag{2.5}$$

Cutting speed, feed, and depth of cut determine the surface finish, power requirements, and material removal rate. However, the primary factor in choosing feed and speed is the material to be cut [49, 50]. In SPDT, the integrity and accuracy of any machined part are accomplished by the relative movement of cutting tool tip over the workpiece, this movement is at an interval of feed per revolution and can be determined by the spindle speed and feed rate.

Variation in cutting speed and feed has a more significant effect on the workpiece surface roughness than the depth of cut [6, 50]. Vijay *et al.*[51]. concluded that feed and speed mostly influence the surface roughness and the material rate removal while using the Taguchi approach and ANOVA to investigate the effect of cutting parameters on surface roughness during CNC turning of EN19 stainless steel. Although the variation of depth of cut has little or no significant effect on surface roughness and tool life, it has a nearly linear proportion with cutting force.

According to previous researches, a decrease in feed rate and an increase in cutting speed result in better surface roughness. At a low cutting speed, the high temperature generated at the machining interfaces can cause a highly unstable large built up edge (BUE) and chip fracture, which may cause adhesive tool wear and increases surface roughness. Therefore, as the cutting speed increases, there is a decrease in machining time - which causes the built up edge to disappear and mitigate chip fracture.

The variation of cutting speed value, if not within the BUE range, determines the surface roughness, R_a. Due to the highly constrained and nonlinearity of the turning process, appropriate parameter settings must be taken into consideration based on work material hardness, shape and machine capability before starting machining [52]. As a result, enhance machine efficiency and ultimately a good surface finish.

It is worth noting that an increase in cutting speed tends to decrease tool life, and cutting at low speed can cause chattering of the tool, thereby, reducing its life span [53, 54]. The decrease in feed rate results in flank wear and shortened tool life, while an increase in cutting tool temperature is as a result of increased feed rate. However, an increase in feed rate enhances machine efficiency and the effect of feed rate on tool life is minimal when compared to the cutting speed. These effects are validated with the experimental studies performed by many researchers through the variation

of machine parameter combination and using different experimental methods to optimize surface roughness.

According to K. Abou-El-Hossein *et al.* [55], during the experiment of diamond turning of RSA 905, it was discovered that the rate of tool wear increases with increasing feed rate. Jithin and Ramesh [56], studied the effect of cutting parameters on surface roughness of aluminium alloy 6063, using the full factorial design of experiment. During the analysis, it was concluded from the experiment that feed rate influences surface roughness more than any other cutting parameters.

Aswathy *et al.* [57] used the Taguchi analysis to optimize the performance characteristics in the turning operation of Ti6Al4V for an orthogonal array. The results revealed that the effect of nose radius, feed rate, cutting speed and depth of cut seem to influence the output parameters.

During Chung and Lee's [58], experiment it was identified that no systematic relationship exists between the depth of cut and surface roughness R_a. Moreover, the effect of spindle speed shows that surface roughness, R_a decreases with an increase in spindle speed and increases when the feed rate was increased [58]. However, at an extremely low feed rate, the surface roughness will increase and the cutting process will experience instability caused by stick-slip motion [36].

Similarly, during the diamond turning of Al061 aluminium alloy to determine the reflectance, Li *et al.* [59] concluded that surface roughness decreases as the feed rate decreases. However, as the feed rate decreases to 3 mm/min, the chip formation becomes unstable, and the reflectance of the machined surface is unfavourably reduced.

Abhanga *et al.* [60] performed turning operations on En-31 steel and studied the effect of process parameters such as cutting speed, feed rate, depth of cut, tool nose radius and lubricant on the surface roughness of the material using factorial design. The results were analysed by looking at the variance and using the F-test (F-test is a statistical tool used to determine if two variances are equal). It was deduced that the aforementioned parameters have a significant effect on measured surface roughness after turning

2.6.5.4   Effect of tool geometry

Tool geometry is the shape and angles at which the cutting parts of a cutting tool are ground. The geometry of a cutting tool is related to SPDT in terms of chip formation, heat generation, tool wear, cutting force and surface finish. Therefore, to achieve adequate high production rates at a reduced cost, the optimization of cutting tool geometry is necessary. The design and influence of cutting-edge geometry and its influence on UPM performance have been a research topic for some time now and various researchers have been able to identify the importance.

In the ultraprecision machining of crystal silicon performed by Fang and Zang [61, 62], it was confirmed that the cutting edge radius has an effect on the negative value of an effective rake angle for good form error and a nanometric finish. Xu *et al*. [63] stated that to achieve a superior surface finish with less tool wear in SPDT, stringent tool rake values for brittle and ductile materials must be considered. For instance, 0° for ductile materials like metals and alloys, and negative values for brittle materials like silicon and electroless nickel.
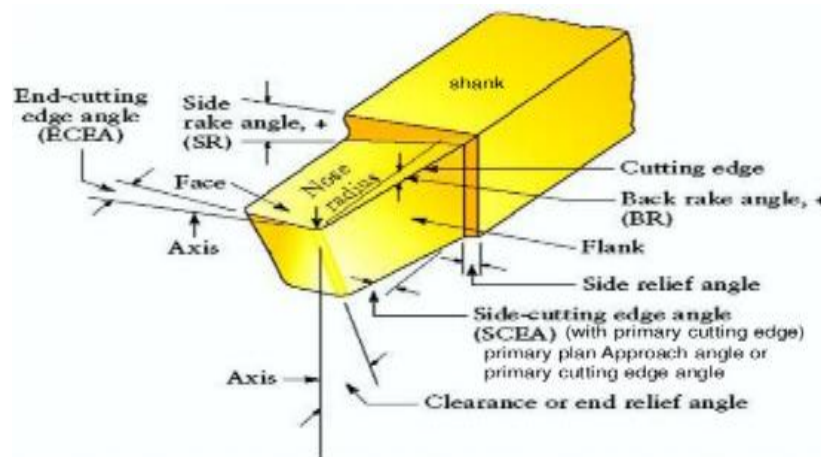
Figure 2.7: Tool geometry of a diamond tool

The radius of the cutting tool edge (sharpness) is considered as the primary reason for the size effect and cutting deformation. The cutting edge radius of a regular monocrystalline diamond tool used in SPDT is between 500 nm to 50 nm, which is 10 to 100 times better than other tools like tungsten carbide tool [36, 64]. The nanometric size of the diamond tool has positively influenced the surface roughness, strain hardening, residual stress and the dislocation density of machine surface. Thus, the tool is suitable for cutting non-ferrous metals like aluminium.

In SPDT, the control that the cutting tool has on surface roughness is stiffly determined properties of the workpiece material. The tool sharpness and extremely low coefficient of friction of diamond cutting are major factors that distinguish SPDT from conventional machining. The relationship between cutting edge and minimum undeformed chip thickness, a_{cmin} can be expressed mathematically as [65];

$$a_{cmin} = \rho \left(1 - \frac{F_y + \mu F_x}{\sqrt{(F_y^2 + F_x^2)(1 + \mu^2)}} \right) \tag{2.6}$$

Where a_{cmin} = minimum undeformed chip thickness, ρ = cutting edge radius of the tool, F_y = vertical force, F_x = horizontal force and μ = coefficient of the friction between the cutting tool and the workpiece material.

Generally, the tool nose radius is specified to be large - to give the cutting edge the strength needed as the cutting tool undergoes multiple passes on the workpiece. The minimum cutting thickness is greatly affected by the sharpness of the diamond tool, small cutting thickness can be attained by the sharpness of the cutting tool [65]. As a result, improving the surface integrity of machined parts.

2.6.5.5   Effect of vibration

Naturally, vibration is a physical process that belongs to ultraprecision machining (UPM). Vibration, which can be described as a classified dynamic response, caused by the excitation of cutting forces at irregular intervals, this significantly results in waves on the machined surface. Vibration in UPM is generally in the form of tool tip vibration, spindle vibration, slide vibration. and table vibration. These dynamic factors influence the surface quality of machined parts. Typically, the relative vibration between the tool and the workpiece (of which the source is not recognized) is called machine-tool vibration [36]. Profound research and analysis have been carried out on different forms of vibration.

In UPM, the depth of cut corresponds to the average grain size of workpiece material due to the differences in the anisotropy / inhomogeneity / irregularity / non-uniformity that causes the

variation of cutting force, shear angle, chip formation, etc. to influence surface generation. These variations, which are self-excited, induces vibration by changing the relative distance between tool and workpiece and accordingly, produces periodical patterns on a machined surface.

Tool tip vibration occurs naturally, caused by the topography of diamond tool. The vibration experienced at the diamond tool tip has been analysed to be at a high frequency of about 12 kHz, which influences the surface roughness at a nonmetric level. The high frequency of vibration experienced at the tool tip has been theoretically and experimentally explained.

However, according to Zang *et al.* [35], more research should be focused on the two-degree-of-freedom vibration characteristics of a tool tip along the cutting direction, rather than the one-degree-of-freedom vibration characteristics along with the cutting and feed directions. Other forms of vibration in UPM such as chatter, spindle, etc. have been analysed to influence surface generation.

2.6.5.6 Effect of material property

SPDT is remarkable for machining non-ferrous metals such as aluminium and its alloys, copper, nickel and many other optical crystals such as germanium and silicon. Other polymer optical plastics like acrylic (PMMA), germanium-based chalcogenide glass and so on, can also be machined using SPDT - because their properties support diamond tuning. In SPDT, the most important factor to consider is the workpiece material that is being machined, due to the chemical reaction with the diamond cutting tool.

The most popular materials that are unsuitable for single-point diamond machining are ferrous metals and optical glass. The graphitization occurrence between the workpiece and the diamond cutting tool reduce machining quality and surface desirability. As mentioned earlier, the effect of the tool edge on surface roughness is greatly determined by the material properties. Additionally, mechanical properties and other properties such as crystallographic orientation, microstructure, impurities, inclusion, among others, have a relevant effect on the diamond-turned surface that should be considered [36, 66].

Mechanical properties include brittleness and ductility of the material. Examples of ductile materials are copper and aluminium, while silicon and germanium are examples of brittle materials. These diamond turnable materials have been extensively used in applications like VCR Cylinder optical quality reflector, laser optical product, etc. Hard and brittle materials generally appear difficult to machine when compared to ductile materials because of the cleavage-based fracture experienced during machining. Hard and brittle materials are best machined in a "ductile-manner" and the technology has been generally recognized to produce a surface finish that is brittle fracture free.

There is a critical depth of cut, which is below the cutting mode of brittle to ductile transition [32]. Puttick *et al.* [67] suggested that at a critical undeformed chip thickness below the crack free machined surface, brittle materials can be machined plastically. Arif *et al.* [68] predicted a model of the critical undeformed chip thickness for ductile-brittle transition points in nano-machining of brittle material.

Crystallographic orientation is the arrangement of crystals in a material such as polycrystalline, monocrystalline or amorphous. The shearing process in SPDT is heavily dependent on the material properties, such as material isotropy and anisotropy and material uniformity and non-uniformity, on surface roughness. As these properties change from one material to another, so does the surface roughness change even under the same cutting conditions.

As observed by To *et al.* [38], the surface roughness of a single crystal aluminium is dependent on the orientation of the crystal, due to the anisotropy. A material plastically deforms due to the orientation of the crystal that is being cut. They also concluded that the cutting force in a single crystal aluminium depends on the orientation of the cutting tool.

In the experiment carried out by Furukawa *et al.* [42, 69], it was concluded that the cutting force for polycrystalline materials, such as aluminium alloys, fluctuates mainly because of the crystal grain boundaries that are influenced by the anisotropy of aluminium alloys. An observation was also made concerning the cutting force and surface finish of single crystalline materials (for example single crystal silicon and pure aluminium). The cutting force and surface finish were different for the various cutting directions, while the cutting properties do not change for

amorphous materials. When compared to crystalline materials, amorphous reflects interesting and distinctive features, the materials have been discovered to possess a structure that composes a random aggregate of atoms [32].

2.7   Aluminium and aluminium alloys

Engineering materials are categorized into three main groups; ceramics, polymers and metals. The other category is called composites, these are a non-homogenous mixture of the other three classifications [6]. Their usage for different manufacturing processes depends on the individual mechanical and physical properties.
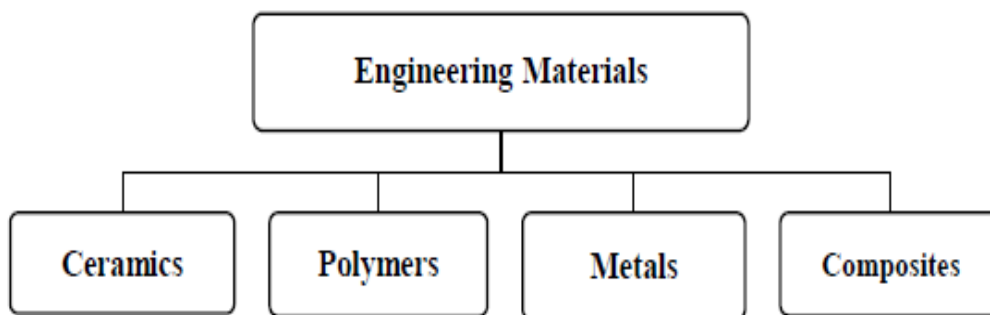
Figure 2.8: Classification of engineering materials

Aluminium is a non-ferrous metal; the base material does not contain iron. Aluminium is considered the most abundant metal in the earth's crust and also the third most abundant chemical element (up to 8% by mass). Unlike all other metals, aluminium exists mainly as oxides (called Bauxite) because of its chemical reaction and attraction with oxygen to form aluminium oxide. Bauxite is often found in clay and many other minerals. Despite its abundance, aluminium metal was first economically extracted from its oxide form to present it as pure metal through electrolytic reduction, by scientists in the year 1886. Ironically, since then aluminium has turned out to be the second-most-widely used naturally occurring metal after iron.

The density of aluminium is 2.7g/cm^3 (which is one-third the density of steel) and a cubic foot of aluminium weighs 170lb (unlike steel which is 490lb). This lightweight property, coupled with high ductility, reflectivity, resistance to corrosion, and good conductors of electricity, have made

the metal suitable for electrical conductors, chemical equipment, optical components, sheet metal works, food and beverages packaging among others.

Table 2.5: Properties for aluminium

Property	Value
Atomic Number	13
Atomic Weight (g/mol)	26.98
Valency	3
Crystal Structure	FCC
Melting Point (°C)	660.2
Boiling Point (°C)	2480
Mean Specific Heat (0-100°C) (Cal/g.°C)	0.219
Thermal Conductivity (0-100°C) (Cal/cms. °C)	0.57
Co-Efficient of Linear Expansion (0-100°C) ($x10^{-6}$/°C)	23.5
Electrical Resistivity at 20°C (Ω.cm)	2.69
Density (g/cm^3)	2.6898
Modulus of Elasticity (GPa)	68.3
Poisson's Ratio	0.34

However, when aluminium exists alone, it is weak and very soft. The aluminium atoms exist at the same size; therefore, it is easy for the atoms to slide past each experiencing "slip panes". The weak and soft nature of pure aluminium limits it for the applications where high strength is an important factor, another limitation is its low melting point [70].

Therefore, by the addition of small quantities of other elements, a soft and weak metal becomes strong and hard, while retaining the lightweight property. The addition process is called alloying, the elements added to the pure aluminium metal are called "alloying elements" (copper, manganese, silicon, magnesium, zinc), while the hard and strong aluminium metal is called "aluminium alloy".

The alloy is strengthened, its chemical composition, structural defects, cast-ability and machinability are also improved. Alloys of aluminium encourage the design and construction of

strong, lightweight structures such as space, land and water-borne vehicles. Nowadays, advanced aluminium alloys are used for optical devices and precision components. They can be classified into four main groups according to how they are produced, machinability and the specified alloying elements. These four groups of aluminium alloys are cast, wrought, strain-hardenable and heat treatable [71].

i. Cast alloys: Produced by pouring molten aluminium metal and its alloying elements (like copper, magnesium, silicon, zinc, and tin) into a sand cast or high strength steel mould, like die casting, and then allowing it to cool and solidify into the desired shapes. In machining cast alloy (where aluminium and silicon are the predominant elements), a cutting tool with a large rake angle must be employed due to build up at the edge of the tool. This has made it economically reasonable to machine at lower machine parameters like speed and feed.

ii. Wrought alloys: These are formed as billets or cast ingots. The ingots are hot worked into semi-fabricated wrought products by processes such as hot rolling and extrusion, some of which are further finished by cold rolling or drawing. Wrought aluminium alloys are characterised by excellent machinability and are suitable for different operation machining.

iii. Strain-hardenable alloys: These are mainly commercially pure aluminium, which contains no alloying elements, but they can be strengthened and as such improve their machining to a certain level by cold work. These alloys can be machined easily, although, during machining a continuous chip is formed that must be directed away from the workpiece by tools with generous side and back rake angles to prevent scratching of the finished surface with the work-hardened chips. Tool pressures are also high as a result of high friction and gummy nature of the alloy. Therefore, a sharp cutting tool should be considered for machining in order to generate a good surface finish.

iv. Heat-treatable alloys: Most of the alloys in this group contain reasonably high percentages of alloying elements such as copper, silicon, magnesium, and zinc. They can be machined to a good finish with or without cutting fluid. Nonetheless, cutting fluid is recommended for most operations for the optimal result. Turnings usually occur as long, continuous curls, except for the free-machining alloys, which contain chip-breaking constituents. Heat-treatable alloys are more machinable in the heat-treated tempers than in the softer as-fabricated or annealed solution.

Today, the economical use of aluminium alloys has gained rapid growth over the past years due to its combination of low weight and high strength - coupled with other properties like reflectivity, formability and high corrosion resistance, among other properties. Its application in areas like aerospace and automotive industries is a better reference for its importance in daily life and industrial use.

Aluminium alloys have gained so many improvements and have successfully replaced iron and steel mostly because of the addition of desirable alloying elements such as Si, Mg, Ce, Cu, Cr, Fe, Mn, Ti, Zn, Ni, Zr, etc. The added alloying elements are either dissolved or form compounds within the alloy microstructure. Over the years, there have been a lot of studies on the effect of these alloying elements in aluminium alloys.

i. Effect of Silicon (Si): This one of the most important and commonly used elements used in alloying aluminium. Generally, silicon is a hard material with low density and alloying it with aluminium produces an aluminium alloy of reduced total weight. It has low solubility and the addition of silicon ensures good cast-ability (high fluidity, low shrinkage) of aluminium alloys [72], good weldability and thermal conductivity. Aluminium Alloys with high silicon content possess improved mechanical properties at high temperatures, thus, resulting in excellent corrosion resistance and machinability. Another effect of silicon on machinability of aluminium is the cutting force, as the silicon content increases, the cutting force at reduced cutting speed decreases - which influences a better surface finish of work material [73]. Alloys with high silicon content are mostly machined with carbide or diamond tool due to abrasion [53, 74, 75].

ii. Effect of Magnesium (Mg): The small presence of magnesium can provide a reasonable amount of strength to the work-hardening characteristics of aluminium alloys. It also offers good wear and corrosion resistance as well as weldability. An aluminium alloy containing a higher content of magnesium can result in low-temperature brittleness and scums.

iii. Effect of Copper (Cu): Copper added to Aluminium (Al) alloy forms an intermetallic phase, which precipitates during solidification and a slight increase in alloy fluidity [76]. Copper (Cu) and magnesium (Mg) are the most common hardening alloying elements added to Al-Si alloys - to increase their strength and hardenability and have been used

extensively in such alloys to improve the mechanical properties.

iv. Effect of Iron (Fe): Iron found in Al is often regarded as an impurity, however, it is intentionally added as an alloying material to provide a slight increase in strength. The negative influence of iron on the mechanical properties of Al alloys – specifically the ductility and fracture toughness is directly related to the volume fraction, size and morphology of the iron-containing phases formed in the metal matrix [77].

v. Effect of Nickel (Ni): Nickel when combined with iron forms insoluble intermetallic in Al when it exceeds 0.04wt% but Nickel content of up to 2wt% increases the strength of high-purity aluminium, however, it reduces ductility. Nickel when added to Al-Cu alloy and to Al-Si alloys, improves hardness and strength at elevated temperatures and is used to reduce the coefficient of thermal expansion.

2.7.1 Machinability aluminium alloys

Worldwide there is high demand for aluminium alloys (approximately around 29 million tons per year) due to their lightweight structure and other physical, mechanical and thermal properties [78, 79]. These properties have made aluminium alloys to be versatile, attractive and economically viable. Therefore, a lot of importance has been attached to these alloys and the machinability, which qualifies the machining performance, is a very important consideration.

The machinability of material reveals how the material can adapt or behave during the machining process and it is evaluated in terms of tool life, surface finish, chip evacuation, cutting force, material removal rate and machine-tool power [75, 80, 81]. Aluminium alloys are easy to machine rapidly and economically when compared to pure aluminium due to the microstructure, which has been improved through heat treatment and alloying elements. In fact, they are considered to have the highest level of machinability when compared to titanium and magnesium alloys, which are in the same category of lightweight metals. The role of machinability is important in the selection of suitable cutting parameters. Machinability varies from one material to another and is dependent on the physical properties, chemical composition and cutting conditions of the material [75].
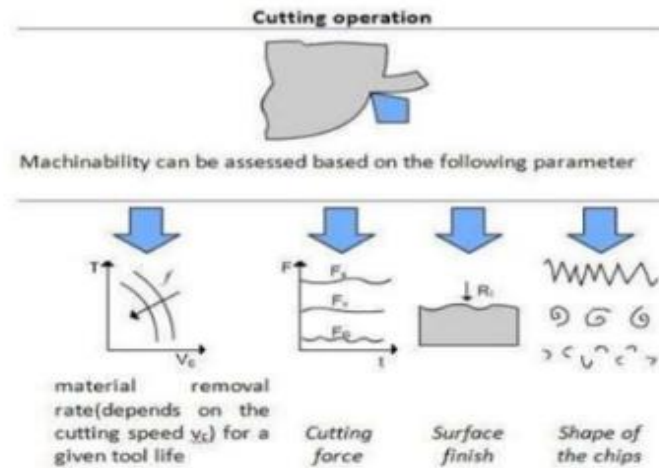
Figure 2.9: Factors affecting machinability of aluminium

The main challenge encountered during single-point machining of aluminium alloys is the built up edge (BUE) experienced at low cutting speeds and sticking at high cutting speeds [82]. BUE occurs mostly in harder alloys such as steel, it preserves the tool life to a certain extent, considering that most of the cutting activity is done by the BUE in lieu of the tool edge.

Nevertheless, there are major disadvantages that come with the effect of BUE such as; excessive work hardening at the surface of the workpiece, poor surface finish and dynamic change in cutting-tool geometry. The best way to minimize built-up edge is to employ potent cutting fluids and engaging tools with surfaces that are free from grinding marks and scratches.

    i.   Cutting forces in machining aluminium alloys:

            The high compressive and frictional contact stresses on the face of the cutting tool are called cutting forces. The cutting force has a significant effect on the surface integrity of the aluminium alloy as a workpiece. The cutting force during machining of aluminium alloys is relatively low, compared to steel when machined under the same condition [83]. The cutting force is affected by the heat treatment as well as the addition of chemical components aimed at improving the hardness of the aluminium alloy. This hardening process reduces the chip tool contact. As a result, the machining force is also reduced, which has covered up for the limiting effects of the increase in mechanical strength and the reduction in the contact area.

Although, aluminium alloys differ from one another, for instance, in-term of hardness and aging particles, cutting forces are responsive to the variation of cutting parameters, like speed and feed [75]; irrespective of the strength or hardness of the aluminium alloys. an increase in cutting speed normally reduces the cutting force, i.e. the higher the cutting speed, *V*, the lower the cutting force experienced [54, 84] and this is in spite of the strength of the alloy. This is due to the low temperature generated at the primary shear zone and secondary shear zone when cutting speed increases.

Nevertheless, in situations like high-speed cutting (HSC), an excessive increase in cutting speed may increase the cutting force [54]. Feed, *f,* is also an important parameter that influences aluminium machining, it determines the chip thickness. Thus, due to the deterrent caused by an increase in the area of the shear plane (primary and secondary), the cutting force increases with feed rate. Other factors that increase the cutting force during aluminium machining include; flank rake angle (an increase in rake angle reduces cutting force), nose radius, flank wear and built up edge.
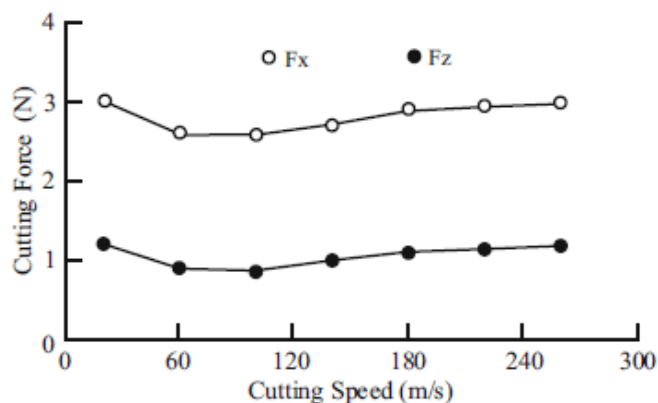
Figure 2.10: Cutting force variation with cutting speed [54]

ii.   Surface finish in machining aluminium alloys.

Surface roughness refers to the irregularities on the surface of the workpiece. In aluminium machining, it may be an intentionally impressed machine tool but can also be created by a wide range of factors. However, the main limiting factor affecting the surface quality in the machining of aluminium is the hard nature of the material and its microstructures. High

hardness signifies lower surface roughness. Another effect is the ductile characteristic of aluminium.

iii. Chips Formation in machining aluminium:

Aluminium alloys are characterized with long and continuous chips formed during machining. Chip formation often depends on work material, tool geometry and cutting conditions. The shape of the chip is a good index for determining the machinability of the work material. According to research, it was observed that the chips' formation of brittle aluminium alloys at low cutting speed is always continuous and long, while ductile workpiece produces discontinuous chips at a moderate speed. Songmene *et al.* [75] concluded that to achieve a good surface roughness (especially for automated production), the recommended chip formation must be discontinuous. Although this is to easily manage chip formation. Continuous and spiral chips can be averted by selecting appropriate machining feeds and cutting speeds.

2.7.2 Rapidly solidified aluminium alloys

Advanced technologies have continued to be developed for the design and production of advanced products made of improved materials. These materials are made up of microstructures such as atoms and molecules. The solidification of molten metals tends to improve some properties of these metals due to how the new atoms are arranged or structured (either closely packed or otherwise).

Rapid solidification, which was developed many years ago by Dewez and his colleagues [85-87], can be defined as the process of extracting thermal heat from metal in its molten state by rapidly cooling it at a temperature of 10^2 - 10^6 K/s; it is a way of improving the microstructures of materials. Water, brine solution, or liquid nitrogen are common means through which the heat can be quenched. The choice of means of quenching has a significant influence on the solidification rate and microstructural development [88].

Rapid solidification is used to produce materials with improved properties by altering the microstructural features like grain size, dendrite arm spacing and extent of segregation. Lobry *et al.* [89] have confirmed in their research that the high mechanical properties possessed by the

aluminium alloy are ascribed to the rapid solidification. Figure 2.11 shows the effect of rapid solidification on the material microstructure.
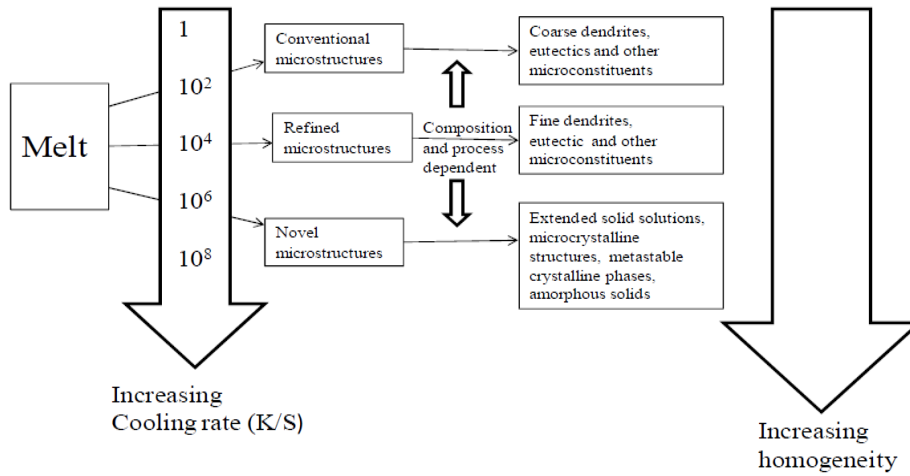

Figure 2.11: Microstructural consequences of rapid solidification [90].

There are different techniques of rapid solidification, these are; powder metallurgy, strip casting, melt spinning, laser spin atomization, droplet quenching and gas atomization [88, 91]. Although the technology behind these techniques is different, the principle is the same. However, melt spinning has proven to be the best and commonly used technique due to the highest cooling rate as well as the fine microstructure it offers [86].

Rapidly solidification of aluminium (RSA) alloy, is an improved aluminium alloy produced by a process of rapid solidification known as melt spinning. It is the rapid solidification technique used for the production of rapidly solidified aluminium at an ultra-fast cooling rate of 1 million degrees per second [92]. According to the RSP technology, melt spinning of aluminium alloy involves the rapid cooling of molten aluminium at about 800°C when poured onto a fast-rotating copper wheel; to form ribbons for further processes like machining. This process produces an excellent homogenous crystalline structure of aluminium alloys, which can be used for the production of light-weight high-end applications in optics, precision equipment, aerospace, medical, electronics and automotive industries [93].
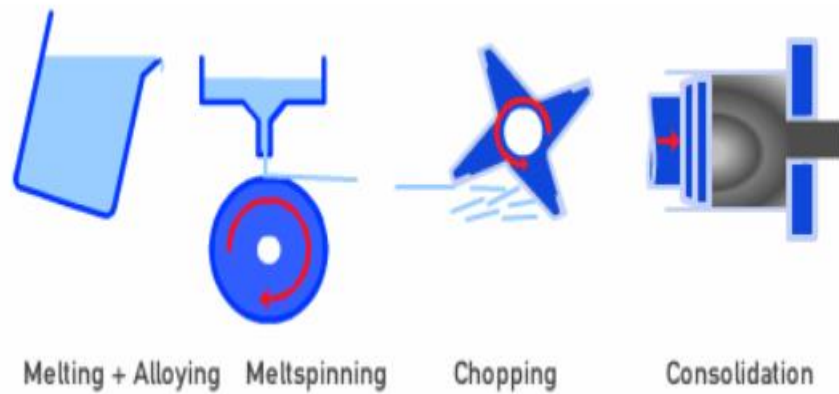
Figure 2.12: Melt spinning technique used by RSP Company[93].

2.8   Cutting fluid

Cutting fluid (sometimes referred to as coolants, metalworking fluids or lubricants) was first introduced by F. W. Taylor, a tool engineer in 1894 when he used a large amount of water as cutting fluid [94]. He observed a significant reduction in tool life during the cutting process, even at increased cutting speed. Since then, different types of cutting fluids have been used for this and other purposes. Smooth surface finish and low friction is the foremost thinking whenever two or more surfaces come in contact with one another. The application of cutting fluids play a fundamental role in the modern manufacturing process and metalworking of workpiece material (except cast iron and brass) [95].

In most machining processes, high friction increases the cutting temperature - which causes challenges like high tool wear, heat affected shear zone, high energy consumption, thermal distortion, high built up edge (BUE), the microstructure of workpiece burning and change in hardness. These challenges eventually result in deteriorated surface finish and flawed dimensions. The use of cutting fluids helps to lubricate the cutting tool at relatively low cutting speed and also cools the cutting tool together with the shearing zone at a relatively high cutting speed [96]. Therefore, a good cutting fluid must have excellent cooling and lubricating properties. Cooling is usually done at a high cutting speed because the fluid has no time to penetrate the chip-tool interface [23].

The PH value of cutting fluid play an important role in tolerance during machining. The PH value can improve the efficiency of machining and reduce its surface roughness. According to Voloshin *et al* [97], the requisite mechanism of cutting fluids have not been adequately explored.

Precision machining requires high surface quality, therefore, the stability and extended life of working parts under the extreme environmental condition are mandatory. In ultraprecision diamond turning, another function of cutting fluid (in addition to lubricating and cooling) is the control of the formation and flow of chips. This is an important function as chips produced during SPDT although are usually few [98], and can easily cause scratches and other types of damage on the optical surface if not effectively controlled. During ultraprecision machining, several other factors affect the cutting performance and surface finish, thus, some machining operations are carried out 'dry' (without cutting fluid). Nevertheless, the proper application has suggested that there is an improvement in the productivity of the machining process and quality of the workpiece. 'Dry' cutting produces high cutting force and low tool life, which causes a high crack.

There are various types of cutting fluids, these include water-based, oil-based, aerosols, spirits, air and other gases. In the performance evaluation of different types of cutting fluids on milling of AISI 01 hardened fluid carried out by Hamdan *et al* [99], it was observed that water-based cutting fluid delivered the best surface roughness when compared to oil-based cutting fluid.

The selection of suitable cutting fluid is as important as selecting the suitable machine tools, cutting tool and machine parameters. However, some requirements must be satisfied before selection.

- Environmental factor: Cutting fluid must be non-hazardous to operators or environmental health. Some cutting fluids have the potential of degrading the ecological systems by contaminating land, water bodies and wildlife if not properly disposed of. In actual fact, the major threat posed by the use of cutting fluid in machining is the waste disposal after use [100], the damaging effect on the environment has made its use limited. There are stringent regulations developed concerning the use of cutting fluids in industrial engineering.

- Economical factor: The goal in conventional metal removal techniques is to increase productivity and reduce cost without compromising the quality of engineering design, cutting fluids must be readily available and affordable.

Application of cutting fluids can be carried out in three major ways, these are [99].

- Flooding method: In this method, the entire machining area is deluged with a high volume of cutting fluid. With this process, the heat generated during machining is efficiently removed. This is the most commonly used method; however, recorded cases of occupational dermatitis and other skin diseases have been credited to the frequent exposure of operators to cutting fluid.
- Jet application method: Here, high pressure is used to apply cutting fluid (either gas or liquid) on the tool and workpiece.
- Mist application method: In this method, the cutting fluids are mixed with a gas (generally air) and applied to tool and workpiece. Mist application combines the properties of above mentioned both methods i.e. flooding and jet application.

Aluminium alloys have good machinability, extreme heat is not generated during machining because of their low melting point, likewise, the diamond cutting tool maintains its properties at high temperatures and can still maintain their properties [101]. Yet, during 'dry' machining, the challenge of BUE at low cutting speed and sticking of chips at high cutting speed is encountered. This owes to the fact that aluminium alloys are generally light and easily stick to the cutting zone to form built up layer [102].

2.9   Automated / Intelligent monitoring systems

An automated/intelligent monitoring system is a system that has the adequacy of sensing, analysing, knowledge learning and error correction capacity when integrated into the machining process. An AI system is expected to imitate as accurate as possible the human operation capabilities, hence, for any AI system to be complete and efficient, it must undergo the following systems:

i.   **Sensing Techniques systems**

47

This simply implies that indirect sensing techniques, such as a Forced-based monitoring system or acoustic emission monitoring system, must be used. There are different types of sensors and sensory data for different systems, which are employed to yield optimum and valuable information.

ii. **Feature Extraction systems**

Signals from sensors are embedded with the necessary information needed to distinguish between different process and machine tool conditions. However, these signals in the form of raw data contain some noise that is needed to be further filtered and processed.

iii. **Decision-making systems**

In Decision-making systems, strategies are used to process incoming signal features and used to perform a pattern association assignment, arranging the signal feature in a proper class.

iv. **Knowledge learning systems**

To make the correct decision, learning algorithms have to be provided. Such algorithms tune system parameters by observing the sample feature corresponding to different tool conditions. Like human operators, automated monitoring systems should have the ability to learn from their experiences, as well as from the new information generated from the machining process [103].

2.9.1 Monitoring techniques with the use of sensors

Monitoring in the manufacturing process involves the supervision and identification of machine conditions during cutting operation without interrupting the process. Various monitoring techniques have been categorized into two traditional methods namely: direct monitoring and indirect monitoring techniques [103].

Direct monitoring techniques measure the actual quantity of variable A. A high degree of accuracy can also be achieved, although the trade-off is that due to numerous practical limitations, they are characterized as laboratory-oriented techniques. Alternatively, indirect techniques are less accurate but more suitable for practical applications, at the machine shop level. Auxiliary quantities are measured using appropriate physical sensors placed in the cutting region and

empirically correlated with machining phenomena. Common indirect methods include vibration, cutting force, acoustic emissions [104].

Sensors convert physical parameters such as vibration, pressure, temperature, etc. to electrical signals, usually as a function of time. Modern machining now requires flexibility, sustainability and operation with minimal human involvement, while the process has to be free of errors. Sensor-based monitoring techniques have been developed and extensively used in modern manufacturing application. These techniques are based on the idea of imitating human sensing capability, although it is impossible to exactly imitate the human operator. The technique has now impelled the development and sustainability of manufacturing industries.

In machine-condition monitoring, the use of advanced sensor-monitoring system enables the collection of information through signals from the machining process for adequate measurements. The signals detected by the sensors are subjected to analog-digital signal processing, to extract useful and correlated features. There is a wide range of sensors available for monitoring machining conditions such as cutting forces, vibrations, acoustic emission, temperature, etc. Depending on the type of application, scope and suitability, various types of sensors have been used to make monitoring useful, easy and reliable. Sensors are used to generate control signals to improve both the control and productivity of manufacturing systems.

2.9.2   Process monitoring in ultraprecision machining

The technological development of ultraprecision machining has been a focus of attention in the past few decades, due to its excellent precision and accuracy across numerous applications. However, under the continuous demand for high accuracy and productivity in precision engineering, it is necessary to minimize cost and machine downtime. Therefore, maximize preventive maintenance and optimize machine performance to meet demand.

Effective monitoring is fast becoming a resolution to these necessities. The application of on-line sensors for monitoring UPM processes detects problems during machining and provides information about the fundamental machine conditions (without disrupting the process). This information is needed for process optimization and data development to ultimately control the

machine parameters. The machine conditions can be used to control machine occurrences such as wear, surface roughness, BUE, chip breakage, etc. Process monitoring systems can be used to characterise, control and improve ultraprecision machining.

The technology of ultraprecision machining is used to produce small and complex features at a sub-micron level of material removal rates (MRR) and has a very high tolerance. Unlike conventional machining, micromachining processes are difficult to monitor because of the related small energy emissions and cutting forces, thus a compact, confident, reliable and sensitive sensor-based monitoring tool is required for accurate detection [105].

There are various techniques available for process monitoring to improve accuracy and productivity, these techniques depend on the type signals which include; cutting force signals, vibration signals, spindle motor current signals and acoustic emission signals. However, the use of a force sensor and accelerometer for detecting cutting force and vibration signals are inadequate for monitoring micromachining processes, due to their low signal-to-noise ratio. An acoustic-emission sensor is the most appropriate process monitoring technique compared to other techniques due to its sensitivity and high signal to noise ratio. In AE sensing technique, the signals are propagated at high frequency and unaffected by environmental noise [106-108].

2.10   Acoustic emission (AE) in ultra-high precision machining

Acoustic emission can be described as transient elastic waves of high frequency emitted within a workpiece material undergoing a dynamic process. These emitted waves are in the form of sound signals and are propagated from the source to the surface - where they can be detected. AE is an efficient technique for studying the demeanour of a workpiece material under plastic deformation. The testing technique of acoustic emission is a versatile and non-invasive method of monitoring and gathering information about a material, structure or machining process.

In ultraprecision machining, where the cutting conditions and the tool dimensions are conceptualized as precise and accurate within the sub-micrometre level, AE is adapted for process monitoring to detect signals at a frequency range higher than the ambient noise and machine

vibration [106]. Figure 2.10 shows the signal-to-noise characteristics of AE compared to force/vibration.
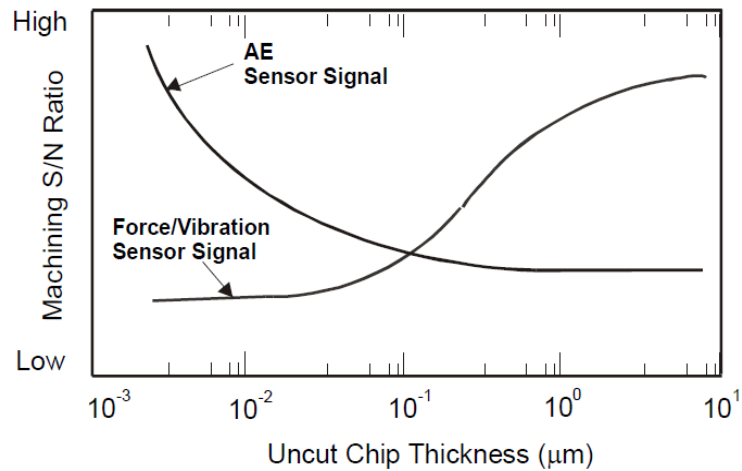

Figure 2.13: AE Signal/Noise ratio [53]

AE enables the identification of specific signals and cutting modes of different materials. As a result of structural deformation of material that occurs during machining, the yield stress is experienced and energy in the form of stress waves or sound wave is released from the surface of the material. AE sensors, devices used to detect AE events, are competent in detecting high-frequency range of elastic waves (typically 20 kHz to 1 MHz) and physical motions as low as 1×10^{-12} [109] at a very high-level precision.

For effective diagnosis in UPM, it is important to note the potential sources of AE signals. There are several sources of acoustic emission during metal cutting in terms of a sudden release of energy in deforming workpiece material. These sources include [107, 110];

- Plastic deformation of workpiece material in the shear zone.
- Sliding friction between the tool rake face and chip, resulting in crater wear.
- Friction mechanisms between workpiece and tool contact, resulting in flank wear.
- The collision between chip and tool.
- Entangling and breakage of chips.
- Tool fracture.

High-frequency of acoustic emission is predominantly generated from the forces in tool and workpiece material. Therefore, of all the AE sources, plastic deformation and fracture have the most significant effect in the machining process. Figure 2.14 depicts the different sources of AE signals in machining.
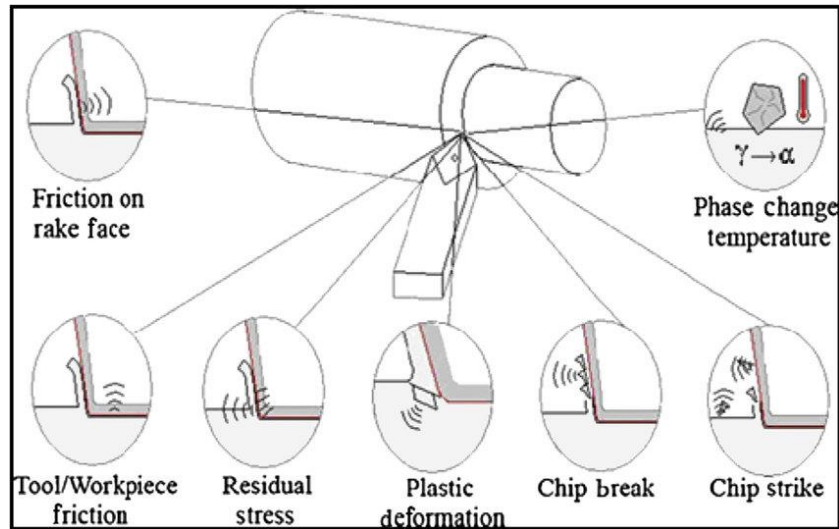

Figure 2.14: Sources of AE in machining [107]

Two distinct forms of AE signals can be generated during precision machining, these are continuous signal and transient signal (also known as bursts). Continuous signals are related to multiple emissions of time-overlapping signals from different sources in which noise could be found. They are emitted from rapidly occurring events and consist of clear, distinctive and varied amplitude and frequency with no end.

Continuous AE signals are produced as a result of shearing in the primary zone and wear on the tool flank and rake face. Transient signals are in the form of bursts or sharp spikes associated with individual emission events like tool fracture or chip breakages. These AE signals consist of start and endpoint signals, which are completely distinguished from background noise. A single burst waveform (Figure 2.15) can be used to simply explain the time-domain features of AE signals used for various statistical signal processing.
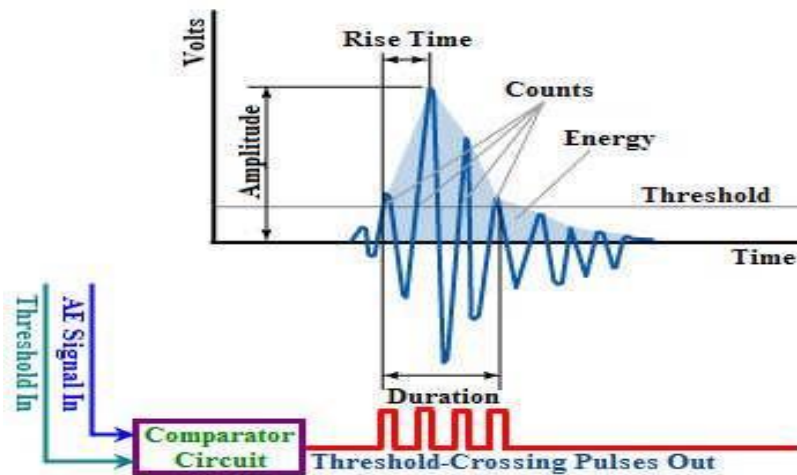
Figure 2.15: Features of transient signal [111].

- **Rise time**: This can be described as the time interval between the first threshold crossing and the peak amplitude. The peak amplitude indicates the measurement of the intensity of the AE source.

- **Threshold**: Threshold is a defined level to distinguish signal from noise. An AE event is counted only if the signal crosses the threshold level.

- **AE event**: This is a micro-structural displacement that produces elastic waves in a loaded/stressed material.

- **Signal amplitude**: This is the maximum (either positive or negative) AE signal attained during an event. The amplitude is expressed in Decibel (dB). It is an important parameter as this is the parameter that makes the AE signals detectable. The amplitude detected below the presented threshold is usually not recorded.

- **Duration**: This is the time interval between the first threshold crossing and the last threshold crossing. This parameter is often used as a filter rather than for measurement. It helps in filtering out interference.

- **Frequency**: Is the number of counts divided by the duration.

- **Ring down counts**: This is the number of threshold crossings. It is a measure of signal size; this implies that the larger the signal the more the number of counts. It is denoted by *n*. Number of counts is given by

53

$$n = \frac{\omega}{2\pi\beta} ln \frac{V_O}{V_{th}} \qquad\qquad (2.7)$$

Where V_O = reference / initial voltage, $\omega = 2\pi f$ = apparent frequency, β = decay constant, and V_{th} = threshold voltage

Counts, n is dependent on the magnitude of the AE source and acoustic properties of the material and the sensor.

- **Energy**: Often referred to as energy count, is the integral of squared amplitude over time of signal duration. It is the total elastic energy emitted by a material undergoing acoustic emission.

- **AE RMS**: Root mean square (RMS) is an electrical engineering power term defined as the rectified time-averaged AE signal measured on a linear scale. It is the continuous measure of varied AE signal "voltage" expressed in volts and it is calculated as

$$AE_{RMS} = \frac{1}{T} \int_0^T V^2(t) \, dt \qquad\qquad (2.8)$$

Where $V(t)$ is the signal function and T is the time period.

The most commonly measured AE parameters in the time-domain are ring-down count, events, energy and amplitude. The RMS of the acoustic emission signal is the best representation of the signal's energy [112]. Other statistical quantities that can be used as AE time-domain features include standard deviation, kurtosis and variance, among others. Time-domain features of AE signals are used to generate frequency domain features based on the power spectrum.

The earliest utilization of acoustic emission analysis began with the study of seismology by Hodgson in 1923 [53, 113]. He related and confirmed the similarity between the AE wave characteristics and an earthquake, except for the scale. However, the first profound, documented and recognized investigation of AE in metal was made by Kaiser in 1950 [113], where he concluded that the observed AE was irreversible occurrence and that repetitive loading of material does not generate repetitive emissions. This was after Tinsmiths noted "Tin cry" during the deformation of Tin metal using acoustic emission.

The use of acoustic emission for machine process monitoring and condition analysis is phenomenal. Over the year, the technique has been applied to monitor several macro and micro machining such as turning, milling and grinding. Mokhtar *et al.* [114] used the acoustic emission for the analysis of surface roughness during an end milling operation. A Fast Fourier transformer was used to transform time-domain features - amplitude, RMS and frequency where a time-domain signal transformed to frequency domain for the analysis. The result confirms that the AE components are responsive to the change in milling parameters that influences surface roughness.

Liu and Donfeld [115] proposed a quantitative model that can be used to estimate the acoustic emission energy released at the cutting and rubbing zones during diamond turning. They observed that the energy content of the AE signal is close to the theoretical predictions. Onwuka *et al.* [86] investigated the AE monitoring of diamond-turned RSA 443 on an ultra-high precision lathe machine to analyse tool condition and surface roughness. The machine parameters selected were feed, speed and depth of cut; which were varied for the experimental study. From the result, it was observed that respective increase in raw AE signal spikes and peak-to-peak signal increases the surface roughness and tool wear values. This indicates that the acoustic-emission-sensing technique proves to be an effective monitoring method.

The application of AE is not limited to machining, there are other applications and field in which the technology is employed, such as; civil engineering for monitoring integrity of structures, automobile industries, gears, etc. Its application can also be employed in the inspection and monitoring of pipelines, pressure vessels, storage tanks and welding processes. The technique of AE testing is also feasible in the detection and location of high-voltage partial discharges in transformers.

2.10.1 Acoustic emission measuring technology and sensors

Detection, amplification, filtering and analysis of signals are some of the qualities of AE technology. A typical AE monitoring system consists of sensor, preamplifier, and an AE acquisition and analysis system (Figure 2.16) [109].
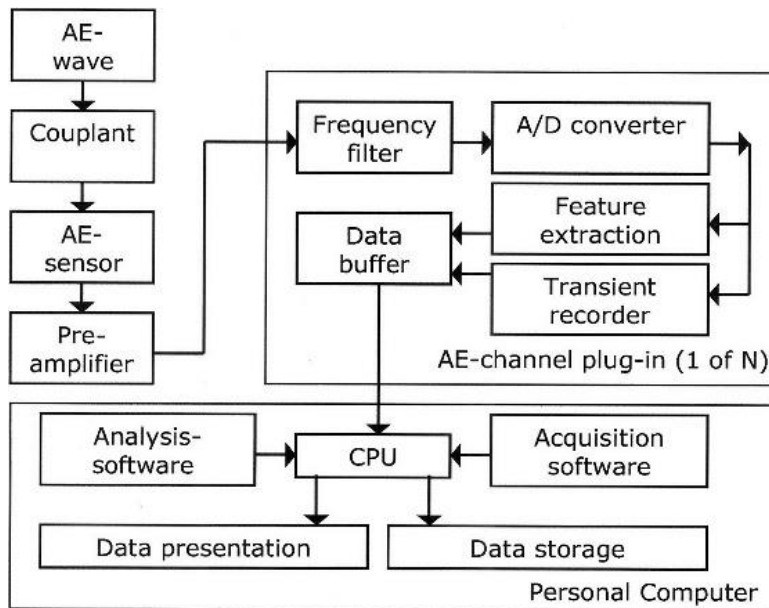
Figure 2.16: AE measurement chain; courtesy of Vallen - Systeme, GmBH [109]

An AE sensor is an integral part of the AE technology in condition monitoring of Ultra-high precision machining (UHPM). The sensor is introduced during machining for continuous monitoring, to quantify the process performance and then give valid information on the optimisation of the process. AE sensors are available for monitoring in-process machining such as force, power and vibration in precision machining. Unlike other sensor-based monitoring in in-process machinings such as force and vibration, AE sensors can detect signals even at a very low depth of cut.
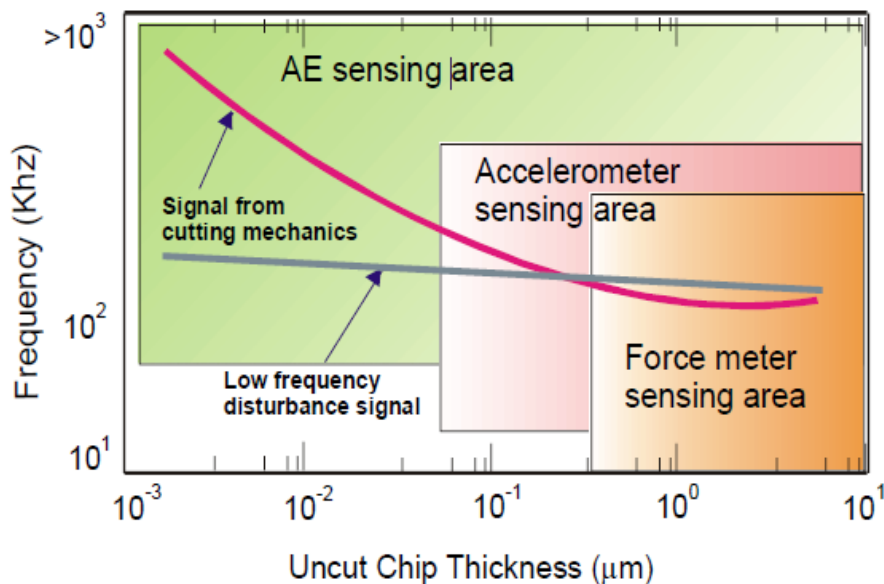
Figure 2.17: Signal Frequencies and Sensor Effectiveness [53]

A piezoelectric transducer is a sensing device commonly used in acoustic emission measurement to generate electric signals when a mechanical force is applied [107, 110, 113, 116]. The piezoelectric elements inside the sensor convert mechanical waves to voltage-time signals and consequently, the signal generated is used in acoustic emission steps. There are several piezoelectric transducers, but the most popular and commonly used at present is lead zirconated titanate (PZT), due to its availability, low financial cost, high performance and user-friendly operation [116]. The dynamic strain in PZT facilitates the acquired voltage-time signal as the sensor output. The signal can be expressed as

$$V = V_O e^{-\beta t} \sin \omega t \qquad (2.9)$$

Where, V_O = reference voltage, $\omega = 2\pi f$ = apparent frequency, t = time and β = decay constant.

The signals detected by the piezoelectric sensor are subjected to analog and digital signal conditioning and then processed to ultimately generate functional signal features. Cognitive decision-making support systems help in the evaluation of the signal features for final analysis, which can be fed numerically into the machine tool by the human machinist to recommend or execute suitable adaptive or corrective actions. The output signal from the piezoelectric-sensor technology is usually fed through a pre-amplifier characterized by high input and low output impedance. The technology is used to transform the small signal (in mV) to a higher range (in volts) for gain. Other technologies that can be used for AE measurement in precision machining include the capacitance principle and the application of a piezoelectric thin-film sensor deposited on a shim and located between cutting the insert and tool holder [107]. Although these sensing methods offer noteworthy advantages in terms of accuracy, calibration and frequency range, they are not readily available and have not been expressly used in industrial applications.

2.11   AE signal processing

Signals are defined as a measure of physical variables over some time and/or space. For example - voltage, current, amount of charge in the electrical system, position, velocity, mass and volume are physical variables in the mechanical system. The price of a stock, commodity and interest rate

are physical variables in the financial system. Finally, electrocardiogram (ECG), electroencephalogram (EEG) and magnetoencephalogram (MEG) are examples of biomedical signals.

There are two distinct types of signals; an analog signal is a continuous signal that always consists of infinite variable values. A digital signal is discrete in time and value. An analog pattern (represented in the curve) together with a digital pattern (represented as the discrete lines) is illustrated graphically in Figure 2.18. An analog signal is continuous in time and value, while the digital signal maintains a constant level and then changes to another constant level.
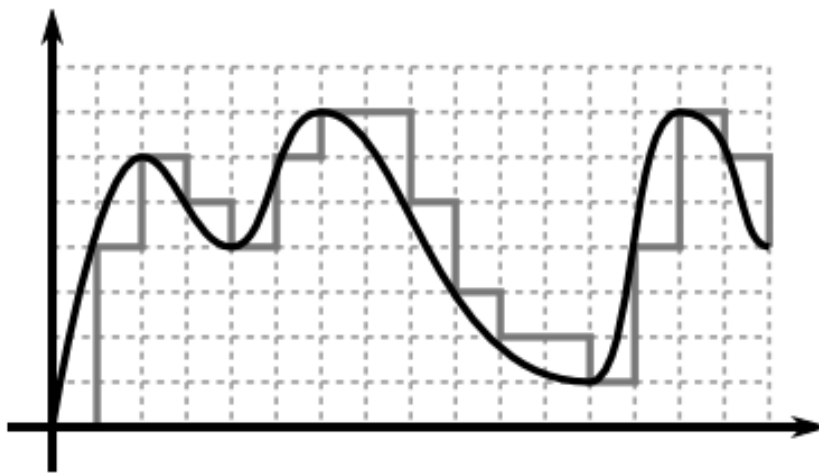
Figure 2.18: Signals Pattern

Signal processing is the act of manipulating a signal to extract useful information. The manipulation is usually done by a computer and special integrated circuits or analog electrical circuits. We now live in a digitalized era; humans rely on the technology of digital signal processing (DSP) as it pervades our everyday activities. Most applications now depend on DSP; ranging from the use of digital/ smartphones, digital computers, cameras, high-definition (HD) televisions, printing machines, watches; most of these devices make use of digital data as their way of representation.

Some of the advanced applications of digital signal processing include machine vision, which is used for automated inspection (e.g. for currency) or robotics guidance and even security systems. In addition, avionics and defence that are used in radar and electronic warfare is another advanced application of DSP. Medical instruments, an example of the advanced technology of DSP would

be less efficient and inaccurate in analysing if there were no digital electrocardiography (ECG) analysers or digitized x-beams and therapeutic image frameworks.

The concept of DSP has dynamically impacted engineering as scientists and researchers are now equipped with a reliable tool to visualize data, analyse and then process it. Figure 2.19 shows the different units through which a basic analog signal can be converted to a digital signal.
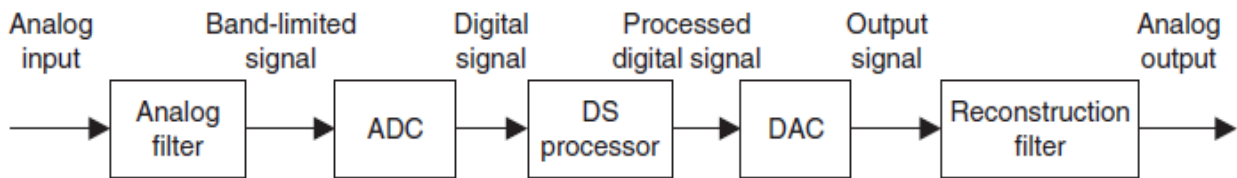
Figure 2.19: Analog to Digital signal processing schemes [117].

Acoustic emission signals occur over a wide range of frequency, (typically from 100 MHz – 1 MHz) [109]. The complexity and multiple sources of AE signals during the cutting process cause the signals to experience changes through multiple reflections at interfaces. Additionally, there is scattering by microstructural defects and refraction when there is a medium change along the travel path from the source to the sensor. This factor together with the consideration of the sensor sensitivity alters the property.

However, AE signals are intricate and random in their final waveform, due to the multiple originating sources during the cutting process, thereby making them difficult to characterise a source. Acoustic signals carry insight about the source event, which requires processing for assessment and extraction of significant features. Signal features can be used to correlate cutting conditions, tool wear, tool geometry, tool breakage, chip formation, surface roughness and other occurrences involved in machining. Pertinent features in an adequate amount are to be extracted to reflect the process conditions [107, 118]; this can be achieved through sufficient signal pre-processing and further signal processing techniques.

The pre-processing of raw AE signals is carried out to amplify small signals for detection and it is necessary to keep the signal within a specific frequency range and avoid overloading of the buffer. Hence, the raw analog signal is not directly fed into the analog /digital converter (A/D converter). The signal is pre-processed through the amplification, filtering, RMS conversion and segmentation

[107]. Further signal processing of the digital AE signal (after pre-processing) involves transformation into time, frequency or time-frequency domains, extraction of signal and feature selection. Figure 2.20 illustrates the logical scheme followed by the signal processing of AE signals [107].
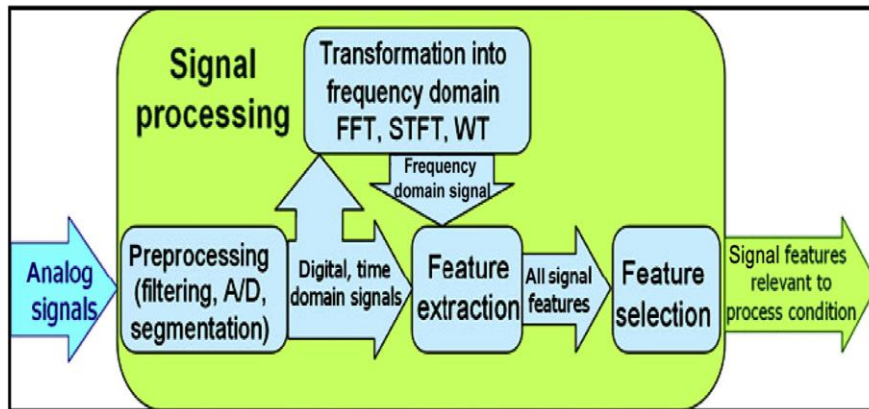
Figure 2.20: Signal processing logical scheme.

2.11.1 Feature extraction and domains

Feature extraction is a process that transforms the original sensory signal into many potentially discriminant features [119]. One of the most important and challenging parts in acoustic emission signal processing is feature extraction, which is usually applied to signals to transform them into a reduced representation set of features. For the reliability of the monitoring process of AE, it is necessary to extract pertinent features that are of importance to the process conditions. Reducing the dimensionality of the signal is not the primary purpose of feature extraction, but also to extract dominant information hidden in the signals by avoiding redundant information.

The extraction of interested feature parameters in AE signal processing can be challenging, therefore, many signal processing methods have been used to analyse AE signals to extract the relevant features for testing and monitoring [120]. Several signal processing methods are used to interpret and identify recorded digital signals, to extract features for monitoring. These methods include time-domain analysis (for time), time series modelling, frequency domain analysis (for frequency) and time-frequency analysis [118, 121, 122]. Lauro *et al.* [122] stressed that selecting

a suitable signal processing method for the most important items used for the cutting process that is assumed to be nonlinear and non-stationary.

2.11.1.1 Time-domain

The time-domain method is used to extract information that is limited to time in an AE signal. Here, the analysis of signals is done with respect to time and the values are known to be real numbers. Time-domain is used to process data without interfering with its raw form. The signal features from this domain are extracted directly from the calibrated time-domain signals as recorded by the sensor and analyser.

There are several features from an AE signal that can be extracted in the time-domain, these features are usually descriptive and sensitive to impulse oscillation [118]. Time-domain features include, arithmetic mean, RMS, crest factor, variance, skewness, kurtosis, power, standard deviation, range, the burst rate (maximum and minimum), ring count, peak-to-peak, range, etc [86, 107, 123-125]. Some of these signal features are explained below:

- **Arithmetic mean (μ)** is the mean of amplitude values of the raw data signal. The mean of n amplitude values of a signal ($x_1, x_2, x_3, \ldots, x_n$) is given by the expression:

$$\mu = \frac{1}{n}\sum_{i=1}^{n}(x_i) \tag{2.10}$$

- **Root mean square (RMS)** is a measurement of the magnitude of a set of n values of raw data. It is expressed mathematically as:

$$RMS = \sqrt{\frac{1}{n}\sum_{i=1}^{n}(x_i)^2} \tag{2.11}$$

  RMS is related to the source of energy and the change in signal RMS can be associated with machine integrity or dynamic behaviour. The advantage of the RMS measurement is that it gives a continuous measurement of a parameter that can be standardized for comparative purposes [118].

- **Crest factor** is the ratio of the peak amplitude of a waveform to its RMS value. Crest factor indicates the extent to which peaks are present in a waveform. In other words, it is the measurement of smoothness of a signal. It is expressed as

$$CF = \frac{Peak\ level}{RMS\ value} \qquad (2.12)$$

The level of RMS increase determines the crest factor, as RMS increases, the spiky signal profile increases.

- **Standard deviation (σ)** is the measurement of the variation of data from the average. It is calculated as:

$$\sigma = \sqrt{\frac{\sum_{i=1}^{n}(x_i - \mu)^2}{n-1}} \qquad (2.13)$$

- **Variance (V)** is described as the variability of the raw data can be regarded as variance and can be defined mathematically as:

$$V = \frac{\sum_{i=1}^{n}(x_i - \mu)^2}{n-1} \qquad (2.14)$$

- **Skewness (S_k)** is the 3rd central moment of mean and it is used to measure the asymmetry of the probability distribution (peak) of the raw data in the signal. It is calculated as:

$$S_k = \frac{1}{n}\frac{\sum_{i=1}^{n}(x_i - \mu)^3}{\sigma^3} \qquad (2.15)$$

- **Kurtosis (k_u)** is the 4th central moment and it is used to measure the "peakedness" of the probability distribution of the signal raw data. Otherwise, it is the measure of the sharpness of a signal peak. The higher the sharpness of distribution of signals, the bigger the kurtosis value and the more likely a defect has occurred. It is expressed mathematically as:

$$k_u = \frac{1}{n}\frac{\sum_{i=1}^{n}(x_i - \mu)^4}{\sigma^4} \qquad (2.16)$$

- **Power (P)** is the measured area under the rectified signal envelope. Power can be described as another measurement of the signal amplitude. However, it is sensitive to amplitude as well as duration, and it is less dependent on the operating frequency. Power is defined mathematically as:

$$P = \frac{1}{n} \sum_{n=1}^{n} (x_i{}^2) \tag{2.17}$$

- **Range** can be described as the difference between the maximum signal raw data value without overflow (or distortion) and the minimum raw data value.
- **Burst rate** is also known as pulse rate. It is the number of times the sign exceeds a pre-set threshold (usually set to $300\mu V$) per second [126]. Burst rate is a feature that applies to AE and vibration.

Time-domain features of AE have been successfully used for online monitoring of tool wear, chip formation surface integrity as well as smearing and plucking. An advantage of time-domain is that the features are fast and easy to calculate, therefore, it is used for online-monitoring. Furthermore, complex pre-processing, like framing, windowing and filtering are not required. The advantage eliminates time and power consumption during pre-processing, although they are not suitable for the measurement of errors and calibration.

2.11.1.2 Time-series modelling

The time-series modelling technique is used to extract parameters from the sensor's signals. The technique is a collection of numerical observations identified in a natural order that show variation in a specified time interval [123]. Many researchers have used time-series analysis. Three main techniques have been frequently used in the machine monitoring process: auto regression (AR) model, moving average (MA) model and the auto regression moving average (ARMA) model [127]. These techniques use model coefficients as features in the monitoring process:

- **Auto regression (AR) model** can be set as follows [120]:

$$\bar{x}(n) = a_1 x(n-1) + a_2 x(n-2) + \cdots + b_p x(n-p) \tag{2.18}$$

63

$$R(n) = \bar{x}(n) - x(n) \tag{2.19}$$

Where $\bar{x}(n)$ = the AR predicted value, $x(n)$ is the acoustic emission–root mean square (AE-RMS) time series, p = AR order, $a_1, a_2....a_5$ = AR model parameters, R(n) is the AR residual signal. The first AR coefficient can be chosen as a feature.

Experimental results [127, 128] revealed that in turning operation, the increase in flank wear of cutter increases the power of AR residual signal of AE.

- **Moving average (MA) model** is given as [123]

$$\bar{u}(n) = b_1 u(n-1) + b_2 u(n-2) + \cdots + b_q u(n-q) \tag{2.20}$$

$$R(n) = u(n+q) - \bar{u}(n+q) \tag{2.21}$$

Where $\bar{u}(n)$ = the moving average predicted value, $u(n)$, n =1, 2, 3, …, n is the time series of acoustic emission, q is the moving average order, $b_1, b_2,.....,$ b_p are MA coefficient parameters, R(n) is the residual components. The first MA coefficient can be chosen as a feature.

- **Auto regression moving average (ARMA) model** is the combination of the AR and MA model. ARMA consists of a notation model (p, q), which represents the time series from auto regression (AR) and moving average (MA).

$$x(n) = -\sum_{k=1}^{p} a_k \big(x(n-k) \big) + \sum_{k=1}^{q} b_1 \big(u(n-k) \big) \tag{2.22}$$

Where k is the coefficient index. The first two coefficients from this model can be chosen as features [123, 129].

2.11.1.3 Frequency and time-frequency domain

Frequency domain is the representation of sinusoidal signals as "single spikes". In a monitoring system using AE signal waveform, there are different techniques used in frequency and time-frequency domains for signal analysis. The methods employed in ultraprecision machining are Fourier transform (FT) [130, 131], fast Fourier transformations (FFT) [132], short-time Fourier

transformation (STFT) [133], wavelet transformation (WT) [134] and Fourier transform (FT). FT is a mathematical technique commonly used to extract fundamental frequency components embedded in time-domain analysis; this is achieved by converting the signal from time-domain to frequency domain. The parameters of frequency domain analysis are more reliable in damage detection than time-domain parameters [135].

A signal x(t) can be decomposed by its Fourier transform F(w) as:

$$x(t) = \frac{1}{2\pi} \int_{-\infty}^{\infty} F(w)e^{j\omega t} dt \tag{2.23}$$

Where

$$F(w) = \int_{-\infty}^{\infty} x(t)e^{-j\omega t} dt \tag{2.24}$$

Equation 2.23 and 2.24 mean the signal x(t) can be decomposed into a family with harmonics $e^{j\omega t}$ and the weighing coefficient $F(w)$ represents the amplitudes of the harmonics in the signal x(t). FT is a powerful tool; its analysed signal can be reconstructed to and from their frequency components. Inverse Fourier transform is used to perform the reverse Fourier transform and constructs a waveform from its Fourier coefficients. To regenerate the time-domain signal x(t) from the frequency domain an inverse Fourier transform must be applied.

FT is useful and precise in calculating the frequency composition of the nonstationary signal, all the same, the main limitation of FT is that information about the time occurrence of the frequency component is usually lost during transformation. However, when describing a stationary signal (even though the detected sensor signals during machining are predominantly nonstationary), FFT is suitable.

During machining, the frequency component of surface roughness and geometries can be characterized using FFT [136]. The working technique of FFT to generate the frequency spectrum of acquired signals is based on the Fourier transformation. Thus, representing a polynomial function or a signal by the sum of sinusoid functions with different frequencies. A major drawback associated with FFT [107] is the averaging of frequency composition throughout the signal with a fixed resolution of the entire frequency spectrum. As a result, sufficient samples are needed to extract an ample measure of frequencies. Usually, in the frequency domain, small sine waves can

be detected in the presence of large signals. To address the limitation, time-frequency analysis is applied.

Analysing the time-frequency domain spectrum of signals causes a larger amount of information to be extracted. Short-time Fourier transform (STFT) and wavelet transform are examples of this time-frequency analysis method.

STFT, also known as windowed Fourier transform or Gabor transform, is a time-frequency method that uses a windowed sliding to provide time-localized frequency information for situations in which the frequency components of a signal vary over time. Signal x(t) is multiplied with a short window function, g(t-τ) centred at time, τ and calculating the Fourier transform of x(t) g(t-τ). The window is then moved to a new position and this calculation is repeated. The main difference between FT and STFT is the window function and the key parameter in STFT is the window width, which determines the spectral resolution and time localization. The challenge with this method is that the resolution depends on the appropriate length of the desired segment of the signal. The mathematical expression for decomposing a signal x(t) using STFT is written as [137]:

$$G(w, \tau) = \int_g f(t)g(t - \tau)e^{-i\omega t}dt \tag{2.25}$$

The application of STFT for signal processing is efficient when used to locate and characterise events with many defined frequency patterns, not overlapping and long relative to the window function [121]. Wavelet transformation (WT) is a recent but most advanced and efficient development in signal processing [138]. It is a technique introduced to beat out the resolution problem of STFT [139].

Wavelet transformation uses window duration for different frequencies: high-frequency components are analysed with a shorter duration window for better time resolution, while the low-frequency components are analysed with a longer duration window for better frequency resolution. The application of wavelet has been successfully utilized in different applications such as data and image compression, transient detection, pattern detection, communication systems and more significantly in the monitoring of machining processes [107, 124, 140, 141]. In the application of

wavelet analysis, the signal can be analysed into its sub-band frequencies, each of these is generated from a combination of shifting and scaling of the original wavelet signal [107].

The term shifting in wavelet analysis simply means the dilating (stretching) or compressing of time-scale signals produced by it. The larger scale will be stretched out and the small scales will be compressed. This connotes that the scale factor, often denoted by *a*, has a relationship with the frequency of the signal and functions the same way as the wavelets. The smaller the scale factor, the more "compressed" the wavelet. High scale or stretched wavelets, or low-frequency indicates approximation (A), while low-scale or compressed wavelets or high frequency indicates detail (D) as shown in Figure 2.21 [135]. Shifting in wavelet transform implies delaying or hastening the commencement (onset) of the process.
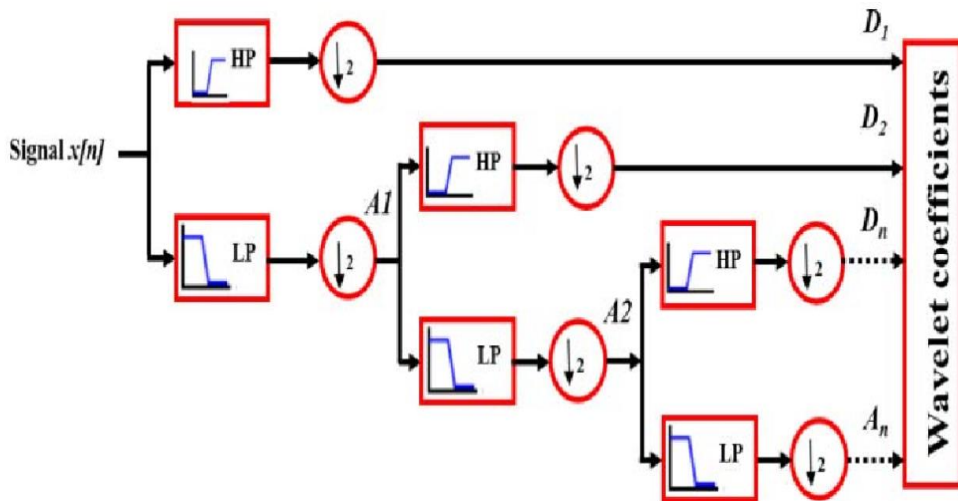
Figure 2.21: Signal decomposition using discrete wavelet transform

There are several types of WT and depending on their application, one may be preferred to the others. For a continuous input signal, the time and scale parameters can be continuous, leading to the continuous wavelet transform (CWT). They may also be discrete to avoid a redundant representation and ease computation, which leads to the discrete wavelet transform (DWT), this is also known as the continuous time wavelet series. Finally, the wavelet transform can be defined for discrete-time signals leading to a Discrete Time Wavelet Series (DTWS)

67

2.11.2 Signal feature selections

The term "feature selection" is often used in the field of machine learning. It is a process whereby relevant, irrelevant, redundant or noisy features are removed from extracted features, based on an evaluation criterion to optimize the performance of machine learning algorithms. Relevant features influence the output performance and the function cannot be performed by another feature. Irrelevant features can be removed without affecting the learning performance. They do not influence the output performance and consist of random values for each instance. Redundant features are correlated, that is, they perform the function of other features.

The purpose of choosing a small subset of the relevant features, using certain relevance evaluation criterion, is not only to optimize performance but also to lower cost of computation, increase the accuracy and give a better interpretation of the model. Depending on how the selected features are evaluated, a different approach could be adopted. Approaches for feature selection can be categorized into filter model, wrapper model and embedded model [142].

- **Filter model:** Generally, a pre-processing step in machine learning, which relies on the characteristic of data. The selection and evaluation of features in a filter model are independent of any machine learning algorithm [143]. This characteristic and its ability to allow the algorithm to have a very simple structure (usually used as straight forward search strategy in backward elimination or forward selection), is an advantage the filter model has over the wrapper and the embedded model. The filter model is easy to design and also easy to understand, this confirms why most feature selection algorithms in real-world application make use of this filter model. Examples of filter models include the Chi-squared test, information and coefficient scores.
- **Wrapper model**: The selection of a set of features is considered as a search problem where different combinations are prepared, evaluated and compared to other combinations. This model searches the space of possible parameters, for a good subset using the induction algorithm as part of the evaluation function. Some examples of the wrapper model of feature selection include forward selection, which refers to a search that starts at the empty set of features (no feature in the model). Backward elimination refers to a search that starts with a full set of features. Lastly, the Recursive feature elimination, which is used to find

the best performing feature subset. It creates the best model and sets aside the best or the worst performing features at every iteration.

- **Embedded model**: The filter and wrapper model of feature selection are concluded to be expensive to run for data with a large number of features, however, an embedded model of feature selection was introduced to compensate for this limitation [143]. The embedded model makes use of the Filter model inside the wrapper model. It learns which feature best contributes to the accuracy of the model while the model is being created. Some common examples of this model include LASSO and RIDGE regression, regularized trees, memetic algorithm and random multinomial logit.

Feature selection can also be approached using the following [124]:

- **Search methods**: Different categories of search method employed for feature selection include: optimal search (exhaustive search, branch and bound algorithms), heuristic search (sequential selection, floating selection and decision tree methods), random search (genetic algorithms, simulated annealing, and Bayesian network algorithm), and weight-based search (fuzzy set theory, fuzzy feature selection, neural networks, neuro-fuzzy approach, and relief).

- **Evaluation criteria**: This is the measure of "goodness" of a particular subset of features, which helps the search methods in the selection process. Commonly used evaluation criteria include (a) distance-based measures, such as Mahalanobis distance, Hausdorff distance and metric approach; (b) entropy measures; (c) statistical measures; (d) correlation based heuristic measures; e) accuracy measures; and (f) relevance measures.

- **Real-world application:** This is the application of feature selection important areas of our day-to-day activity. Feature selection is an essential tool in areas like statistics, pattern recognition, machine learning, data mining and more importantly, it is of interest in machine condition monitoring to improve performance [144].

2.11.3 Decision making

Artificial intelligence (AI) is used to imitate human behaviour, it is simply a means of using a computer or machine to reason intelligently like humans. Its technique is increasingly extending;

however, AI is inspired by the strategy of decision making. The strategy is significant in the development of an automated machining process and tool condition monitoring.

A decision-making strategy in the machine monitoring process is established on the existing relationship between the process/ tool conditions and the feature-bearing signal [103]. There is a wide range of decision-making methods developed for feature-based monitoring, these include pattern recognition, fuzzy systems; decision trees, expert systems and neural networks. These methods have been successfully applied in many cases of monitoring tasks and found to be superior to regression due to their ability to learn from experience in a complex system such turning, milling, drilling and other metal cutting processes[103, 145].

2.12 Artificial neural network (ANN)

Artificial neural networks (ANN), also known as neural networks, are pieces of a computing system that work like the human brain and learn from experience. They are used to develop models just as the human brain processes information, neural networks attempt to imitate the function of the biological neural system to make intelligent decisions.

The basic building block of every ANN is called an artificial neuron. Artificial neuron (also known as a node) is the processing unit that stores local memory and performs localised information processing operations. A neuron is linked with other neurons with unidirectional signal channels (known as connections) to form multilevel networks. Each neuron has a single output signal that splits into many multilevel networks. This signal is the same throughout the network and can take any mathematical form. In general, a neural network has an input layer, hidden layer and output layer (Figure 2.22), these layers are basically for receiving, processing and transmitting the information.
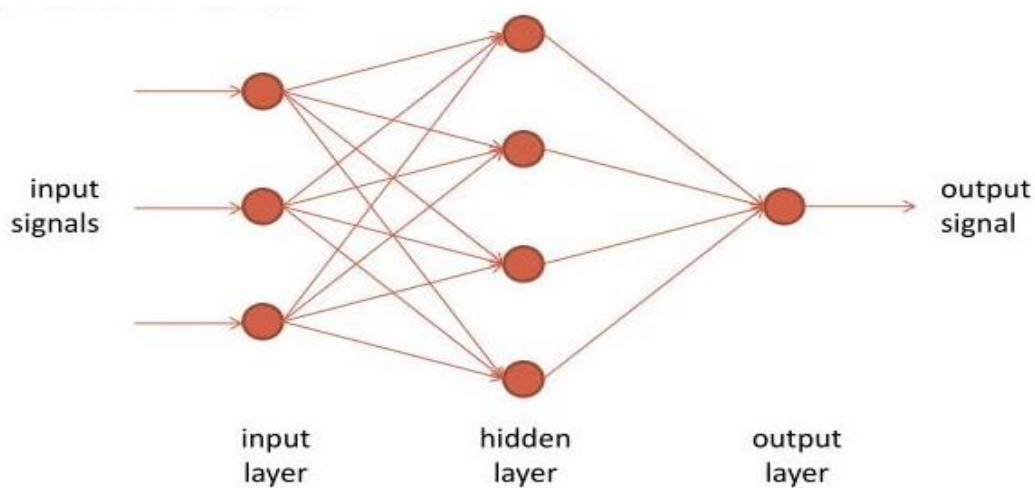
Figure 2.22: A simple artificial neural network

The input layer receives data from the outside world to the network, an output layer computes the data and then sends information back to the outside world (users or external devices). Hidden layers lie between the input and output layer, they have no direct contact with the outside world (hence the name "hidden"). Hidden layers perform computations and transfer information from the input. Although a feedforward network will have a single input layer and output layer, it may have zero or multiple hidden layers [146].

Different kinds of artificial neural networks have been developed to achieve different learning and processing speed capabilities, based on the mathematical operations and a set of parameters required to determine the output. Some of them include; feedforward, radial basis function, Kohonen self-organizing, convolutional, modular and recurrent neural network (RNN) and Long short-term memory.

The feedforward neural network is the most commonly used, it can be either single-layer or multi-layer. A neural network is a simple form of ANN, where input data travels in one direction, that is, the data passes through the input nodes and exit in the output. As previously mentioned, this type of network may or may not have hidden layers. In other words, it has a front propagation wave and no back-propagation by always using classifying activation function. A multi-layer feedforward network consisting of an input layer, one hidden layer and an output layer is shown in Figure 2.23.

71
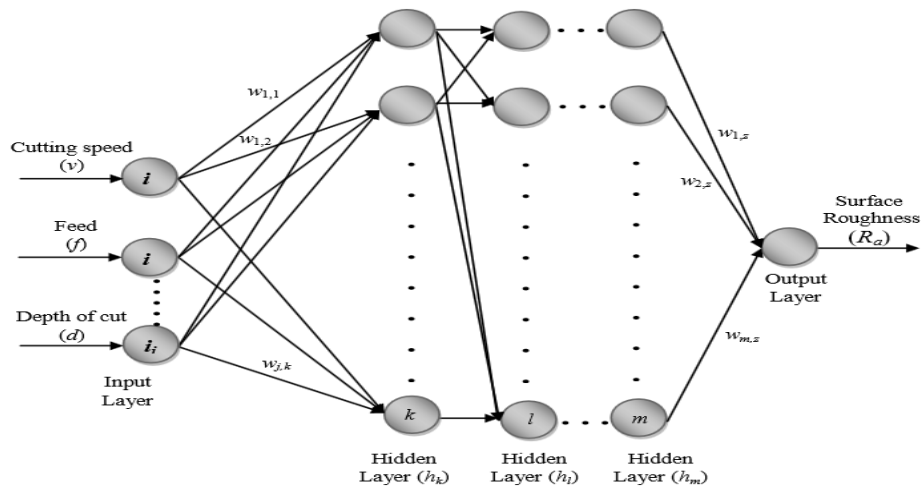
Figure 2.23: A typical multi-layer feedforward artificial neural network [147]

2.12.1 Working principle of ANN

A typical architecture of ANN can be characterized by interconnection links among neurons, the activation/ transfer function for converting input signals to outputs and the learning algorithm. The data is fed into the system through the input layer, the information is stored in the inter-neurons connections at the hidden layer, and there they are processed and transferred to the output layer. Whenever the input is supplied to the network, each neuron in the hidden and output neuron gets some weighted input signals and generates only one output value, the output network is then compared with the target.
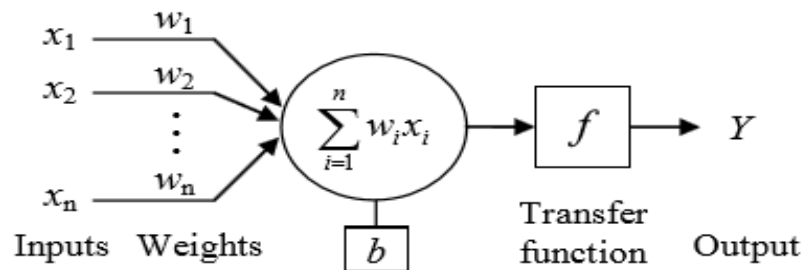
Figure 2.24: Working principle of an artificial neuron

Neural network training is carried out by adjusting the connection weights between neurons to produce the desired output pattern corresponding to the target. The difference between the target output and the network output is calculated as an error. Figure 2.23 shows the structure of a

network with a single neuron. Here, $x\{x_i, i = 1, 2, \dots, n\}$ represent the inputs received by the neuron and Y represents the output. Each input is multiplied by the weight (for instance: $x_i w_i$). The summation of all the products and associated bias, b are fed to a transfer function (activation function), f to generate a result and this result is sent to the output. The main objective of an ANN is to establish some connections between input and output patterns and using the relationship to develop a model that would work as a machine that imitates human intelligence. The relationship between input and output in a neural network can be described as [148]:

$$Y = f\left(\sum_{i=1}^{n} w_i x_i + b\right) \tag{2.26}$$

The activation function is an algebraic equation of the linear and non-linear form, the use of a non-linear activation function is to introduce non-linearity into the output of a neuron. Most real-world data are non-linear, and the aim is to make the neuron learn these non-linear representations.

The distinct feature of ANN is learning [149], is that it learns by itself and does not need to be programmed. The ability to learn complex non-linear and multivariable relationships between process parameters made this intelligent system suitable for modelling various manufacturing operations, such as the prediction of surface roughness in turning operation. Some other abilities of ANN include:

- ANN can perform tasks that are impossible for a linear program.
- ANN is more successful in terms of speed, simplicity and a capacity to learn more than the conventional approaches.
- ANN performance for model prediction could be further improved by defining more levels for the input process parameters, which can be achieved by trial and error methods and repeated training simulations.
- An ANN allows for simple complementing of the model by new input parameters without modifying the existing model structures.

Neural networks are used in diverse applications such as modelling and design, mapping and system identification, control, robotics, pattern recognition, forecasting, signal processing and many more. Despite the numerous limitations and many applications, the effectiveness, speed and accuracy of the neural network is firmly influenced by the following factors [150]: Network

73

structure, network algorithm, training, testing data, transfer function, training function, learning function and performance function

2.12.1.1 Network Structure

The structure of ANN consists of layers and neurons. Taking the multilayer feedforward the ANN network of Figure 2.22 for instance, the network has a structure that contains three layers – input layer has one node with three neurons that represent cutting speed (*f*), feed rate (*v*), depth of cut (*d*). The second layer is the hidden layer with three nodes – *k*, *l,* and *m.* The third layer is the output layer with one neuron. The network model structure can then be defined as a 3-*k-l-m*-1.

ANN permits the process of trial and error by adjusting the number of layers and the number of nodes in the hidden layer(s) to obtain the best possible results. The hidden layers play significant roles in the efficacious application of neural networks, they allow the network to detect the features to capture data pattern and to perform a nonlinear mapping between input and output variables. However, increasing the number of hidden layers might improve the accuracy and it might not, depending on the complexity of the problem.

According to Shafi *et al*. [99], increasing the number of hidden layers seems to further increase the complexity of the network, in terms of mapping, computer memory and desired data control. Computation time also increases when there are too many hidden layers. It has been rigorously proven that the performance achieved with one hidden layer can match that of any number of hidden layers [150, 151]. Various researchers have tried applying different model structures to generate the desired result. Basheer *et al.* [152] applied the 5-8-1 structure, Gupta [153] 3-10-3 structure, Sanjay and Jyothi [154] applied 5 different structures in their research and concluded that the 4-1-1 network structure was the most accurate and reliable to predict surface roughness. Zang [155] suggested that an approximate number of neurons for the hidden layer can be calculated by ''*n*/2'', ''1*n*'', ''2*n*'', and ''2*n* + 1'' where *n* is the number of input neurons.

2.12.1.2 Training and testing data

The quantity of training and testing data are important requirements for the effective performance of the neural network. Training data are used for ANN model development, while the test data are

used for evaluating the predicting ability of the model. Increasing the amount of training data will increase the accuracy of the ANN model, the more the training data, the more reliable the model is.

It is expedient to divide available experimental data into the training data and testing data. The testing data is usually smaller than the training data, inappropriate separation of training data and testing data will undermine the selection of optimal ANN structure and evaluation of ANN prediction. As recommended by Zhang *et al.* [155], the ratio of training and testing data in percentage is given by 90%:10%, 85%:15% and 70%:30%. When the testing data has never been used in training, such test data is called a "holdout dataset". There are two main training approaches used by ANN, these are supervised learning and unsupervised or adaptive training.

- **Supervised learning**: Here, both the inputs and outputs are provided. The training data which entails the input and target, which represent the output, are provided to enable the training process. The inputs' data are processed by the network then the results/outputs are compared with the provided targets, this implies that there is prior knowledge of what the result should be. Errors are propagated back through the network system, which caused the system to adjust the weights that control the network, thus, improving the performance of the network. This process is continuous as the weights are adjusted over and over.
- **Unsupervised or adaptive learning**: In this type of learning approach, the inputs are provided but the target is not. Here, the network itself will have to detect the similarities and generate pattern classes through the previous training pattern. Even without being told whether it's right or wrong, the network must have some information about how to organize itself. There is no external influence to adjust their weights, instead, they internally monitor their performance. One of the most common applications of unsupervised learning is when categorizing data into different clusters using their similarities.

In machining, acquired data are from actual experimental tests, which are usually a challenge due to constraints such as the cost and time in conducting the actual experiment. The acquisition of relevant and reliable data during the process is also a challenge.

2.12.1.3 Network algorithm

Different ANN network algorithms have been proposed by researchers for modelling purposes - feedforward Back Propagation (BP), Elman BP, Time-delay BP, Perceptron, Radial Basis and Self-Organizing map. The most common and successfully used algorithm by researchers, in modelling of machining process, is the feedforward back propagation network. It is a supervised learning algorithm and is mainly used by multilayer perceptions. The algorithm uses the repetitive altering of connection weight values for neurons, based on the computed error when the output value is compared with the target value. The computed output error alters the weight values in a backward direction.

The technology of feedforward BP is greatly adapted for decision making, diagnosis, prediction and control. Zuperl and Cus [156] used two neural network algorithms in their experimental research – feedforward back propagation and radial basis neural network for optimization of cutting parameters during machining of cast steel with HSS tool. They discovered that feedforward BP gives more accurate results, although more training and testing time is required when compared to radial bias - which took less time but produces worse results.

2.12.1.4 Transfer function, training function, learning function and performance function

The transfer function (activation function) determines the total signal a neuron receives, by connecting the weights of a neuron to the input. Transfer functions are differential, continuous and increasing. They introduce non-linear properties to the network by mapping non-linear complex functions between the inputs and output. There are ranges of transfer functions available to process the weighted and biased inputs in ANN modelling, among them are tangential-sigmoid transfer function, hard limit transfer function, liners transfer function, competitive transfer function, etc. [157].

- **The logarithmic-sigmoid transfer function (LOGSIG)** takes an input valued between negative infinity and positive infinity and outputs a value between zero and positive one.

- **The tangential-sigmoidal transfer function (TANSIG)** takes an input valued between negative infinity and positive infinity and outputs a value between negative one and positive one.

- **The hard limit transfer function (HARDLIM)** outputs zero if the net input of a neuron is less than zero, and outputs one if the net input of a neuron is greater than or equal to zero.

- **Linear transfer function (PURELIN)** produces a linear mapping of input to output.

- **The competitive transfer function** is used in competitive learning and accepts a net input vector for a layer and returns neuron outputs of zero for all neurons except for the winner, the neuron associated with the most positive element of the net input.

According to Beale *et al.* [157], the three most used transfer functions in feedforward BP are LOGSIG, TANSIG, and PURELIN. Nalbant *et al.* [158] concluded that the choice of transfer function depends on the nature of the problem. Zhang *et al.* [155] confirmed that LOGSIG activation function seems well suited for the output node for various classification problems where the target values are often binary.

Therefore, if the output is for binary classification then the sigmoid function is a very natural choice for the output layer. Additionally, for a prediction problem that involves continuous target values, it advisable to use a linear activation function for the output nodes. Although, Kohli and Dixit [150] applied both LOGSIG and ANSIG and confirmed that these transfer functions produced almost the same performance.

Network performance is the measure of performance in the prediction accuracy a network can achieve beyond the training data. Accuracy measurement is usually described in terms of predicting error, that is, the difference between the actual (target) and output value. There are different kinds of measurements of accuracy in ANN. The most common types are; mean absolute deviation (MAD), sum of squared error (SSE), mean squared error (MSE), root mean squared error (RMSE) and mean absolute percentage error (MAPE). Each of these has advantages and disadvantages, although there is no specific measurement of accuracy that is generally accepted

for a given problem. Of all the types of performance measure mentioned above, MSE is the most frequently used accuracy measurement according to literature.

Various training algorithms are applied by researchers to train networks. Here, nine training functions have been classified into four types of training algorithms, they are gradient descent algorithms (TRAINGD, TRAINGDX, TRAINGDM, TRAINRP), conjugate gradient algorithms (TRAINSCG, TRAINCGF, TRAINCGP), Quasi-Newton algorithms (TRAINBFG, TRAINOSS) and Levenberg–Marquardt (TRAINLM). According to past researches [147], TRAINGD and TRAINGDX of gradient descent algorithms are the most popular and most applied training algorithms. These algorithms are simple and require less memory. They implement the basic gradient descent algorithm by measuring the output error and then calculate the gradient of the error through modification of weights in the gradient direction. The limitation associated with this training algorithm is that it is slow.

The learning rate, η in a neural network is simply how fast weights change. To have a successful network, the selected learning rate must be low enough so the network can converge to something useful and at the same time as high as possible to speed up the convergence. The best learning rate is the one taking the minimum number of epochs. Momentum parameter, α can be used to allow for larger learning rates resulting in faster convergence while minimizing the tendency for oscillation. The effect of the momentum factor for the updated weights.

2.13   Design of Experiment (DOE)

An experiment is a test or series of tests or scientific processes conducted systematically to discover or demonstrate a fact. It is solely used to generate a better and robust process that is not influenced by any external parameter. Experimentation is important, and its procedures are mostly the source of scientific and engineering knowledge or conviction about a product and process in the engineering and scientific discipline today.

Design of experiments (DOE) is a mathematical methodology used to determine the most relevant relationship between different factors or input variables influencing a process and its output [159]. It was introduced in the 1920s by Ronald A. Fisher while the work of Box and Wilson in 1951

contributed to it. The controversial but significant impact of Genichi Taguchi in the 1980s made the design popular and acceptable [160].

The technique of DOE enables designers or analysts to determine both individual and interactive effects of many factors that can affect the output results in any design at the same time. In other words, it gives the full knowledge of the relationship between design elements and the output response. DOE is an effective tool used for maximizing the amount of information acquired from a study while minimizing the amount of data to be collected. DOE techniques are commonly used in engineering for the manufacturing of new products and processes where scientific theories or principles are directly irrelevant [161].

Its applications are also relevant in many non-manufacturing fields such as marketing, service operations and general business operations. In machining, DOE can be used to generate the necessary combination of the machining parameters (such as feed, speed, and depth of cut) or conditions as inputs (independent variables) and the corresponding surface roughness as output (dependent variable). Generally, DOE is done to identify, investigate and evaluate the performance of a system or process, which includes a combination of operations, machines, methods, people, and other resources that changes the input into an output. In most cases, the system or process contains one or more observable response variables. DOE has helped to meet the ever-increasing demand for new and quality products.

2.12.1 Common design techniques

Numerous DOE techniques are available and used for different experimental purposes. The under-listed gives the most commonly used design types [160]:

1. For comparison:
   - One factor design
2. For variable screening:
   - 2-level factorial design
   - Taguchi orthogonal array
   - Plackett-Burman design

3. Response surface methodology (for transfer function identification and optimization):
   - Central composite design
   - Box-Behnken design
4. For system robustness:
   - Taguchi robust design

Response Surface Methodology (RSM) are designs used for transfer function identification and optimization. For this study, the experiment is planned and conducted according to a Box-Behnken design of response surface methodology using Design-Expert software. The three cutting parameters considered during the turning operation are cutting speed, feed rates and depth of cut.

2.12.2 Response surface methodology

Response surface methodology (RSM) is an advanced technique of experimental design introduced by George Box and Wilson 1951. The objective for the development of RSM is to use statistical and mathematical tools for analysing, modelling and optimising engineering processes [162]. The tasks are realized by studying the relationship between optimized responses and various process parameters affecting such responses. It is a process whereby experimental data are used for fitting and identifying a response surface model, which can be applied to numerical modelling studies [163].

The approach employed in RSM uses the controllable and uncontrollable factors to help the researcher or experimenter identify the optimum response surface. Its application is often used to model after the important factors that have been determined using factorial design. For instance, in a process where curvature in the response surface is suspected. When many factors and interactions influence the desired response, RSM is an effective tool for the optimization process.

The quadratic model is used in RSM, while linear regression and ANOVA are the tools for data analysis. In this research work, RSM is selected for the optimization of the response surface that is influenced by various process parameters, the technique is adopted due to the orthogonality, rotatability, uniformity, and efficiency. Several researchers have successfully applied the

technique of RSM in their research works to prove that the technique is suitable for prediction and optimization.

Rajeev *et al* [164] varied cutting parameters to analysed roughness of hard turned AISI 4140 steel when heat treated to 47 HRC. The analysis was carried out using RSM as a method of design of experiment. Result of this study indicate RSM regression model can predict roughness based on the cutting parameters, with minimum roughness produced at low value of feed rate and higher value of speed.

Otieno [165] in his research work on SPDT of RSA alloy for optical mould inserts, employed RSM to create and evaluate model for surface roughness, tool wear, cutting force and acoustic emission while varying the cutting parameters - cutting speed, feed rate and depth of cut. He concluded that Optimising the cutting parameters using RSM to minimise surface roughness and tool wear as well as predicting average cutting force and AERMS greatly improves machining performance and enhances machinability of the material

Balasubramanian *et al* [166]. investigated machining performance during CNC turning. of stir-casted aluminium metal matrix using the same RSM approach. An empirical relationship among the desired performance characteristics – minimized cutting temperature, vibration and roughness of machined surface - and their effects of interaction among those selected variables was developed. A mathematical model was developed, and the confirmation test carried out confirmed RSM approach as an efficient tool for modelling and perform desirability in an effective manner

2.12.2.1 Box-Behnken design

Box-Behnken design (BBD) is an experimental design used for response surface methodology (RSM) developed in 1960 by George Box and Donald Behnken. It is an independent quadratic design built mainly for fitting response surfaces that are three-level factorial designs. These surfaces can be successfully coded as +1, 0 and -1 (high, intermediate, and low values respectively) and are available in 3 to 10 number of factors.

BBD is a spherical and revolving design, which appears as a cube - it consists of a central point and the middle points of the edges. It can, however, be viewed as consisting of three interlocking

2^2 factorial designs and a central point. The treatment combinations of BBD are located at the mid-point of the edges and centre of the process space. The method is considered rotatable (or nearly rotatable) because the variance of the predicted repose at any point is a function of the distance from the central point. Figure 2.5 below illustrates a three-dimensional representation in X_1, X_2, X_3 space of a 3 Level, 3-factor Box-Behnken design.
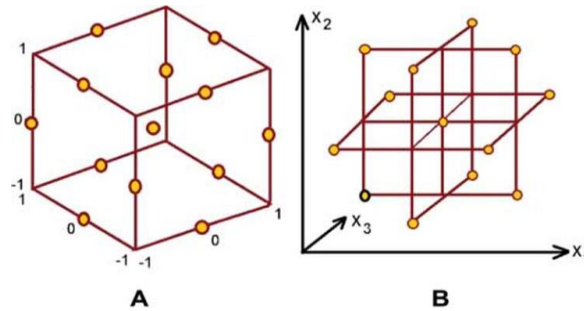
Figure 2.25: A three-factor Box-Behnken design.

In Box-Behnken design geometry, all points lie on a sphere of the radius, and not on the vertices of the cubic region created by the upper and lower limits for each variable (no corner points). Due to fewer design points, BBD has fewer experimental runs (15 runs for 3 factors, 27 runs for 4 factors, unlike central composite design) and can be less expensive. Its methodology allows for efficient estimation for the first and second-order coefficients and is selected for optimization of the main effect, interaction effect and quadratic effect. However, the design is limited in capacity when providing orthogonal blocking compared to other methods of RSM like central composite designs.

Table 2.6: Summary of comparison of primary response surface designs [124].

	Central Composite Design	**Box-Behnken Design**	**D-optimal Design**
1	Created from a 2-level factorial design, augmented with centre points and axial points.	Has specific positioning of design points.	The position of design points chosen mathematically according to the number of factors and the desired model. Therefore, the points are not at any specific position - they

			are simply spread out in the design space to meet the D-optimality criteria.
2	Regular central composite designs have five levels for each factor, although this can be modified by choosing alpha = 1.0, a face-centred CCD. The face-centred design has only three levels for each factor.	Always has three levels for each factor.	D-optimality mathematically chooses points to minimise the integrated variation of the coefficients for the model – it has precise coefficients.
3	Created for estimating a quadratic model.	Created for estimating a quadratic model.	Can be used to create a good design for fitting a linear, quadratic, or cubic model. You can also change the user preferences to get up to a sixth-order model.
4	Rather insensitive to missing data.	Provides strong coefficient estimates near the centre of the design space (where the presumed optimum is), but weaker at the corners of the cube (where there are no design points).	If you have subject matter knowledge, you can edit the desired model by removing terms that you know aren't significant or cannot exist. This will decrease the required number of runs.
5	Replicated centre point provides excellent prediction capability near the centre of the design space (where the presumed optimum is).	If you end up missing any runs, the accuracy of the remaining runs becomes critical to the dependability of the model. The Box-Behnken	Generally, the D-optimal design has 1-2 more runs than a Box-Behnken design, so this provides a little more protection for the model

			design is not recommended if it is common to have a bad run or have missing data. The central composite designs have more runs initially and this makes them more robust to problems.	coefficients if you end up losing some data.
6				Can add constraints to your design space, for instance, to exclude a particular area that you can't get responses.
7				For a quadratic model, factors may have either 3 or 4 levels.

2.14   Conclusion

An extensive number of researches have carried out on the effects of cutting parameters such as depth of cut, feed and speed on responses such surface roughness among others. Till now few researches have been carried out on novel RSA 431 for optical use. Fundamental task in science and engineering practice is to develop models that give an adequate description of the physical systems being observed. The main goal of this study is to attain a mathematical model that relates the responses to the three cutting parameters in SPDT, precisely to the spindle speed, feed rate and depth of cut. Two different approaches have been adopted to attain the mathematical models. The first approach is DOE together with analysis of variance (ANOVA) and regression analysis. The second method is by means of the artificial neural network technique. Generally, the machining parameters are chosen based on the machine data handbook, trial and error method or by literature. Adopting this can lead to wastage of time and increase cost. Hence, to overcome the intricacy, it is necessary to develop a technique to predict the appropriate machining parameters for desired machined surface. In the present study desirability technique is used to identify the optimal process parameters.

Chapter Three

3.0 Experimental Procedure

3.1 Introduction

In this chapter, the major processes and methods applied in the diamond turning of RSA 431 will be explained. To start with, the relationship between the surface roughness and process parameters using experimental design methods will be established. Response surface methodology (RSM) based on the Box-Behnken design and Artificial neural network (ANN) will be introduced and comparisons between these methods will be identified and analysed. The single-point diamond turning machine system, choice of tool, workpiece material and acoustic emission sensing setup will be utilised in the research and briefly described. Design-Expert software and NI LabVIEW employed in the research for experimental design and AE data acquisition devices will also be explained.
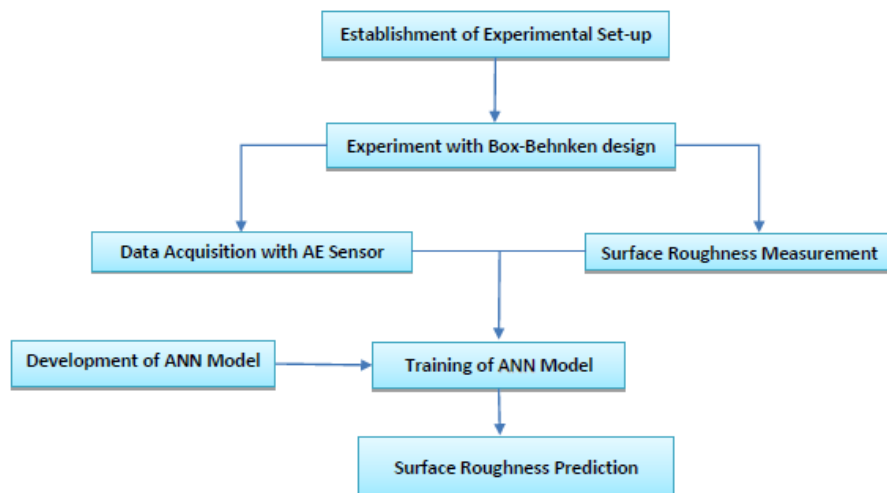
Figure 3.1: Methodology-Design of Experiment

As discussed earlier, it is noteworthy that machine parameters such as depth of cut, feed and speed have significant effects on the surface roughness of the machining process. Therefore, the research experiments were planned and conducted according to a three-factor, three-coded level BBD using these parameters as independent variables. Based on past research, available literature and

experience, the independent variables and their associated levels were fixed and shown in table 3.1.

Table 3.1: Combination of the selected level of cutting parameter from BBD

Variable Parameters	Symbol	Levels		
		-1	0	+1
Depth of cut (µm)	x_1	5	15	25
Feed (mm/min)	x_2	5	15	25
Speed (rpm)	x_3	750	1375	2000

The design of the expected number of experiments to be carried out as calculated [167]:

$$N = 2k \ (k-1) + c_P \tag{3.1}$$

Where N is the number of experimental runs, k is the number of factors and, c_p is the replicate number of central points.

In the three-level three-factorial Box–Behnken experimental design for this research, a total of 15-runs was allotted by the statistical software, Design-Expert, to establish the optimum levels. A combination of twelve different levels of independent variables and three centre point runs were used to fit a second-order response surface. Table 3.2 shows the design matrix along with the experimental run combination. From the 15-run order of BBD, repeatability and randomisation are ensured. The repeated combinations (run order 7, 11 and 14) in table 3.2 correspond to the centre point (0, 0, 0) and is distributed to confirm that the experimental data is dispersed normally. Repeatability also helps to check process instability or drift. Randomisation helps to create a balanced effect of conditions that are irrelevant and uncontrollable, which can influence experimental results - it also helps to make correct logical conclusions from the experiment. For this research work, odourless kerosene mist and water as used as cutting fluid for each experiment run and the surface roughness's are compared.

Table 3.2: BBD experimental runs with coded values

Run	Code level			Factors		
	A	**B**	**C**	**Depth of Cut (µm)**	**Feed (mm/min)**	**Speed (rpm)**
1	1	1	0	25	25	1375
2	1	-1	0	25	5	1375
3	1	0	-1	25	15	750
4	0	1	-1	15	25	750
5	1	0	1	25	15	2000
6	-1	0	1	5	15	2000
7	0	0	0	15	15	1375
8	-1	-1	0	5	5	1375
9	0	-1	1	15	5	2000
10	0	1	1	15	25	2000
11	0	0	0	15	15	1375
12	-1	0	-1	5	15	750
13	0	-1	-1	15	5	750
14	0	0	0	15	15	1375
15	-1	1	0	5	25	1375

3.2   Workpiece: RSA-431

The experiment was carried out on a workpiece material called RSA-431. The workpiece was produced by RSP Technology Ltd through a rapid solidification process known as melt spinning. This process is carried out at an ultra-fast cooling rate of about 10^6 K/s, to produce a fine nanostructured composition with high-end properties. This material exhibits improved mechanical, physical, chemical and thermal properties - which have made it suitable for precision equipment, optical mirrors and moulds' application. Alloy composition and unique properties of RSA 431 are shown in the tables (Table 3.3 and Table 3.4) below;

Table 3.3: Alloy composition of RSA 431 [168]

Aluminium, Al	66.5 %
Silicon, Si	30 %
Copper, Cu	1.5 %
Magnesium, Mg	1.2 %
Iron, Fe	0.4 %
Nickel, Ni	0.4 %

Table 3.4: Properties of RSA 431 [168].

Density, ρ	2.6 gr/cm^3
Thermal Expansion, α	15.5×10^{-6}/K
Stiffness	95 GPa
Specific Stiffness	36 g/cc
Thermal Conductivity, k	120 W/m-K
Ultimate Tensile Strength	435 MPa
Yield Strength	375 MPa
Elongation, e	1%
Hardness	190 HB

The workpiece material, RSA 431, was a 60 mm diameter disk as shown in Figure 3.2. The workpiece was fitted in an adapter, which can be mounted on the machine spindle for easy attachment/detachment and workpiece balancing.
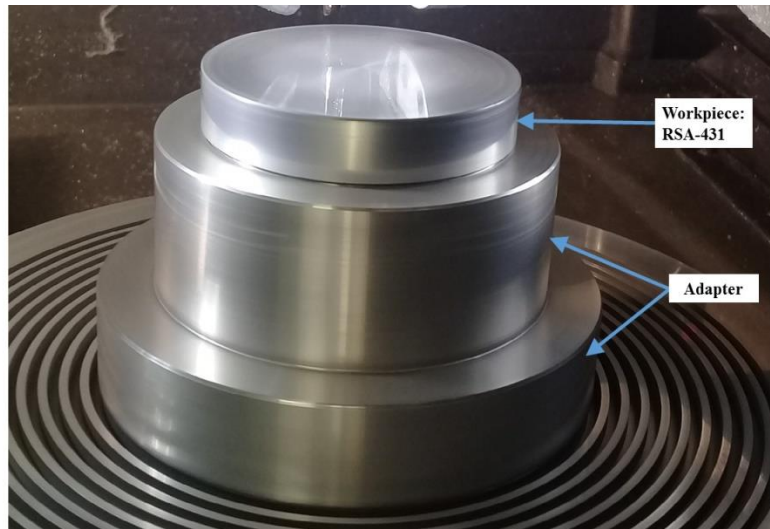
Figure 3.2: Workpiece (RSA-431) Setup

3.3   Machine tool: ultra-high precision machine

Ultra-high precision machining (UHPM) of RSA 431 is in its novelty stage as the material is relatively new, so little is known about the machining of this material for optical application. Single-point diamond turning (SPDT), is an advanced machining process designed for ultraprecision machining of metallic alloys, polymeric materials and precious crystals. SPDT is used to produce different kinds of surfaces that exhibit optical qualities in both surface finish and form accuracy. Presently, SPDT has demonstrated to be the most efficient UHPM process for generating good surface quality with fewer defects in the superficial surface layer [39, 79].

In this research, experimental tests on SPDT of RSA 431 were performed on a precision machine called Nanoform® 250 ultra-grind precision lathe machine situated in a temperature-controlled environment. The machine manufactured by Precitech (specifications are given in the appendix) is a 4-axis (X, Y, Z, and B) ultraprecision freeform machine, which makes use of its high-technology machine characteristics like high rigidity and extreme precision to produce a nanometric level of surface roughness and submicron level dimensional accuracy. Figure 3.3 is a Nanoform® 250 ultra-grind precision diamond turning Lathe machine at the Precision Engineering laboratory, Nelson Mandela University.

Figure 3.3: Nanoform® 250 Ultra-Grind Lathe

The machine can also produce flat, spherical, aspheric or diffractive optical surfaces. Some of the machine's key features are [169];

- High-performance work holding Spindle speed (Maximum speed = 7000 rpm)
- Slide travel of 200 mm
- Capable of performing turning and grinding
- The maximum feed rate of 4000 mm/min
- 200 mm vacuum chuck
- Natural granite base with flood coolant stainless steel enclosure
- Windows® interface for easy network integration with Diffsys® Basic
- FEA optimized dual sub-frames for the ultimate in environment isolation
- Air bearing work spindle bearing
- Oil hydrostatic machine slides
- Optimally located air isolation mounts

- Chiller for work spindle and slides. This chiller is powered and operates separately from the machine to help control the temperature of the machine and spindle
- Optical tool setter
- Integrated gauge head

The Nanoform® 250 ultra-grind also comes with a standard Precitech UPx CNC machine control. The Precitech UPx is a true real-time control system with a user-friendly interface; the features are designed specifically to increase output relative to the input. UPx operates with QNX operating system (OS) to serve the demands of ultraprecision machining.

3.4   Mono-crystalline diamond tool

In ultraprecision machining, the selection of the cutting tool is significant as it influences the final surface quality. A single crystal natural diamond tool is usually the preferred cutting tool because of its high hardness, stiffness, thermal conductivity, honed sharp edge and ability to hold on to the edge while cutting. The tool also has low friction and relative inertness when interacting with aluminium. Although, diamond has its shortcomings that affect the surface finish and accuracy of machined parts, among them, is the chemical reaction with elements such as carbon and iron which has made it limited to non-ferrous alloys and face-centred cubic (FCC) materials. Another is the breakout when machining under high temperatures, however, this can be controlled by the proper selection of machining parameters such as feed, speed and depth of cut during turning[48].

Table 3.5: Properties of Diamond [39]

Symbol	C
Atomic Number	6
Atomic Weight	12.011
Hardness	7000 Knoop Hardness (W = 2100 Knoop Hardness)
Density	3.51 g/cm^3
Most Common Valence	+4
Electron Configuration	$1s^22s^22p^2$
Melting Point	$> 3550\ ^0$C

Bonding Type and Energy	Covalent; 713 kJ/mol
Mechanical Properties	E = 1035 GPa
Electrical Conductivity	10-14 [(Ω-m)-1]
Thermal Conductivity	2000-2500 W/m-K

For this experiment, a mono-crystalline diamond cutting tool manufactured by Contour Fine Tooling is used for the single-point turning of RSA-431. The selection of suitable tool parameters is influenced by previous experiments, workpiece manufacturer's suggestions, and experience to ensure that the turning parameters do not wear the tool. The monocrystalline diamond tool insert is mounted on a tool holder using M5 screws as shown in Figure 3.4 (a). A new diamond tool is used for the experiment and the same tool is used for all the cutting combinations:

(a)   (b)
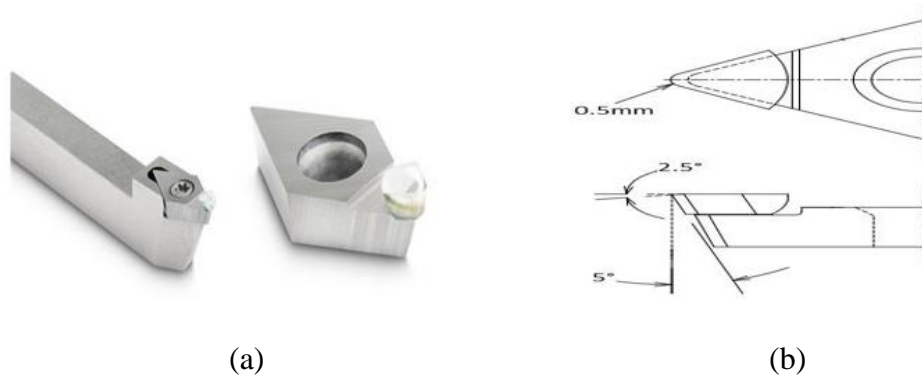
Figure 3.4: (a) Tool holder and diamond insert (b) Diamond tool dimensions.

As specified in the manufacturer's catalogue, the dimension features Figure 3.4 (b) are:

Nose radius = 0.5mm

Clearance angle = 5°

Tool height = 3.163mm

Suggested rake angle by the manufacturer is 0, hence, this tool rake is used throughout the experiment.

3.7 Data acquisition and control

Data acquisition (DAQ) is the process of acquiring and sampling signals from the measurement of real-world physical conditions such as temperature, force, sound, etc. and then converting the samples into electrical signals. These signals are numerically digitalized and displayed on the computer for manipulation.

In DAQ systems, the three main components involved are:

- Sensors that convert physical parameters to electrical signals.
- Signal conditioning circuitry, which consists of hardware devices like DAQ boards and analog-to-digital converters. It serves as an interface between a computer and the acquired signals. The primary function is to convert analog signals from the sensor into a digital form that can be visualized by the computer. Analog-to-digital converters convert conditioned sensor signals to digital values.
- Computer and application software; this is a computer with a software program used for controlling the operation of DAQ devices. The application software installed on the computer helps in processing, visualizing and storing measured data. Software programs used for controlling data acquisition are generally developed using different programming languages such as BASIC, C, FORTRAN, Java, Lisp and Pascal.

3.7.1 Acoustic emission sensor and coupler setup

Acoustic emission (AE) has been used to monitor the behaviour of machine processes through emitted sound during machining [53, 108, 110, 124], as it provides information on the cutting tool characteristics. In the acoustic emission setup, the signal from acoustic emission was acquired using Kistler Piezotron AE Sensor Type 8152B (Figure 3.6 (a)) positioned close to the tool holder (Figure 3.7).

| (a) | (b) |

Figure 3.6: (a) AE Sensor (Kistler 8125B) (b) AE coupler (Kistler 5125B)

The sensor capable of capturing high-frequency signals consists of a piezoelectric sensing element and an in-built impedance converter housed in a small rugged device made of steel. The device is attached, using an M6 bolt to a magnetic steel diaphragm, which is sensitive to elastic waves emitted during machining and ensures easy mounting of the sensor. The design also determines the sensitivity and response of the sensor and prevents the sensing element from external noise.
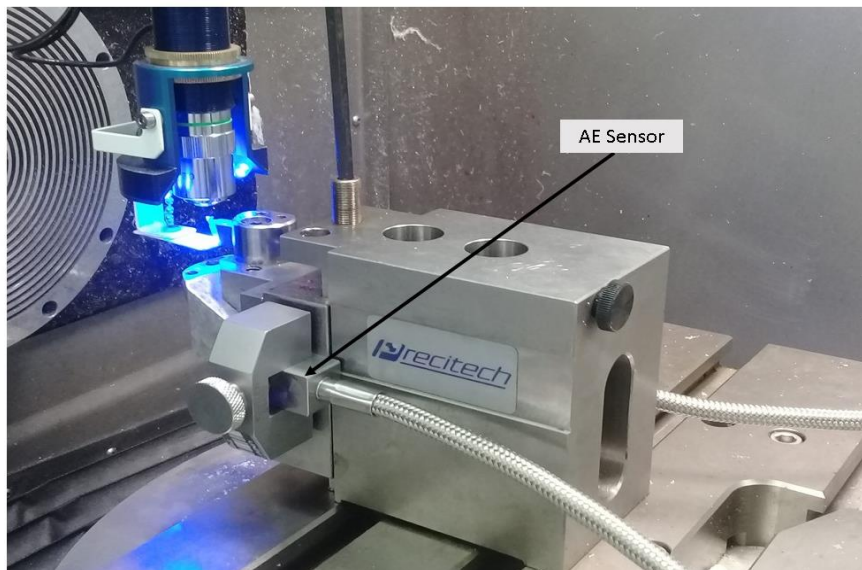
Figure 3.7: AE sensor setup

The sensor is connected to the Kistler AE Piezotron Coupler Type 5125B (Figure 3.6 (b)) to supply power and for signal processing of high-frequency output signals, amplification, filtration and RMS conversion. The power supply input was set at 220V and the output voltage stepped down to

24V with reference to "ground". Thus, regulating the amount of current that goes into the energizer of the sensor.

The coupler design includes the gain amplifier, filters (50 kHz to 700 kHz high-pass filter and 1000 kHz to 1MHz low-pass filter) and an in-built RMS converter with a standard integration time constant of 0.12 ms to 120 ms. Filters are configured to remove noise embedded with the signal, they also minimize the amount of processing required and permit best conceivable adaptation to the specific monitoring function. The coupler was attached behind the tool holder on the hydrostatic oil bearing slideways, to allow free movement of the tool holder on the Z-axis. Figure 3.8 describes AE coupler workflow.
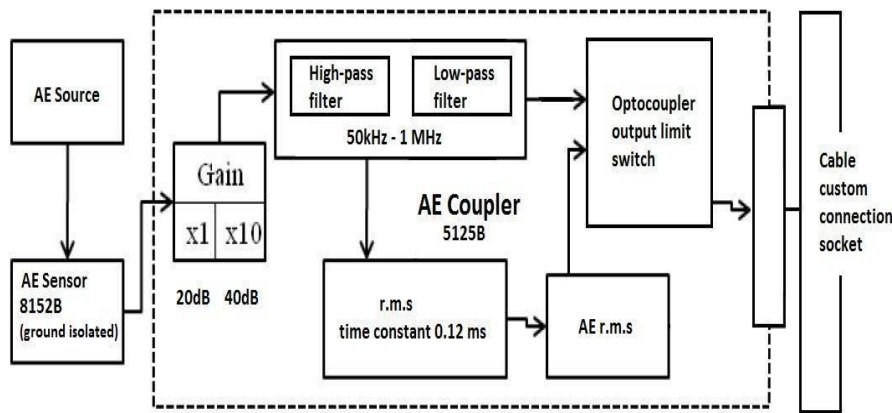
Figure 3.8: AE coupler circuit framework

3.7.2 Data acquisition system

Control and data acquisition from the AE sensor can be achieved using the national instruments' hardware devices. These devices (Figure 3.9) - NI BNC-2110 connector module and NI PXIe-1071 - serve as a link between the AE sensor and PC running NI LabView. The NI BNC-2110 is a simplified connection block and custom cable design that transmits signals from the sensor to the NI PXIe-1071 for further processing. The NI PXIe-1071 is a 4 – slot wide system controller, designed for a wide range of test and measurement applications which provides high - bandwidth backplane. It is compact and rugged, making it suitable for portable, desktop and industrial control applications. NI PXIe-1071 is also flexible and offers each slot to populate with either PXI express module or PXI module.

95

Figure 3.9: AE measuring equipment: (a) NI BNC-2110 (b) NI PXIe-1071

3.7.3 Data acquisition software and program

Finally, data from the acoustic emission are actualised and displayed on the computer through a programmed data acquisition software called NI LabVIEW (National Instruments Laboratory Virtual Instrument Engineering Workbench) (Figure 3.10). LabVIEW is a visual programming language software used for acquiring, analysing, and presenting real-world data. The software has a user-friendly interface and consists of two panels: the front panel that shows a graphical process for monitoring the AE signals in real-time and the block diagram panel, where high-level graphical programming codes in G are developed.

Block panel defines the functionality, at the same time providing a visual representation. The concept function is based on the incorporated graphical user interface (GUI) approach. Programs created by LabVIEW are called VI (virtual instruments). The design pattern used in LabVIEW is known as the producer/consumer loop approach, which is based on the master/slave pattern to enhance high sampling rate and data sharing between multiple loops running asynchronously. The producer loop composes of data acquisition VI, buffer, sequence structure, incorporating a stack sequence structure and a for-loop. On the other hand, the consumer loop was dedicated to saving and storing the samples in the queued sequence. The producer loop produces data for the consumer loop and they communicate using data queues. The concept establishes the simultaneous, independent acquisition and storage of AE data, thereby facilitating efficient acquisition and storage of samples that are saved for further processing.
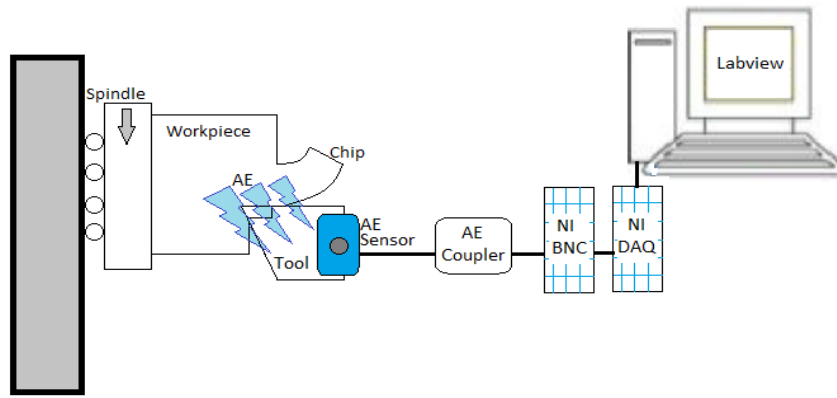
Figure 3.10: Acoustic Emission measurement workflow

Figure 3.11 shows the front panel of NI LabVIEW data acquisition for RSA 431 machining and the block diagram can be viewed in the appendix section.
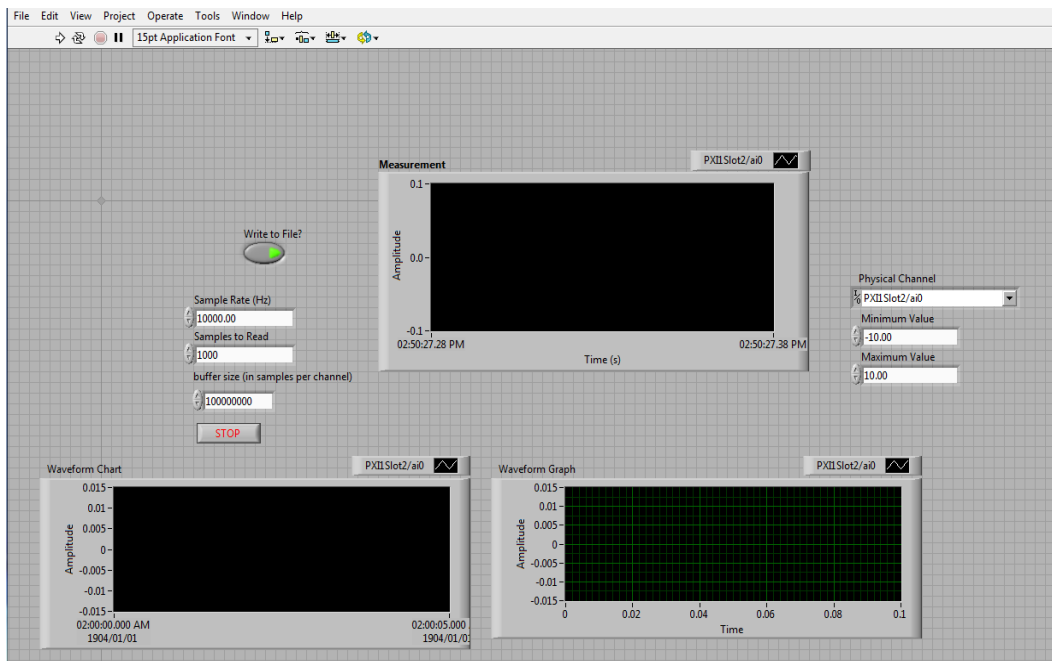
Figure 3.11: Front panel design from LabVIEW

3.8 Roughness measurement of diamond-turned RSA 431

As previously stated, surface roughness is an index used to determine the product quality of ultraprecision machining, consequently, there is a need for effective and reliable means to measure roughness. Since the individual roughness irregularities are too small to the naked eye, a roughness measuring instrument is required. In this experiment, roughness measurements of diamond-turned

97

RSA 431 were conducted after each experimental run using Taylor Hobson PGI Dimension XL surface Profilometer at the Precision Engineering Laboratory, Nelson Mandela University (Figure 3.12). This measuring equipment consists of three important elements, these are: the stylus, pick up and instrument.

Figure 3.12**:** Taylor Hobson PGI Dimension XL Surface Profilometer

The profilometer is an efficient instrument due to the following features [170]:

- Precision measurement of shallow and steep aspherical lenses and moulds from less than 2 mm to 300 mm diameter;
- Firm and fast stylus trace speed of 100 mm/s;
- Automated 3D aspheric measurement, analysis and surface astigmatism display;
- Automated centre and level;
- Superior accuracy and repeatability with very low noise;
- Improved roughness measurements of up to 0.2 nm resolution;
- Ability to measure steep slope surfaces up to 85^0 and
- Taylmap advanced analysis with excellent report building tools.

Before the roughness measurement, the measuring instrument was calibrated. This was carried out after the stylus tip and calibration ball were checked for adhering dirt and damage, and the surrounding confirmed to be isolated from low-frequency floor vibration. The method of

calibration specified by the manufacturer is - Calibration ball. In this method, the gauge is calibrated by calculating the stylus tip shape (curve) and corrections, gauge linearity and gain.

To perform a routine ball calibration, the stylus is "run" through the surface of the ball (with a known radius and form errors) as shown in Figure 3.13. The measurement data from the process is compared to a LS arc (straightness error) and Pt value (maximum deviation/form error). A situation where the form error is greater than the maximum permissible form error for the stylus indicates an error within the measurement loop. The ISO standard for roughness measurement is a 60^0 or 90^0 conical stylus with a spherical tip of 2 µm. The gauge of inductive Form Talysurf instruments ranges from 1mm, 200 microns and 40 microns. The choice of gauge depends on the component to be measured.
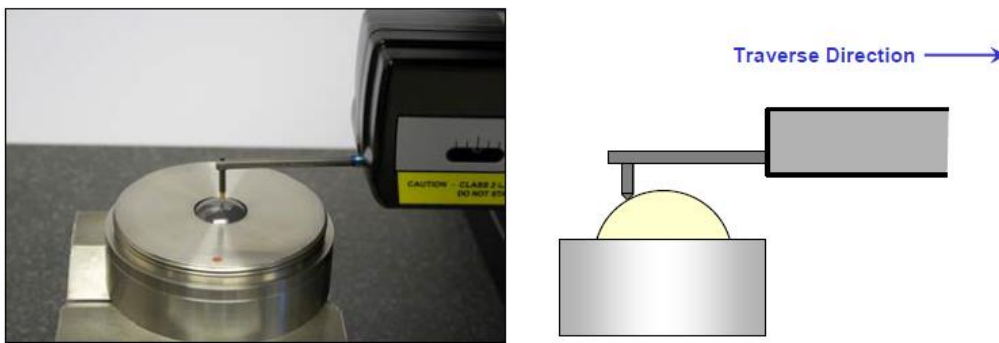
Figure 3.13: Process of calibration balls – known radius and form error

After calibration and accuracy is ensured, the workpiece was placed on the Taylor Hobson PGI Dimension XL Surface Profilometer air-bearing spindle table (Figure 3.14) and the stylus of the profilometer is allowed to drag across the surface (direct contact measuring technique). The measured profile was processed and digitalized through an advanced surface finish analysing software, which evaluates the roughness parameter. The roughness parameter utilized to accomplish the study on surface roughness is the average roughness absolute or centreline average or arithmetic average (R_a), which is defined as the mean deviation of the surface height from the mean profile line.
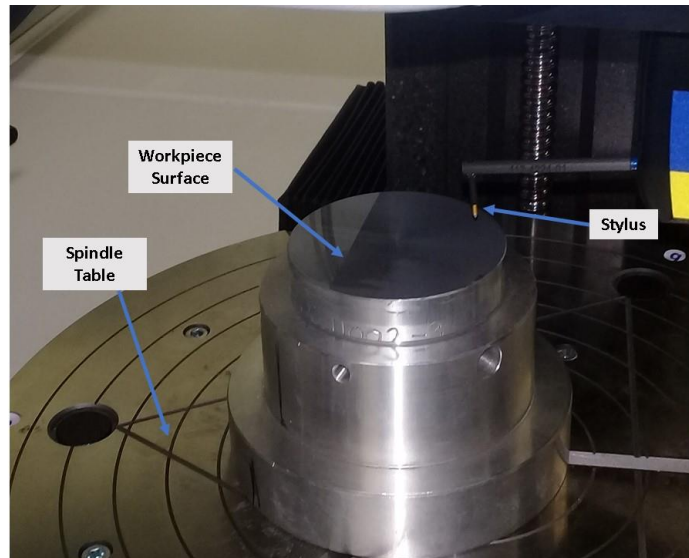
Figure 3.14: Taylor Hobson Profilometer stylus measuring workpiece surface

3.9 Experimental setup and procedure

- The cutting process was carried out on the Nanoform 250 ultra-grind machine tool. The tool was situated in a temperature-controlled environment at a stabilized temperature of 22^0c with constant humidity of 52%.

- Before the main experiment, the workpiece was firmly placed in the adapter, it was mounted and fastened on the machine's vacuum chuck (Figure 3.15). The cutting tool edge and vacuum chuck were ensured to be aligned using the integrated tool gauge while monitoring the spindle balance on the UPx with the aid of DIFFSYS 2D Basic (Figure 3.16). An optical tool setter (LVDT) was used to adjust the height of the diamond tool including the X and YZ position about the centreline of the spindle. The process is known as tool centring and spindle balancing; the process prevents oscillation patterns that can deteriorate the surface quality of the workpiece. After tool centring and spindle balancing, the cutting tool tip was wiped using an alcohol pre-saturated wipe to clean off dirt, oxides, etc.
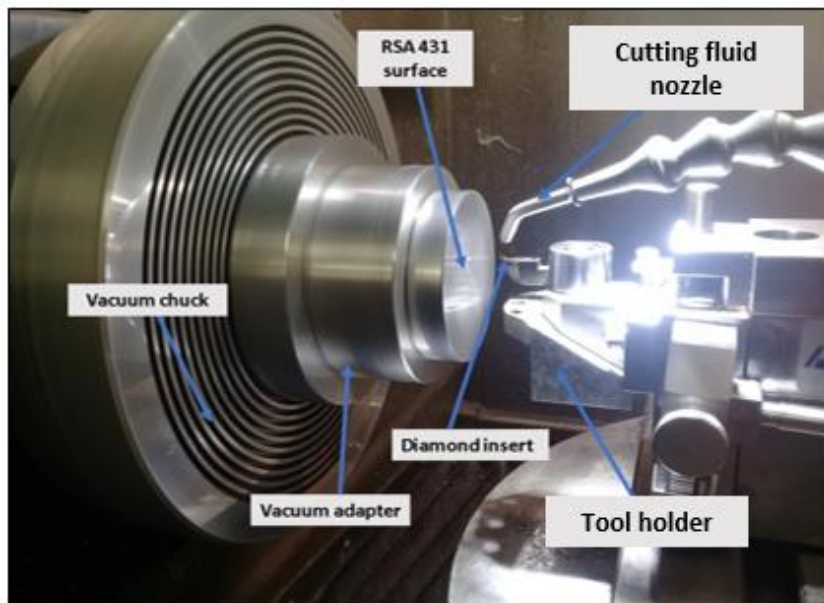
Figure 3.15: Setup of diamond turning of RSA 431
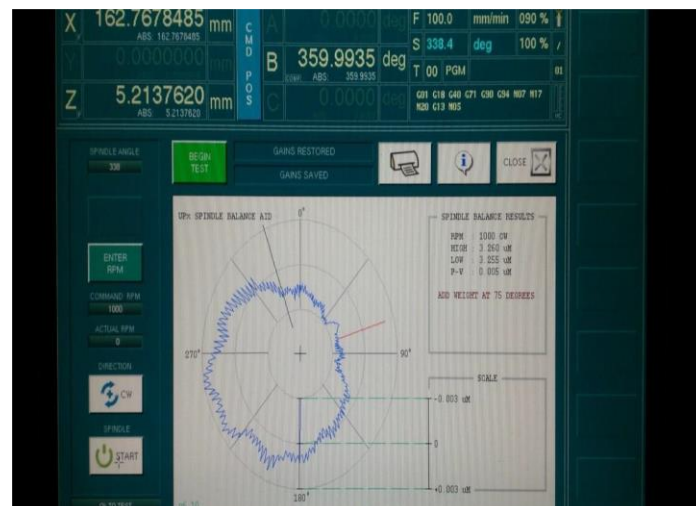
Figure 3.16: Spindle balancing platform DIFFSYS

- Before the main experiment was performed, the workpiece was "face-cleaned". The importance of face cleaning is to remove impurities on the surface of the workpiece to get clear and consistent results when the main cutting commenced. During the face turning, the AE sensor position was verified to determine whether there were actual magnitude and frequency that were different from random noise.

- Machining tests were conducted according to parameter combinations (DOC, feed rate, and speed) specified by Box-Behnken design of experiment. Odourless kerosene mist and water were used as the cutting fluid. These fluids were applied separately for each run.

- At each run, the acoustic emission signal was observed and recorded on the computer through LabVIEW software. To have enough sample measurement and capture of AE data, the software was programmed with 100 samples to read at a rate of 1000Hz. The data were acquired and saved LVM file format, which was then converted to an excel format for analysis.

- After each run, the adapter together with the workpiece was removed from the spindle and taken to the profilometer for surface roughness measurement.

- The same cutting tool was used throughout the cutting pass.

Chapter Four

4.0   Results and discussion

4.1   Introduction

In this chapter, the first section gives a detailed report on the experimental results of SPDT of RSA 431. The surface roughness results of machining process when kerosene mist is used as cutting fluid were further compared with the results of water as cutting fluid. The second section explains the application of response surface methodology (RSM) to develop a response surface model used for predicting the surface roughness values and to investigate the influence of machining parameters on the developed models, validation of models and optimisation.

Acoustic emission and extracted features were highlighted in the previous chapter. AE models were developed using RSM and the relationship between AE and machining parameters was investigated. Time-domain features from acoustic emission raw data were extracted and analysed. In the last section, an artificial neural network (ANN) approach was employed for training and testing selected features to predict surface roughness values. The analysis in this chapter was made possible using Design-Expert 10, Excel, Matlab, Minitab and LabVIEW.

4.2   Surface roughness experimental results

The importance of surface roughness cannot be over-emphasized. It determines the quality, integrity and productivity of a machined surface. The surface roughness is a key factor as it influences functional properties such as light reflection, corrosion resistance, lubrication retentiveness, tolerance and so on.

Consequently, there is a need for optimisation of cutting parameters to improve the quality of the product through surface roughness. With regards to previous research on aluminium turning [171, 172], it was observed that feed is the most significant factor of all the cutting parameters affecting surface roughness. As the feed increases, the surface roughness also increases.

For this research, two sets of experiments were carried out on SPDT of RSA-431. The workpiece material was diamond-turned using kerosene mist and water respectively as cutting fluid for each

turning process. The experiments were performed according to a set of input parameter combinations (as shown in Table 4.1) provided by Box-Behnken design. Depth of cut, feed and speed were selected to establish the relationship between surface roughness and machining parameters.

An acoustic emission signal was acquired during each run of turning and after each experiment, the surface roughness of the machined surfaces was measured using Taylor Hobson PGI Dimension XL surface profilometer and the values were recorded. The surface roughness values measured as output parameters (responses) for the 15 runs of each experiment. Table 4.2 (a-b) shows the surface roughness of diamond-turned RSA 431. Experiment 1 represents the diamond turning of RSA 431 using kerosene mist as cutting fluid. On the other hand, experiment 2 represents the diamond turning of RSA 431 using water as cutting fluid. The parameter used for surface roughness evaluation on the surface profilometer is average roughness (R_a). This is the arithmetic average of the value of peaks and valleys of the roughness profile.

Table 4.1: (a) Surface roughness values of diamond-turned RSA 431 for experiment 1

Experiment Number	Depth of Cut, d (µm)	Feed, f (mm/min)	Speed, v (rpm)	Surface roughness, R_a (nm)
1	25	25	1375	27
2	25	5	1375	12
3	25	15	750	25
4	15	25	750	50
5	25	15	2000	16
6	5	15	2000	13
7	15	15	1375	13
8	5	5	1375	10
9	15	5	2000	9
10	15	25	2000	15
11	15	15	1375	13
12	5	15	750	19

13	15	5	750	12
14	15	15	1375	13
15	5	25	1375	17

Table 4.2: (b) Surface roughness values of diamond-turned RSA 431 for experiment 2

Run Order	Depth of Cut, d (µm)	Feed, f (mm/min)	Speed, v (rpm)	Surface roughness, R_a (nm)
1	25	25	1375	17
2	25	5	1375	11
3	25	15	750	19
4	15	25	750	40
5	25	15	2000	11
6	5	15	2000	12
7	15	15	1375	13
8	5	5	1375	9
9	15	5	2000	8
10	15	25	2000	14
11	15	15	1375	13
12	5	15	750	17
13	15	5	750	12
14	15	15	1375	13
15	5	25	1375	14

Figure 4.1: Series plot of surface roughness for experiment 1
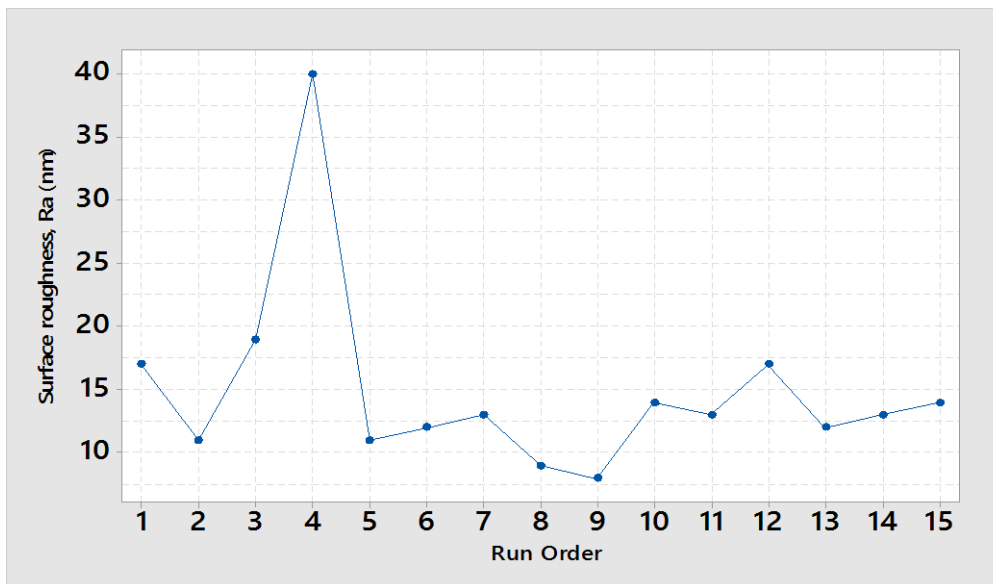
Figure 4.2: Series plot of surface roughness for experiment 2

Figure 4.1 and 4.2 show the series plot chart of the variation of measured surface roughness with a change in the combination of cutting parameters. The best and worst measured surface roughness of RSA 431 for each experiment is presented. Experiment 2, with water as cutting fluid, gives a better surface roughness value when compared to experiment 1 with kerosene mist as cutting fluid.

106
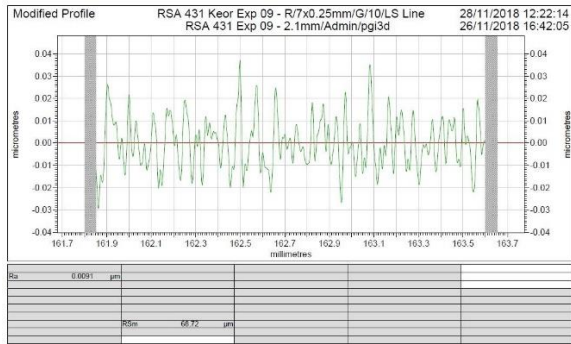
Surface profile chart for Ra 9nm
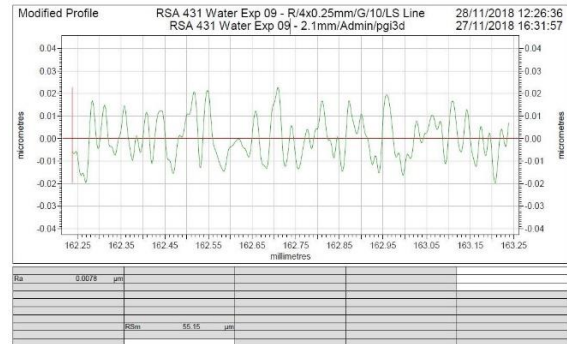
Surface profile chart for Ra 8nm
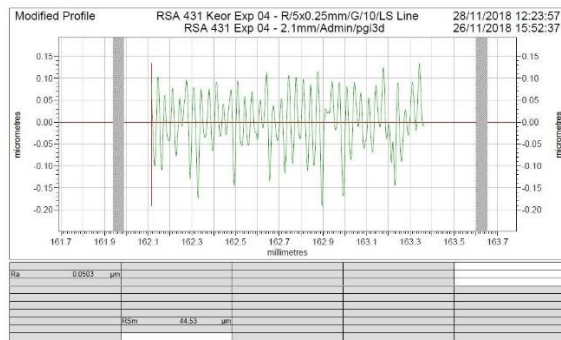
Surface profile chart for Ra 50nm
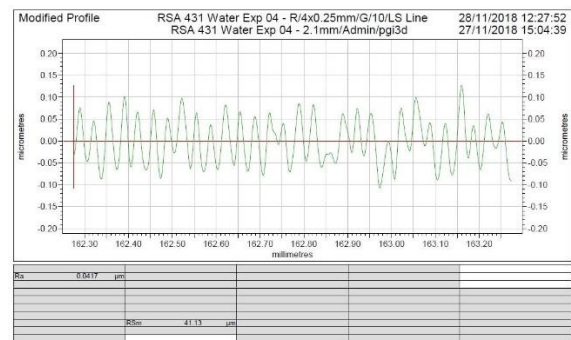
Surface profile chart for Ra 50nm

Figure 4.3: Surface profile chart for Ra 40nm

The minimum roughness, which is the best, for each experiment occurred at run order 9, while the maximum roughness, considered as the worst, occurred at run order 4. Figure 4.3 depicts the surface profile for the measured surface roughness of experiment 1 and 2. A minimum roughness value of 9 nm for experiment 1 and 8 nm for experiment 2 was recorded at feed of 5 mm/min, DOC of 15 μm and high speed 2000 rpm. Moreover, the maximum roughness value of 50 nm for and 40 nm for experiment 2 occurred at feed 25 mm/min, DOC of 15 μm and speed of 750 rpm. Other better roughness values occur at the low/medium level of feed and a high/medium level of speed. These suggest that feed and speed influence the surface roughness of RSA-431, although feed plays a more significant role. It also confirms previous conclusions that the best values of surface roughness are recorded at the maximum cutting speed [173].

The main effects plots for means in experiment 1 and 2 are shown in Figure 4.4 (a-b), which support the findings. Main effect plot can be used to determine the best combination of cutting

parameters (depth of cut, feed, and speed) that can result in the best surface roughness. The variation of response with the considered cutting parameters is revealed in the plot.

From the plot, the x-axis represents the value of each cutting parameter and the y-axis represents the surface roughness as the response value, the reference (horizontal) line represent the overall mean of the response. Since the factor lines are not parallel to the x-axis, then we can say that each level of the cutting parameter affects the response differently. This is revealed in the plot, as minimum R_a is recorded at high speed, low depth of cut and feed.
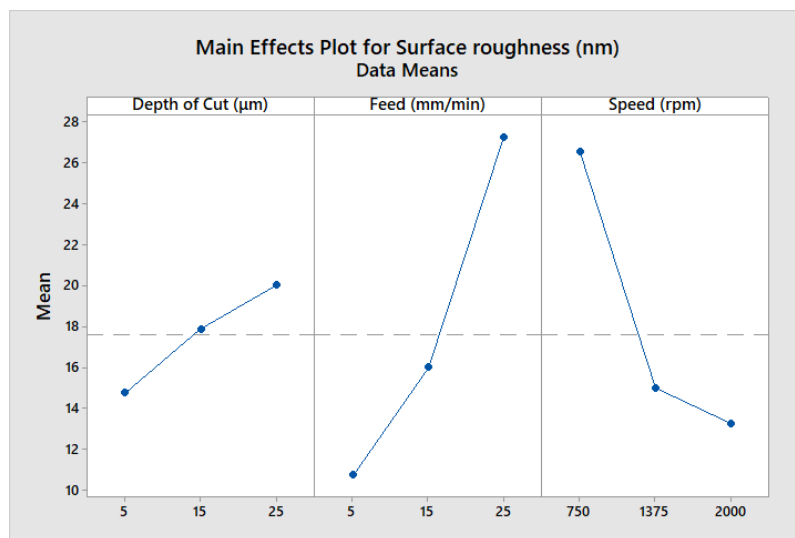
(a)
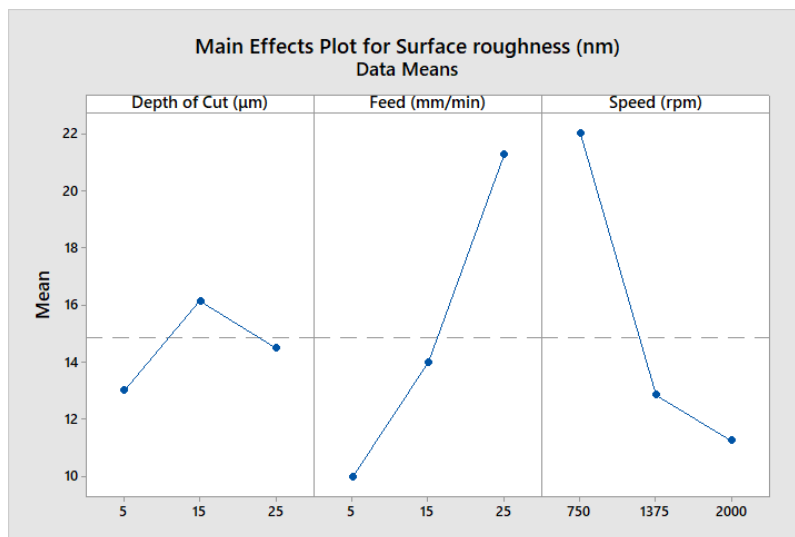
(b)

Figure 4.4: Main effects plot for Ra in (a) experiment 1 (b) experiment 2

From Figure 4.4 (a), it can be observed that the plot is in an increasing trend. As the depth of cut increases from 5 μm to 25 μm, the surface roughness increases. This means for machining with kerosene mist as cutting fluid, the surface roughness is smoother when the depth of cut is low. In experiment 2, the plot shows a similar trend, although inconsistency was noticed on surface roughness. Notably, there is a sharp decrease when the depth of cut increases from 15 μm to 25 μm. This might be due to some errors or disturbance during the cutting process. At higher feed, the effects plot for experiment 1 and 2 reveals that surface roughness deteriorates. Finally, the relationship between cutting speed and surface roughness is inversely proportional as shown in the Figure 4.4 (a-b), increase in speed causes roughness to decrease

4.3   Statistical analysis of surface roughness

4.3.1   Response surface modelling approach

In the machinability study of materials, statistical design of experiments (DOE) is required and must be done comprehensively. The statistical design of an experiment is referred to as the process of planning and executing an experiment to obtain appropriate results. These results are then analysed to make an objective and valid conclusion.

RSM, discussed earlier in the previous, has also been adopted. It is a statistical method used for modelling and analysing engineering problems [174] with the main aim of optimising the response surface influenced by various process parameters. RSM exclusively makes use of a regression method, which involves fitting the response into a polynomial model for the analysis of this response.

Considering RSM for modelling and analysing, selection of independent variables, their levels and proper experimental design are consequential. The understanding and evaluation of contributing parameters and their interaction with one another to bring about the best response or responses is the main advantage of adopting RSM. RSM design procedures used in analysing is as follows;

> i.   Select the factors to be involved in the process and choose the levels of these factors.

ii. Conduct experiments at all possible factor level combinations randomly that satisfy adequate and reliable measurement of desired response(s).

iii. Collect the results and analyse data using analysis of variance (ANOVA).

iv. Develop a mathematical model of the second-order response surface with the best fittings.

v. Validate the model.

vi. Determine the optimal set of experimental values that can produce the minimum and maximum value of the response.

RSM is used to quantify the relationship between the measured response (roughness, R_a) and the process parameters (d, f, V). R_a is a function of the process parameters and can be expressed mathematically as"

$$R_a = \varphi(V, f, d) + \varepsilon \tag{4.1}$$

Where ε is the observed error in the response.

This existing relationship can be investigated statistically using the regression equation. Regression is performed to describe the acquired data by which an observed, empirical variable (response) is approximated based on a functional relationship between the response surface, y, and the input variables, $x_1, x_2, \ldots x_n$. The regression equation is formulated based on the relation, as shown in equation 4.2:

$$y = \beta_0 + \sum_i^k \beta_i x_i + \sum_{i=1}^k \beta_i x_i^2 + \sum \sum_{i<j} x_i x_j + \varepsilon \tag{4.2}$$

Where y is the output (roughness, R_a), x is the input variables (V, f, d), β_0 is the constant coefficient, ε is the random error. ($\beta_1, \ldots \beta_k$), ($\beta_{11}, \ldots \beta_{kk}$), and ($\beta_{12}, \beta_{13}, \ldots$) are the linear, quadratic and interacting compounds respectively. Equation (4.1) can be re-written as;

$$y = \beta x + \varepsilon \tag{4.3}$$

Where $y = \begin{bmatrix} y_1 \\ y_2 \\ \vdots \\ y_k \end{bmatrix}, x = \begin{bmatrix} 1 & x_{11} & x_{12} & \cdots & x_{1k} \\ 1 & x_{21} & x_{22} & \cdots & x_{2k} \\ \vdots & \vdots & \vdots & \vdots & \vdots \\ 1 & x_{12} & x_{12} & \cdots & x_{12} \end{bmatrix}, \beta = \begin{bmatrix} \beta_o \\ \beta_1 \\ \vdots \\ \beta_k \end{bmatrix}, \varepsilon = \begin{bmatrix} \varepsilon_1 \\ \varepsilon_2 \\ \vdots \\ \varepsilon_k \end{bmatrix}$

4.3.1.1 Normality test and transformation

Adequate statistical analysis and modelling require checking the normality of data. Most statistical tests and intervals are based on the assumption of normality, this makes the tests simple, accurate and mathematically tractable. To check whether the experimental data is normally distributed, probability tests (Figure 4.5 (a-b)) were plotted using Anderson-Darling's test for normality. Anderson-Darling's test is a powerful statistical test for normal distribution, it is more precise, especially in the outer parts of the distribution and gives more weight to the tails than other tests.
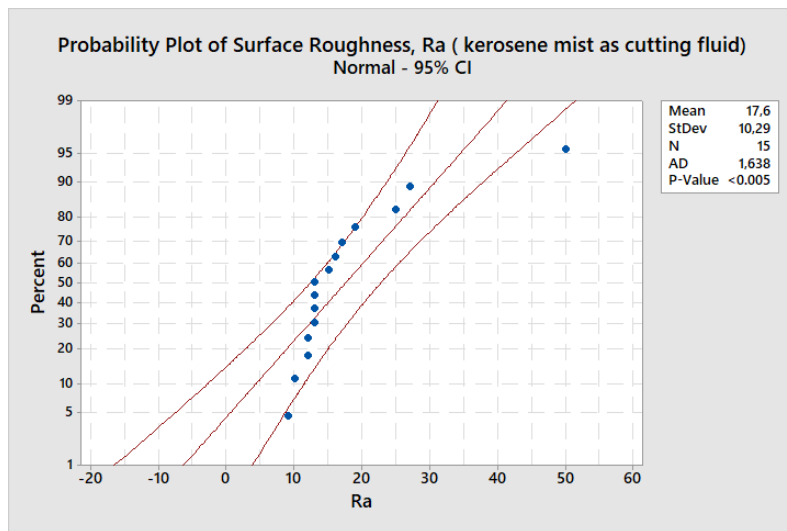
(a)
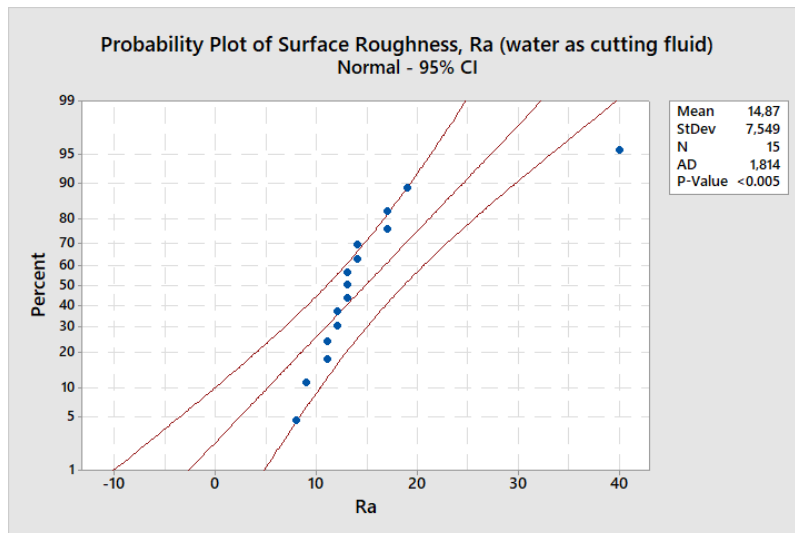
(b)

Figure 4.5: Normal Probability plot for (a) experiment 1 (b) experiment 2

In a normality test, a p-value that is greater or equal to 0.05 (≥ 0.05) is considered normal. If the p-value is greater than 0.05, the researcher fails to reject the null hypothesis (H_o). From the probability plot above, the p-value for the two sets of experiments is less than 0.05 (< 0.05). Further examination of the graph indicates that the data points are not relatively close to the fitted normal distribution line (the middle solid line of the graph). There is enough evidence to conclude that the data set for the two experiments do not follow a normal distribution, therefore it is imperative to transform the data sets.

The appropriate transformation of the data set into normality can be carried out using Box-cox transformation. In this type of transformation, the distributional shape of a set of data is modified to be more normally distributed to ensure suitable use of tests and confidence limits that require normality. In the research analysis, the Box-Cox plotting technique from Design-Expert is used for the selection of transformed scale model.
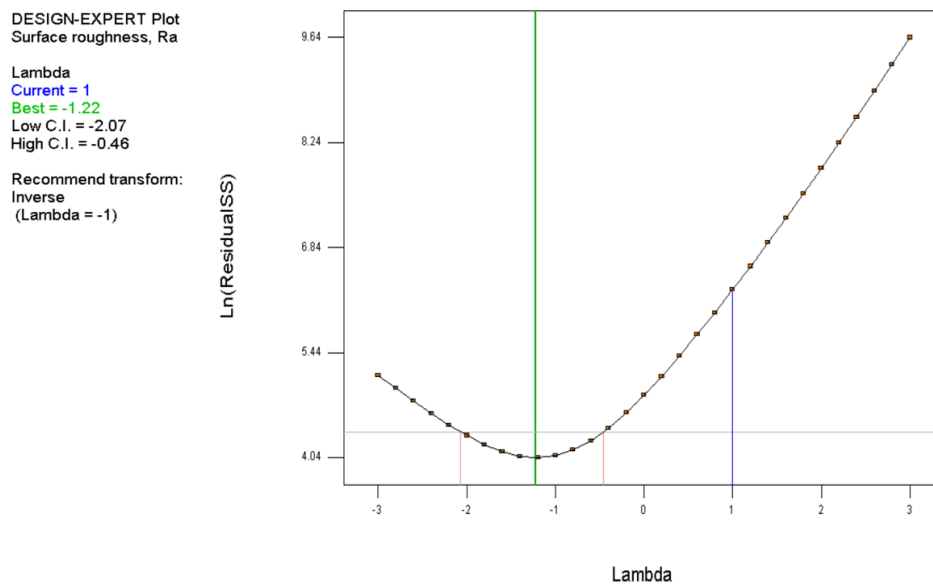
(a)

DESIGN-EXPERT Plot
Surface roughness, Ra

Lambda
Current = 1
Best = -1.1
Low C.I. = -1.81
High C.I. = -0.48

Recommend transform:
Inverse
(Lambda = -1)
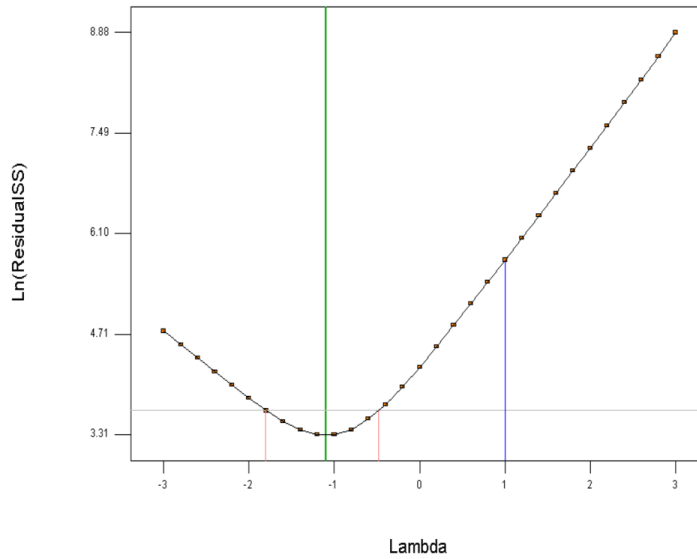
(b)

Figure 4.6: Box-Cox plot "before" transformation for (a) experiment 1 (b) experiment 2

From the Box-cox plots (Figure 4.6 a-b), it was observed that the lambda, λ values are not within the limits of the confidence interval (the two red lines). Therefore, the inverse transformation was recommended to improve the analysis. The transformation is in a model form of:

$$y' = \frac{1}{y + k}$$

(4.4)

Where k is the constant and is kept at 0. Figure 4.7 and 4.8 present a transformed Box-Cox plot of R_a model. The lambda, λ value of data sets for each experiment is now within the confidence level and the difference between the current lambda and best value is low. The transformation has also improved the data set.

DESIGN-EXPERT Plot
1.0/(Surface roughness, Ra)

Lambda
Current = -1
Best = -1.3
Low C.I. = -2.66
High C.I. = -0.16

Recommend transform:
Power
(Lambda = -1.3)

Ln(ResidualSS)

Lambda
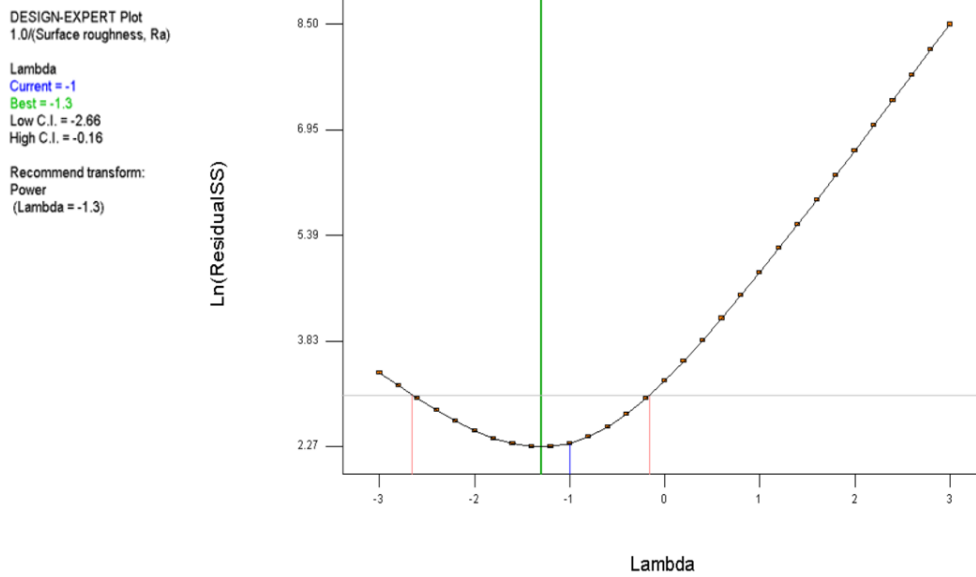
Figure 4.7: Box-Cox plot of R_a model after transformation for experiment 1

DESIGN-EXPERT Plot
1.0/(Surface roughness, Ra)

Lambda
Current = -1
Best = -1.1
Low C.I. = -1.81
High C.I. = -0.48

Recommend transform:
Inverse
(Lambda = -1)

Ln(ResidualSS)

Lambda
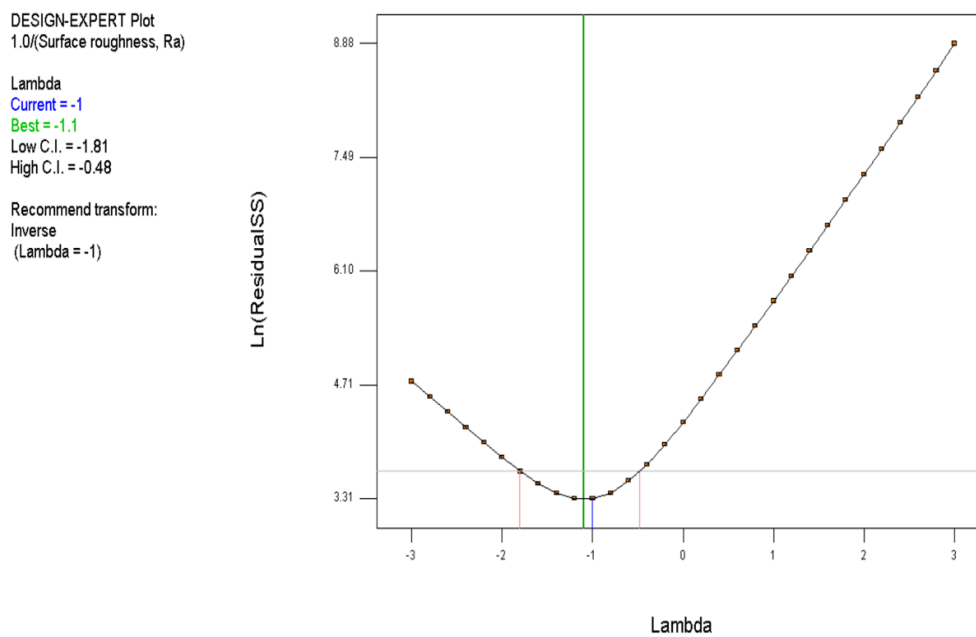
Figure 4.8: Box-Cox plot of R_a model after transformation for experiment 2

Figure 4.9 and 4.10 confirm the normality of the data set after transformation with p-values of 0.564 and 0.430 for experiment 1 and 2 respectively. Accuracy or acceptance of the experiment is decided by the distribution of the response points around the straight line. The p-values are greater

114

than the significance level of 0.05, thus, it can be concluded that data for the two experiments do follow a normal distribution [175].
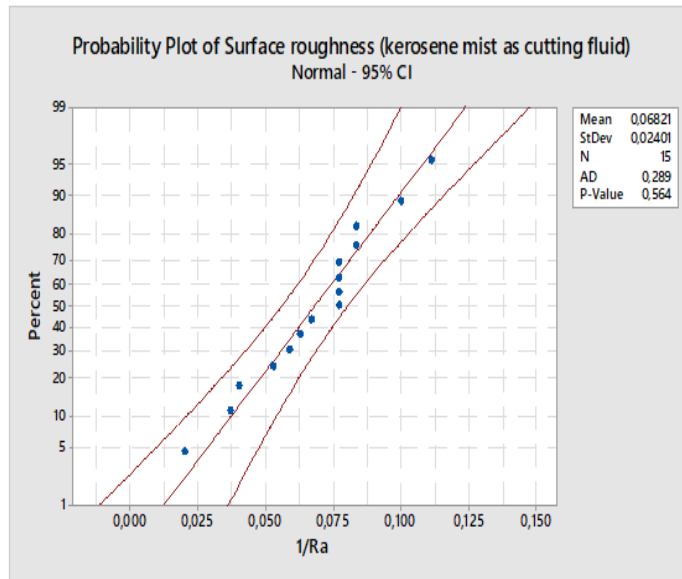
Figure 4.9: Normal probability plot for experiment 1 after transformation.
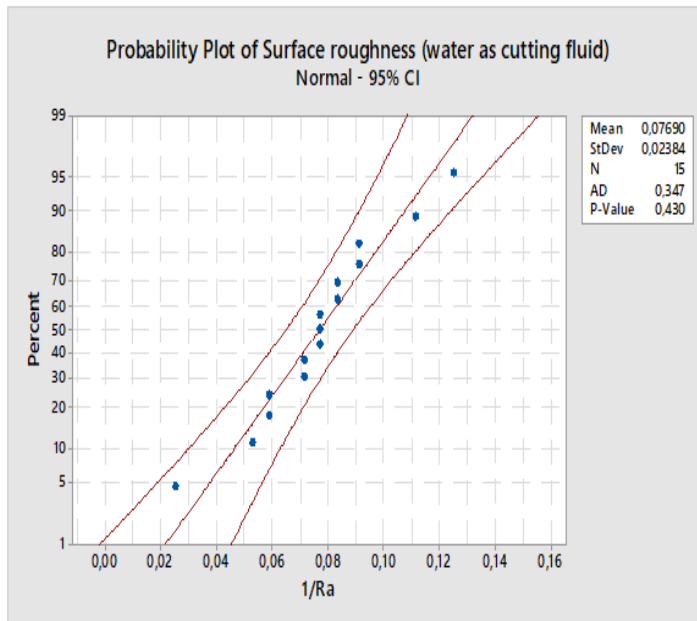
Figure 4.10: Normal probability plot for experiment 2 after transformation.

Table 4.3 (a-b) presents the result of the quadratic response model fitting for the two experimental data in the form of sum of squares sequential model. Moreover, the adequacy of the model was tested through the lack of fit test (Table 4.4 (a-b)). The result of the sequential model suggests

115

linear vs. mean and quadratic vs. 2FI approach for experiment 1. While linear vs. mean is suggested for experiment 2. The cubic model has been aliased in the fit summary of both experiments, this implies that the effects of each variable that caused different signals to become indistinguishable, cannot be considered.

In this study the significance level of $\alpha = 0.05$ is used, that means results are valid for a confidence level of 95%. The lack of fit is the variation of data in a fitted model. Lack of fit for the models can be said to be insignificant, it is projected that lack of fit is insignificant for the model to fit. The R² value (0.9798) of the quadratic model for experiment 1 (Table 4.5a) is closer to 1, although the linear model is also suggested for this experiment, it has a lower R^2 and adjusted-R^2 (0.8847 and 0.8532) values when compared to the quadratic model. The linear model came out best in experiment 2 model summary (Table 4.5b) due to the low standard deviation (Std. Dev. = 0.0084), high R^2 value (0.9033), and a low PRESS (0.0016).

Table 4.3: (a) Sequential Model Sum of Squares of R_a for experiment 1

Source	Sum of Squares	df	Mean Square	F-value	p-value	
Mean vs. Total	0.0698	1	0.0698			
Linear vs. Mean	0.0071	3	0.0024	28.12	< 0.0001	Suggested
2FI vs. Linear	0.0001	3	0	0.3087	0.8187	
Quadratic vs. 2FI	0.0007	3	0.0002	6.84	0.0321	Suggested
Cubic vs. Quadratic	0.0002	3	0.0001			Aliased
Residual	0	2	0			
Total	0.0779	15	0.0052			

Table 4.3: (b) Sequential Model Sum of Squares of R_a for experiment 2

Source	Sum of Squares	df	Mean Square	F-value	p-value	
Mean vs. Total	0.0887	1	0.0887			
Linear vs. Mean	0.0072	3	0.0024	34.26	< 0.0001	Suggested
2FI vs. Linear	0.0001	3	0	0.2565	0.8547	

Quadratic vs. 2FI	0.0003	3	0.0001	1.07	0.4409	
Cubic vs. Quadratic	0.0004	3	0.0001			Aliased
Residual	0	2	0			
Total	0.0967	15	0.0064			

Table 4.4: (a) Lack of Fit Tests for surface roughness for experiment 1

Source	Sum of Squares	df	Mean Square	F-value	p-value
Linear	0.0009	9	0.0001		
2FI	0.0008	6	0.0001		
Quadratic	0.0002	3	0.0001		
Cubic	0	0			
Pure Error	0	2	0		

Table 4.4: (b) Lack of Fit Tests for surface roughness experiment 2

Source	Sum of Squares	df	Mean Square	F-value	p-value
Linear	0.0008	9	0.0001		
2FI	0.0007	6	0.0001		
Quadratic	0.0004	3	0.0001		
Cubic	0	0			
Pure Error	0	2	0		

Table 4.5: (a) Statistical summary for each model in experiment 1 analysis

Source	Std. Dev.	R^2	Adjusted R^2	Predicted R^2	PRESS	
Linear	0.0092	0.8847	0.8532	0.7811	0.0018	Suggested
2FI	0.0102	0.8966	0.8191	0.5674	0.0035	
Quadratic	0.0057	0.9798	0.9433	0.6761	0.0026	Suggested
Cubic	0	1	1		*	Aliased

Table 4.5: (b) Statistical summary for each model in experiment 2 analysis

Source	Std. Dev.	R²	Adjusted R²	Predicted R²	PRESS	
Linear	0.0084	0.9033	0.8769	0.7929	0.0016	Suggested
2FI	0.0094	0.9118	0.8456	0.5303	0.0037	
Quadratic	0.0092	0.9463	0.8495	0.1401	0.0068	
Cubic	0	1	1		*	Aliased

4.3.1.2 Analysis of variance (ANOVA) for response surface model

Analysis of variance (ANOVA) is a statistical tool used for investigating how model factors significantly affect the output response. The technique makes use of the sum of squares and F-statistics to analyse the processing parameters, measurement errors and uncontrolled parameters. An ANOVA table, as presented in Table 4.6 (a-b), shows the response surface quadratic model for surface roughness of experiment 1 and a linear model for surface roughness of experiment 2. The tables also present the summary of the test performed for the significance of the regression model, significance on individual model coefficient and test for lack of fit.

Table 4.6: (a) ANOVA table for the quadratic model (Experiment 1)

Response 1: Surface roughness, R_a

Transform: Inverse

Source	Sum of Squares	df	Mean Square	F-value	p-value	
Model	0.0079	9	0.0009	26.89	0.001	significant
A-Depth of Cut	0.0005	1	0.0005	16.42	0.0098	
B-Feed	0.0048	1	0.0048	145.85	< 0.0001	
C-Speed	0.0018	1	0.0018	56.23	0.0007	
AB	6.55E-06	1	6.55E-06	0.2006	0.673	
AC	8.02E-07	1	8.02E-07	0.0246	0.8816	
BC	0.0001	1	0.0001	2.73	0.1594	

A²	0.0003	1	0.0003	10.62	0.0225	
B²	0.0000	1	0.0000	0.7463	0.4271	
C²	0.0003	1	0.0003	9.60	0.0269	
Residual	0.0002	5	0.0000			
Lack of Fit	0.0002	3	0.0001			
Pure Error	0.0000	2	0.0000			
Cor Total	0.0081	14				

The ANOVA table of the quadratic model for experiment 1 (Table 4.6 (a)) shows the "p-value" for the model to be 0.001 (which is less than 0.05). This indicates the adequacy of the quadratic model and signifies that some model terms have a significant effect on the response. The main effect of depth of cut (A), feed (B), speed (C), and the second-order effect of depth of cut (A^2), speed (C^2) are the significant model terms. Other terms can be concluded to be insignificant due to the high p-value. To improve the model, these insignificant terms can be eliminated.

The backward elimination procedure was selected to automatically reduce the insignificant model terms. This procedure starts by selecting a significance level, fit the model with all possible independent variables, after which the variable with the highest p-value is considered. If the p-value is greater than the significance level, such a variable is considered insignificant and removed. The resulting ANOVA for the modified quadratic model for surface roughness of experiment 1 is shown in Table 4.6 (b). The result shows that the model is still significant with an improved F-value of 49.29 and it also shows there is a 0.01% chance that an F-value this large could come about due to noise.

Table 4.6: (b) ANOVA for the modified quadratic model (Experiment 1)

Response 1: Surface roughness, R_a

Transform: Inverse

Source	Sum of Squares	df	Mean Square	F-value	p-value	
Model	0.0078	5	0.0016	49.29	< 0.0001	significant
A-Depth of Cut	0.0005	1	0.0005	16.98	0.0026	significant

B-Feed	0.0048	1	0.0048	150.86	< 0.0001	significant
C-Speed	0.0018	1	0.0018	58.16	< 0.0001	significant
A²	0.0004	1	0.0004	11.51	0.008	significant
C²	0.0003	1	0.0003	10.42	0.0104	significant
Residual	0.0003	9	0			
Lack of Fit	0.0003	7	0			
Pure Error	0	2	0			
Cor Total	0.0081	14				

The linear model is suggested for the surface roughness of experiment 2. The ANOVA linear model is presented in table 4.7. The model F-value of 34.26 indicates that the model is significant and there is a 0.01% chance that an F-value this large could come about due to noise. The model terms are considered significant, their p-value is less than 0.05 (α - value). Although the p-value of "depth of cut" is greater than 0.05, it is considered significant and cannot be eliminated from our model terms because it is required to support hierarchy in the model. Moreover, DOC is always required during the turning process.

Table 4.7: ANOVA table for the linear model (Experiment 2)

Response 1: Surface roughness, R_a

Transform: Inverse

Source	Sum of Squares	df	Mean Square	F-value	p-value	
Model	0.0072	3	0.0024	34.26	< 0.0001	significant
A-Depth of Cut	0.0001	1	0.0001	1.77	0.2109	
B-Feed	0.0042	1	0.0042	60.31	< 0.0001	significant
C-Speed	0.0028	1	0.0028	40.7	< 0.0001	significant
Residual	0.0008	11	0.0001			
Lack of Fit	0.0008	9	0.0001			
Pure Error	0	2	0			
Cor Total	0.008	14				

Table 4.8: ANOVA summary for experiment 1 and 2

	Experiment 1 Values	Experiment 2 Values		Experiment 1 Values	Experiment 2 Values
Std. Dev.	0.0056	0.0084	R²	0.9648	0.9033
Mean	0.0682	0.0769	Adjusted R²	0.9452	0.8769
C.V. %	8.24	10.87	Predicted R²	0.8881	0.7929
PRESS	0.0009	0.0016	Adeq Precision	22.2587	19.3691

Table 4.8 shows the Summary of the regression coefficient for the response of experiment 1and 2. The summary table demonstrates the significance of the models using a desirable high R-squared (R^2) value for the model that is close to 1 (0.9648 and 0.9033) It indicates 96.48% and 90.33% of the total variations are explained by the models, these high percentage accuracies support the claim that the experimental data fit well into the model.

The "Predicted R-squared" value of each response is in reasonable agreement with the "Adjusted R-squared" value, the difference between these two values is expected to be less than 0.2 to confirm the significance of the model. "Adeq Precision" measures the signal to noise (S-N) ratio, generally, a ratio greater than 4 is desirable for the model to be effectively used. The obtained ratios of 22.2587 and 19.3691 for each experiment indicate the adequacy of the selected model's experimental data.

Generally, the "R^2" value and "adjusted R^2" value are the major statistical parameters used to determine the fitness of a model. The coefficient of variation (CV), which remains at a relatively low value, is also an indication of precise and reliable experimental results.

4.3.1.3   Regression model

Models can be described as an abstract system, similar to the real system in terms of key properties and characteristics. Models can be employed for investigation, calculation, explanation and demonstration purposes, which would otherwise be too expensive or not possible. These models are useful in the academic field, and in industries to help improve machine performance and

ultimately reduce the cost of production. With a model, important machine performance such as roughness, cutting forces, temperatures, chip morphology, strains and stresses can be calculated before the actual cutting is carried out on a machine tool.

The correlation between the factors, depth of cut, feed, cutting speed and the measured surface roughness of both experiments was obtained by regression, predictive modelling. The obtained regression model equations for both experiments are as follows:

$$R_a = (0.026242 + 0.002149d - 0.002441f + 0.000091v - 0.000099d^2$$
$$- 0.000000024v^2)^{-1} \tag{4.5}$$

$$R_a = (0.075739 - 0.000393d - 0.002296f + 0.000030v)^{-1} \tag{4.6}$$

Where d is the depth of cut in μm, f is the feed rate in mm/min, v is the cutting speed in rpm and, R_a is the surface roughness in nm. Equation (4.5) is the final model to determine the surface roughness for RSA-431 with kerosene mist as cutting fluid, while equation (4.6) is the final model to determine the surface roughness for RSA-431 with water as the cutting fluid.

The model presented by equation (4.5) provides evidence that as the cutting speed increases, the surface roughness decreases. However, at a significant increase, the negative coefficient of speed squared term (v2) would come into effect and increase the surface roughness. An increase in the depth of cut will have similar effects on surface roughness as cutting speed does, although, the squared term will have a quicker effect on surface roughness at lower values. That is, at the initial stage the depth of cut would decrease surface roughness to an extent after which the surface roughness starts to increase. Feed rate has a direct effect on the surface roughness -as it increases so does surface roughness.

A good model needs to be adequately checked for accuracy. Further analysis was carried out on the RS model by comparing the predicted and experimental surface roughness (Figure 4.11 to Figure 4:14). The results from the plots confirm the suitability of the proposed models for predicting surface roughness of RSA-431. It is observed that the predicted and the measured roughness are comparatively close.

The R-squared value of 0.9 which is close to 1 signifies a good model. Percentage errors show how much error occurred in an experiment. A small percentage error signifies how close the measured and predicted values are and vice versa. In the percentage error plot (Figure 4.15 and Figure 4.16) for both experiments, an error with high percentage was discovered during run order 4, and this could be as a result of machine parameter combination (speed of 750rpm, feed of 25mm/min and DOC of 15μm) chosen.
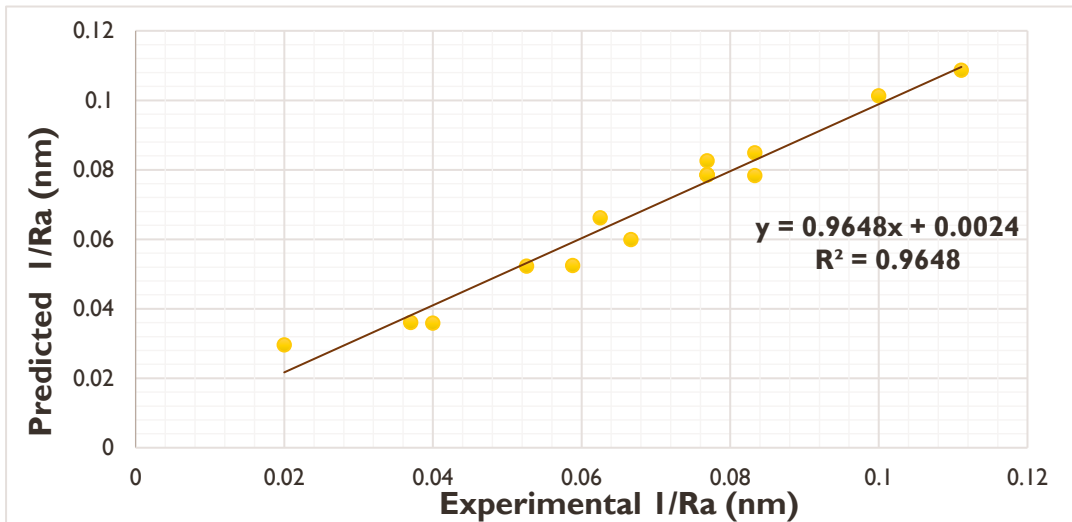
Figure 4.11: Data visualization for experiment 1 (kerosene mist as cutting fluid)
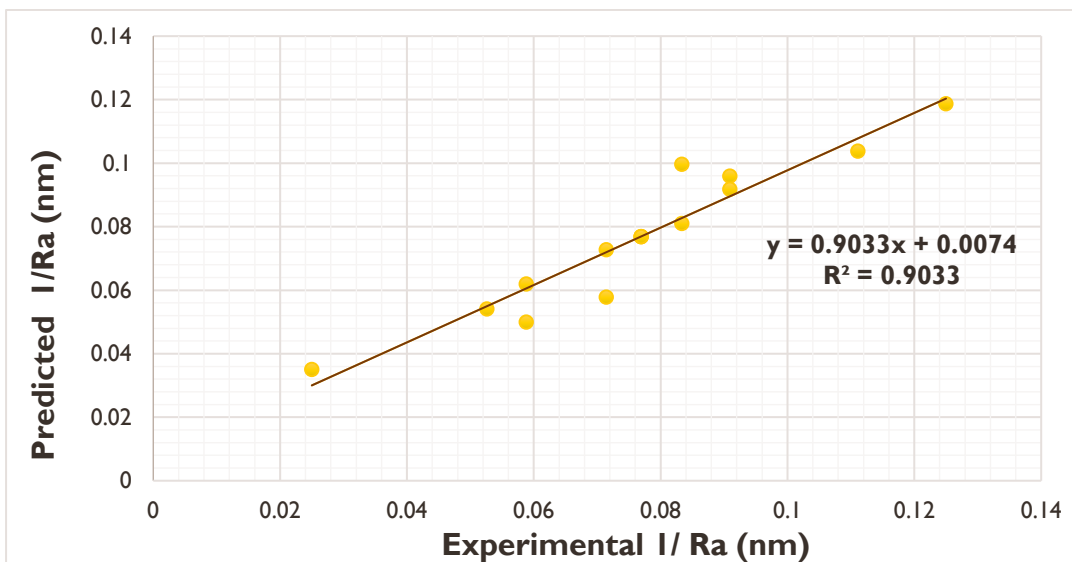
Figure 4.12: Data visualization for experiment 2 (water as cutting fluid)

Figure 4.13: Comparison of measured and predicted surface roughness of the RS model 1

Figure 4.14: Comparison of measured and predicted surface roughness of the RS model 2
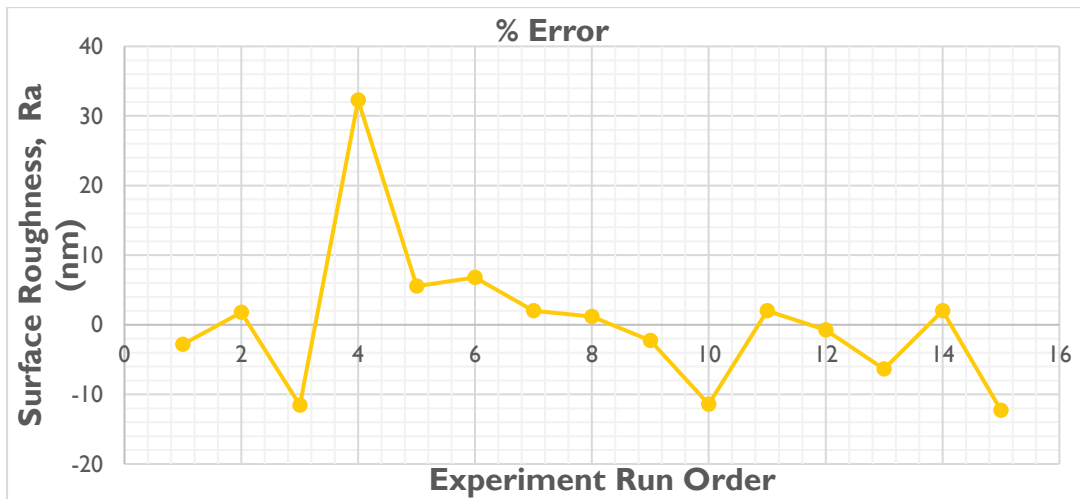
Figure 4.15: Plot of % error for experiment 1
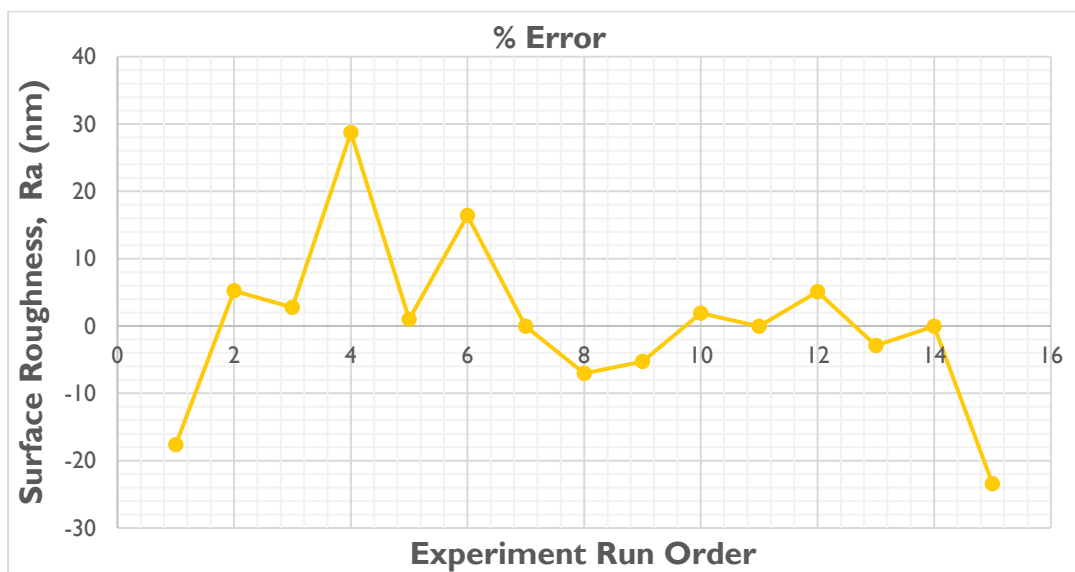
Figure 4.16: Plot of % error for experiment 2

4.3.1.4   Diagnosis of statistical properties of the model

For better understanding and verification of the effect of the factors on the response surface, the model is further analysed. Design-Experts software was used to obtain the normal probability plot of the residuals and the plots of the residuals versus the predicted response for surface roughness. Residuals help to determine the degree to which a model satisfies the assumptions of ANOVA.

Figure 4.17 and Figure 4.18 illustrate the normal probability plot of the studentized residuals. Normal probability is the most important diagnostic that checks for normality of residuals.

Studentized residual is recommended because it offers an alternative basic idea for identifying outliers. A rare chance of occurrence within a given data set is known as an outlier and if not detected and handled properly, it can distort predictions and affect the accuracy.

The plots reveal that the residuals follow a normal distribution. This conclusion is made based on the fact that the residuals emerge generally on a straight line, suggesting that the error is normally distributed [175]. Definite patterns like an "S-shaped" curve would require a response transformation for better analysis. Figure 4.19 and Figure 2.20 present plots of the residual versus the ascending predicted response values. In this type of diagnostic plot, the assumption of constant variance is tested. The plots show randomly scattered points, which indicate a constant range of residual across the graphs.

Figure 4.17: Normal Probability plot of residuals in R_a modelling for experiment 1
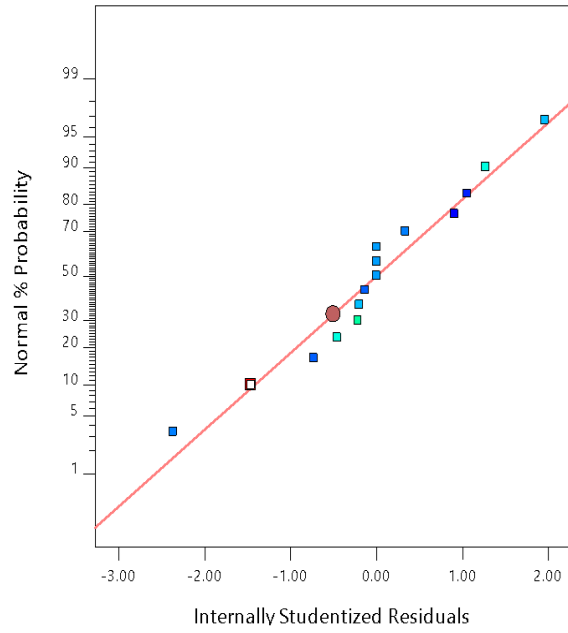
Figure 4.18: Normal Probability plot of residuals in R_a modelling for experiment 2
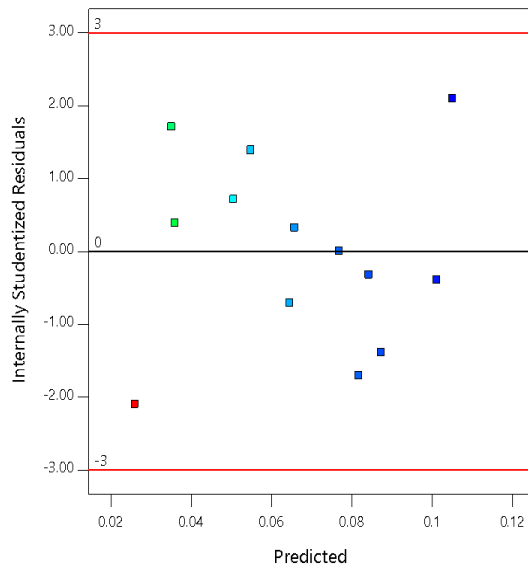
Figure 4.19: Plot of residuals vs. predicted response for experiment 1 R_a data

Figure 4.20: Plot of residuals vs. predicted response for experiment 2 R_a data

Residuals versus run order plot can also be used to determine how well the model fits experimental data, by verifying the assumption that the residuals are independent of one another. Independent residuals display a graph with no trends or pattern when plotted against a run order. Patterned points may indicate that residuals are correlated. Figure 4.21 to Figure 4.22 shows that the residuals are independent because residuals on the plots fall randomly around the centre-line.
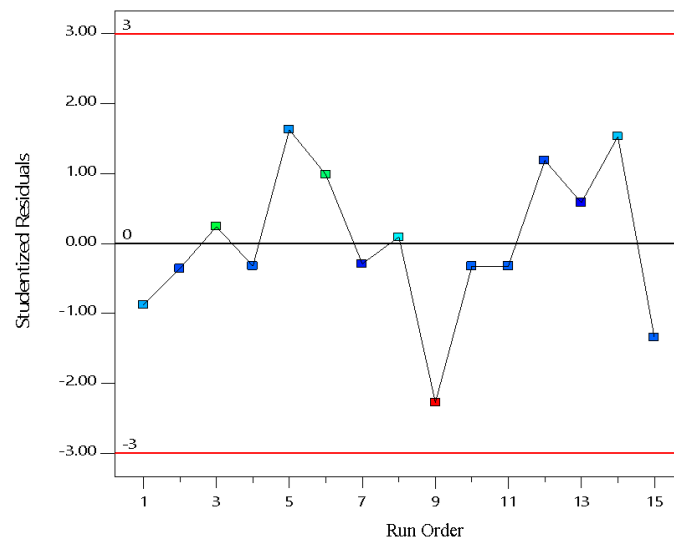
Figure 4.21: Plot of residuals vs. run order for experiment 1 R_a data

128
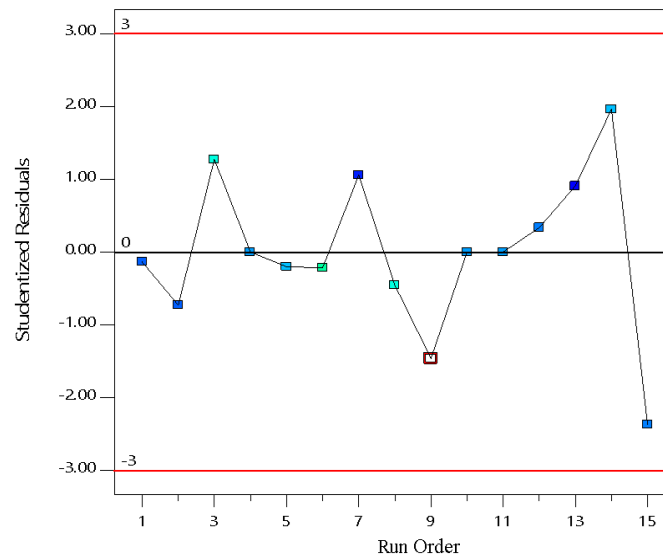
Figure 4.22: Plot of residuals vs. run order for experiment 2 R_a data

4.3.1.5 Influence of factors on the selected model

In this section, various graphs are used to interpret the model selected for the two experiments. The effect of all the factors at a point in the design space can be compared using the perturbation plot. The effect of each factor is considered by keeping the other variables constant. A perturbation plot shown in Figure 4.23 and Figure 2.24 for model 1 and 2 represent the comparison of the effect of selected cutting parameters at the midpoint (coded 0).

A curvature or steep slope of factors signifies the response that surface roughness is sensitive to all factors. Additionally, it is observed that the most influencing factor in both models on surface roughness is B (feed) as a result of its curvature in the perturbation plots. This is predictable because the effect of tool radius on surface roughness is greatly influenced by feed. This confirms the conclusion made by Khan *et al.* [176] that feed is a predominant factor in the surface roughness of machined surfaces. Besides this, speed is another close influencing factor but when compared to feed, the influence of speed (C) is less. The depth of cut (A) is the least affecting variable among the selected variables as indicated by the plots. The blunt edge of diamond cutting tool and the selected range of depth of cut (5 – 25 μm) may have contributed to this observation. Diamond tool is not impeccably sharp, therefore the tool engagement in terms of nose radius and rake angle cannot achieve a high material removal rate capable of compromising surface roughness [79, 177].

129
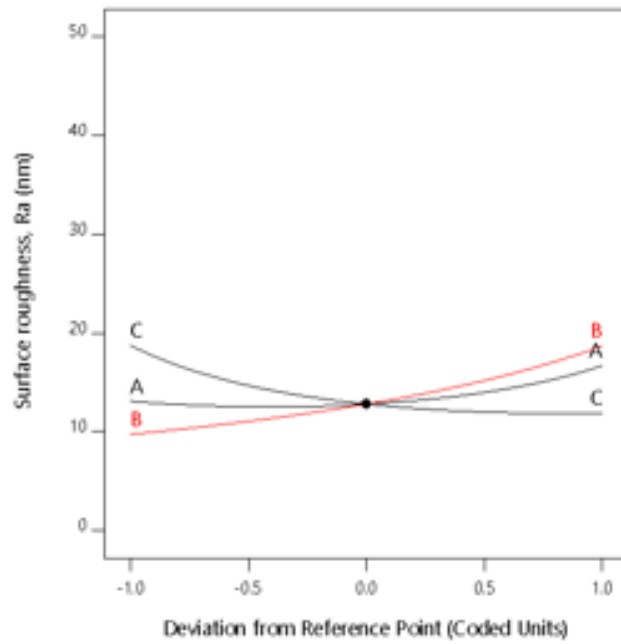
Figure 4.23: Perturbation plots for model 1 surface roughness in the original scale
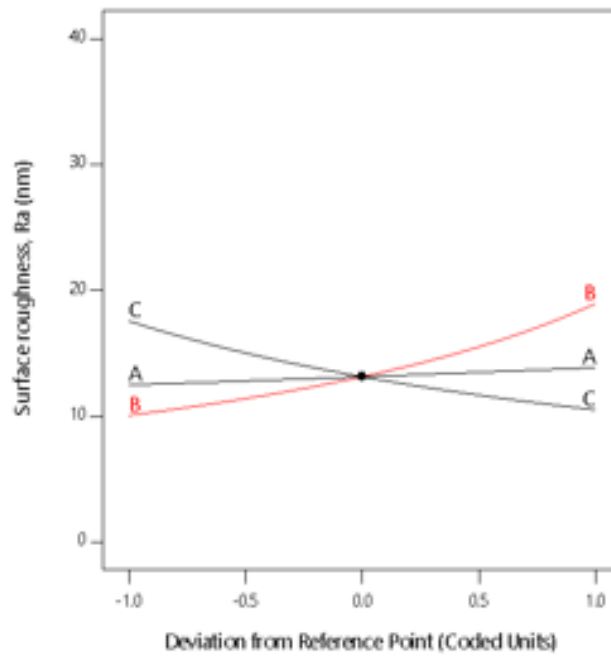
Figure 4.24: Perturbation plots for model 2 surface roughness in the original scale

4.3.1.5.1   Effect of depth of cut on surface roughness

Figure 4.25 (a) shows the effect of depth of cut on the transformed scale of surface roughness of model 1 (using kerosene mist as cutting fluid). The graph shows a negative curve, it can be seen

that as the depth of cut increases, inverse surface roughness also increases. However, as DOC increases to a certain level (12 µm), the inverse surface roughness takes a significant turn and starts to decrease. Figure 4.25 (b) depicts a negative linear relationship between the depth of cut of model 2 (using water as cutting fluid) and the inverse surface roughness. This relationship indicates that as the depth of cut increases, the inverse of surface roughness decreases, thereby increasing surface roughness.

(a)   (b)
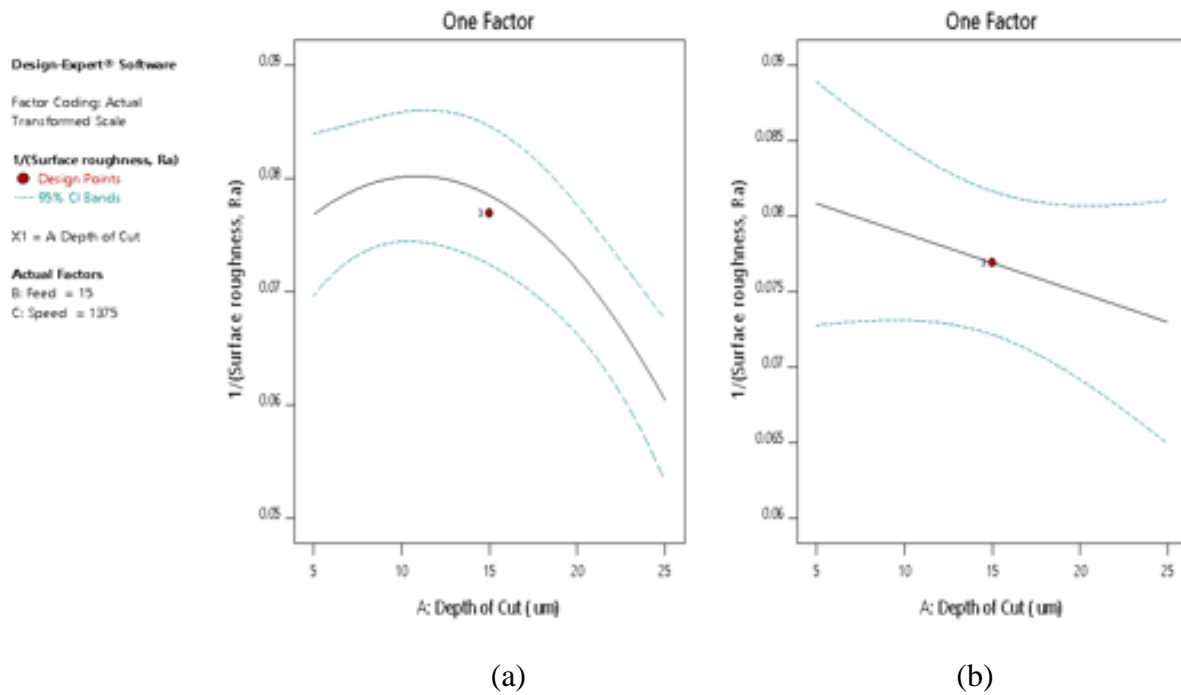
Figure 4.25: Variation of R_a with depth of cut for (a) model 1 (b) model 2

The observed influence of depth of cut on surface roughness corresponds with the main effects plot in Figure 4.4 (a-b) whereby depth of cut positively influence the surface roughness. This observation can be ascribed to the relationship between depth of cut and cutting force – at increased cutting depth, the width between the workpiece and cutting tool becomes wider and this leads to high friction. Besides, as the cutting force increases during machining, high chip deformation occurs which affects machined surface [178, 179]. Despite this fact, it is evident that this parameter does not show much significance on surface roughness (between 13 - 16 nm) compared to other parameters. This conforms with other researchers of various research works with different tool, machine process or material combination [180, 181].

4.3.1.5.2 Effect of feed on surface roughness

Figure 4.26 (a-b) shows a negative linear relationship between feed and the inverse of surface roughness. This implies that, when the feed is increased, the inverse surface roughness decreases linearly for both models, hence surface roughness increases as feed increases. This imitates other researcher's observation that at small feed, surface roughness is reduced [182]. At higher feed, there is a high amount of material deposits at the interface between the cutting tool and the workpiece surface.[114, 178]. These deposits are due to the incomplete removal of the workpiece material at higher feed rate, hence, more heat and friction which deteriorate the surface roughness is generated. Nonetheless, in SPDT or any precision machining, roughness starts to increase again as feed decreases below a certain critical value [41]. Feeding mechanism has the tendency of producing "stick-slip" motion at extremely low feed.

(a)   (b)
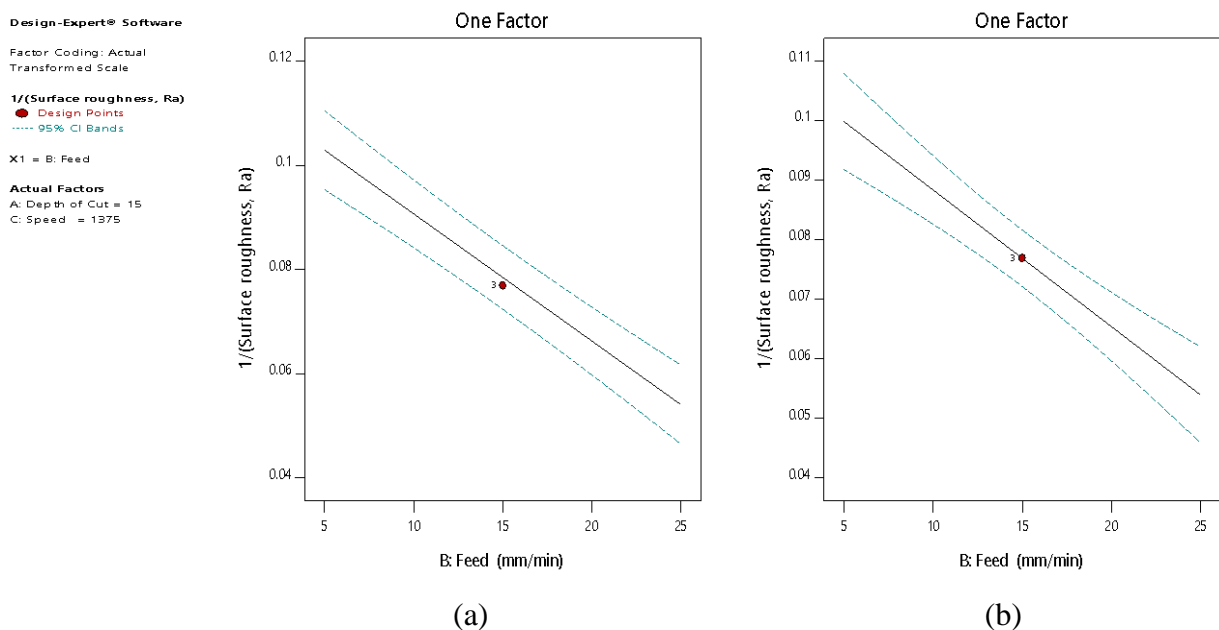
Figure 4.26: Variation of R_a with feed for (a) model 1 (b) model 2

4.3.1.5.3 Effect of speed on surface roughness

The relationship between speed and inverse surface roughness is in the form of the squared curve, as illustrated in Figure 4.27 (a-b). For model 1 the effect of speed on inverse surface roughness is a nonlinear relationship it is in the form of a positive curve as shown in Figure 4.27 (a). As shown, the inverse of surface roughness increases significantly as speed increases. The increase in inverse

surface roughness peaks at approximately 1700 rpm, after which it is stagnant or inconspicuous. The effect of speed in model 2 has a linear relationship with the inverse surface roughness similarly with the effect of feed although, this relationship is positively linear. The inverse surface roughness increases with speed, eventually, surface roughness increases as speed increases. Productivity is maximised at increased cutting speed [183]. As the cutting speed increases during machining, high rate of material removal occur due to excessive temperature generated at the cutting zone [178, 184], this produces a softening phenomenon that refines the cutting process. Notwithstanding, an increase in cutting speed is a pivotal factor in tool wear [185]
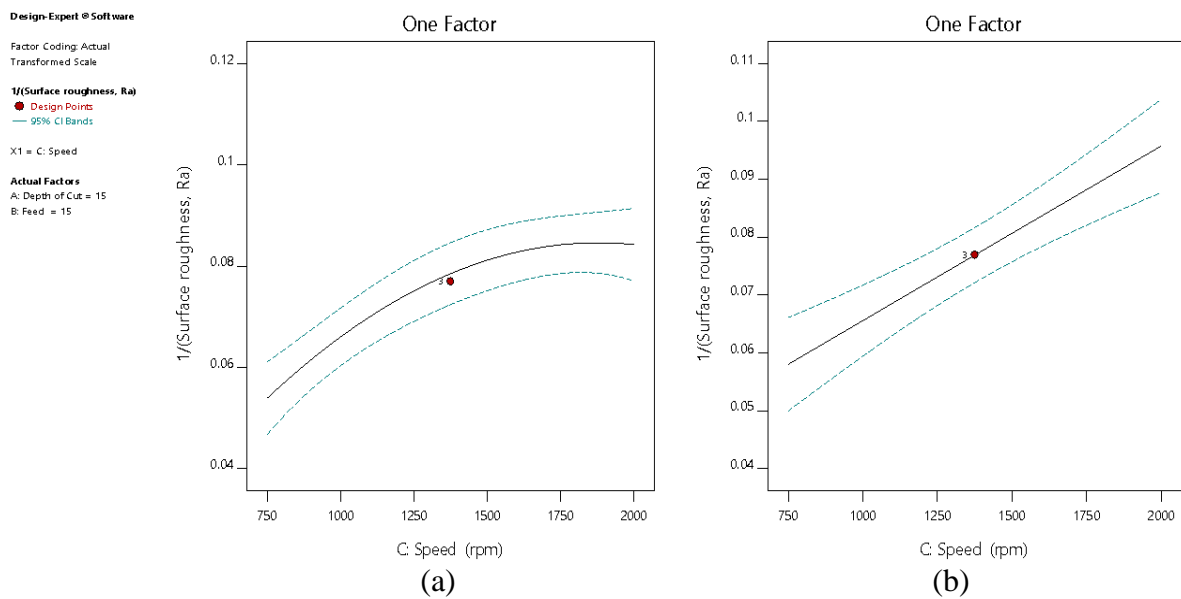
Figure 4.27: Variation of R_a with feed for (a) model 1 (b) model 2

From the two models, it is observed that there is no interaction effect existing between the selected parameters. However, in section 4.4.5 feed and speed were identified as the most influencing factor in the models. Therefore, contour and 3-D plots for these factors are considered to determine the trend of variation of response within the selected range of input parameters and also their combined influence with the other factor on inverse surface roughness.

Figure 4.28 to Figure 4.35 show the contour plot and 3D plot of model 1 and 2 for combined influence of feed and depth of cut on inverse surface roughness at a constant speed of 2000 rpm. It is observed that at very low feed and high cutting speed low surface roughness can be achieved. As the feed increases from 15 mm/min to 25 mm/min, the colour changes from blue to green, the

inverse of surface roughness reduces. Depth of cut (DOC) has little or no significant influence on inverse surface roughness of SPDT of RSA 431.
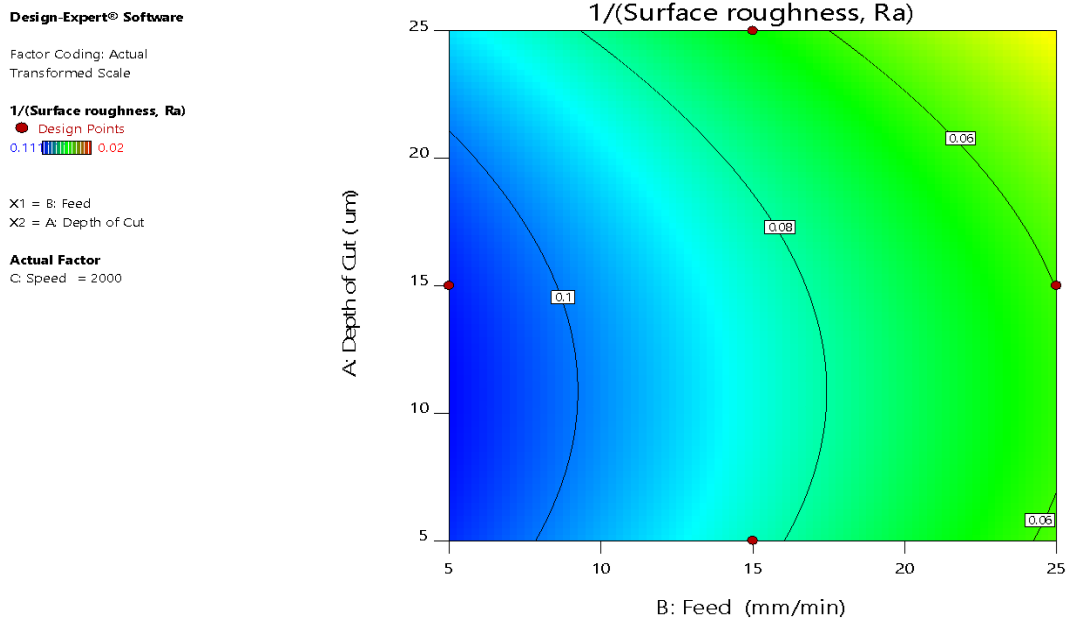
Figure 4.28: Model 1 R_a contours in feed – DOC plane at cutting speed of 2000 rpm
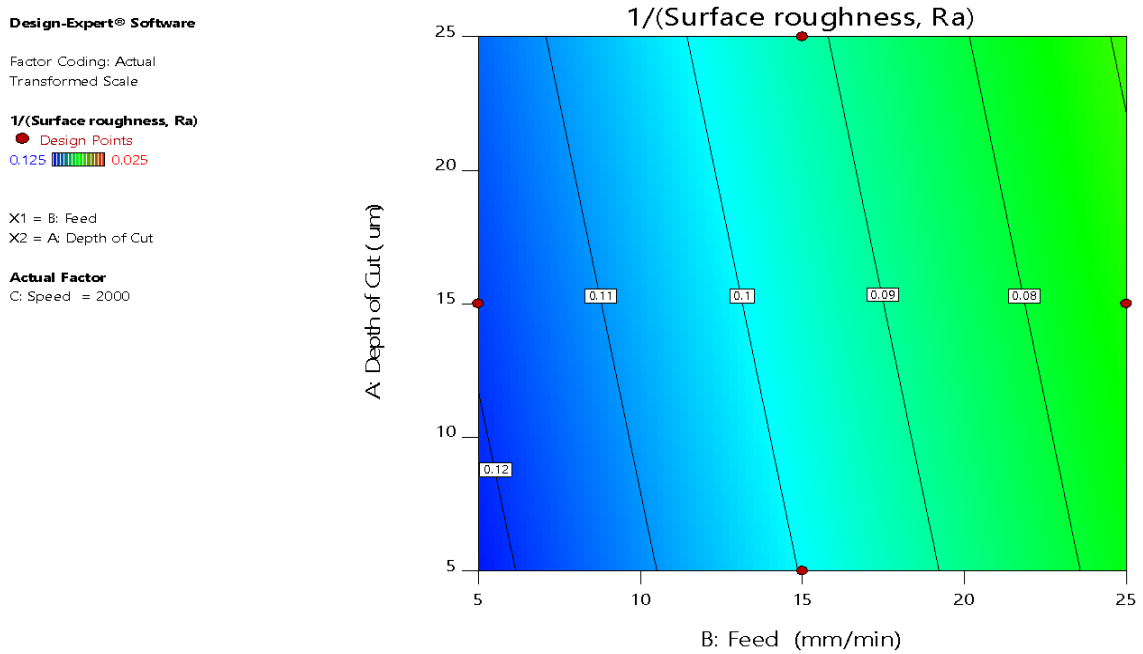
Figure 4.29: Model 2 R_a contours in feed – DOC plane at cutting speed of 2000 rpm
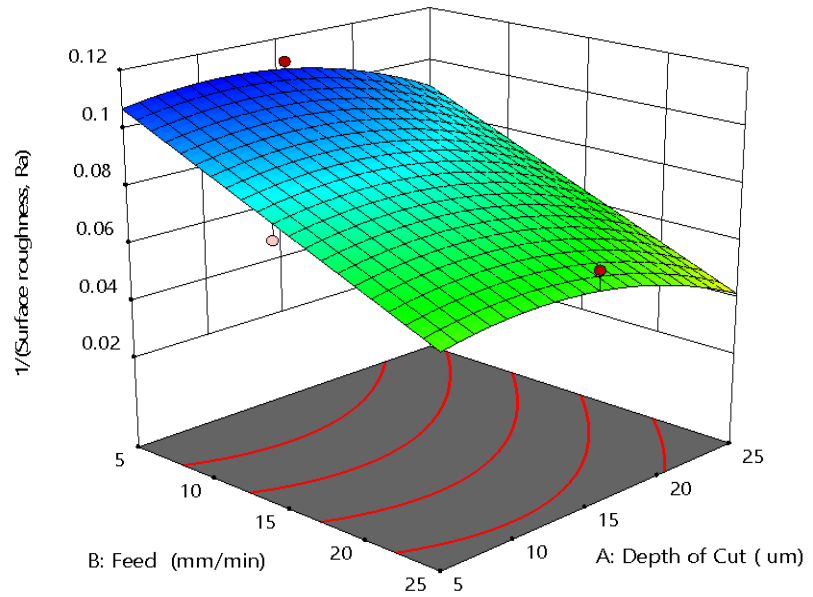
Figure 4.30: Model 1 3D surface graph of inverse surface roughness against feed and DOC
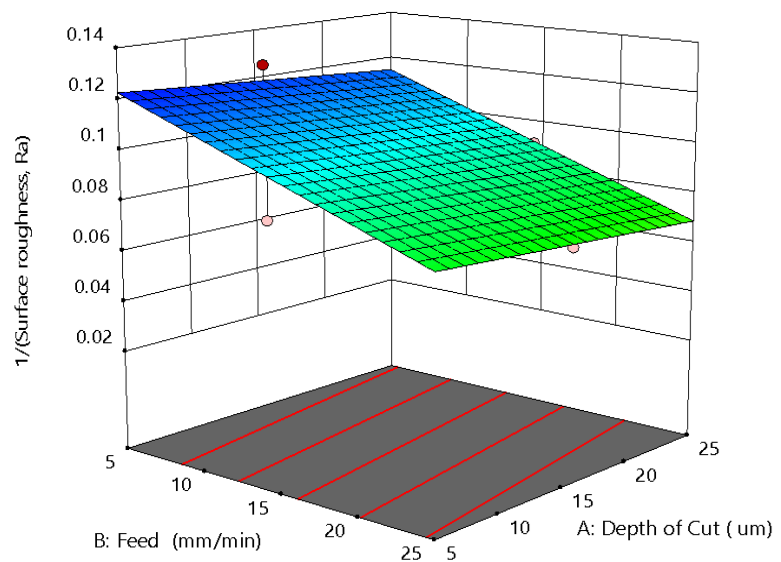
(b)

Figure 4.31: Model 2 3D surface graph of inverse surface roughness against feed and DOC

135
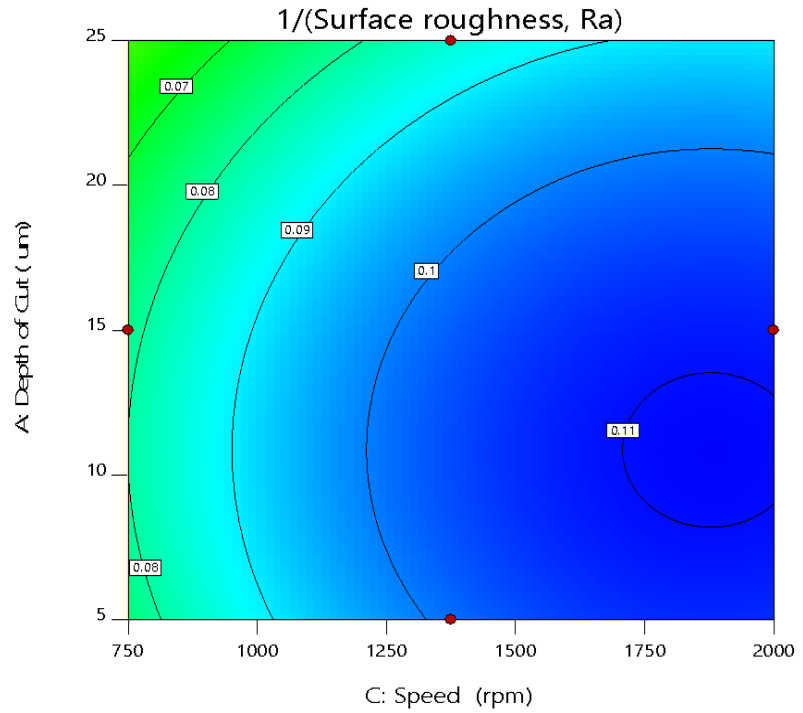
Figure 4.32: Model 1 R_a contours in speed – DOC plane at feed of 5 mm/min
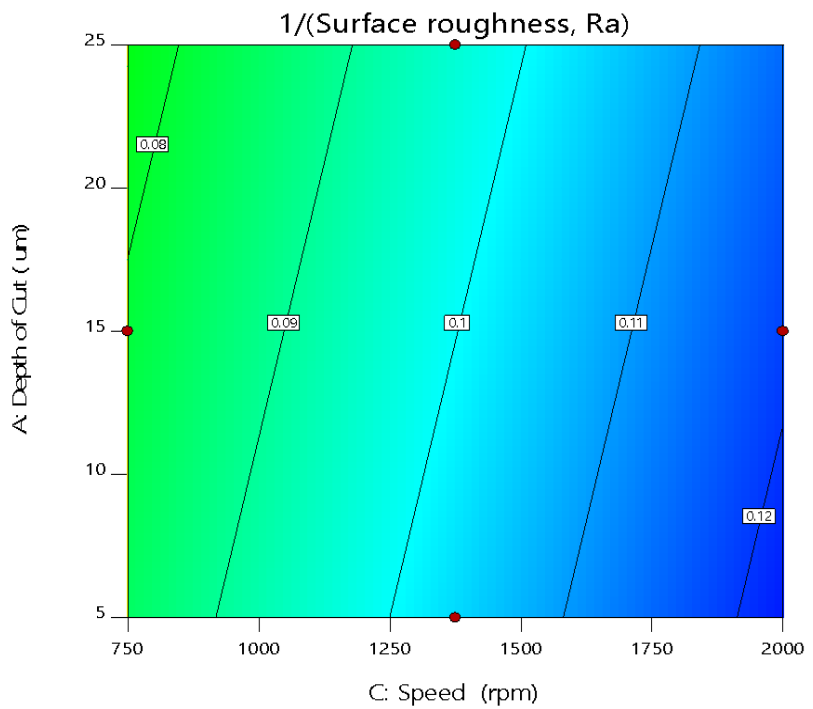
Figure 4.33: Model 2 R_a contours in speed – DOC plane at feed of 5 mm/min

136
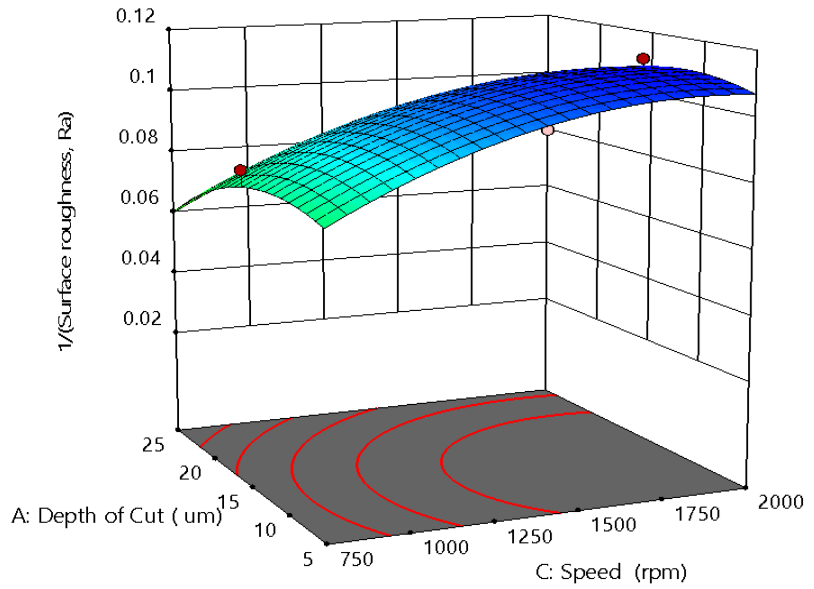
Figure 4.34: Model 1 3D surface graph of inverse surface roughness against speed and DOC
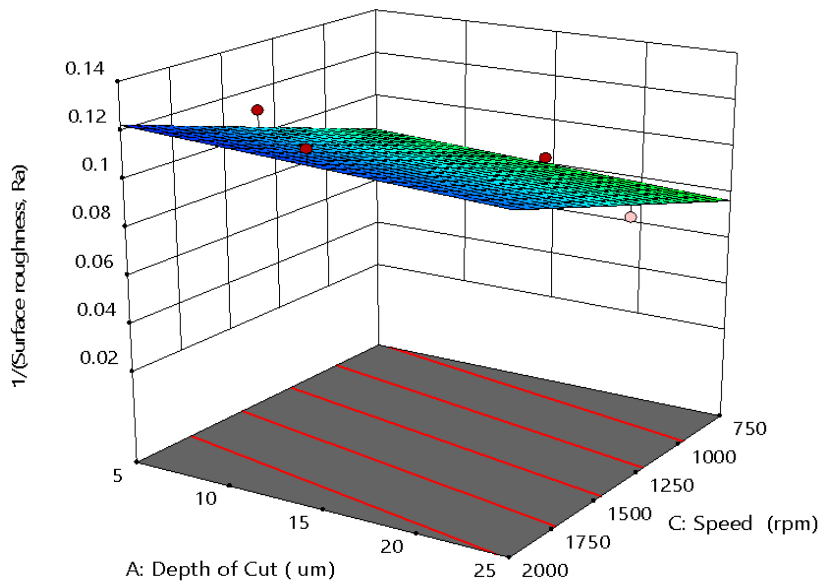
(b)

Figure 4.35: Model 2 3D surface graph of inverse surface roughness against speed and DOC

137

4.3.1.6   Optimisation analysis

The aim of this research work is not just to investigate how cutting parameters (depth of cut, feed, and speed) influence surface roughness of RSA 431 during turning, but also to identify which combination of these parameters will give the minimum surface roughness value. Profile plot and response optimisation analysis can be used in obtaining the desired surface roughness.

Profile plots are used to show how the combination of these parameters can be used to achieve a good surface roughness. Figure 4.36 (a-b) represents the profile plots for DOC that shows that during turning of RSA 431 when kerosene mist is used as cutting fluid. The best surface roughness (about 12 nm) can be achieved when DOC is between 10 µm -12µm, while feed and speed are at very low - moderate values.

Similarly, optimum surface roughness can be reached with minimum values of DOC, feed, and speed, when water is used as cutting fluid. The best *Ra* is achieved at DOC of 5µm, feed of 5 mm/min and speed of 750 rpm. The profile plot for feed (as shown in Figure 4.37 (a-b)) illustrates that at the lowest feed, the minimum surface roughness is experienced at moderate DOC and speed for experiment 1. While the lowest feed combined with high DOC and speed generate the lowest *Ra* when water is used as cutting fluid. Maximum value of speed and lowest value of DOC and feed low surface roughness can be achieved when water or kerosene mist is used as cutting fluid (Figure 4.38 (a-b)).
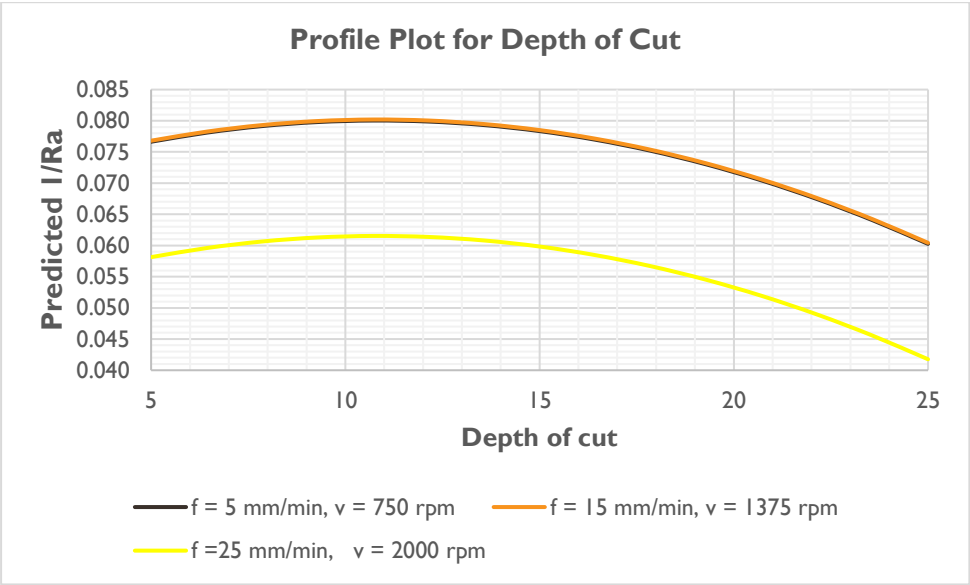
(a)
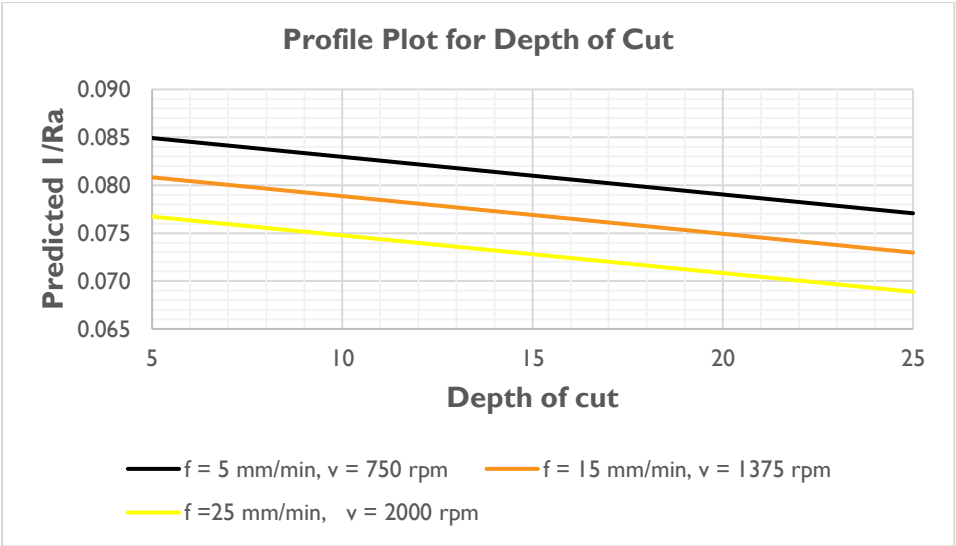
(b)

Figure 4.36: (a-b) Profile plot for depth of cut
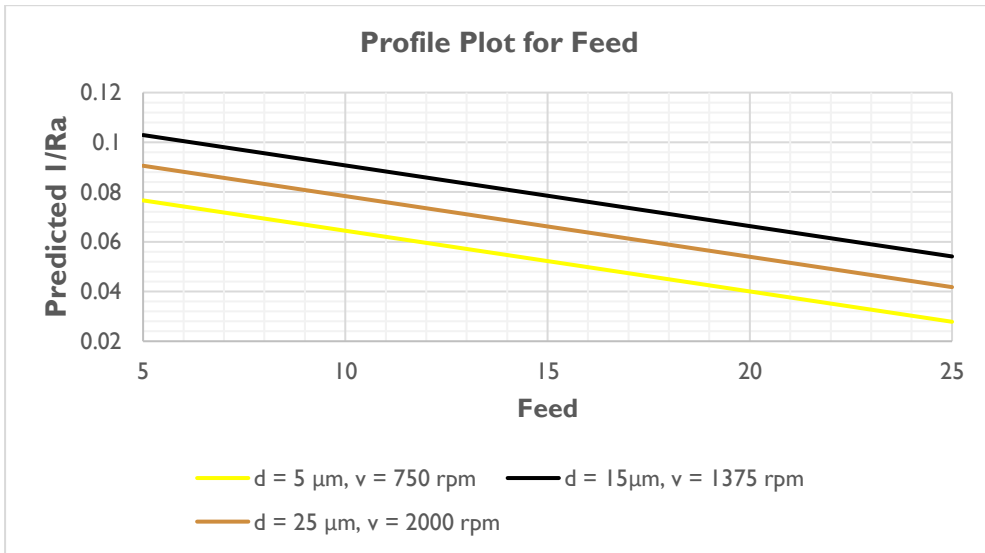
(a)
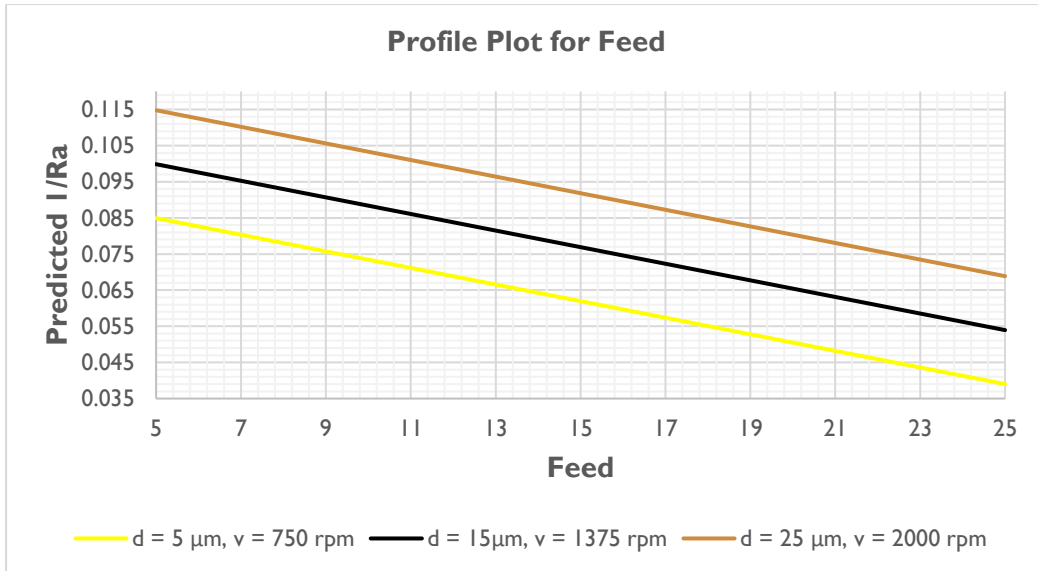
(b)

Figure 4.37: (a-b) Profile plot for feed
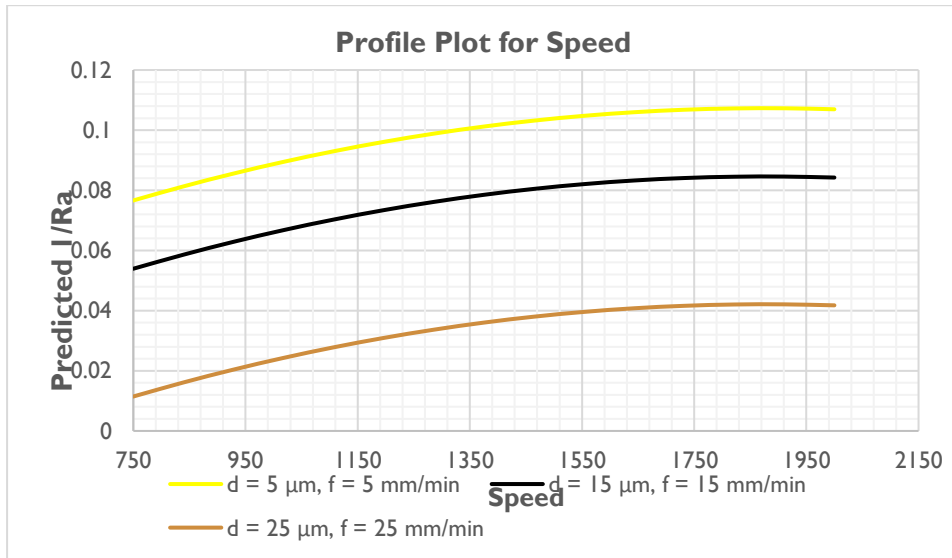
(a)
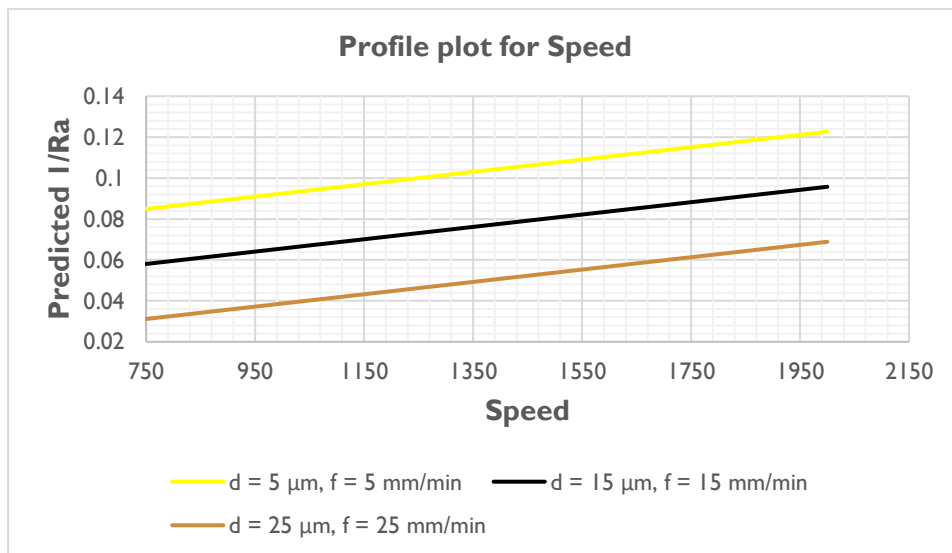
(b)

Figure 4.38: (a-b) Profile plot for speed

Optimisation is the process whereby the best combination of variable factors that jointly improve response or set of responses, are identified after satisfying the conditions for such factors and response(s) in the set. In machining, economic efficiency is improved with optimization of cutting parameters to achieve the optimal surface roughness [186]. The process of optimization is accomplished using RSM technique to obtain desirability (d) for the response.

The desirability investigates whether the parameters are within their working range or not. Desirability of 0 indicates that the response is outside the working range while desirability of 1 concludes the parameters are within the working range. Several researchers have employed the technique of desirability to determine optimum cutting conditions [187, 188].

Optimisation analysis was performed using Design-Experts software for achieving minimum surface roughness based on the mathematical model given by equation (4.4) and equation (4.5) and for the two models based. The goal weights for the two models are set at 1 (lower) and 1 (upper), this is to ensure that the best solution is provided by the optimization process and equal importance is allotted on the goal and the bounds.
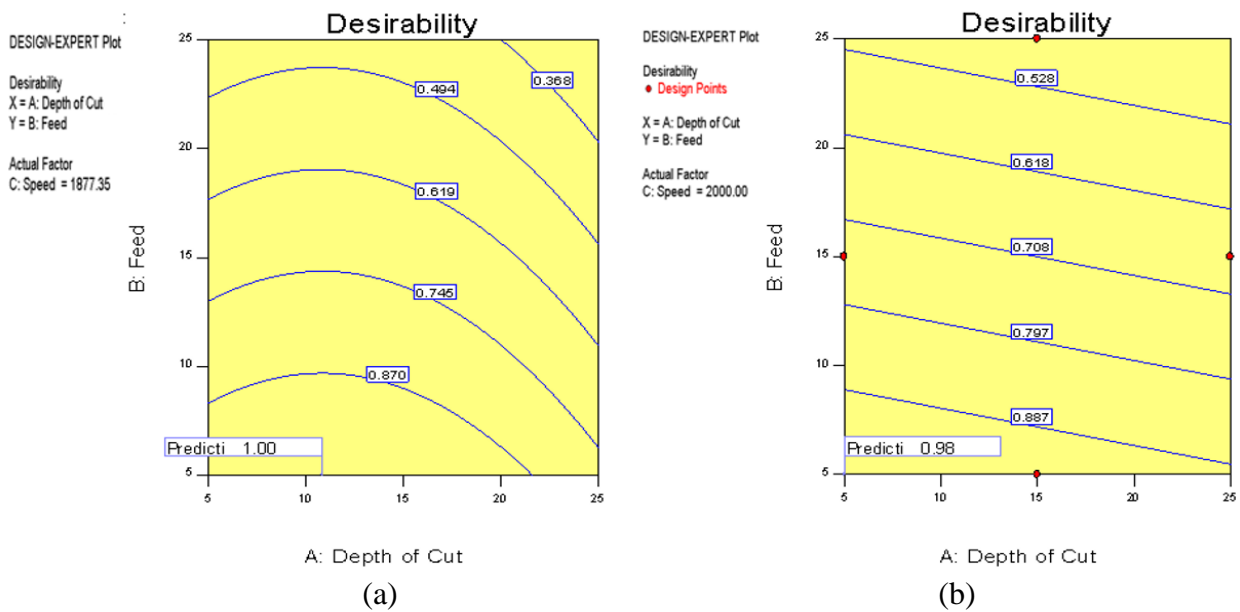
Figure 4.39: (a-b) Desirability plot for model 1 and 2

Figure 4.39 (a-b) shows the desirability plot for both models, 4.39 (a) represents the model with kerosene mist as cutting fluid, while 4.39 (b) represents the model with water as cutting fluid. The first contour from the base of the graphs, especially the predicted spots, represents the area with the best combination for machining RSA-431.

The optimization report for the two models is presented in the tables below. Table 4.9 shows a summary of the criteria constraints, which shows all the criteria applied to attain the optimal setting. This summary is used to produce the optimal solution for the process as shown in Table

4.10. The tables give the optimal machining parameters for the two models. The desirability values for the models (0.99 and 0.98) are acceptable because of their closeness to 1.

Table 4.9: (a) Constraints for model 1 optimization

Name	Goal	Lower Limit	Upper Limit	Lower Weight	Upper Weight	Importance
Depth of cut	is in range	5	25	1	1	3
Feed	is in range	5	25	1	1	3
Speed	is in range	750	2000	1	1	3
Surface roughness	minimize	9.00001	50	1	1	3

Table 4.9: (b) Constraints for model 2 optimization

Name	Goal	Lower Limit	Upper Limit	Lower Weight	Upper Weight	Importance
Depth of Cut	is in range	5	25	1	1	3
Feed	is in range	5	25	1	1	3
Speed	is in range	750	2000	1	1	3
Surface roughness	minimize	8	40	1	1	3

Table 4.10: Solution to model 1 and 2 optimization

Experimental Model	Depth of Cut (μm)	Feed (mm/min)	Speed (rpm)	Surface Roughness (nm)	Desirability	
1	10.88	5	1877.68	9	0.99	**Selected**
2	5	5	2000	8	0.98	**Selected**

4.4   AE analysis and feature extraction

The acoustic emission (AE) signals captured during the machining process are complex waveforms and they consist of thousands of basic signals' data. These signals are processed and analysed to extract important information about occurrences in machining. Feature extraction can

be carried out in time-domain analysis, frequency domain and time-frequency domain. Feature extraction was achieved in this section using Excel and Matlab.

4.4.1 Time-domain observations and analysis

The acoustic emission signal in time-domain was observed to change as the machining parameter combination changes in both experiments. There were variations in the amplitude levels of the AE as the machining parameters combination changes, although these variations are not a continuous trend for the result of the two experiments. The difference in amplitude levels of some raw AE signals was consequently observed to increase with some of the measured surface roughness values of the workpiece material. Spikes were noticed in the raw AE signals, which could be an indicator of surface imperfection or deep grooves. Figure 4.40 (a-b) shows the AE amplitude variations in the time-domain for various machining parameter combinations.

In experiment 1, high AE in terms of the amplitude level was noticed for experimental run order 4. This experimental run produced the worst surface roughness with combination 15 μm, 25 mm/min and 750 rpm for depth of cut, feed and speed respectively. The same was observed for run order 3, with higher amplitude voltage of AE signal at the same speed and feed of 15 mm/min. Experimental run order 9 has the best surface roughness value at 15 μm, 5 mm/min and 2000 rpm produced low AE amplitude level.

Run order 2 with high speed (1375 rpm) and low feed, produced low surface roughness and low AE amplitude value when compared to the value of experimental run order 4. Experiment 2 also produced the same pattern of AE results as experiment 1. High amplitude of AE signals was observed in experimental run order 4 and 3 with high feed and low speed. Furthermore, the combination of low feed and high speed of experiment 9 and 2 also generated low acoustic emission.

144
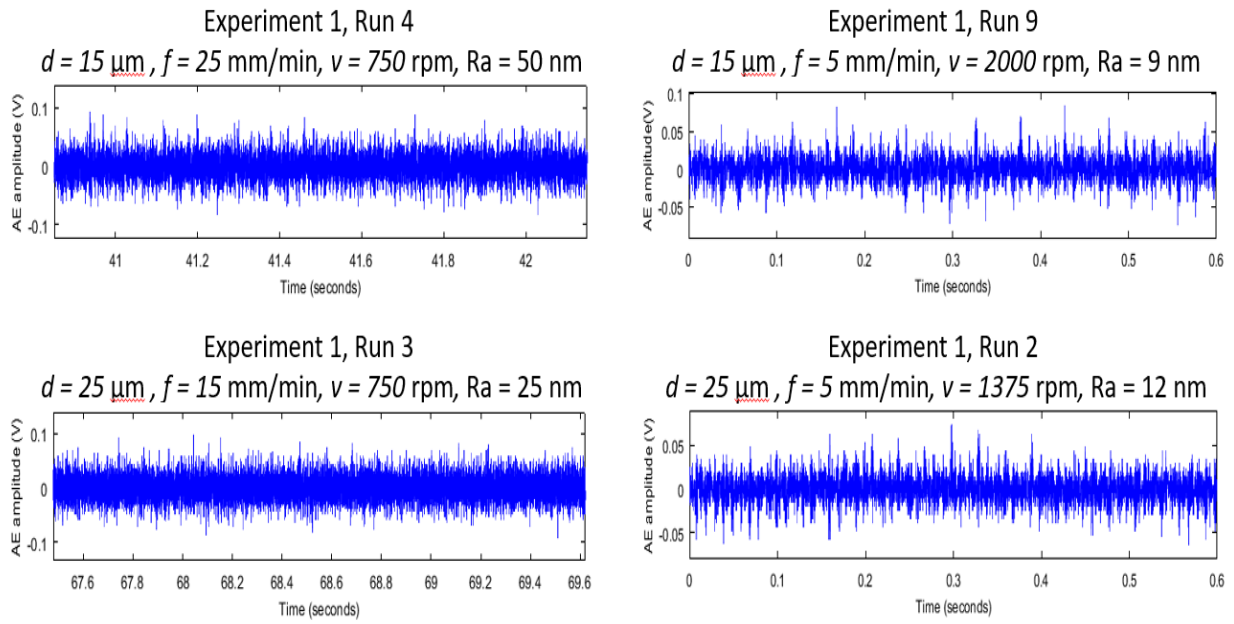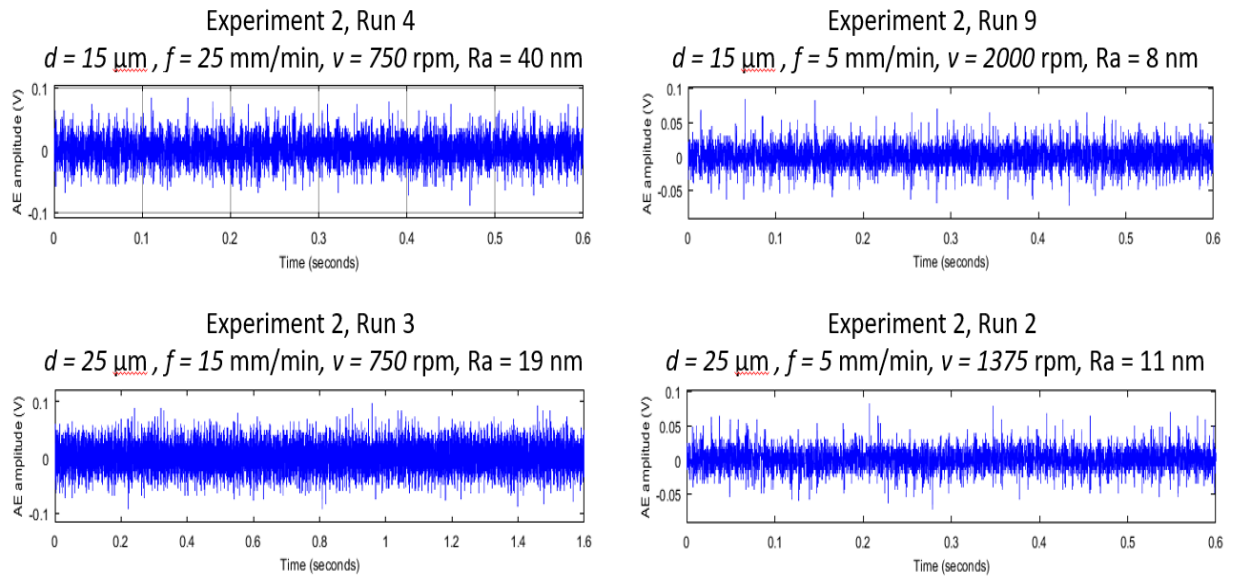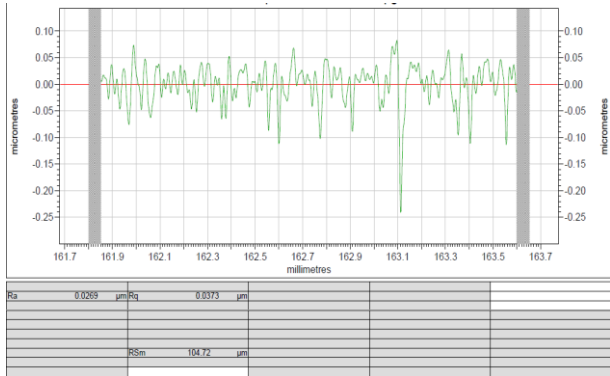
Figure 4.40: (a-b) AE amplitude variation in time-domain for different experimental order.
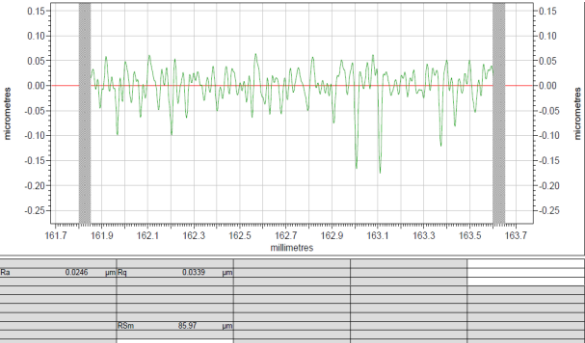
In time-domain, the following features were extracted from the raw AE data: AE mean, AE_{RMS}, standard deviation of frequency, skewness, kurtosis, peak-to-peak, power, energy, maximum amplitude, minimum amplitude and range.
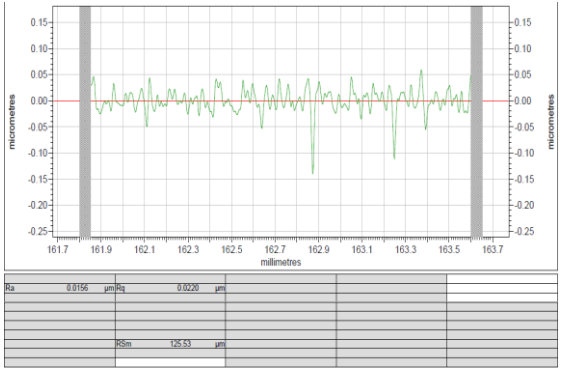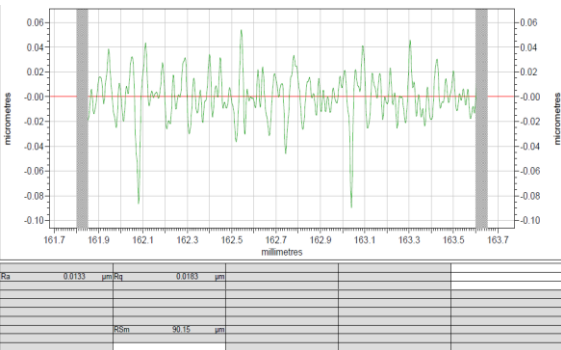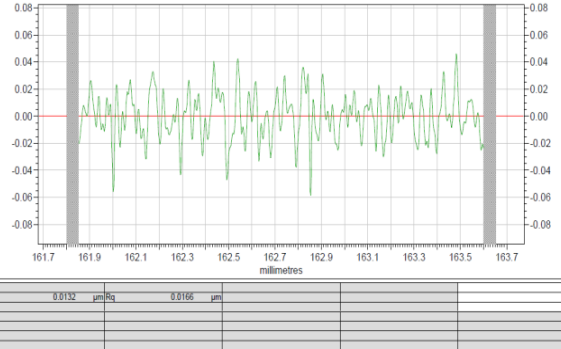
4.4.2 Acoustic Emission Statistical Analysis
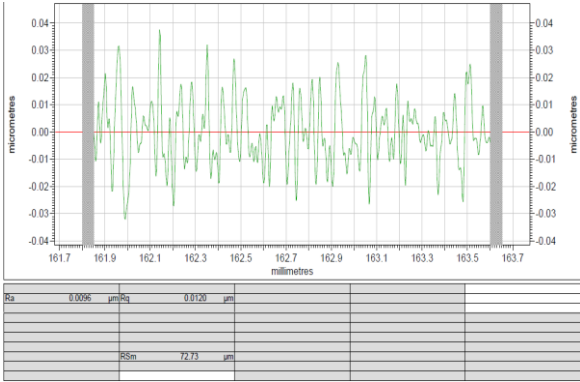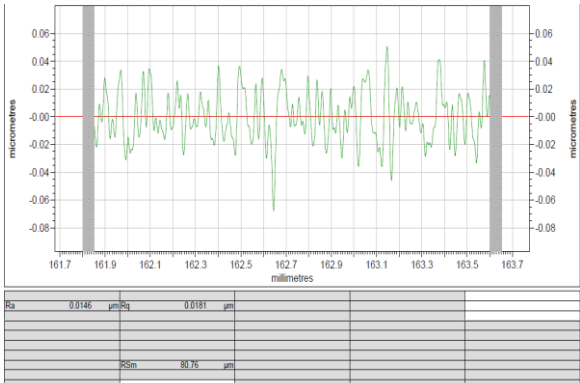
Table 4.11 (a-b) presents the machining parameters during SPDT of RSA 431 when kerosene mist and water are used as cutting fluid. The surface roughness profile was obtained from Taylor Hobson Talysurf's measuring instrument and the root mean square (RMS) value of the acoustic emission signal. Root mean square (RMS) is one of the most common time-domain features used in analysing AE signals. The RMS of AE voltage values of the raw signal was observed to increase with an increase in some surface roughness values.
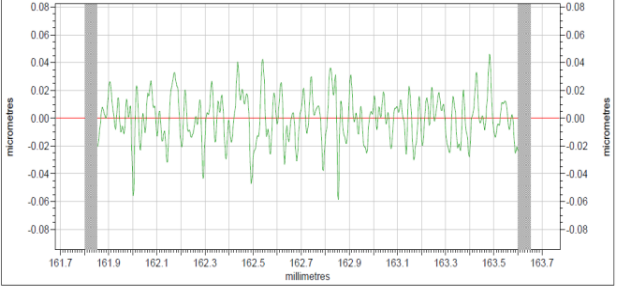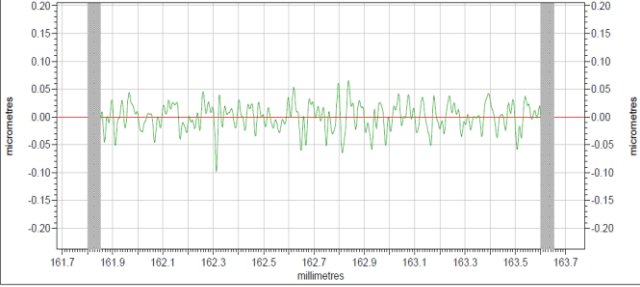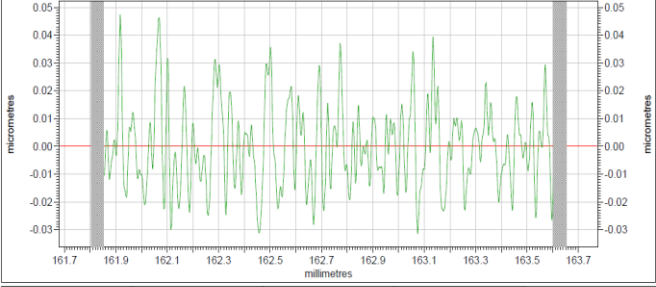
Table 4.11: (a) Surface profile and acoustic emission result for experiment 1

Run	d (µm)	f (mm/min)	v (rpm)	Surface roughness profile
1	25	25	1375	$AE_{RMS} = 0.02739$ V

2	25	5	1375	AE$_{RMS}$ = 0.02158 V Ra 0.0124 µm Rq 0.0153 µm RSm 72.02 µm
3	25	15	750	AE$_{RMS}$ = 0.02285 V Ra 0.0246 µm Rq 0.0339 µm RSm 85.97 µm
4	15	25	750	AE$_{RMS}$ = 0.02220 V Ra 0.0503 µm Rq 0.0620 µm RSm 44.53 µm

5	25	15	2000	AE_RMS = 0.02226 V
6	5	15	2000	AE_RMS = 0.0226 V
7	15	15	1375	AE_RMS = 0.02158 V

AE$_{RMS}$ = 0.02226 V

Ra 0.0156 µm Rq 0.0220 µm

RSm 125.53 µm

AE$_{RMS}$ = 0.0226 V

Ra 0.0133 µm Rq 0.0183 µm

RSm 90.15 µm

AE$_{RMS}$ = 0.02158 V

Ra 0.0132 µm Rq 0.0166 µm

RSm 65.44 µm

8	5	5	1375	$AE_{RMS} = 0.02117$ V
9	15	5	2000	$AE_{RMS} = 0.01668$ V
10	15	25	2000	$AE_{RMS} = 0.02143$ V

149

11	15	15	1375	AE$_{RMS}$ = 0.02158 V Ra 0.0132 µm Rq 0.0166 µm RSm 65.44 µm
12	5	15	750	AE$_{RMS}$ = 0.0169 V Ra 0.0185 µm Rq 0.0233 µm RSm 71.82 µm
13	15	5	750	AE$_{RMS}$ = 0.01639 V Ra 0.0119 µm Rq 0.0149 µm RSm 61.36 µm

14	15	15	1375	$AE_{RMS} = 0.02158$ V
15	5	25	1375	$AE_{RMS} = 0.01579$ V

Table 4.11: (b) Surface profile and acoustic emission result for experiment 2

Run	d (μm)	f (mm/min)	V (rpm)	Surface roughness profile
1	25	25	1375	AE$_{RMS}$ = 0.01579 V
2	25	5	1375	AE$_{RMS}$ = 0.02255 V

3	25	15	750	$AE_{RMS} = 0.02270$ V

$AE_{RMS} = 0.02270$ V

| Ra | 0.0186 | µm | Rq | 0.0232 | µm |
| RSm | 75.00 | µm |

4	15	25	750	$AE_{RMS} = 0.02229$ V

$AE_{RMS} = 0.02229$ V

| Ra | 0.0417 | µm | Rq | 0.0492 | µm |
| RSm | 41.13 | µm |

5	25	15	2000	$AE_{RMS} = 0.02221$V

$AE_{RMS} = 0.02221$V

| Ra | 0.0109 | µm | Rq | 0.0137 | µm |
| RSm | 68.20 | µm |

153

| 6 | 5 | 15 | 2000 | AE_{RMS} = 0.02220V |

$$AE_{RMS} = 0.02220V$$

| Ra | 0.0117 | µm | Rq | 0.0145 | µm |
| RSm | 58.64 | µm |

$$AE_{RMS} = 0.02167 \text{ V}$$

| 7 | 15 | 15 | 1375 |

| Ra | 0.0128 | µm | Rq | 0.0160 | µm |
| RSm | 66.77 | µm |

$$AE_{RMS} = 0.01695 \text{ V}$$

| 8 | 5 | 5 | 1375 |

| Ra | 0.0087 | µm | Rq | 0.0112 | µm |
| RSm | 76.98 | µm |

154

9	15	5	2000	AE$_{RMS}$ = 0.01685 V
10	15	25	2000	AE$_{RMS}$ = 0.01648 V
11	15	15	1375	AE$_{RMS}$ = 0.02167 V

12	5	15	750	AE$_{RMS}$ = 0.01544 V
13	15	5	750	AE$_{RMS}$ = 0.01552V
14	15	15	1375	AE$_{RMS}$ = 0.02167 V

15	5	25	1375	$\text{AE}_{\text{RMS}} = 0.01536 \text{ V}$

RSM of the Design-Expert software was applied to analyse the acoustic emission responses and develop a model. The response ranges from 0.1367 to 0.2197 V and the ratio of maximum to minimum response is 1.6072. Although this ratio is greater than 10, further investigation on the response data reveals that the p-values of response data are below 0.05 for experiment 1 and 2 as shown in Figure 4.41 (a-b). Therefore, the data are concluded not normally distributed.

The null hypothesis (H_O) for the normality test is that the data is normally distributed. Therefore, there was a need for the transformation of the AE_{RMS} data. Johnson transformation of Minitab 18 software was utilised for transforming the data. This transformation option is a powerful tool that can be used with data that include zero and negatives values. The Johnson transformation provides an overall capability statistic and is applied when other types of transformation tools do not give a suitable transformation. The respective p-value of 0.218 and 0.444 for experiment 1 and 2 data from the probability plot for transformed data support the null hypothesis and the low Anderson-Darling statistic indicates a good fit.
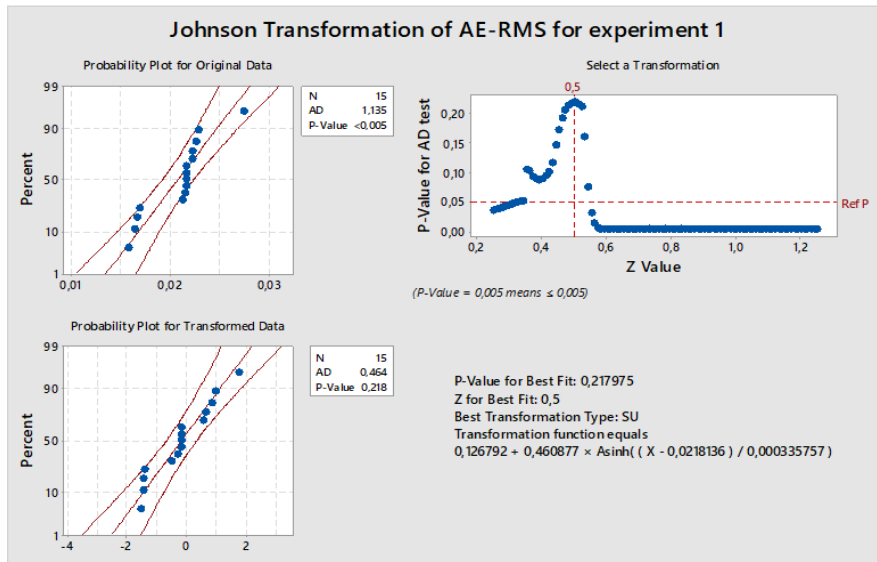
(a)
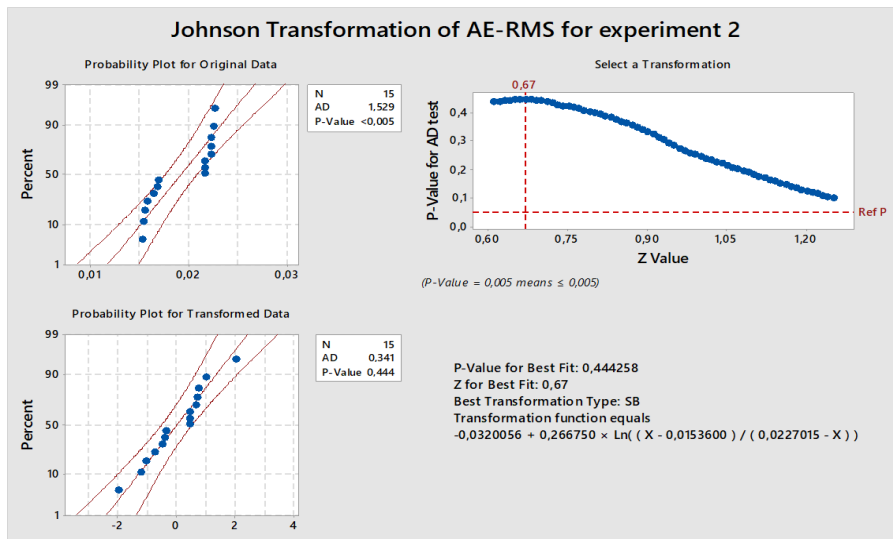
(b)

Figure 4.41: (a-b) Transformation plots of AE_{RMS} value for experiment 1 and 2

Table 4.12 (a-b) displays the fit summary of the models evaluated by the software of Design-Expert to find models that can efficiently and satisfactorily describe the desired response (AE_{RMS}). As seen from the tables, a two-factor interaction (2FI) vs. linear was suggested for experiment 1 and quadratic vs. 2FI form for experiment 2. These suggestions are based on the highest order polynomial where the additional terms are significant, and the model is not aliased. A simplified general form of a second-order (quadratic) polynomial equation is used to model this:

$$y = \beta_0 + \sum_{i=1}^{n} \beta_i x_i + \sum_{i=1}^{n} \beta_{ii} x_i^2 + \sum_{i=1}^{n} \sum_{j=1}^{n} \beta_{ij} x_i x_j + e \qquad (4.7)$$

Where y is the response model, x represents the independent variables, β is the regression coefficient, and e is an error. β_0 is a constant value. $\beta_i x_i$ and $\beta_{ii} x_i^2$ represent linear terms (first-order effects of variables) and quadratic terms (second-order effects of the variables), respectively, and $\beta_{ij} x_i x_j$ is a two-factor interaction (2FI) term. A two factor (2FI) model can be derived from equation (4.7) by replacing β_{ii} with 0.

Table 4.12: (a) Sequential Model Sum of Squares for AE$_{RMS}$ model of experiment 1

Source	Sum of Squares	df	Mean Square	F-value	p-value	
Mean vs. Total	0.460016	1	0.460016			
Linear vs. Mean	6.421954	3	2.140651	3.055995	0.073666	
2FI vs. Linear	4.075823	3	1.358608	2.994659	0.09546	Suggested
Quadratic vs. 2FI	1.738277	3	0.579426	1.53195	0.315162	
Cubic vs. Quadratic	1.891138	3	0.630379			Aliased
Residual	0,0000	2	0,0000			
Total	14.58721	15	0.972481			

Table 4.12 (b): Sequential Model Sum of Squares for AE$_{RMS}$ model of experiment 2

Source	Sum of Squares	df	Mean Square	F-value	p-value	
Mean vs. Total	0.000685	1	0.000685			
Linear vs. Mean	4.672538	3	1.557513	1.685426	0.227338	
2FI vs. Linear	3.463814	3	1.154605	1.378354	0.317633	
Quadratic vs. 2FI	3.261545	3	1.087182	1.580294	0.304951	Suggested
Cubic vs. Quadratic	3.439808	3	1.146603			Aliased
Residual	0	2	0			
Total	14.83839	15	0.989226			

Results for the suggested models were evaluated using ANOVA, as shown in table 4.13 (a-b). Generally, the insignificant terms (terms with p-value > 0.05) are removed to improve the models. However, the actual terms with p-values higher than 0.05 were included in the model since they are control variables that are expected during the machining process and also to support hierarchy. Furthermore, in model 1, the insignificant model terms such as the interacting factors do not improve the model, hence they are not considered. The results show that the two models are significant with F-values of 3.86 and 4.23 for model 1 and 2 respectively.

Table 4.13: (a) ANOVA result for 2FI model of AE_{RMS} for experiment 1

Source	Sum of Squares	Df	Mean Square	F-value	p-value	
Model	10.50	6	1.75	3.86	0.0414	significant
Depth of Cut, (d)	4.19	1	4.19	9.25	0.0160	
Feed, (f)	2.09	1	2.09	4.60	0.0644	
Speed, (v)	0.1415	1	0.1415	0.3120	0.5918	
Depth of cut * feed, ($d * f$)	2.12	1	2.12	4.68	0.0625	
Depth of cut * speed, ($d * v$)	1.74	1	1.74	3.83	0.0860	
Feed * Speed, ($f * v$)	0.2145	1	0.2145	0.4727	0.5112	
Residual	3.63	8	0.453			
Lack of Fit	3.63	6	0.6049			
Pure Error	0	2	0			
Cor Total	14.13	14				

Table 4.13: (b) ANOVA result for the quadratic model of AE_{RMS} for experiment 2

Source	Sum of Squares	df	Mean Square	F-value	p-value	
Model	10.41	5	2.08	4.23	0.0295	significant
Depth of Cut, (d)	4.29	1	4.29	8.73	0.0161	
Feed, (f)	0.3796	1	0.3796	0.7718	0.4025	
Speed, (v)	9.57E-06	1	9.57E-06	0	0.9966	

Depth of cut * speed, ($d * v$)	2.60	1	2.60	5.28	0.0472	
Feed * Feed, (f^2)	3.14	1	3.14	6.39	0.0324	
Residual	4.43	9	0.4919			
Lack of Fit	4.43	7	0.6324			
Pure Error	0	2	0			
Cor Total	14.84	14				

The final models developed to predict the resulting acoustic emission response (AE_{rms}) for each experiment is given in equation (4.8) and (4.9) as:

$$AE_{rms} = -3.6200743 + 0.108156d - 0.007282f + 0.002351v + 0.007285df -$$
$$0.000106dv - 0.00000371fv \tag{4.8}$$

$$AE_{rms} = -4.996623 + 0.250529d + 0.253391f + 0.001932164v - 0.000128928dv$$
$$- 0.009172498f^2 \tag{4.9}$$

Equation (4.8) is the AE_{rms} model, when kerosene mist is used as cutting fluid, likewise, equation (4.9) is the AE_{rms} model when water is used as cutting fluid. Where AE_{rms} is the acoustic emission RMS in volts (V), d is the depth of cut in μm, f is the feed (mm/min) and v is speed (rpm).

(a)   (b)
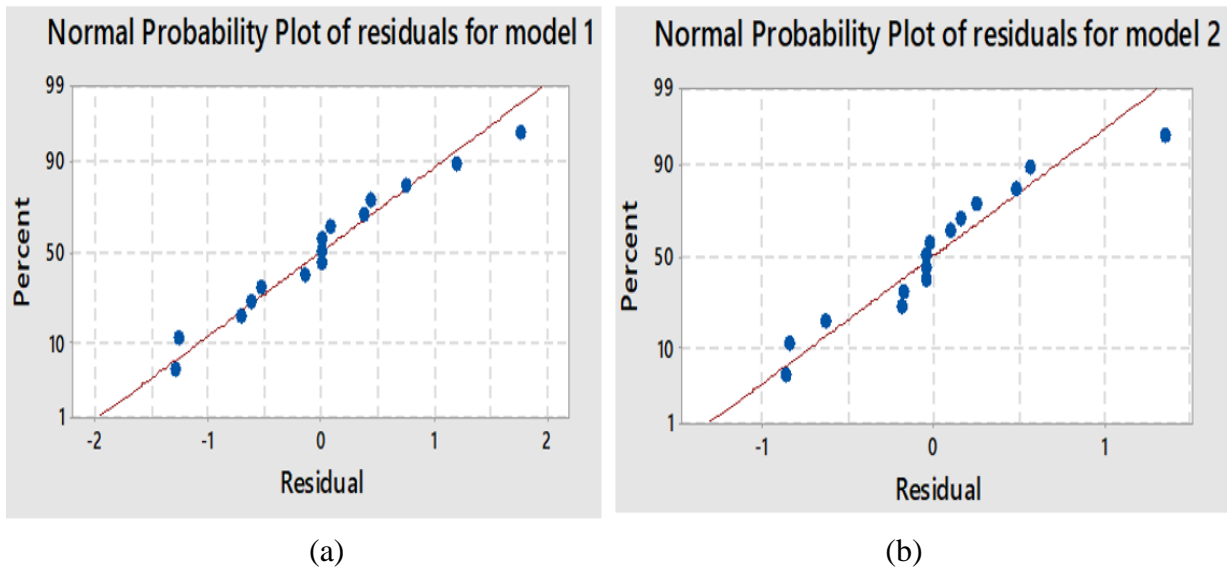
Figure 4.42: (a-b) Normal probability plot of residuals for AE_{RMS} models for experiment 1 and 2

The normality of the residuals for model 1 and 2 in Figure 4.42 (a-b) verifies, through the proximity of the points to the probability line, that the models are adequate, and the assumptions of regression are met. The model equations elucidate the relationships between each term and the AE_{RMS} response. The terms positively added to the model equation have synergistic effects, while negative terms have antagonistic effects on the model [189].

4.4.2.1   Effects of machining parameters and Interactions in the AE response of model 1

As observed from the model equation 4.8, an increase in depth of cut and speed will increase the AE response. On the contrary, feed will affect the AE response negatively. As feed increases, the AE response will decrease. This conclusion is made due to the positive and negative sign of the terms in the model.

Figure 4.31 shows the single main effect plot of the machining parameters in model 1 for the SPDT of RSA 431 when water is used as a cutting fluid. The plot displays the means for each value of a categorical variable. From the plot, an increase in depth of cut, feed and speed was seen to increase AE response. However, the increment of AE response as speed increases is smaller when compared to other effect plots. Further investigation reveals through the perturbation plot (Figure 4.45 (a)) that depth of cut has the greatest impact in the model due to its steepest slope.

The single plot shows that the lowest AE would be achieved with a low depth of cut, feed and speed. However, the effect of one factor of a plot is dependent on the level of interaction with other terms. The two-factor interaction between the depth of cut and feed ($d * f$) is synergistic, while the other interactions terms ($d * v$ and $f * v$) with a negative sign has an adverse influence on AE_{RMS}.
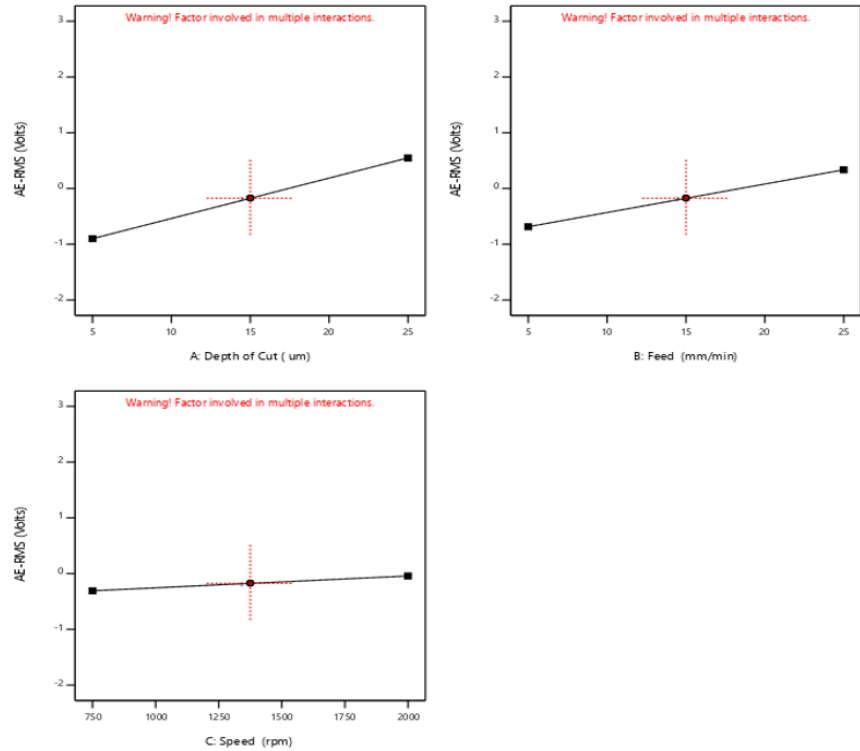
Figure 4.43: Effect plots of machining parameters on AE_{rms} for model 1

All existing interactions in the model equation 4.9 are shown in Figure 4.44. As mentioned earlier, the depth of cut contributes the strongest effect to AE response. Therefore, the two-factor interaction between depth of cut and feed shows that high feed with the combination of low depth of cut at a constant speed, AE_{RMS} will decrease steadily. In addition, the interaction between depth of cut and speed reveals that at the lowest depth of cut and speed with constant feed, AE_{RMS} will reduce. As mentioned earlier, feed contributed more to the model after depth of cut. However, the interaction between feed and speed through the interaction plot shows that as feed and speed increases, AE_{RMS} increases.

163
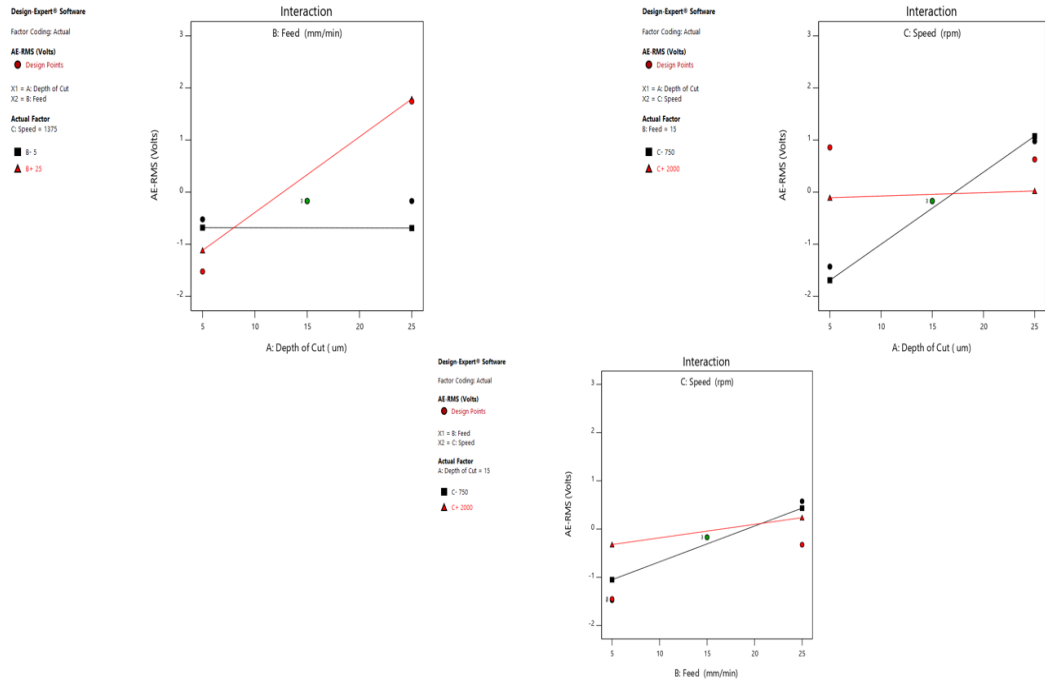
Figure 4.44: Interaction plot of model 1 terms and AE$_{RMS}$

(a) (b)
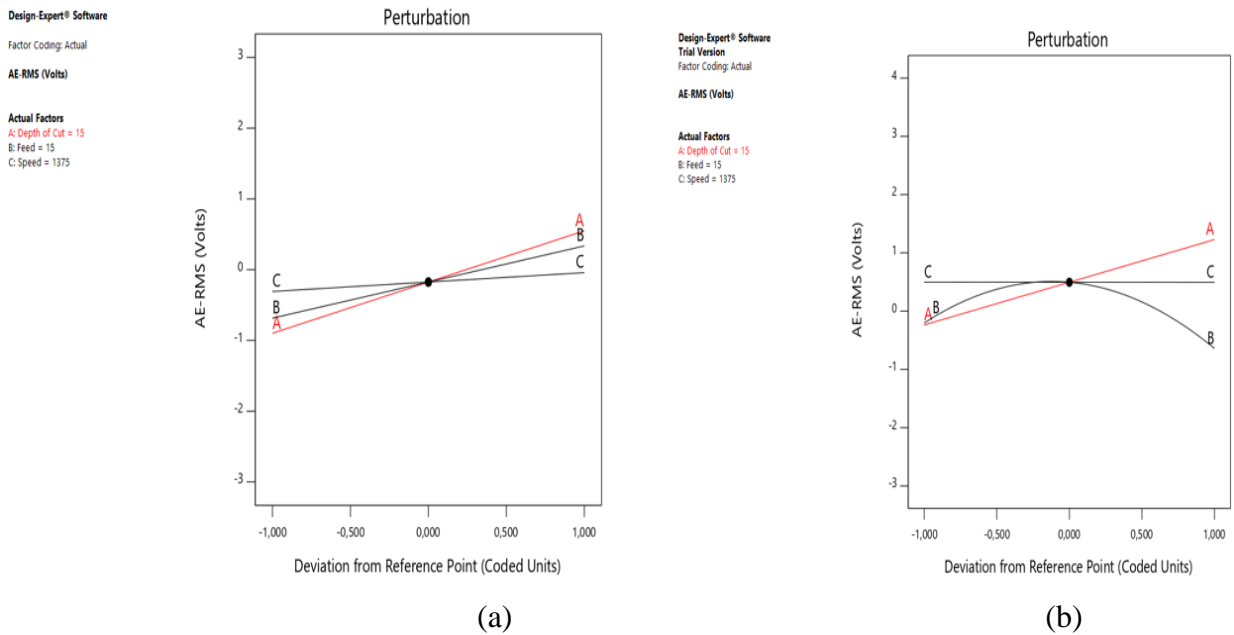
Figure 4.45 (a-b): Perturbation Plot (A= Speed, B = Feed and C = Depth)

164

4.4.2.2 Effects of machining parameters and Interactions in the AE response of model 2

Considering model equation (4.9), increasing all the machining parameters (depth of cut, feed and speed), which are the main factors will increase the acoustic emission response. Meanwhile, as feed increases, the negative squared term of feed would have an influence, causing the AE_{RMS} to decrease slowly. In the perturbation plot (Figure 4.45 (b)), the slope steepness of depth of cut explains why it contributed more to the model, followed by feed.
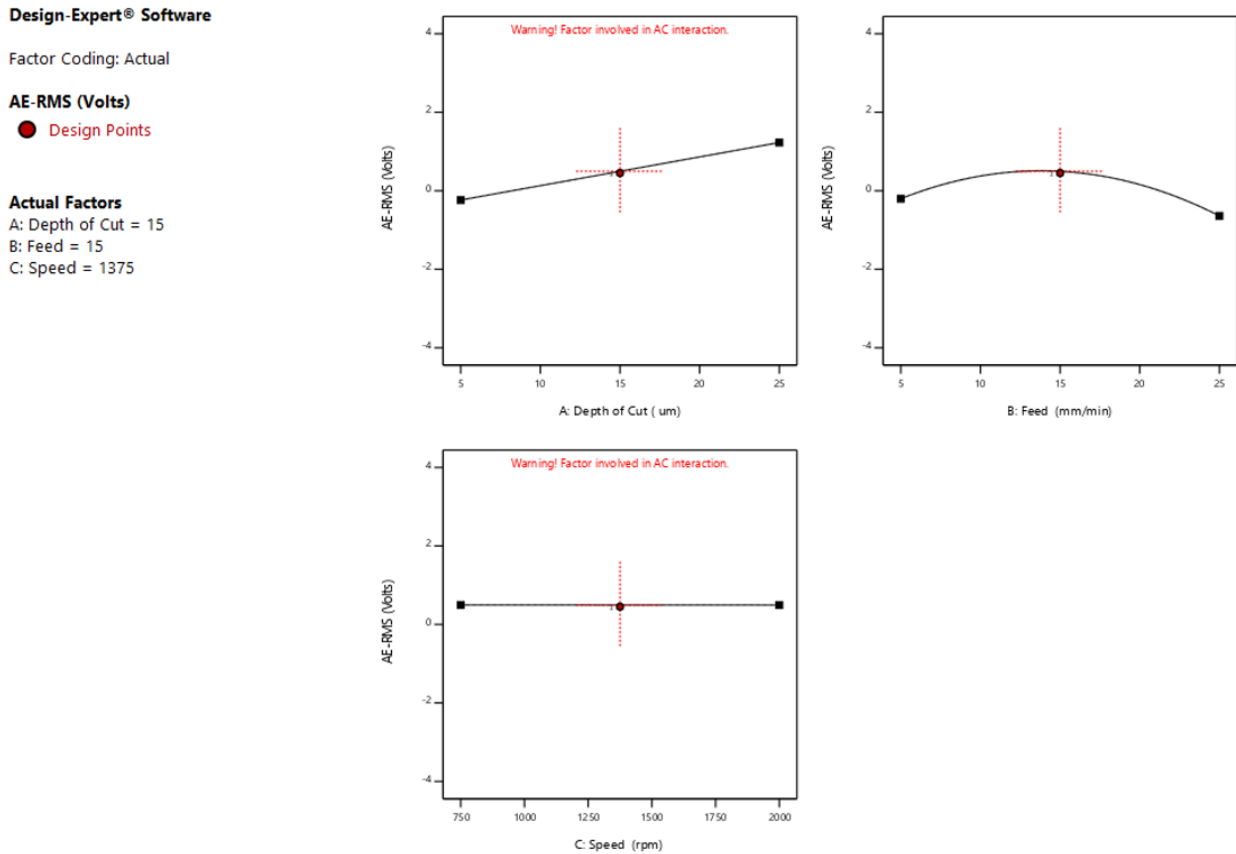
Figure 4.46: Effect plots of machining parameters on AE_{rms} for model 2

The effect of machining parameters is described in Figure 4.46. As seen from the plot, the depth of cut has a linear relationship with the AE response, as the depth of cut increases, AE_{RMS} also increases. The relationship between feed and the AE response is non-linear compared to the depth of cut. An increase in feed caused the AE_{RMS} to increase initially, but then subsequently decreased. AE response decreases slightly with an increase in speed, the decrease is so small it can almost be assumed that the effect of speed on AE_{RMS} is constant. The effect plots of machining parameters

on AE_{RMS} for model 2 show that the highest AE would be as a result of high depth of cut, medium feed and low speed.
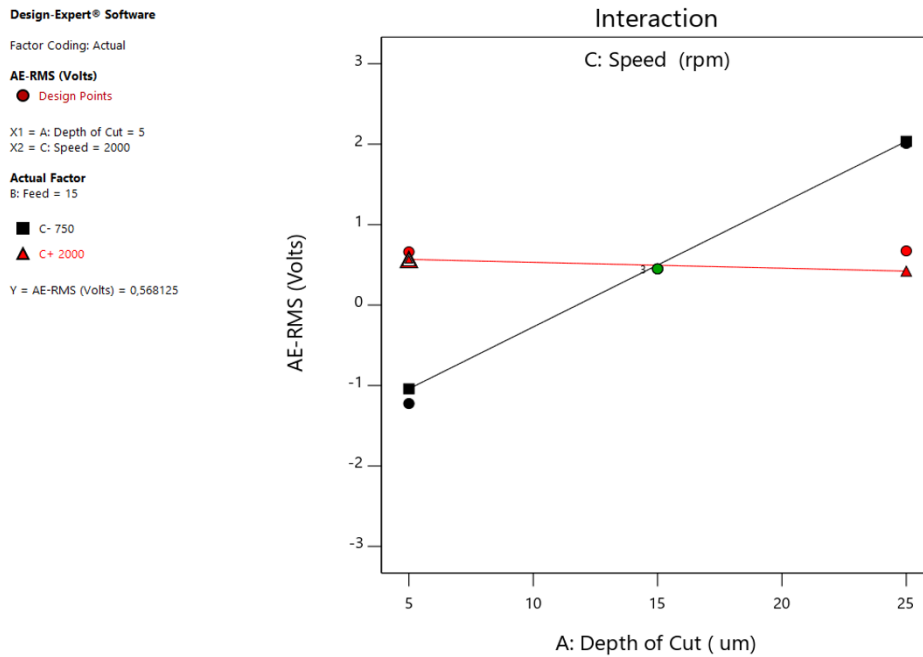
Figure 4.47: Interaction plot of model 2 terms and AE_{RMS}

In the ANOVA table for the quadratic model of experiment 2, there is a significant interaction between the depth of cut and speed. This means the effect of one parameter on AE_{RMS} is dependent on the other parameter. The interaction plot is presented in Figure 4.47. Observation from the plot reveals that AE_{RMS} value increases at low speed, high depth of cut and constant feed. Likewise, at a high speed and high depth of cut, AE reduces.

4.6   Predictive modelling for surface roughness using ANN

The machining process is very complex and pure analytical physical modelling is not permitted, thus, empirical models are developed [190]. The recent trend in AI-based models has caused it to be preferred by most researchers to develop models for near-optimal conditions in machining. ANN is a powerful data-modelling tool that utilizes the AI, which can be used to represent complex input-output relationships to predict surface roughness.

Section 2.11 provides comprehensive literature on ANN; therefore, only a brief explanation will be done in this section. A total of fourteen features were selected for the building of the neural

network, these include cutting parameters and time-domain features of AE signal. These features are the inputs and the output is the surface roughness. The experimental data set (total of fifteen) are randomly divided into training data (ten) and testing data (five) and according to literature and previous researches, the training data used in this research is more than the testing data.

4.6.1   Normalisation of data

The numerical values of the dataset exist in different ranges, therefore, the selected features are normalized so that their values lie between 0 and 1, where 0 and 1 correspond to the lowest and highest feature value in the subset respectively. Normalisation of data helps to standardise feature values and reduce redundancy before feeding them into the network. For the percentage error in the prediction to be more or less uniform, normalized values of logarithmic surface roughness are used [191]. The normalisation of data is carried out using the following equation:

$$t_n = \frac{(f_o - f_{min})}{(f_{max} - f_{min})} \tag{4.10}$$

Where t_n is the normalized value of f_o, f_o is the observed value, f_{min} is the minimum observed value in the subset and f_{max} is the maximum value of the observed value in the subset. Normalised data for ANN modelling of surface roughness is shown in the appendix section.

4.6.2   Selected ANN parameters

ANN is a powerful tool for data modelling used to capture and represent complex input-output relationships to classify surface roughness. The design of the ANN model is based on trial and error mainly because obtaining a successful model in ANN depends on the selection of optimum parameters. Therefore, different researchers have tried different model structures to obtain the best model for prediction.

167
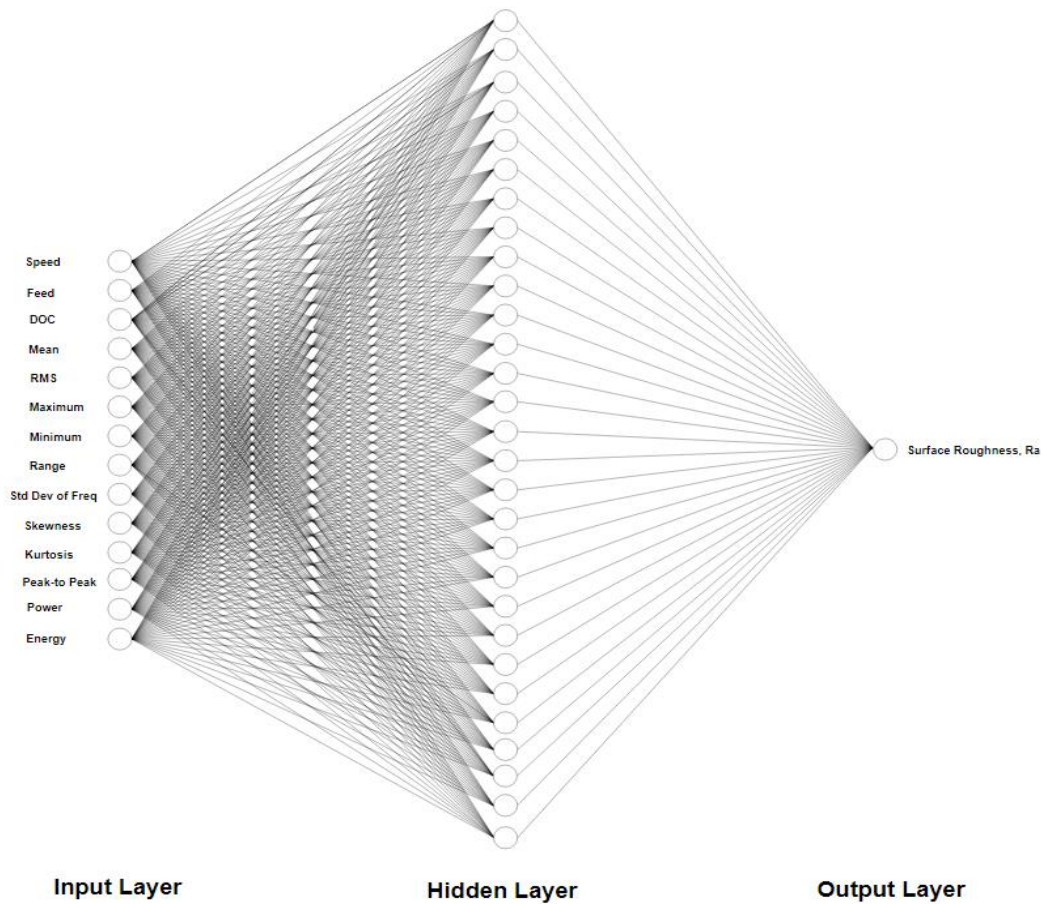
Figure 4.48: Structure of the Artificial Neural Network model

In this research work, a multilayer feed-forward-back propagation neural network structure was used with 14 input, 1 hidden and 1 output layer (Figure 4.48). This algorithm is a supervised learning algorithm and the training and testing were done through the MATLAB software package.

A logsig transfer function is applied in this study to determine the output for individual layers. A logsig function is preferred because it has a simple derivative and is self-limiting. According to Liu *et al*. [192], the function is easy to converge and provides fast learning speed. An advantage of the sigmoid function is that the output cannot grow infinitely large or small [147]. The Logsig (Log-Sigmoid) transfer function is written as follows:

$$f = \frac{1}{1 + e^{-x}} \tag{4.11}$$

In this study, a learning rate of 0.3 on a gradient descent training function with a momentum of 0.9 was used. The adaptive learning rate method assists in rapid improvement of back propagation neural network and the algorithm's accuracy. If an error occurs during learning, it is determined by MATLAB software using performance function. The commonly used performance function for predicting surface is the MSE (mean square error), therefore, this performance function is used. MSE is calculated as follows:

$$MSE = \left(\frac{1}{N} \sum_i [t_1 - o_i]^2 \right) \tag{4.12}$$

Where N is the number of samples, t is the target value and o is the output value.

The selected ANN parameters for surface roughness modelling for both experiments (experiment 1 for kerosene as cutting fluid and experiment 2 for water as cutting fluid) are shown in table 4.11.

Table 4.14: Network parameters

Selected ANN parameter	Value
Network structure	14-29-1
Training/Testing data	10/5
Network algorithm	Feedforward back propagation
Transfer Function	logsig
Training function	traingdx
Learning function	learngd
Performance function	MSE
Learning rate	0.3
Epochs	1000
Momentum	0.9
Weights	Random from [-1 1]

4.6.3 Results and discussion

As stated in the previous section, the network was trained using traingdx of gradient descent with momentum and adaptive LR for both experimental models. Throughout the analysis, the training, validation, and testing were performed several times; to choose the best model with the best fit and

minimum MSE. The training stopped when the validation error increased at iteration 1 000 and iteration 85 for experiment 1 and experiment 2 respectively.

A regression plot is used for validating network performance. Data falling along the 45^0 lines signifies a perfect fit, that is, the network outputs are equal to the targets. As shown in Figure 4.49 (a-b), it is important to note that the circles represent the data points and the coloured line represents the best fit between outputs and targets (as they are aligned along the dotted line). Furthermore, it is desired that correlation coefficient R values be very high, that is close to 1[39, 147, 193, 194]. Correlation coefficient R provides a measure of how close a model is to the actual values. It a measure of the explanatory power of the model and it can be computed as [195]:

$$R = \sqrt{\frac{\sum_{m=1}^{M}(y_m - \bar{y})^2 - \sum_{m=1}^{M}(y_m - \hat{y}_m)^2}{\sum_{m}^{M}(y_i - \bar{y})^2}} \quad (4.13)$$

Where, y_m is the observed dependent variable, $\hat{y}_m$ is the fitted dependent variable for the independent variable X_m, X_m is the independent variable in the Mth trial, $\bar{y}$ is the mean, $\sum_{m=1}^{M}(y_m - \bar{y})^2$ is the total sum of squares and $\sum_{m=1}^{M}(y_m - \hat{y}_m)^2$ is the residual sum of squares.
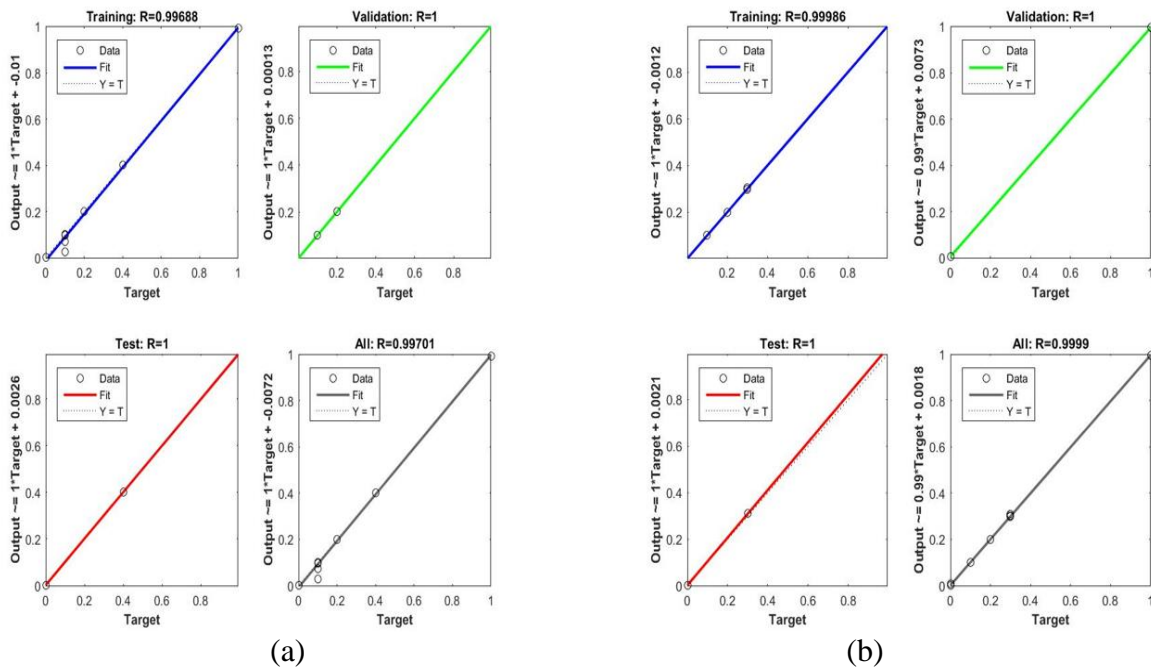
Figure 4.49: (a-b) Regression plots for surface roughness model by feed-forward neural network model for training, validation, testing samples and all data set for experiment 1 and 2.

170

The best R-value for experiment 1 (Figure 4.49 (a)) surface roughness model is 0.997, 1 and 1 for training, validation and testing respectively. While experiment 2 (Figure 4.49 (b)) is 0.9999, 1 and 1 for training, validation and testing respectively. The overall R-value for the surface roughness model of experiment 1 and 2 can be observed as all data are properly fitted to the line, which indicates that the neural network is correct and can be used for predicting the output for other input data sets.

(a)　　　　　　　　　　　　　　　　(b)
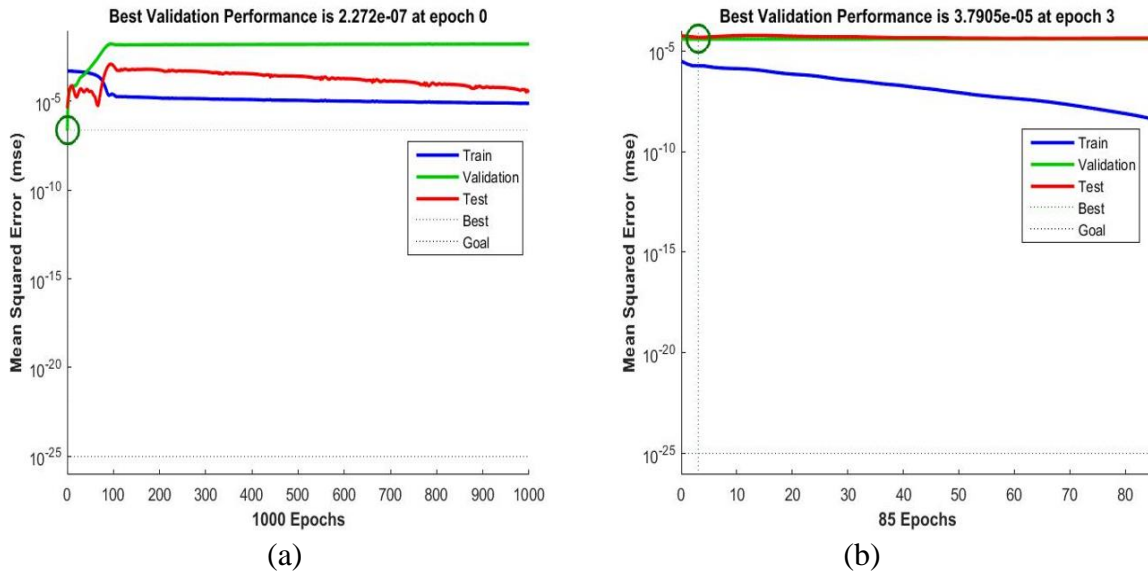
Figure 4.50: (a-b) Performance plot in ANN for surface roughness model for experiment 1and 2

The performance plot is shown in Figure 4.50 (a-b) represents the iteration number (epoch) versus the mean square error of the network. The mean square error dynamics for all datasets are presented in logarithmic scale. The plot consists of the training, validation and test errors recorded during the training of the network. Usually, the error decreases after more epoch of training and could start to increase on the validation data set as the network starts over-fitting the training data. However, the training stopped as the validation error started to increase, and the best performance is taken at the epoch with the lowest validation error.

When choosing the best validation performance of a network, the following must be ensured [194]: the final mean-square error is small, and the characteristics of test and the validation set error are the same. As shown in Figure 4:50 (a), the process stopped at epoch 1 000 for experiment 1 model and epoch 85 for experiment 2 model. The best validation performance occurred at epoch 0 with

171

MSE of 2.272e-07 for experiment 1 model, while the MSE of 3.7905e-05 occurred at epoch 3 for experiment 2 model. These error values show perfect training.

Figure 4:51 (a-b) shows the training state for the artificial neural model of surface roughness for experiment 1 and 2. The plot consists of the variation of the gradient error, validation failure and learning rate. The gradient is a value of back propagation (BP) gradient on each iteration in logarithmic scale and the validation fails are iterations that occur when validation MSE increases in value. As described in the validation performance plot, the training state plot confirmed that the errors in experiment 1 are repeated 1000 times and stopped at epoch 1000. On the other hand, the errors are repeated 81 times and stopped at epoch 85 for experiment 2. The repetition of error in model 2 implies that over-fitting of data starts after epoch 3 and at epoch 0 for model 1. That is the reason why epoch 3 and 0 are selected as the base and its weights are chosen as the final weights.

(a)   (b)
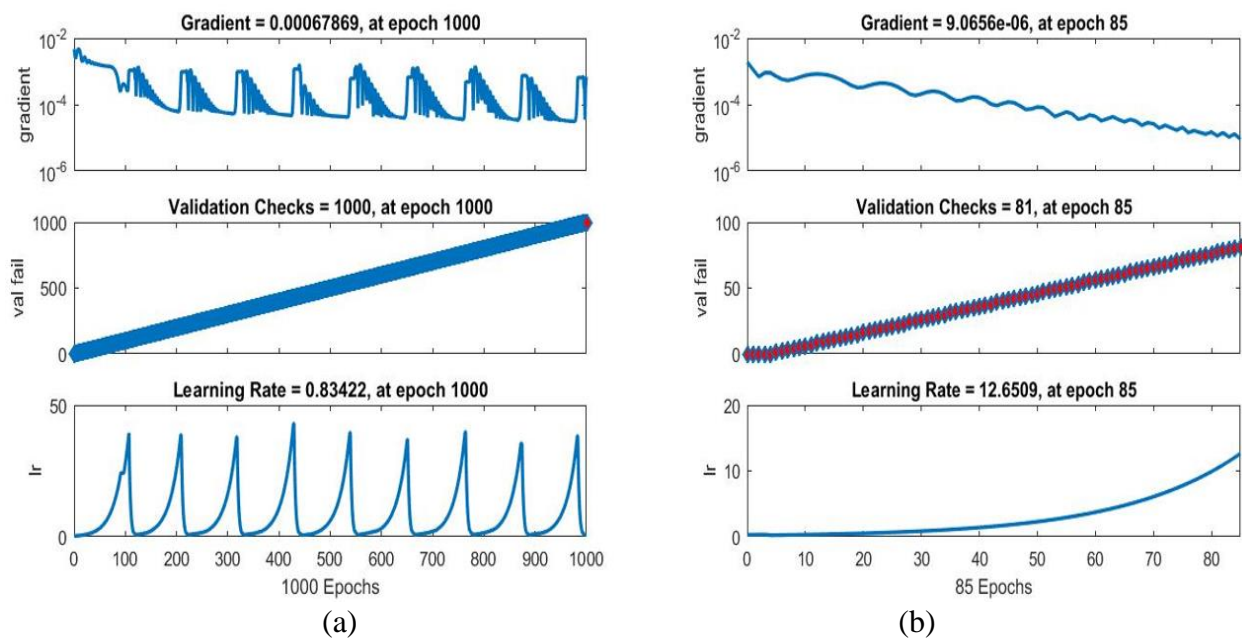
Figure 4.51: (a-b) Training state for the artificial neural network model for experiment 1 and 2

As specified in table 4.11, neural network training was performed using ten (experiment 1-10) from fifteen experimental data (the reason for this had been explained in section 2.11). The remaining five experimental data (experiment 11-15) were used for network testing. The same amount and order of training and testing data were used for both experiments. The predicted results

of the testing process from the ANN models are compared with the experimental test results as shown in Table 4.12. Figure 4.51 and Figure 4.52present the graph that shows the pattern of the data between the measured surface roughness and the ANN predicted output.

Table 4.15: Comparison of ANN testing outputs with experimental findings

Run	Experiment 1 (With Kerosene mist as cutting fluid)			Experiment 2 (With water as cutting fluid)		
	Experimental Ra Value (nm)	ANN Predicted Ra Value (nm)	% Error	Experimental Ra Value (nm)	ANN Predicted Ra Value (nm)	% Error
11	13	13	1.160	13	14	10.611
12	19	17	9.358	17	18	3.158
13	12	13	8.435	12	11	6.853
14	13	13	0.052	13	14	10.611
15	17	17	1.325	14	14	2.548
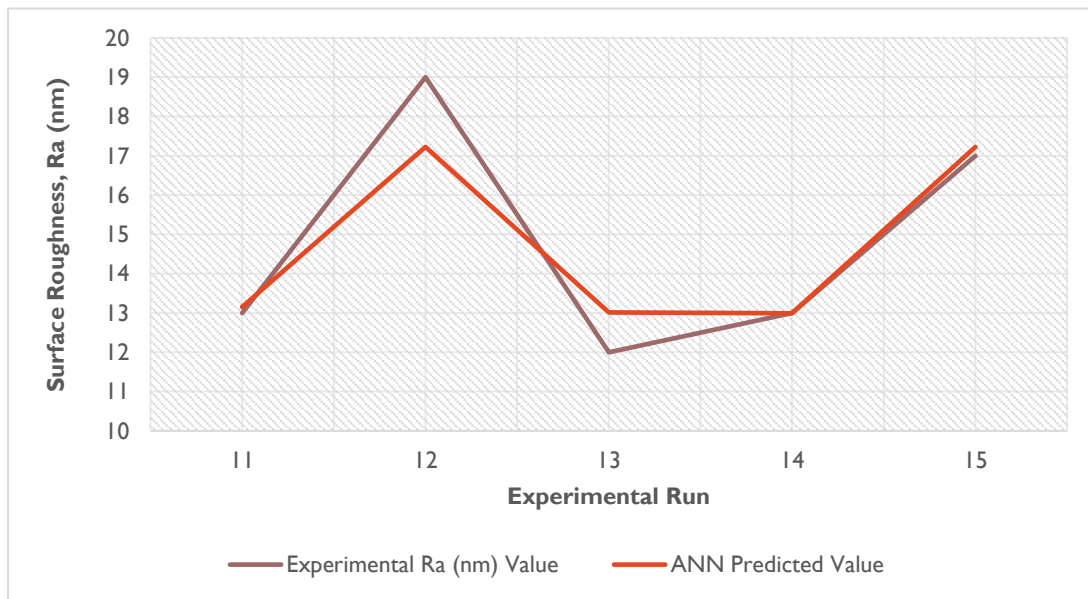
Figure 4.52: Comparison between the measured and ANN predicted surface roughness for experiment 1 "test" data.

173
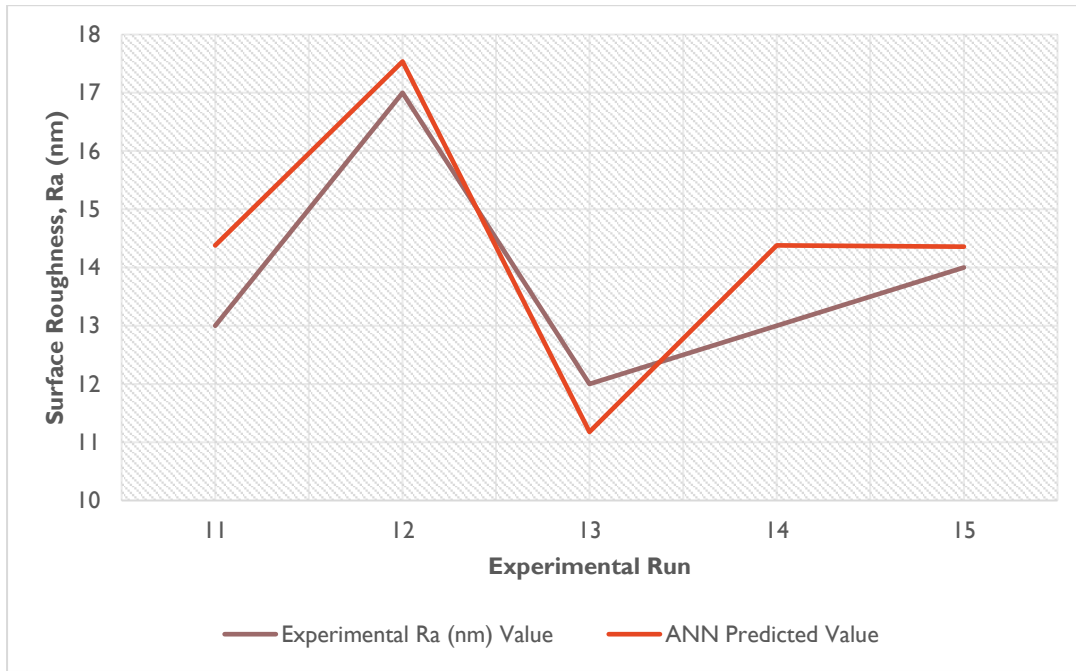
Figure 4.53: Comparison between the measured and ANN predicted surface roughness for experiment 2 "test" data.

Small variations were observed between the predicted and the original experimental values for the selected testing data, notably at experimental order 12 and 13 of experiment 1; and experimental order 11, 13 and 14 of experiment 2. Nonetheless, there is a close margin between the experimental values and predicted values for both experiments. Furthermore, the results follow the same pattern in the charts, which indicate that the ANN prediction is in agreement with the experimental results.

4.6.4 Comparison of RSM and ANN models for surface roughness

A previously mentioned, ANN and RSM models have been developed to predict the surface roughness of RSA 431 during diamond turning. The predictive ability of these two tools can be evaluated, based on their predictive accuracy. The evaluation is done by comparing the model surface roughness prediction results with the experimental results. The mean absolute percentage error (MAPE) is used as a performance criterion to show the accuracy values of RSM and ANN model. The MAPE value for each predictive tool can be estimated as:

$$MAPE = \left(\frac{1}{n}\sum_{i=1}^{n}\left|\frac{R_{a,i}-R_{a,i}^{P}}{R_{a,i}}\right| \times 100\right) \tag{4.13}$$

174

Where; n = the total number of measurements, i = the estimated measurement for a specific run, $R_{a,}$ = the measured surface roughness for a specific run, $R_{a,i}^{P}$ = the predicted surface roughness for a specific run.

Table 4.16 shows the summary of surface roughness values for ten experimental runs obtained during the diamond turning of RSA 431 as well as the corresponding predicted values obtained by the RSM and ANN models. The calculated MAPE for each model was presented for accuracy validation.

Table 4.16: Comparison of RSM and ANN predictive modelling tools

Experimental Run	Experiment 1 (Kerosene mist as cutting fluid)			Experiment 2 (Water as cutting fluid)		
	Experimental Ra Value (nm)	RSM Predicted Ra Value (nm)	ANN Predicted Ra Value (nm)	Experimental Ra Value (nm)	RSM Predicted Ra Value (nm)	ANN Predicted Ra Value (nm)
1	27	28	25	17	20	18
2	12	12	13	11	10	11
3	25	28	25	19	18	18
4	50	34	49	40	29	40
5	16	15	17	11	11	11
6	13	12	13	12	10	11
7	13	13	13	13	13	14
8	10	10	10	9	10	8
9	9	9	9	8	8	8
10	15	17	13	14	14	14
MAPE		7.77 %	4.66 %		8.60 %	4.28 %

The MAPE results obtained from the two predictive tools, RSM and ANN, for each experiment shows that the ANN model could predict surface roughness for training data set with MAPE of 4.66% and 4.282% for experiment 1 and 2 model respectively. Alternatively, RSM could predict with MAPE of 7.765% and 8.6% for experiments 1 and 2 model respectively. A MAPE value that

is less than 10% implies a reasonable/ good model. Therefore, ANN is suggested as the better prediction model when compared to the RSM model, due to its high accuracy and it can be used further for surface roughness prediction of diamond turning of RSA 431.

Chapter Five

5.1 Conclusion

This research work aims to investigate the surface roughness of RSA 431 during diamond turning. RSA 431 is a relatively new material in micro-manufacturing for the production of optical and precision components. Therefore, curiosity and industrial demands for miniaturised products with quality surface finish motivated this research work.

During the research, the effect of cutting parameters - depth of cut, feed, and speed, on the quality of the surface of RSA 431 during SPDT were investigated when kerosene mist and water were used as the cutting fluids. The principle of AE sensing technique was adopted to monitor the cutting conditions of SPDT operation, and the mathematical models from RSM and ANN were obtained to ensure surface roughness prediction. Optimisation was carried out using RSM to find the values of machining parameters leading to minimum surface roughness. From this study, the following conclusions were drawn:

- The lowest surface roughness value for machining with water as the cutting fluid was recorded as 8 nm, while that of machining with kerosene mist as cutting fluid was 9 nm. The low surface roughness recorded can be attributed to the general effect of cutting fluids, which penetrate the cutting interface and reduce the coefficient of friction. Moreover, the cutting fluids reduce the adhesion between the tool face and chips through a chemical reaction.
- Water as a cutting fluid offers better surface roughness than kerosene mist. This could be a result of the reaction of the high content of silicon in RSA 431 with water. Water molecules prevent micro-plasma generation from occurring between the diamond tool and silicon-content workpiece, thereby, reducing surface roughness. The difference could also be attributed to the organic nature of kerosene mist, which forms carbide on the workpiece surface during machining and retards the surface finish.
- The effect of water as cutting fluid on surface roughness can also be linked to its potency in terms of chip clearing and elimination of built up edge.

177

- The results of ANOVA show that the developed mathematical model using RSM allows for the prediction of surface roughness with a 95% confidence level. The models obtained from the experimental data have coefficients of determination of $R^2 = 0.9648$ and 0.9033 for experiment 1 and 2 respectively. The prediction error of RSM for each experiment is 7.77% and 8.60%. In order of influence, feed has the most significant effect during SPDT of RSA 431, followed by speed and lastly, depth of cut. Surface roughness increases as feed increases. This may be caused by the high stress experienced on the cutting tool, which results in vibration and heat generated between workpiece and cutting tool, vibration and surface roughness are directly proportionate. Increasing the cutting speed leads to high surface roughness, this can be attributed to the reduced time for contact between the workpiece material and tool holder. Generally, an increase in DOC increases the cutting force and the uncut chip. Nonetheless, due to the low depth of cut values used for this research, DOC has little or no effect on the surface roughness of RSA 431 when diamond-turned.

- The increasing trend of the amplitudes of raw AE signals do not follow a consistent pattern with increase in surface roughness, hence, it may be unsuitable for online monitoring. Nevertheless, online monitoring can be initiated by analysing the real-time burst AE signals in the time-domain.

- Time-domain features show a good correlation with surface roughness; therefore, they can be used as input parameters in a neural network scheme.

- The predictive models developed using ANN indicate that surface roughness could be obtained with the selected parameters. The predicted values by the ANN model are in close relation with the experimental results. It has been established that the model developed using ANN is capable of predicting surface roughness accurately using a small number of training data. The prediction error values for each experiment is 4.66% and 4.28%.

- The developed predictive models have been compared using MAPE, it was discovered that ANN performs better than RSM for predicting surface roughness.

- The optimal cutting combination for the lowest surface roughness of 8 nm when water is used as cutting fluid, has been achieved with low values of feed and depth of cut about 5 µm and 5 mm/min respectively. The lowest surface roughness of 9 nm when kerosene mist

is used as cutting fluid, has been achieved at low feed about 5 mm/min and an average depth of cut with high values of speed. Hence, feed has a pronounced effect on surface roughness, followed by speed and then depth of cut.

5.2 Recommendations

In this study, three cutting parameters were used for the investigation of surface roughness of RSA 431. Cutting conditions such as forced vibration and cutting force can also be monitored to analyse surface roughness. Furthermore, a Polycrystalline diamond tool can also be used as a cutting tool for RSA 431 turning, as an alternative to the monocrystalline diamond tool used in this research. The polycrystalline diamond tool has a higher cutting removal rate with a uniform surface finish. It was observed that alloy elements of the workpiece material have significant effects on the surface finish. In future works, the effect of microstructure distribution of alloying elements on surface roughness could be investigated using molecular dynamics. The signal processing of AE signals in time-frequency and frequency domain may also be utilised in the future study. Possible investigation of tool wear and the relationship with the surface roughness can also be considered.

References

[1]   "Merriam-Webster's collegiate dictionary," in *Merriam-Webster's collegiate dictionary*, Springfield, Ed., 11 th ed: MA: Merriam-Webster Incorporated, 2019.

[2]   Ikawa N *et al.*, "Ultraprecision metal cutting —the past, the present and the future," *Annals of the CIRP,* vol. 40, pp. 587-594, 1991.

[3]   Chiu M and B. Lee W, "Development of ultraprecision machining technology," *Fifth International Conference on FACTORY 2000,* pp. 486-490, 1997.

[4]   J. Roblee. "Factors affecting surface finish in diamond turning, Precitech ultra precision technology." http://precitech.com/FactorsAffectingSurfFinish.pdf (accessed.

[5]   J. Yuan, B. Lyu, W. Hang, and Q. Deng, "Review on the progress of ultra-precision machining technologies," *Frontiers of Mechanical Engineering,* vol. 12, no. 2, pp. 158-180, 2017/06/01 2017, doi: 10.1007/s11465-017-0455-9.

[6]   M. P.Groover, *Fundamentals of Modern Manufacturing : Materials, Process, and Systems*, 4th ed. 111 River Street, Hoboken, NJ: JohnWiley & Sons, Inc, 2010.

[7]   S. S. Joshi, "Ultraprecision Machining (UPM)," *Encyclopedia of Nanotechnology,* pp. 4254-4324, 2016, doi: 10.1007/978-94-017-9780-1.

[8]   A. E. D. J. Caldeirani Filho, "Influence of Cutting Conditions on Tool Life, Tool Wear and Surface Finish in the Face Milling Process," *Journal of the Brazilian Society of Mechanical Sciences,* vol. 24, 2002. [Online]. Available: http://dx.doi.org/10.1590/S0100-73862002000100002

[9]   Venkatesh.V.C and S. Izman, *Precision Engineering*. USA: Tata McGraw-Hill Publishing Company Limited., 2007, pp. 1-406.

[10]   S. Goel, X. Luo, A. Agrawal, and R. L. Reuben, "Diamond machining of silicon: A review of advances in molecular dynamics simulation," *International Journal of Machine Tools and Manufacture,* vol. 88, pp. 131-164, 2015/01/01/ 2015, doi: https://doi.org/10.1016/j.ijmachtools.2014.09.013.

[11]   D. Dornfeld and D.-E. Lee, *Precision Manufacturing*. 233 Spring Street, New York, NY 10013, USA: Springer science +business media, LLC, 2008, pp. 1-775.

[12]   S. Kalpakjian and S. Schmid, R, *Manufacturing Engineering and technology*. Prentice Hall, 2001.

[13]   ASPE. "Precison Engineering." http://www.aspe.net (accessed.

[14]   M. Weck, *Handbook of Machine Tools*. John Wiley, 1984.

[15]   J. Chae, S. S. Park, and T. Freiheit, "Investigation of micro-cutting operations," *International Journal of Machine Tools and Manufacture,* vol. 46, no. 3, pp. 313-332, 2006/03/01/ 2006, doi: https://doi.org/10.1016/j.ijmachtools.2005.05.015.

[16]   N. Taniguchi, "Current status in, and future trends of, ultraprecision machining and ultrafine materials processing," *CIRP annals,* vol. 32, no. 2, pp. 573-582, 1983.

[17]   M. C. Gerchman, "Specifications and manufacturing considerations of diamond machined optical components," *Proc. SPIE,* vol. 0607, pp. 36–45, 1986.

[18]   S. Zhang, J, S. To, Z. W. Zhu, and G. Zhang, Q, "A review of fly cutting applied to surface generation in ultra-precision machining," *International Journal of Machine Tools & Manufacture,* vol. 103, pp. 13 - 27, 2016, doi: 10.1016/j.ijmachtools.2016.01.001.

[19]   J. Ramsden, *Description of an Engine for Dividing Strait Lines on Mathematical Instruments: By Mr. J. Ramsden, Mathematical Instrument-maker, and Optician. Published by Order of the Commissioners of Longitude*. William Richardson; and sold by John Nourse; and Mess. Mount and Page, 1779.

[20]   C. Evans, *Precision Engineering: an Evolutionary View*. Cranfield Press, 1989.

[21]   M. A. Davies, C. J. Evans, R. R. Vohra, B. C. Bergner, and S. R. Patterson, "Application of precision diamond machining to the manufacture of microphotonics components," in *Optical Science and Technology, SPIE's 48th Annual Meeting*, 2003, vol. 5183: SPIE, p. 15.

[22]   Hannah.P.R, "A personal prospective on the quest for higher precision diamond turning lathes," *Proc. Int. Congress for Ultraprecision Technology (Aachen),* pp. 237-251, 1988.

[23]   L. Li, "Investigation of the Optical Effects of Single Point Diamond Machined Surfaces and the Applications of Micro Machining," The Ohio State University, 2009. [Online]. Available: http://rave.ohiolink.edu/etdc/view?acc_num=osu1252435737

[24]   Zhenghong Zhu and Q. Jiang, "Research on Precision and Ultra-precision Machining Technology Development," presented at the International Conference on Intelligent Systems Research and Mechatronics Engineering, China, 2015.

[25]   O. T and k. Abou-El-Hossein, "Surface roughness analysis when diamond turning optical grade rapidly solidified aluminium RSA 905," *The Optical Society of India,* vol. 46, no. 4, pp. 446-455, December 2017 2017, doi: 10.1007/s12596-017-0405-2.

[26]   S. Shimada, N. Ikawa, H. Tanaka, G. Ohmori, J. Uchikoshi, and H. Yoshinaga, "Feasibility study on ultimate accuracy in microcutting using molecular dynamics simulation," *CIRP annals,* vol. 42, no. 1, pp. 91-94, 1993.

[27]   A. Novan. "Surface Roughness." http://arknovin.com/en/quality-control/surface-quality/surface-roughness.html (accessed.

[28]   B. Bhushan, "Surface roughness analysis and measurement techniques," in *Modern Tribology Handbook, Two Volume Set*: CRC press, 2000, pp. 74-144.

[29]   E. Gadelmawla, M. Koura, T. Maksoud, I. Elewa, and H. Soliman, "Roughness parameters," *Journal of Materials Processing Technology,* vol. 123, no. 1, pp. 133-145, 2002.

[30]   S. M. O. Tavares, "Analysis of surface roughness and models of mechanical contacts," *Thesiss, Facolta di Ingegneria–Universita di Pisa, Italy,* 2005.

[31]   T. Hobson and G. PRECISION'S, "Exploring Surface Texture: A fundamental guide to the measurement of surface finish," *Leicester–Inglaterra, 4th edition, ed. Taylor Hobson Ltda,* vol. 100, 2003.

[32]   C. F. Cheung and W. B. Lee, *Surface Generation in Utra-precision Diamond Turning: Modelling and Practices* (Engineering Research Series, no. 10). London and Bury St Edmunds, UK, 2003, p. 267.

[33]   H. Haitjema, "Uncertainty analysis of roughness standard calibration using stylus instruments," *Precision Engineering,* vol. 22, no. 2, pp. 110-119, 1998/04/01/ 1998, doi: https://doi.org/10.1016/S0141-6359(97)00090-1.

[34]   D. R. Burada *et al.*, "Metrology techniques for ultra-precision diamond turned freeform optics," in *Optical Design and Fabrication 2019 (Freeform, OFT)*, Washington, DC, 2019/06/10 2019: Optical Society of America, in OSA Technical Digest, p. JW2A.4, doi: 10.1364/FREEFORM.2019.JW2A.4.   [Online].   Available: http://www.osapublishing.org/abstract.cfm?URI=Freeform-2019-JW2A.4

[35]   S. Zhang, J, S. To, G. Zhang, Q , and Z. W. Zhu, "A review of machine-tool vibration and its influence upon surface generation in ultra-precision machining," *International Journal of Machine Tools and Manufacture,* vol. 91, pp. 34-42, 2015, doi: 10.1016/j.ijmachtools.2015.01.005.

[36]   S. Zhang, J, S. To, S. J. Wang, and Z. W. Zhu, "A review of surface roughness generation in ultra-precision machining," *International Journal of Machine Tools & Manufacture,* vol. 91, pp. 76-95, 2015, doi: 10.1016/j.ijmachtools.2015.02.001.

[37]   C. Cheung and W. Lee, "A theoretical and experimental investigation of surface roughness formation in ultra-precision diamond turning," *International Journal of Machine Tools and Manufacture,* vol. 40, no. 7, pp. 979-1002, 2000, doi: 0890-6955.

[38]   S. To, W. B. Lee, and C. Y. Chan, "Ultraprecision diamond turning of aluminium single crystals," *Journal of Materials Processing Technology,* vol. 63, no. 1, pp. 157-162, 1997/01/01/ 1997, doi: https://doi.org/10.1016/S0924-0136(96)02617-9.

[39]   M. M. Liman, "Diamond Turning of Contact Lens Polymers," Masters, Mechatronics, Nelson Mandela University, South Africa, 2016.

[40]   H. Mohammadi, H. Bogac Poyraz, D. Ravindra, and J. Patten, *An Experimental Study on Single Point Diamond Turning of an Unpolished Silicon Wafer via Micro-Laser Assisted Machining*. 2014.

[41]   S. S. To, H. Wang, and W. B. Lee, *Materials characterisation and mechanism of micro-cutting in ultra-precision diamond turning*. Springer, 2018.

[42]   Y. Furukawa, N. Moronuki, and K. Kitagawa, "Development of ultra precision Machine Tool made of Ceramics," *CIRP Annual Manufacturing Technology,* vol. 35, pp. 279–282, 1986.

[43]   P. McKeown, "From Micro-to Nano-Machining -Towards the Nanometre Era," Sens Rev, 1996, ch. 16, pp. 4-10.

[44]   Kim.J.D. and Kim.D.S., "Development and Application of an Ultra-precision Lathe,"*, International Journal Advanced Manufacturing Technology,* vol. 13, pp. 164–171, 1997.

[45]   Y.-B. Bang, K.-m. Lee, and S. Oh, "5-axis micro milling machine for machining micro parts," *International Journal of Advanced Manufacturing Technology,* vol. 25, pp. 888-894, 05/01 2005, doi: 10.1007/s00170-003-1950-1.

[46]   T. Moriwaki, A. Horiuchi, and K. Okuda, "Effect of cutting heat on machining accuracy in ultraprecision diamond turning," *Annals of the CIRP,* vol. 39, no. 1, p. 81, 1990.

[47]   T. Moriwaki and E. Shamoto, "Analysis of thermal deformation of an ultra precision air spindle system," *CIRP Ann. - Manuf. Technol,* vol. 47, pp. 315–319, 1998.

[48]   A. Yip, "Factors Affecting Surface Topography in Diamond Turning," Master of Applied Science, Mechanical Engineering, McMaster University, Canada, 2014.

[49]   C. Cheung, F, and W. Lee, B, "Study of Factors Affecting the Surface Quality in Ultra-Precision Diamond Turning," *Materials and Manufacturing Processes,* vol. 15, no. 4, pp. 481-502, 2000/07/01 2000, doi: 10.1080/10426910008913001.

[50]   H. Hatem, "Study the Effect of Cutting Conditions for turning process," *ALNAHRAIN JOURNAL FOR ENGINEERING SCIENCES,* vol. 14, no. 1, pp. 61-66, 2011.

[51]   M. Vijay Kumar, B. J. Kiran Kumar, and N. Rudresha, "Optimization of Machining Parameters in CNC Turning of Stainless Steel (EN19) By TAGUCHI'S Orthogonal Array Experiments," *Materials Today: Proceedings,* vol. 5, no. 5, Part 2, pp. 11395-11407, 2018/01/01/ 2018, doi: https://doi.org/10.1016/j.matpr.2018.02.107.

[52]   C. Natarajan, Muthu.S, and Karuppuswamy.P, "Investigation of cutting parameters of surface roughness for a non-ferrous material using artificial neural network in CNC turning," *Journal of Mechanical Engineering Research,* vol. 3, no. 1, pp. 1-14, 22 November, 2010 2011.

[53]   O. O. A and A.-E.-H. K, "Acoustic Emission Monitoring in Ultra-High Precision Machining of Rapidly Solidified Aluminium," in *COMA'13*, 2013.

[54]   Mário.C.Santos.Jr., Alisson.R.Machado., Wisley.F.Sales., Marcos.A.S.Barrozo., and Emmanuel.O.Ezugwu., "Machining of aluminum alloys: a review," *Int J AdvManuf Technol,* 2016, doi: 10.1007/s00170-016-8431-9.

[55]   K. Abou-El-Hossein, O. Olufayo, and Z. Mkoko, "Diamond tool wear during ultra-high precision machining of rapidly solidified aluminium RSA 905," *Wear,* vol. 302, no. 1-2, pp. 1105-1112, 2013, doi: 10.1016/j.wear.2012.12.060.

[56]   J. Babu.R. and Ramesh.Babu.A., "Correlation Among the Cutting Parameters, Surface Roughness and Cutting Forces in Turning Process by Experimental Studies," *All India Manufacturing Technology, Design and Research Conference,* 2014.

[57]   Aswathy.V.G., Rajeev.N., and Vijayan.K., "Effect of machining parameters on surface roughness, material removal rate....wet turning of Ti-6Al-4V alloy," *Int. Journal of Applied Sciences and Engineering Research,* vol. 4, no. 1, 2015, doi: 10.6088/ijaser.04001.

[58]   C. F. Cheung and W. B. Lee, "Characterisation of nanosurface generation in single-point diamond turning," *International Journal of Machine Tools and Manufacture,* vol. 41, no. 6, pp. 851-875, 2001/05/01/ 2001, doi: https://doi.org/10.1016/S0890-6955(00)00102-4.

[59]   L. Li, N. Yu, C. Chan, and W. Lee, "Al6061 surface roughness and optical reflectance when machined by single point diamond turning at a low feed rate," *PloS one,* vol. 13, no. 4, 2018.

[60]   Abhanga.L.B. and Hameedullaha.M., "Parametric Investigation of Turning Process on En-31 steel," *Procedia Materials Science,* vol. 6, pp. 1516 – 1523, 2014.

[61]   F. Fang and G. Zhang, "An experimental study of edge radius effect on cutting single crystal silicon," *The International Journal of Advanced Manufacturing Technology,* vol. 22, no. 9-10, pp. 703-707, 2003.

[62]   K. Abou-El-Hossein, "Quality of silicon convex lenses fabricated by ultra-high precision diamond machining," *South African Journal of Industrial Engineering,* vol. 24, no. 1, pp. 91-97, 2013.

[63]   H. Xu, X. Zhang, M. Xu, and X. Li, "Study on the control of surface roughness in single point diamond turning," in *6th International Symposium on Advanced Optical Manufacturing and Testing Technologies: Advanced Optical Manufacturing Technologies*, 2012, vol. 8416: International Society for Optics and Photonics, p. 84161D.

[64]   A. Gani and R. Zareena, "Extension of ultra precision machining to titanium alloys," 2010.

[65]   Z. J. Yuan, M. Zhou, and S. Dong, "Effect of diamond tool sharpness on minimum cutting thickness and cutting surface integrity in ultraprecision machining," *Journal of Materials Processing Technology,* vol. 62, no. 4, pp. 327-330, 1996/12/01/ 1996, doi: https://doi.org/10.1016/S0924-0136(96)02429-6.

[66]   Xu H, Zhang X, Xu M, and L. X., "Study on the control of surface roughness in single point diamond turning," *6th International Symposium on Advanced Optical Manufacturing and Testing Technologies (AOMATT 2012),* pp. 84161D-84161D-7, 2012.

[67]   K. E. Puttick, M. R. Rudman, K. J. Smith, A. Franks, and K. Lindsey, "Single-point diamond machining of glasses," *Proceedings of the Royal Society of London. A. Mathematical and Physical Sciences,* 10.1098/rspa.1989.0116 vol. 426, no. 1870, p. 19, 1989. [Online]. Available: http://rspa.royalsocietypublishing.org/content/426/1870/19.abstract.

[68]   M. Arif, Z. Xinquan, M. Rahman, and S. Kumar, "A predictive model of the critical undeformed chip thickness for ductile–brittle transition in nano-machining of brittle materials," *International

Journal of Machine Tools and Manufacture, vol. 64, pp. 114-122, 2013/01/01/ 2013, doi: https://doi.org/10.1016/j.ijmachtools.2012.08.005.

[69]   Y. Furukawa and N. Moronuki, "Effect of Material Properties on Ultra Precise Cutting Processes," *CIRP Annals,* vol. 37, no. 1, pp. 113-116, 1988/01/01/ 1988, doi: https://doi.org/10.1016/S0007-8506(07)61598-4.

[70]   K. Rathod. "Aluminium and it's alloys." https://www.slideshare.net/KunalRathod2/aluminium-and-its-alloys (accessed.

[71]   NA, "Machining of Aluminum and Aluminum Alloys," in *Machining*, vol. 16: ASM Handbook, 1989, ch. 761-804.

[72]   M. G. Kalhapure and P. M. Dighe, "Impact of silicon content on mechanical properties of aluminum alloys," *Int. J. Sci. Res,* vol. 4, pp. 38-40, 2015.

[73]   R. Rana, R. Purohit, and S. Das, "Reviews on the influences of alloying elements on the microstructure and mechanical properties of aluminum alloys and aluminum alloy composites."

[74]   W. König and D. Erinski, "Machining and Machinability of Aluminium Cast Alloys," *CIRP Annals,* vol. 32, no. 2, pp. 535-540, 1983/01/01/ 1983, doi: https://doi.org/10.1016/S0007-8506(07)60180-2.

[75]   V. Songmene, R. Khettabi, I. Zaghbani, J. Kouam, and A. Djebara, "Machining and Machinability of Aluminum Alloys," in *Aluminium Alloys, Theory and Applications*, P. T. Kvackaj Ed. Canada: InTech, 2011, ch. 18, pp. 377-400.

[76]   N. A. Belov, D. G. Eskin, and N. N. Avxentieva, "Constituent phase diagrams of the Al–Cu–Fe–Mg–Ni–Si system and their application to the analysis of aluminium piston alloys," *Acta Materialia,* vol. 53, no. 17, pp. 4709-4722, 2005/10/01/ 2005, doi: https://doi.org/10.1016/j.actamat.2005.07.003.

[77]   G. H. Garza Elizondo, "Effect of Ni, Mn, Zr and Sc additions on the performance of Al-Si-Cu-Mg alloys," Université du Québec à Chicoutimi, 2016.

[78]   G. V Galevsky, V. V Rudneva, and V. S Aleksandrov, "Current state of the world and domestic aluminium production and consumption," *IOP Conference Series: Materials Science and Engineering,* vol. 411, p. 012017, 10/19 2018, doi: 10.1088/1757-899X/411/1/012017.

[79]   T. Otieno, "The machinability of rapidly solidified aluminium alloy for optical mould inserts," Masters, Mechatronics, Nelson Mandela University, South Africa, 2017.

[80]   A. I. H. Committee, "Machining of aluminum and aluminum alloys," *Metals Handbook,* 1989.

[81]   E. M. Trent and P. K. Wright, *Metal cutting*. Butterworth-Heinemann, 2000.

[82]   P. Roy, S. K. Sarangi, A. Ghosh, and A. K. Chattopadhyay, "Machinability study of pure aluminium and Al–12% Si alloys against uncoated and coated carbide inserts," *International Journal of*

Refractory Metals and Hard Materials, vol. 27, no. 3, pp. 535-544, 2009/05/01/ 2009, doi: https://doi.org/10.1016/j.ijrmhm.2008.04.008.

[83]   I. Zaghbani and V. Songmene, "A force-temperature model including a constitutive law for Dry High Speed Milling of aluminium alloys," *Journal of Materials Processing Technology,* vol. 209, no. 5, pp. 2532-2544, 2009/03/01/ 2009, doi: https://doi.org/10.1016/j.jmatprotec.2008.05.050.

[84]   H. Demir and S. Gündüz, *The effects of aging on machinability of 6061 aluminium alloy*. 2009, pp. 1480-1483.

[85]   G. P. H.Gubbels, W. H. v. V. Bart, A. J. Bosch, and R. Senden, "Rapidly solidified aluminium for optical applications," *Advanced Optical and Mechanical Technologies in Telescopes and instrumentation,* vol. 7018, pp. 70183A-9, 2008.

[86]   G. Onwuka, K. Abou-El-Hossein, and Z. Mkoko, "AE Monitoring of Diamond Turned Rapidly Soldified Aluminium 443," *International Conference on Recent Trends in Physics 2016,* vol. 843, p. NP, 2017, doi: 10.1088/1742-6596/755/1/011001

10.1088/1742-6596/843/1/012059.

[87]   F. Alshmri, "Rapid Solidification Processing: Melt Spinning of Al-High Si Alloys," in *Advanced Materials Research*, 2012, vol. 383: Trans Tech Publ, pp. 1740-1746.

[88]   E. J. Lavernia and T. S. Srivatsan, "The rapid solidification processing of materials: science, principles, technology, advances, and applications," *Journal of Materials Science,* vol. 45, no. 2, p. 287, 2010.

[89]   P. Lobry, L. Błaż, M. Sugamata, and A. Kula, "Effect of Rapid Solidification on Structure and Mechanical Properties of Al–6Mn–3Mg Alloy," *Archives of Material Science and Engineering,* vol. 49, no. 2, pp. 97-102, 2011.

[90]   M. Cohen, B. H. Kear, and R. Mehrabian, "Rapid Solidification Processing. An Outlook," MASSACHUSETTS INST OF TECH CAMBRIDGE, 1980.

[91]   B. Cantor, "Fundamentals of rapid solidification," in *Science and Technology of the Undercooled Melt*: Springer, 1986, pp. 3-28.

[92]   L. Katgerman and F. Dom, "Rapidly solidified aluminium alloys by meltspinning," *Materials Science and Engineering: A,* vol. 375-377, pp. 1212-1216, 2004/07/01/ 2004, doi: https://doi.org/10.1016/j.msea.2003.10.094.

[93]   H. Group. "High-performance alloys and Melt Spinning." https://hittech.com/en/portfolio-posts/high-performance-alloys-and-melt-spinning/ (accessed.

[94]   R. F. Ávila and A. M. Abrão, "The effect of cutting fluids on the machining of hardened AISI 4340 steel," *Journal of Materials Processing Technology,* vol. 119, no. 1, pp. 21-26, 2001/12/20/ 2001, doi: https://doi.org/10.1016/S0924-0136(01)00891-3.

[95] J. P. Byers, "Metalworking fluids," (in English), 2017. [Online]. Available: http://app.knovel.com/hotlink/toc/id:kpMFE00022/metalworking-fluids-3rd?kpromoter=marc.

[96] N. Dhar and M. Kamruzzaman, "Cutting temperature, tool wear, surface roughness and dimensional deviation in turning AISI-4037 steel under cryogenic condition," *International Journal of Machine Tools and Manufacture,* vol. 47, no. 5, pp. 754-759, 2007.

[97] A. Voloshin, E. Dolzhenkova, L. Lytvynov, A. Petukhov, and E. Slyunin, "The influence of coolant pH on efficiency of machining sapphire," *Journal of Superhard Materials,* vol. 35, 03/01 2013, doi: 10.3103/S1063457613020093.

[98] Jared and B. Howell, *Chip dynamics in diamond turning.* 2019.

[99] A. Hamdan, F. Jamaludin, K. Abou-El-Hossein, and M. Abd Shukor, "PERFORMANCE EVALUATION OF DIFFERENT TYPES OF CUTTING FLUID IN THE MACHINING OF AISI 01 HARDENED STEEL USING PULSED JET MINIMAL QUANTITY LUBRICATION SYSTEM," *ASEAN Engineering Journal,* vol. 1, p. 1, 07/01 2011.

[100] M. Uddin, S. Kumar Saha, and M. Sulaiman Hossain, *Effect of Lubrication Condition on Surface Roughness in Facing Operation.* 2015, pp. 227-232.

[101] O. Çakīr, A. Yardimeden, T. Ozben, and E. Kilickap, "Selection of cutting fluids in machining processes," *Journal of Achievements in materials and Manufacturing engineering,* vol. 25, no. 2, pp. 99-102, 2007.

[102] L. N. López de Lacalle, C. Angulo, A. Lamikiz, and J. A. Sánchez, "Experimental and numerical investigation of the effect of spray cutting fluids in high speed milling," *Journal of Materials Processing Technology,* vol. 172, no. 1, pp. 11-15, 2006/02/20/ 2006, doi: https://doi.org/10.1016/j.jmatprotec.2005.08.014.

[103] M. A. Elbestawi and M. Dumitrescu, "Tool condition monitoring in machining-neural networks," in *Information Technology for Balanced Manufacturing Systems*: Springer, 2006, pp. 5-16.

[104] P. Stavropoulos, D. Chantzis, C. Doukas, A. Papacharalampopoulos, and G. Chryssolouris, "Monitoring and control of manufacturing processes: A review," *Procedia CIRP,* vol. 8, pp. 421-425, 2013.

[105] P. Piljek, Z. Keran, and M. Math, "Micromachining–review of literature from 1980 to 2010," *Interdisciplinary Description of Complex Systems: INDECS,* vol. 12, no. 1, pp. 1-27, 2014.

[106] H. Silva, J. Duduch, R. Jasinevicius, and A. Gee, "Monitoring single point diamond turning through acoustic emission," *WIT Transactions on Engineering Sciences,* vol. 23, 1999.

[107] R. Teti, K. Jemielniak, G. O'Donnell, and D. Dornfeld, "Advanced monitoring of machining operations," *CIRP Annals-Manufacturing Technology,* vol. 59, no. 2, pp. 717-739, 2010.

[108] D. Dornfeld, A, Y. Lee, and A. Chang, "Monitoring of Ultraprecision Machining Processes," *Advanced Manufacturing Technology,* vol. 21, pp. 571–578, 2003, doi: 10.1007/s00366-003-1294-3.

[109] P. E. Mix, *Introduction to nondestructive testing: a training guide*. John Wiley & Sons, 2005.

[110] C. XiaoQi, Z. Hao, and D. Wildermuth, "In-process tool monitoring through acoustic emission sensing," *Automated Material Processing Group, Automation Technology Division,* vol. 1, 2001.

[111] H. Vallen, "AE testing fundamentals, equipment, applications," *Journal of Nondestructive Testing(Germany),* vol. 7, no. 9, pp. 1-30, 2002.

[112] T. Otieno and K. Abou-El-Hossein, "Cutting forces and acoustic emission in the diamond turning of rapidly-solidified aluminium," *Insight-Non-Destructive Testing and Condition Monitoring,* vol. 60, no. 1, pp. 11-18, 2018.

[113] D. Eitzen and H. Wadley, "Acoustic emission: establishing the fundamentals," *Journal of research of the National Bureau of Standards,* vol. 89, no. 1, pp. 75-100, 1984.

[114] N. Mokhtar, I. Y. Ismail, M. Asmelash, H. Zohari, and A. Azhari, "Analysis of acoustic emission on surface roughness during end milling," *ARPN Journal of Engineering and Applied Sciences,* vol. 12, no. 4, pp. 1324-1328, 2017.

[115] J. J. Liu and D. Dornfeld, *Modeling and Analysis of Acoustic Emission in Diamond Turning*. 1996.

[116] R. Liptai, D. Harris, R. Engle, and C. A. Tatro, "Acoustic emission techniques in materials research," California Univ., Livermore. Lawrence Radiation Lab., 1970.

[117] L. Tan and J. Jiang, *Digital signal processing: fundamentals and applications*. Academic Press, 2013.

[118] A. Terchi and Y. Au, "Acoustic emission signal processing," *Measurement and Control,* vol. 34, no. 8, pp. 240-244, 2001.

[119] T. W. Liao, "Feature extraction and selection from acoustic emission signals with an application in grinding wheel condition monitoring," *Engineering Applications of Artificial Intelligence,* vol. 23, no. 1, pp. 74-84, 2010.

[120] X. Li, "A brief review: acoustic emission method for tool wear monitoring during turning," *International Journal of Machine Tools and Manufacture,* vol. 42, no. 2, pp. 157-165, 2002.

[121] M. Bhuiyan and I. Choudhury, "Review of sensor applications in tool condition monitoring in machining," *Comp. Mater. Process,* vol. 13, pp. 539-569, 2014.

[122] C. Lauro, L. Brandão, D. Baldo, R. Reis, and J. Davim, "Monitoring and processing signal applied in machining processes–A review," *Measurement,* vol. 58, pp. 73-86, 2014.

[123]   O. A. Olufayo, "Tool Wear Monitoring in End Milling of Mould Steel Using Acoustic Emission," Nelson Mandela Metropoltan University, 2011.

[124]   O. P. B., "Tool Wear Monitoring in Machining of Stainless Steel," Master of Engineering (Mechatronics), Mechatronics, Nelson Mandela University, 2017.

[125]   B. Sick, "On-line and indirect tool wear monitoring in turning with artificial neural networks: a review of more than a decade of research," *Mechanical Systems and Signal Processing,* vol. 16, no. 4, pp. 487-546, 2002.

[126]   S. Binsaeid, S. Asfour, S. Cho, and A. Onar, "Machine ensemble approach for simultaneous detection of transient and gradual abnormalities in end milling using multisensor fusion," *Journal of Materials Processing Technology,* vol. 209, no. 10, pp. 4728-4738, 2009.

[127]   S. Liang and D. Dornfeld, "Tool wear detection using time series analysis of acoustic emission," *Journal of Engineering for Industry,* vol. 111, no. 3, pp. 199-205, 1989.

[128]   H. Ravindra, Y. Srinivasa, and R. Krishnamurthy, "Acoustic emission for tool condition monitoring in metal cutting," *Wear,* vol. 212, no. 1, pp. 78-84, 1997.

[129]   C. Scheffer, "Monitoring of tool wear in turning operations using vibration measurements," University of Pretoria, 1999.

[130]   M. R. Kaphle, "Analysis of acoustic emission data for accurate damage assessment for structural health monitoring applications," Queensland University of Technology, 2012.

[131]   L. Xiaoli and Y. Zhejun, "Tool wear monitoring with wavelet packet transform—fuzzy clustering method," *Wear,* vol. 219, no. 2, pp. 145-154, 1998.

[132]   M. P. Vogler, S. G. Kapoor, and R. E. DeVor, "On the modeling and analysis of machining performance in micro-endmilling, Part II: Cutting force prediction," *Journal of manufacturing science and engineering,* vol. 126, no. 4, pp. 695-705, 2004.

[133]   R. Sturges, "Monitoring milling processes through AE and tool/part geometry," *ASME Journal of Engineering for Industry,* vol. 114, pp. 8-14, 1992.

[134]   X. Chen, J. Tang, and D. Dornfeld, "Monitoring and analysis of ultraprecision metal cutting with acoustic emission," in *Mechanical Engineering Congress and Exposition, ASME, Atlanta, GA*, 1996, p. 387.

[135]   A. A. Jaber and R. Bicker, "A Simulation of Non-stationary Signal Analysis Using Wavelet Transform Based on LabVIEW and Matlab," in *Modelling Symposium (EMS), 2014 European*, 2014: IEEE, pp. 138-144.

[136]   I. Bogrekci and P. Demircioglu, "SURFACE ROUGHNESS DETERMINATION USING SIGNAL PROCESSING TECHNIQUES," 2016.

[137] J. J. Scholey, P. D. Wilcox, M. R. Wisnom, and M. I. Friswell, "A practical technique for quantifying the performance of acoustic emission systems on plate-like structures," (in eng), *Ultrasonics,* vol. 49, no. 6-7, pp. 538-548, 2009/06// 2009, doi: 10.1016/j.ultras.2009.02.001.

[138] V. K. Kakar and M. Kandpal, "Techniques of acoustic feature extraction for detection and classification of ground vehicles," *International Journal of Emerging Technology and Advance Engineering,* vol. 3, no. 2, pp. 419-426, 2013.

[139] A. J. Mian, "Size effect in micromachining," The University of Manchester (United Kingdom), 2011.

[140] N. Instruments. "Time Frequency Analysis Application Areas (Advanced Signal Processing Toolkit)." http://zone.ni.com/reference/en-XX/help/372656C-01/lvasptconcepts/tfa_application/ (accessed 2018).

[141] M. Misiti, Y. Misiti, G. Oppenheim, and J.-M. Poggi, "Wavelet toolbox," *The MathWorks Inc., Natick, MA,* vol. 15, p. 21, 1996.

[142] C. Sammut and G. I. Webb, *Encyclopedia of machine learning*. Springer Science & Business Media, 2011.

[143] J. Tang, S. Alelyani, and H. Liu, "Feature selection for classification: A review," *Data classification: Algorithms and applications,* p. 37, 2014.

[144] K. Goebel and W. Yan, "Feature selection for tool wear diagnosis using soft computing techniques," in *The ASME International Mechanical Engineering Congress and Exhibition, Orlando*, 2000, pp. 5-10.

[145] S. H. Krishna, K. Satyanarayana, and K. B. Raju, "Surface roughness prediction model using ANN & ANFIS," *International Journal of Advanced Engineering Research and Studies,* vol. 1, pp. 102-113, 2011.

[146] G. D'Mello and S. Pai, "Prediction of surface roughness in high speed machining: a comparison," *Proc. Int. J. Res. Eng. Technol,* vol. 1, pp. 519-525, 2014.

[147] G. Kant and K. S. Sangwan, "Prediction and optimization of machining parameters for minimizing power consumption and surface roughness in machining," *Journal of cleaner production,* vol. 83, pp. 151-164, 2014.

[148] J. Jiang, P. Trundle, and J. Ren, "Medical image analysis with artificial neural networks," *Computerized Medical Imaging and Graphics,* vol. 34, no. 8, pp. 617-631, 2010.

[149] M. K. M. Amin, "Multiple self-organised spiking neural networks," University of Aberdeen, 2009.

[150] A. Kohli and U. Dixit, *A neural-network-based methodology for the prediction of surface roughness in a turning process*. 2005, pp. 118-129.

[151] A. Sinha, "An improved recognition module for the identification of handwritten digits," Massachusetts Institute of Technology, 1999.

[152] A. C. Basheer, U. A. Dabade, S. S. Joshi, V. V. Bhanuprasad, and V. M. Gadre, "Modeling of surface roughness in precision machining of metal matrix composites using ANN," *Journal of Materials Processing Technology,* vol. 197, no. 1, pp. 439-444, 2008/02/01/ 2008, doi: https://doi.org/10.1016/j.jmatprotec.2007.04.121.

[153] A. K. Gupta, "Predictive modelling of turning operations using response surface methodology, artificial neural networks and support vector regression," *International Journal of Production Research,* vol. 48, no. 3, pp. 763-778, 2010/02/01 2010, doi: 10.1080/00207540802452132.

[154] C. Sanjay and C. Jyothi, *A study of surface roughness in drilling using mathematical analysis and neural networks*. 2006, pp. 846-852.

[155] G. Zhang, B. Eddy Patuwo, and M. Y. Hu, "Forecasting with artificial neural networks:: The state of the art," *International Journal of Forecasting,* vol. 14, no. 1, pp. 35-62, 1998/03/01/ 1998, doi: https://doi.org/10.1016/S0169-2070(97)00044-7.

[156] U. Zuperl and F. Cus, "Optimization of cutting conditions during cutting by using neural networks," *Robotics and Computer-Integrated Manufacturing,* vol. 19, no. 1, pp. 189-199, 2003/02/01/ 2006, doi: https://doi.org/10.1016/S0736-5845(02)00079-0.

[157] M. H. Beale, H. B. Demuth, and M. T. Hagan, "Neural network toolbox™ User's Guide R 2014a," *For Use with MATLAB. The MathWorks Inc,* vol. 2000, 2014.

[158] M. Nalbant, H. Gökkaya, İ. Toktaş, and G. Sur, "The experimental investigation of the effects of uncoated, PVD- and CVD-coated cemented carbide inserts and cutting parameters on surface roughness in CNC turning and its prediction using artificial neural networks," *Robotics and Computer-Integrated Manufacturing,* vol. 25, no. 1, pp. 211-223, 2009/02/01/ 2009, doi: https://doi.org/10.1016/j.rcim.2007.11.004.

[159] F. Koçer and J. Pajot, *Introduction into Design of Experiments DOE with HyperStudy*, A. University, ed., 1 ed. USA, 2017.

[160] H. Guo. and A. Mettas, "Design of Experiments and Data Analysis," presented at the 2011 Annual RELIABILITY and MAINTAINABILITY Symposium San Jose, CA, USA, January, 2011, 2011.

[161] G. Jacques., W. L. Creighton, and S. Institute, *Introduction to design of experiments with JMP examples* (SAS Press series). SAS Publishing (in English), 2007.

[162] R. H. Myers, *Response surface methodology; Process and product optimization using designed experiments* (no. 04; QA279, M84.). 1995.

[163] K. M. Carley, N. Y. Kamneva, and J. Reminga, "Response surface methodology," CARNEGIE-MELLON UNIV PITTSBURGH PA SCHOOL OF COMPUTER SCIENCE, 2004.

[164] D. Rajeev, D. Dinakaran, G. Lead, and S. Muthuraman, "Prediction of roughness in hard turning of AISI 4140 steel through artifical neural network and regression models," *Int. J. Mech. Eng. Technol,* vol. 7, no. 5, pp. 200-208, 2017.

[165]   T. Otieno and K. Abou-El-Hossein, "Molecular dynamics analysis of nanomachining of rapidly solidified aluminium," (in English), *The International journal, advanced manufacturing technology.*, vol. 94, no. 1-4, pp. 121-131, 2018.

[166]   B. K, N. M, and P. Duraisamy, "Machinability analysis and application of response surface approach on CNC turning of LM6/SiCp composites," *Materials and Manufacturing Processes,* vol. 34, no. 12, pp. 1389-1400, 2019/09/10 2019, doi: 10.1080/10426914.2019.1660787.

[167]   M. A. Bezerra, R. E. Santelli, E. P. Oliveira, L. S. Villar, and L. A. Escaleira, "Response surface methodology (RSM) as a tool for optimization in analytical chemistry," *Talanta,* vol. 76, no. 5, pp. 965-977, 2008.

[168]   R. Technology. "RSP Technology RSA-441 T6 Aluminum Super Alloy." http://www.matweb.com/search/datasheet.aspx?matguid=a2f8e7b296884177bdbacb5def945a8c&ckck=1 (accessed.

[169]   *Precitech Nanoform® 250 Ultragrind*, AMETEK®Precitech, Inc., 2016.

[170]   *Taylor Hopson Pgi Dimension Profilometer*, Precitech, Inc, 2016.

[171]   S. Gupta, V. Chadha, V. Sardana, V. Setia, and R. Singari, *Experimental Analysis of Surface Roughness in CNC Taper Turning of Aluminum 6061 Using Taguchi Technique*. 2017.

[172]   Varsha Pathak, Ranganath M. Singari, Vipin, Ravi Butola, and M. Tayyab, "Influence of The Machining Parameters for Surface Roughness in Turning of Aluminium Metal Matrix Composites," *International journal of advanced production and industrial engineering,* vol. 3, no. 4, pp. 35-43, 2018. [Online]. Available: www.ijapie.org.

[173]   S. Hussein, "An Experimental Study of the Effects of Coolant Fluid on Surface Roughness in Turning Operation for Brass Alloy," 03/03 2014.

[174]   M. Y. Noordin, V. C. Venkatesh, S. Sharif, S. Elting, and A. Abdullah, "Application of response surface methodology in describing the performance of coated carbide tools when turning AISI 1045 steel," *Journal of materials processing technology,* vol. 145, no. 1, pp. 46-58, 2004.

[175]   R. Kumar, A. Kumar Sahoo, P. Chandra Mishra, A. Panda, R. Kumar Das, and S. Roy, "Prediction of Machining Performances in Hardened AISI D2 Steel," *Materials Today: Proceedings,* vol. 18, pp. 2486-2495, 2019/01/01/ 2019, doi: https://doi.org/10.1016/j.matpr.2019.07.105.

[176]   G. S. Khan, R. G. V. Sarepaka, K. Chattopadhyay, P. Jain, and V. Narasimham, "Effects of tool feed rate in single point diamond turning of aluminium-6061 alloy," 2003.

[177]   D.-D. Cui and L.-C. Zhang, "Nano-machining of materials: understanding the process through molecular dynamics simulation," *Advances in Manufacturing,* vol. 5, no. 1, pp. 20-34, 2017/03/01 2017, doi: 10.1007/s40436-016-0155-4.

192

[178] A. Chaijareenont and S. Tangjitsitcharoen, "Monitoring of Surface Roughness in Aluminium Turning Process," *IOP Conference Series: Materials Science and Engineering,* vol. 303, p. 012013, 01/01 2018, doi: 10.1088/1757-899X/303/1/012013.

[179] B. de Agustina, E. M. Rubio, and M. Á. Sebastián, "Surface roughness model based on force sensors for the prediction of the tool wear," (in eng), *Sensors (Basel),* vol. 14, no. 4, pp. 6393-6408, 2014, doi: 10.3390/s140406393.

[180] J. C. Chen and B. Huang, "An In-Process Neural Network-Based Surface Roughness Prediction (INN-SRP) System Using a Dynamometer in End Milling Operations," *The International Journal of Advanced Manufacturing Technology,* vol. 21, no. 5, pp. 339-347, 2003/02/01 2003, doi: 10.1007/s001700300039.

[181] V. Sivaraman, S. Sankaran, and L. Vijayaraghavan, "Effect of cutting parameters on cutting force and surface roughness during machining microalloyed steel: Comparison between ferrite–pearlite, tempered martensite and ferrite–bainite–martensite microstructures," *Proceedings of the Institution of Mechanical Engineers, Part B: Journal of Engineering Manufacture,* vol. 232, no. 1, pp. 141-150, 2018/01/01 2016, doi: 10.1177/0954405416635479.

[182] M. A Kuttolamadom, S. Hamzehlouia, and L. Mears, *Effect of Machining Feed on Surface Roughness in Cutting 6061 Aluminum*. 2010.

[183] K. Kadirgama, M. Noor, M. Rahman, M. Rejab, C. H. C. Haron, and K. A. Abou-El-Hossein, "Surface roughness prediction model of 6061-T6 aluminium alloy machining using statistical method," 2009.

[184] O. Zurita, V. Di-Graci, and M. Capace, "Effect of cutting parameters on surface roughness in turning of annealed AISI-1020 steel," *Revista Facultad de Ingeniería,* vol. 27, p. 109, 01/15 2018, doi: 10.19053/01211129.v27.n47.2018.7928.

[185] L. N. Abdulkadir, K. Abou-El-Hossein, A. I. Jumare, P. B. Odedeyi, M. M. Liman, and T. A. Olaniyan, "Ultra-precision diamond turning of optical silicon—a review," *The International Journal of Advanced Manufacturing Technology,* vol. 96, no. 1, pp. 173-208, 2018/04/01 2018, doi: 10.1007/s00170-017-1529-x.

[186] K. Nabil, Z. Hessainia, and M. Yallese, *Optimisation of machining parameters in hard turning by desirability function analysis using response surface methodology*. 2015.

[187] Z. Hessainia, A. Belbah, M. A. Yallese, T. Mabrouki, and J.-F. Rigal, "On the prediction of surface roughness in the hard turning based on cutting parameters and tool vibrations," *Measurement,* vol. 46, no. 5, pp. 1671-1681, 2013/06/01/ 2013, doi: https://doi.org/10.1016/j.measurement.2012.12.016.

[188] R. K. Bhushan, "Optimization of cutting parameters for minimizing power consumption and maximizing tool life during machining of Al alloy SiC particle composites," *Journal of Cleaner Production,* vol. 39, pp. 242-254, 2013/01/01/ 2013, doi: https://doi.org/10.1016/j.jclepro.2012.08.008.

[189] A. Houshmand, W. Daud, and M. S. Shafeeyan, *Tailoring the Surface Chemistry of Activated Carbon by Nitric Acid: Study Using Response Surface Method*. 2011, pp. 1251-1260.

[190] A. M. Zain, H. Haron, and S. Sharif, "Prediction of surface roughness in the end milling machining using Artificial Neural Network," *Expert Systems with Applications,* vol. 37, no. 2, pp. 1755-1768, 2010/03/01/ 2010, doi: https://doi.org/10.1016/j.eswa.2009.07.033.

[191] K. A. Risbood, U. Dixit, and A. D. Sahasrabudhe, *Prediction of Surface Roughness and Dimensional Deviation by Measuring Cutting Forces and Vibrations in Turning Process*. 2003, pp. 203-214.

[192] X. Liu and H. Gu, *Hyperbolic tangent function based two layers structure neural network*. 2011.

[193] G. Kant and K. S. Sangwan, "Predictive Modelling and Optimization of Machining Parameters to Minimize Surface Roughness using Artificial Neural Network Coupled with Genetic Algorithm," *Procedia CIRP,* vol. 31, pp. 453-458, 2015/01/01/ 2015, doi: https://doi.org/10.1016/j.procir.2015.03.043.

[194] MATLAB. "Function Approximation and Nonlinear Regression " https://fr.mathworks.com/help/deeplearning/examples/body-fat-estimation.html (accessed 8/4/2019, 2019).

[195] D. Yadav, R. Naresh, and V. Sharma, *Stream flow forecasting using Levenberg-Marquardt algorithm approach*. 2011.

[196] G. V. Yeole and S. R. Shinde, "Acoustic Emission Signal Analysis using Data Acquisition System," *International Journal of Engineering Trends and Technology,* vol. 11, no. 8, pp. 384-387, 2014.

Appendix A: Technical Specifications of Precitech Nanoform 250 Ultra-grind [196].

Technical Product Specification Nanoform® 250 ultragrind

Machine Base and Control	Description
Machine Base	Natural, high-stability, sealed granite, with flood coolant stainless steel enclosure
Machine Type	Ultra precision, two, three, four or five axes CNC contouring machine
Vibration Isolation	FEA optimized dual sub-frames for the ultimate in environmental isolation
Control System	UPx™ Control System with Optional Adaptive Control Technology
Operating System	QNX real time operating system
Programming Resolution	0.01 nanometer linear / 0.0000001° Rotary
File Transfer Storage	USB, CD, Ethernet, On-board data storage backup
Performance (SPDT)	Surface Roughness (Ra) < 1.5 nm, Form Accuracy (P-V) < 0.15 micron
Performance (Grinding)	Surface Roughness (Ra) < 5 nm, Form Accuracy (P-V) < 0.15 micron Tungsten carbide

Linear Hydrostatic Slideways	Description
Type	Hydrostatic oil bearing slideways with symmetrical linear motor placement
Material	Durabar cast iron
Travel	X and Z: 220 mm (8.6 inch)
Maximum Feedrate	4,000 mm/minute (157 inch/minute)
Drive System	AC linear motor
Motor Location	Located centrally and mounted vertically eliminating offset drive forces and minimizing thermal distortions
Position Feedback Resolution	16 picometers (0.016 nanometers)
X-axis Straightness	**Horizontal:** 0.2 micron (8 micro inch) full travel 0.05 micron/25 mm (2 micro inch)
Z-axis Straightness	**Horizontal:** 0.2 micron (8 micro inch) full travel 0.05 micron/25 mm (2 micro inch)
Vertical Straightness	0.375 micron (15 micro inch) full travel

Workholding/Positioning Spindle	High Performance SP150 Spindle
Type	Slot-type thrust bearing
Material	Steel shaft/Bronze journal
Standard Swing Capacity	250 mm (9.8 inch) diameter
Motor	Integral brushless motor
Ultimate Load Capacity	114 Kg (250 pounds) 50 mm (2 inch) out from spindle nose
Axial Stiffness	230 N/micron (1,314,000 pounds/inch)
Radial Stiffness	130 N/micron (743,600 pounds/inch)
Motion Accuracy	Axial/Radial ≤ 15nm (0.6 micro inch)
Thermal Control Optional	Liquid cooled chiller +/- 0.1C Accuracy
C-axis Feedback Resolution	0.010 arc-sec
C-axis Position Accuracy	+/- 1 arc-sec
C-axis Max Speed	1,500 RPM
Work Holding Spindle Max Speed	7,000 RPM

Rotary B-axis	HydroRound Rotary B-axis
Type	Bi-conical, self compensated, Oil hydrostatic bearing, DC Brushless direct drive motor
Material	Stainless Steel
Tabletop Size	330 mm (13 inch)
Standard Swing Capacity	220 mm (8.75 inch) diameter over tabletop / 440 mm otherwise
Load Capacity	225 Kg (500 pounds)
Maximum Speed	10 RPM continuous / 50 RPM intermittent
Motor Torque	36 inch-pounds/ 4.0 N-m
Position Feedback Resolution	0.004 arc-sec
Positioning Accuracy	+/- 1 arc-sec
Radial Error Motion	0.10 µm (4 micro inch) @ 1 in. above table and can be improved with optional error mapping
Coning Error	1.0 nm/mm (1.0 micro inch/inch)
Radial Stiffness	225 N/micron (1,280,000 pounds/inch)
Axial Stiffness	600 N/micron (3,428,000 pounds/inch)
Moment Stiffness	3.4 N-m/micro radian (30 inch-pounds/micro radian) (144 inch-pounds inch-pounds/arc-sec)

High Speed Milling/Grinding Spindle	High Speed SP75FF Spindle	High Speed PI ISO 2.25 Spindle
Air Supply Pressure	690 KPA (100 PSI)	690 KPA (100 PSI)
Air Consumption	2.8 l/s (6.0 SCFM)	0.9 l/s (2.0 SCFM)
Radial Load Capacity	20.5 Kg (45 lbs)	10 Kg (20 pounds)
Axial Stiffness	70 N/micron (400,000 pounds/inch)	69 N/micron (392,000 lbs/inch)
Radial Stiffness	22 N/micron (125,000 pounds/inch)	23 N/micron (130,000 lbs/inch)
Axial Error Motion	< 0.05 micron (2 micro inch)	< 0.05 micron (2 micro inch)
Radial Error Motion	< 0.05 microns (2 micro inch)	< 0.05 micron (2 micro inch)
Maximum Speed	15,000 RPM	50,000 RPM

Facility Requirements	Nanoform® 250 ultragrind
Power	208 +/-10% or 230 +/-10% VAC - 3.0 KVA 1 phase - 50/60Hz
Air Supply	Typical: 12 SCFM @100 PSIG
Machine Footprint	914 mm x 2120 mm x 1700 mm (36 inch x 83.5 inch x 67 inch)
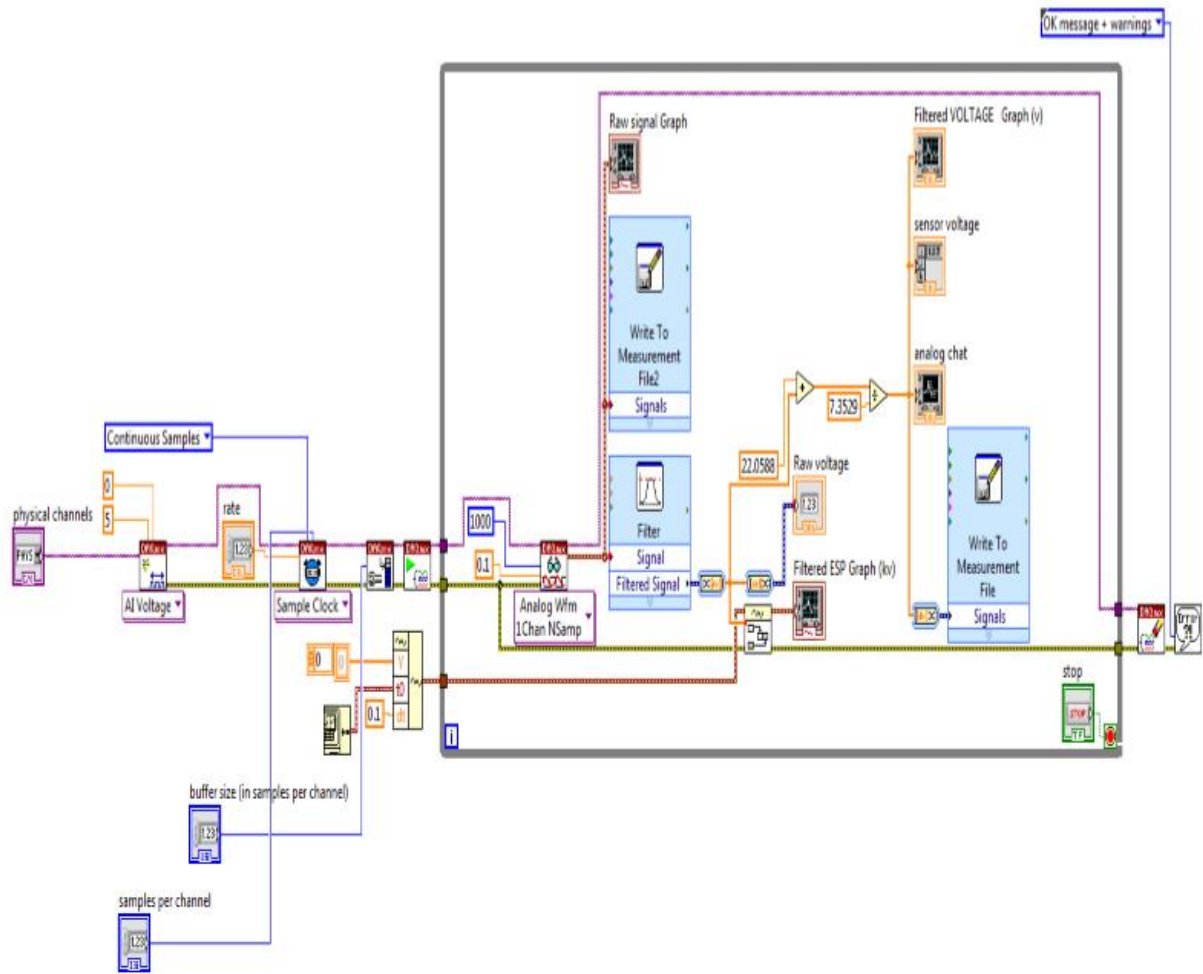
Appendix C: Features extracted for experiment 1 (Kerosene mist as Cutting fluid)

EXPERIMENT	DOC	Feed	Speed	SK	KT	RMS	Power	Energy	Std Dev of Freq	P-P	Mean	Maximum	Minimum	Range	Ra
1	25	25	1375	0.0115	3.2681	0.020948	4.39E-04	191.7674	0.0209	0.2051	6.07E-04	0.1074	-0.0977	0.2051	27
2	25	5	1375	0.0111	3.1633	0.022195	4.93E-04	5.4186	0.0222	0.1953	6.33E-04	0.0977	-0.0977	0.1953	12
3	25	15	750	0.0066	3.276	0.021145	4.47E-04	468.8221	0.0211	0.2148	3.36E-04	0.1074	-0.1074	0.2148	25
4	15	25	750	0.0091	3.2615	0.021169	4.48E-04	371.9572	0.0212	0.21	1.61E-04	0.1123	-0.0977	0.21	50
5	25	15	2000	0.0136	3.2523	0.021429	4.58E-04	618.5889	0.0214	0.2148	2.60E-04	0.1123	-0.1025	0.2148	16
6	5	15	2000	0.0085	3.2424	0.0216	4.65E-04	629.1611	0.0216	0.2197	3.53E-04	0.1123	-0.1074	0.2197	13
7	15	15	1375	0.0087	3.2594	0.021582	4.66E-04	408.017	0.0216	0.2148	2.27E-04	0.1123	-0.1025	0.2148	13
8	5	5	1375	0.0029	3.2856	0.022255	4.95E-04	17.3348	0.0223	0.1855	4.33E-04	0.1025	-0.083	0.1855	10
9	15	5	2000	0.0027	3.5633	0.017388	3.02E-04	9.3726	0.0174	0.1709	3.17E-04	0.083	-0.0879	0.1709	9
10	15	25	2000	0.0273	4.0576	0.016392	2.69E-04	1.6119	0.0164	0.1563	3.65E-04	0.083	-0.0732	0.1563	15
11	15	15	1375	0.0087	3.2594	0.016632	4.66E-04	408.017	0.0216	0.2148	2.27E-04	0.1123	-0.1025	0.2148	13
12	5	15	750	0.0155	3.8357	0.0169	2.77E-04	2.7661	0.0166	0.1611	6.07E-04	0.1074	-0.0977	0.2051	19
13	15	5	750	-0.0216	4.0162	0.016684	2.78E-04	7.2351	0.0167	0.1758	4.52E-04	0.0977	-0.0781	0.1758	12
14	15	15	1375	0.0087	3.2594	0.021582	4.66E-04	408.017	0.0216	0.2148	2.27E-04	0.1123	-0.083	0.2148	13
15	5	25	1375	-0.0591	3.8271	0.015787	2.49E-04	1.4955	0.0158	0.1367	1.81E-04	0.0732	-0.0635	0.1367	17

Appendix D: Normalized feature for experiment 1 (Kerosene mist as Cutting fluid)

EXPERIMENT	DOC	Feed	Speed	SK	KT	RMS	Power	Energy	Std Dev of Freq	P-P	Mean	Maximum	Minimum	Range	Ra
1	1.0	1.0	0.5	0.8	0.1	0.8	0.8	0.3	0.8	0.8	0.9	0.9	0.2	0.8	0.4
2	1.0	0.0	0.5	0.8	0.0	1.0	1.0	0.0	1.0	0.7	1.0	0.6	0.2	0.7	0.1
3	1.0	0.5	0.0	0.8	0.1	0.8	0.8	0.7	0.8	0.9	0.4	0.9	0.0	0.9	0.4
4	0.5	1.0	0.0	0.8	0.1	0.8	0.8	0.6	0.8	0.9	0.0	1.0	0.2	0.9	1.0
5	1.0	0.5	1.0	0.8	0.1	0.9	0.8	1.0	0.9	0.9	0.2	1.0	0.1	0.9	0.2
6	0.0	0.5	1.0	0.8	0.1	0.9	0.9	1.0	0.9	1.0	0.4	1.0	0.0	1.0	0.1
7	0.5	0.5	0.5	0.8	0.1	0.9	0.9	0.6	0.9	0.9	0.1	1.0	0.1	0.9	0.1
8	0.0	0.0	0.5	0.7	0.1	1.0	1.0	0.0	1.0	0.6	0.6	0.7	0.6	0.6	0.0
9	0.5	0.0	1.0	0.7	0.4	0.2	0.2	0.0	0.2	0.4	0.3	0.3	0.4	0.4	0.0
10	0.5	1.0	1.0	1.0	1.0	0.1	0.1	0.0	0.1	0.2	0.4	0.3	0.8	0.2	0.1
11	0.5	0.5	0.5	0.8	0.1	0.1	0.9	0.6	0.9	0.9	0.1	1.0	0.1	0.9	0.1
12	0.0	0.5	0.0	0.9	0.8	0.2	0.1	0.0	0.1	0.3	0.9	0.9	0.2	0.8	0.2
13	0.5	0.0	0.0	0.4	1.0	0.1	0.1	0.0	0.1	0.5	0.6	0.6	0.7	0.5	0.1
14	0.5	0.5	0.5	0.8	0.1	0.9	0.9	0.6	0.9	0.9	0.1	1.0	0.6	0.9	0.1
15	0.0	1.0	0.5	0.0	0.7	0.0	0.0	0.0	0.0	0.0	0.0	0.0	1.0	0.0	0.2

Appendix E: Features extracted for experiment 2 (Water as Cutting fluid)

EXPERIMENT	DOC	Feed	Speed	SK	KT	RMS	Power	Energy	Std Dev of Freq	P-P	Mean	Maximum	Minimum	Range	Ra
1	25	25	1375	-0.0591	3.8271	0.015787	2.49E-04	1.4955	0.0158	0.1367	1.81E-04	7.32E-02	-6.35E-02	1.37E-01	17
2	25	5	1375	0.0285	3.1457	0.022554	5.09E-04	15.2604	0.0225	0.2002	6.30E-04	1.03E-01	-9.77E-02	2.00E-01	11
3	25	15	750	0.0092	3.1359	0.022698	5.15E-04	8.243	0.0227	0.1904	5.31E-04	9.77E-02	-9.28E-02	1.90E-01	19
4	15	25	750	0.0156	3.1426	0.022285	4.97E-04	2.9792	0.0223	0.1709	7.00E-04	8.30E-02	-8.79E-02	1.71E-01	40
5	25	15	2000	0.0298	3.2931	0.022214	4.94E-04	5.428	0.0222	0.1904	6.93E-04	1.03E-01	-8.79E-02	1.90E-01	11
6	5	15	2000	0.0111	3.1639	0.022195	4.93E-04	5.4171	0.0222	0.1953	6.29E-04	9.77E-02	-9.77E-02	1.95E-01	12
7	15	15	1375	0.0021	3.2096	0.021667	4.69E-04	5.6321	0.0217	0.2002	6.19E-04	1.03E-01	-9.77E-02	0.2002	13
8	5	5	1375	0.0469	3.7668	0.016954	2.87E-04	9.1976	0.0169	0.1758	6.76E-04	9.28E-02	-8.30E-02	1.76E-01	9
9	15	5	2000	-0.0122	3.7201	0.016845	2.84E-04	9.3633	0.0168	0.2002	7.53E-04	1.03E-01	-9.77E-02	2.00E-01	8
10	15	25	2000	0.0026	3.8411	0.016479	2.71E-04	1.6282	0.0165	0.1563	2.28E-04	8.30E-02	-7.32E-02	1.56E-01	14
11	15	15	1375	0.0021	3.2096	0.021667	4.69E-04	5.6321	0.0217	0.2002	6.19E-04	1.03E-01	-9.77E-02	2.00E-01	13
12	5	15	750	-0.0533	4.0328	0.015443	2.38E-04	2.6232	0.0154	0.1563	5.01E-04	8.30E-02	-7.32E-02	1.56E-01	17
13	15	5	750	-0.0099	3.9383	0.01552	2.41E-04	7.7075	0.0155	0.1709	8.56E-04	9.28E-02	-7.81E-02	1.71E-01	12
14	15	15	1375	0.0021	3.2096	0.021667	4.69E-04	5.6321	0.0217	0.2002	6.19E-04	1.03E-01	-9.77E-02	0.2002	13
15	5	25	1375	-0.023	4.1639	0.015364	2.36E-04	1.6524	0.0154	0.1563	5.50E-04	8.30E-02	-7.32E-02	1.56E-01	14

Appendix F: Normalized features for experiment 2 (Water as Cutting fluid)

EXPERIMENT	DOC	Feed	Speed	SK	KT	RMS	Power	Energy	Std Dev of Freq	P-P	Mean	Maximum	Minimum	Range	Ra
1	1.0	1.0	0.5	0.0	0.7	0.1	0.0	0.0	0.1	0.0	0.0	0.0	1.0	0.0	0.3
2	1.0	0.0	0.5	0.8	0.0	1.0	1.0	1.0	1.0	1.0	0.7	1.0	0.0	1.0	0.1
3	1.0	0.5	0.0	0.6	0.0	1.0	1.0	0.5	1.0	0.8	0.5	0.8	0.1	0.8	0.3
4	0.5	1.0	0.0	0.7	0.0	0.9	0.9	0.1	0.9	0.5	0.8	0.3	0.3	0.5	1.0
5	1.0	0.5	1.0	0.8	0.2	0.9	0.9	0.3	0.9	0.8	0.8	1.0	0.3	0.8	0.1
6	0.0	0.5	1.0	0.7	0.0	0.9	0.9	0.3	0.9	0.9	0.7	0.8	0.0	0.9	0.1
7	0.5	0.5	0.5	0.6	0.1	0.9	0.8	0.3	0.9	1.0	0.6	1.0	0.0	1.0	0.2
8	0.0	0.0	0.5	1.0	0.6	0.2	0.2	0.6	0.2	0.6	0.7	0.7	0.4	0.6	0.0
9	0.5	0.0	1.0	0.4	0.6	0.2	0.2	0.6	0.2	1.0	0.8	1.0	0.0	1.0	0.0
10	0.5	1.0	1.0	0.6	0.7	0.2	0.1	0.0	0.2	0.3	0.1	0.3	0.7	0.3	0.2
11	0.5	0.5	0.5	0.6	0.1	0.9	0.8	0.3	0.9	1.0	0.6	1.0	0.0	1.0	0.2
12	0.0	0.5	0.0	0.1	0.9	0.0	0.0	0.1	0.0	0.3	0.5	0.3	0.7	0.3	0.3
13	0.5	0.0	0.0	0.5	0.8	0.0	0.0	0.5	0.0	0.5	1.0	0.7	0.6	0.5	0.1
14	0.5	0.5	0.5	0.6	0.1	0.9	0.8	0.3	0.9	1.0	0.6	1.0	0.0	1.0	0.2
15	0.0	1.0	0.5	0.3	1.0	0.0	0.0	0.0	0.0	0.3	0.5	0.3	0.7	0.3	0.2